Degradation Mechanisms and Service Life Estimation of Fiber Reinforced Polymer (FRP) Concrete Reinforcements

Adel ElSafty, Ph.D., P.E. (Principal Investigator)

Dr. Brahim Benmokrane, P.E. (Co-PI)   **Dr. Sami Rizkalla, P.E. (Co-PI)**

Dr. Ahmed H. Ali, Ph.D.   **Dr. Mohammad Pour-Ghaz, (Co-PI)**

Dr. Hamdy M. Mohamed, Ph.D.   **Dr. Omar Khalaf, Ph.D.**

School of Engineering
College of Computing, Engineering, and Construction
University of North Florida
Jacksonville, Florida 32224

DISCLAIMER

The opinions, findings, and conclusions expressed in this publication are those of the authors and not necessarily those of the State of Florida Department of Transportation.

SI CONVERSION FACTORS

SYMBOL	WHEN YOU KNOW	MULTIPLY BY	TO FIND	SYMBOL
		LENGTH		
in	inches	25.4	millimeters	mm
ft	feet	0.305	meters	m
yd	yards	0.914	meters	m

SYMBOL	WHEN YOU KNOW	MULTIPLY BY	TO FIND	SYMBOL
		AREA		
in^2	square inches	645.2	square millimeters	mm^2
ft^2	square feet	0.093	square meters	m^2
yd^2	square yard	0.836	square meters	m^2

SYMBOL	WHEN YOU KNOW	MULTIPLY BY	TO FIND	SYMBOL
		VOLUME		
ft^3	cubic feet	0.028	cubic meters	m^3
yd^3	cubic yards	0.765	cubic meters	m^3

NOTE: volumes greater than 1,000 L shall be shown in m^3

SYMBOL	WHEN YOU KNOW	MULTIPLY BY	TO FIND	SYMBOL
		MASS		
oz	ounces	28.35	grams	g
lb	pounds	0.454	kilograms	kg

SYMBOL	WHEN YOU KNOW	MULTIPLY BY	TO FIND	SYMBOL
		FORCE and PRESSURE or STRESS		
lbf	pound force	4.45	newton	N
lbf/in^2	pound force per square inch	6.89	kilopascals	kPa
kip	1,000 pounds force	4.45	kilonewton	kN

TECHNICAL REPORT DOCUMENTATION

1. Report No. BDV34 TWO 977-05	2. Government Accession No.	3. Recipient's Catalog No.
4. Title and Subtitle Degradation mechanisms and service life estimation of fiber reinforced polymer (FRP) concrete reinforcements		5. Report Date April 2019
		6. Performing Organization Code
7. Author(s) Dr. Adel ElSafty, Dr. Brahim Benmokrane, Dr. Sami Rizkalla, Dr. Mohammad Pour-Ghaz, Dr. Ahmed H. Ali, Dr. Hamdy Mohamed, Dr. Omar Khalaf Alla		8. Performing Organization Report No.
9. Performing Organization Name and Address University of North Florida School of Engineering, 1 UNF Drive Jacksonville, FL 32224		10. Work Unit No. (TRAIS)
		11. Contract or Grant No. **BDV34-977-05**
12. Sponsoring Agency Name and Address State of Florida Department of Transportation 605 Suwannee St. MS 30 Tallahassee, FL 32399		13. Type of Report and Period Covered Final Report
		14. Sponsoring Agency Code
15. Supplementary Notes 		

16. Abstract

Fiber-reinforced-polymer (FRP) reinforcement, such as glass and carbon, have emerged as an acceptable construction material for both new constructions as well as for the rehabilitation and strengthening of existing structures. The proven track records of superior performance of FRP materials in terms of strength, durability, resistance to corrosion, and versatility of fabrication have made these materials attractive to civil engineers. This research study aims at investigating glass fiber reinforced polymer (GFRP) bars and carbon fiber prestressing tendons. The research team of this study investigated the physical and mechanical properties, and durability to concrete of the FRP composites. For GFRP bars and CFRP prestressing tendons, the research team investigated the physical characteristics, tensile properties, and long-term durability in alkaline solution and elevated temperatures under sustained load and without load. The investigated physical characteristics included the fiber content, thermal expansion, void content, water absorption, glass transition temperature T_g, and cure ratio. Scanning electronic microscopy (SEM) analysis, tensile properties tests, shear strength tests in high pH under sustained load and without load, and other tests for GFRP and CFRP reinforcements were performed. In addition, the investigators studied the structural behavior of concrete beams prestressed with CFRP strands. The researchers conducted comparisons between the predicted and experimental ultimate load, strains, and deflection. The researchers analyzed the results and drew conclusion regarding the FRP performance.

17. Key Word FRP, Degradation, Carbon, Prestressing, Glass, Prediction Models, Sustained Load		18. Distribution Statement No restrictions.		
19. Security Classif. (of this report) Unclassified		20. Security Classif. (of this page) Unclassified	21. No. of Pages 286	22. Price

ACKNOWLEDGEMENTS

EXECUTIVE SUMMARY

In recent years, fiber-reinforced-polymer (FRP) materials have emerged as an acceptable construction material for both new constructions as well as for the rehabilitation and strengthening of existing structures. The proven track records of superior performance of FRP materials in terms of strength, durability, resistance to corrosion, and versatility of fabrication have made these materials attractive to civil engineers. Due to the excellent corrosion resistance of the FRP reinforcing bars currently on the market, the use of continuous glass and carbon fiber reinforcement in concrete structural applications seems to be promising for reinforcing new concrete structures, strengthening applications, and for replacement of steel reinforcement. From the literature, the material characteristics show that the carbon fibers offer a higher ultimate strength than glass fibers at similar ultimate strain, providing a higher modulus of elasticity. However, the carbon fibers may experience a brittle rupture at relatively low strains. Some literature indicates that there is a need for more investigation to study the alkali resistance of glass-FRP reinforcement under sustained load. In addition, due to the very limited amount of research on the use of carbon-FRP, as prestressed tendons, for structural applications, further investigations are still required to provide confidence in the use of the carbon-FRP bars or tendons to reinforce concrete structures in place of steel bars. It was determined that mechanical properties, durability, and physical properties are the most important characteristics that should be examined for glass and carbon reinforcing tendons before their use as reinforcement for concrete structures.

The main objective of the this project was to evaluate the characteristics of the glass fiber reinforced polymer (GFRP) bars and the carbon fiber prestressing strands, including the tensile strength, the modulus of elasticity, behavior, and durability under severe environmental exposures and sustained loading. The investigators of this study investigated the physical and mechanical properties, and durability preformance of the FRP composites. For GFRP and CFRP prestressing tendons, the research team investigated the physical characteristics, tensile properties, and long-term durability in alkaline solution and elevated temperatures under load and without load. The investigated physical characteristics included the fiber content, thermal expansion, void content, water absorption, glass transition temperature $Tg,$ and cure ratio. Scanning electronic microscopy (SEM) analysis, tensile properties, shear strength in high pH under load and without load, and

other tests for GFRP and CFRP reinforcements were performed. In addition, the investigators studied the structural behavior of concrete beams prestressed with CFRP strands. The researchers conducted comparisons between the predicted and experimental ultimate load, strains, and deflection. The researchers analyzed the results and drew conclusion regarding the FRP performance.

.

TABLE OF CONTENTS

CHAPTER 5   QUANTIFYING THE DEGRADATION OF RESIN MATRIX AND FIBERS IN HIGH ALKALI ENVIRONMENT 212

LIST OF TABLES

LIST OF FIGURES

CHAPTER 1
INTRODUCTION

1.1 Background

The Florida Department of Transportation has commenced the implementation of fiber reinforced polymer (FRP) products as alternatives to traditional materials. One of the key areas of implementation is reinforcing concrete with FRP bars, which eliminates the issues associated with the corrosion of steel. While FRP rebar will not corrode in the traditional sense, studies have shown that FRP constituent materials may experience degradation when exposed to the concrete environment. In the case of carbon fiber reinforced polymers (CFRP), degradation of the fibers themselves is not a concern. However, there is more concern when glass fiber reinforced polymers (GFRP) are exposed to certain environments because the glass fibers themselves may be prone to degradation.

The problem is that there are no established methods to determine the service life of GFRP rebar. Studies have mainly focused on analyzing the reduction of mechanical properties after exposure to accelerated conditions that are not directly correlated to real time. From a material degradation standpoint, physical properties (such as tensile strength) alone may not tell the full story. An ideal service-life estimation method should also include the actual mechanisms of degradation. This becomes complicated considering there are multiple components of FRPs and may involve the combination of multiple models. For example, one model may look at the cross-link density of the polymer matrix while another looks at the integrity of the silica network in the glass fibers while yet another looks at the fiber/matrix interface. Another possible outcome is that one mode of degradation is determined to be 'critical' to the lifetime of the material, thus a model of that particular mechanism could be used to predict the service life.

For carbon fiber strands (CFRP) under sustained load, there is a need for further investigation. The results of the first phase of the FDOT assessment investigation indicated that the strengths of the CFRP specimens without load were slightly affected by increasing the immersion duration at higher temperature levels. Therefore, long-term durability characterization of CFRP was needed to evaluate the effect of alkaline environment at different temperature exposures and under different sustained tensile load levels (from 40% up to 65% of guaranteed tensile strength).

1.2 Research Significance

The outcome of this research indicates that the carbon CFRP strands can be highly recommended for use as corrosion-resistant reinforcing material for prestressed concrete bridge components and pile applications in Florida's marine environment. The research asseses the duability characteristics and degradation of CFRP strands and GFRP bars under sustained load in aggressive environments. Moreover, the research evaluates the feasibility of using the CFRP prestressing strands in prestressed concrete applications. In addition, the models of service life for FRP recinforcements in concrete were developed and evaluated based by on degradation mechanisms. The mechanical properties and durablilty performance of the constituent materials, including carbon fiber and resin were also investigated to evaluate the effect of environmental conditioning on the durability of FPR constituent materials.

1.3 Objectives and Originality

The main objective of the research project is to determine the alkali resistance of carbon fiber pre-stressing strand under load, the degradation mechanisms of carbon fiber pre-stressing strand in concrete, the degradation mechanisms of GFRP rebar in concrete, and develop testing protocol to evaluate the service life of FRP reinforcements in concrete based on degradation mechanisms. The evaluated characteristics of CFRP strands and GFRP bars were included the tensile strength, the modulus of elasticity, performance, and durability under sustained load and severe environmental exposures. The researchers conducted the tests in accordance to the requirements of the ACI Committee Report 440.3R-04, which provides a guide for the test methods for Fiber-Reinforced Polymers (FRPs) for reinforcing and strengthening concrete structures. The researchers also investigated the FRP materials according to the CAN/CSA S6-14 and CAN/CSA-S806-12. The objectives also included providing a comprehensive state-of-the-art review of fiber-reinforcing materials, providing a baseline verification of structural and bonding capacity of fiber-reinforcing material in concrete, and identifying possible material degradation of fiber, filler, and outer epoxy material components. The researchers also determined the implications of possible material degradation on mechanical behavior of FRP materials. The research objectives also included quantifying mechanical resiliency of fiber-reinforced concrete with possible material deficiencies.

1.4 Methodology

In this study, the researchers investigated the physical and mechanical properties, performance and durability of the FRP composites. For carbon fiber (CFRP) prestressing strands, the researchers performed physical characterization and long-term durability in alkaline solution and elevated temperature under load and without load. The applied sustained loads on the CFRP tendons were equivalent to 40% and 65% of their guaranteed strength. For GFRP bars, the research team also investigated the physical characteristics, tensile properties, and alkali resistance of GFRP in high pH levels under sustained load that was equivalent to 30% of the their guaranteed strength. For both of CFRP and GFRP bars, the researchers conducted tests on physical characteristics (fiber content, thermal expansion, void content, water absorption, glass transition temperature "Tg", and cure ratio), tensile properties, shear strength in high pH under load and without load, and SEM analysis. In addition, the researchers evaluated the mechanical properties of the constituent materials of the CFRP strands and examined the effect of environmental conditioning on their durability. The CFRP strands are comprised of carbon fibers and epoxy resin. Both fibers and resin were tested. The researchers tested concrete beams reinforced with CFRP strands and investigated the structural behavior of beams prestressed with CFRP strands. The researchers used the prediction models to predict the residual strengths at different times and service life, thereby providing the designer with possible estimates of bar capacity at later ages.

CHAPTER 2
LITERATURE REVIEW

2.1 Introduction

The long-term durability of reinforced and prestressed concrete structures has become a major concern in the construction industry. One of the main factors reducing durability and service life of reinforced and prestressed concrete structures is the corrosion of steel reinforcement. Many steel-reinforced and prestressed concrete structures exposed to deicing salts and marine environments require extensive and expensive maintenance (Benmokrane et al. 2017). Fiber reinforced polymers (FRPs) are a promising alternative to steel due to their high tensile strength, light weight, and resistance to electrochemical corrosion. Different types of FRP tendons have been developed to potentially replace steel tendons in areas where corrosion is a problem. Several design guides and codes on reinforcing structural concrete members with FRP reinforcement were developed and published in several countries (ISIS design manual No. 3, 2007; CSA S6, 2014; ACI 440.1R, 2015); CNR-DT 204-06, 2006); FIB Task Group 9.3, 2007; and CSA S806, 2012). Countries such as, Canada, United States (USA), Japan, and some other European countries have already implemented the use of FRP in bridges deck slabs, parking structures, barrier walls, continuous pavement, and other concrete structures. To date, however, FRPs have not realized their full potential within the construction industry. One of the contributing factors is limited information regarding their long-term performance. In particular, since the service life of a civil engineering structure is typically 50 to 100 years, knowledge of the long-term durability of FRPs is of prime importance (Ali et al. 2018). The durability of FRP materials depends on numerous factors including fiber properties, resin properties, and manufacturing process used. Therefore, knowledge of durability and degradation mechanisms of construction materials will play a crucial role to build confidence within the industry and to identify both the limits and potential of FRPs in structural applications (Benmokrane et al. 2016 and 2017; Ali et al. 2017 and 2018). In this report, the following sections provide a general review on the durability of FRP reinforcing and prestressing reinforcements.

2.2 FRP Reinforcing Bars and Prestressing Cables

2.2.1 FRP reinforcing bars

The FRP bars commonly used are composites reinforced with glass FRP (GFRP), carbon FRP (CFRP), Aramid FRP (AFRP), and Basalt FRP (BFRP). Today, glass-FRP (GFRP) bars are becoming more attractive to the construction industry because they cost less than other types of FRP materials. Moreover, the cost of GFRP bars has been dropping in recent years primarily due to a larger market and greater competition. GFRP bars have been used successfully as main reinforcement in concrete bridges, parking garages, tunnels, and water tanks (Mohamed and Benmokrane

2014). Therefore, the development of reinforced concrete with GFRP bars and their application in infrastructure is gaining considerable interest in the civil-engineering community.

Advanced FRP bars have many desirable properties, such as high performance, high strength-to-weight ratio, high stiffness-to-weight ratios, high-energy absorption, and outstanding corrosion and fatigue damage resistance. Besides, FRP reinforcement bars have more flexibility, elasticity, and minimal environmental impact particularly when used in infrastructure such as tunnel application as soft-eyes (Grace et al. 2012). Therefore, partial or complete adoption of FRP composites can significantly enhance structural safety and sustainability. FRP products are manufactured in several forms such as bars, fabrics, 2D grid, 3D grid, or standard structural shapes. Figure 2.1 shows various types and shapes of currently available FRP products (Elsafty 2014).

2.2.2 Carbon-fiber composite cables (CFRP)

Carbon-fiber composite cables (CFRP) are of interest to the Florida Department of Transportation and other DOTs for use as a corrosion-resistant reinforcing material for prestressed precast-concrete bridge beams (as a competitive material of stainless-steel prestressing cables). The researchers in this study investigated CFRP manufactured by Tokyo Rope Manufacturing Co. Ltd., Japan. The Tokyo Rope carbon-fiber composite cable (CFCC) is a stranded cable comprising a number of individual strands. In general, these cables are made with 7, 19, or 37 twisted carbon strands, with nominal diameters varying from 5 to 40 mm (0.2 to 1.6 in.) as presented in Table 2.1 and Figure 2.2. Individual strands of Tokyo Rope (CFRP) consist of carbon fibers impregnated with thermosetting epoxy resin; in addition, each strand is protected with wrapping material of polyester resin (Benmokrane et al. 2016).

Table 2.1: Standard specification of CFRP

Strand configuration Section of CFRP		Diameter (mm)	Effective cross section (mm^2)	Guaranteed Capacity (kN)	Nominal mass density (g/m)	Tensile elastic modulus (kN/mm^2)
●	U 5.0	5.0	15.2	38	30	167
	1x7	7.5	31.1	76	60	155
	1x7	10.5	57.8	141	111	155
	1x7	12.5	76.0	184	145	155
	1x7	15.2	115.6	270	221	155
	1x7	17.2	151.1	350	289	155
	1x7	19.3	186.7	445	355	155
	1x19	20.5	206.2	316	410	137
	1x19	25.5	304.7	467	606	137
	1x19	28.5	401.0	594	777	137
	1x37	35.5	591.2	841	1,185	127
	1x37	40.0	798.7	1,200	1,508	145
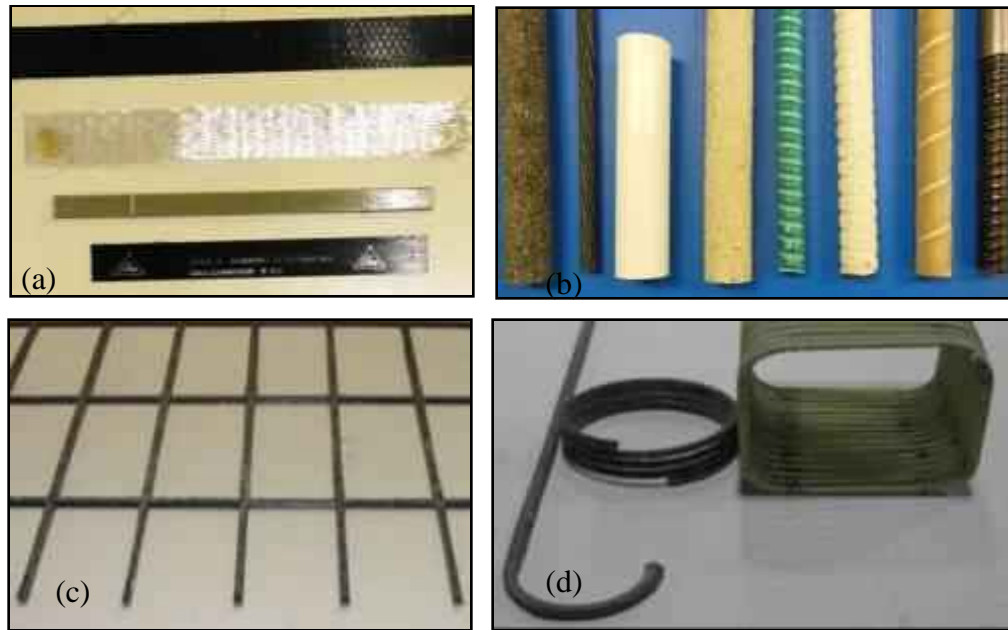
Figure 2.1: Different FRP products: (a) fabrics and strips; (b) straight bars; (c) grids; (d) spiral stirrups and curved bars.

Figure 2.2: Carbon fiber composite cables (CFRPs) (Vistasp M. Karbhari 1998)

2.3 Characteristics of GFRP Reinforcing Bars

GFRP reinforcing bars are manufactured from continuous glass fibers embedded in matrices (thermosetting or thermoplastic). A key element in evaluating the GFRP properties is the characterization of the relative volume and/or mass content of the various constituent materials. The physical and mechanical properties influence the GFRP reinforcing bars in concrete structures. Design variables include the choice of constituents (fiber and polymeric matrix), the volume fractions of fiber and matrix, fiber orientation, and the manufacturing process. Other factors such as dimensional effects and quality control during fabrication play an important role in determining the characteristics of GFRP bars. The loading history, duration of loading, temperature, and humidity also affect FRP materials. FRP bars are produced in different diameters, depending on the manufacturing process. FRP bars normally have tensile strength higher than the tensile strength of conventional steel bars. This relatively high tensile strength makes FRP bars suitable as reinforcement for concrete structures. The tensile behavior of FRP bars having one type of fiber material is characterized by a linearly elastic stress-strain relationship up to failure. The FRP bars do not exhibit any plastic

behavior before rupture. Figure 2.3 shows typical tensile stress-strain relationships of FRP rein-forcement compared to conventional steel bars. The figure also shows that the modulus of elasticity of FRP bars is lower than that of steel bars. The CFRP has the highest modulus of elasticity, which ranged from 60% to 75% of that for steel. While the GFRP bars has the lowest modulus of elasticity, which ranged from 20% to 25% of that for steel.
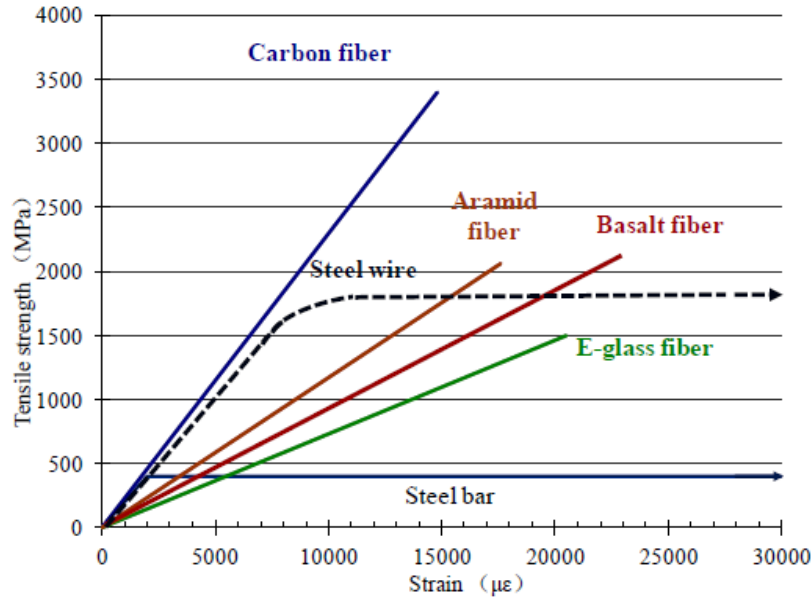
Figure 2.3: Typical stress-strain relationships of different FRPs compared to steel bars (Zhishen et al., 2012)

Bond behavior of an FRP bar depends on the surface preparation and mechanical properties of the bar itself as well as the environmental conditions. The FRP bar surface preparations can be cate-gorized in two forms according to the bond stresses transfer between the FRP bar and the concrete, friction forming preparations and bearing forming preparations. The bars in the first category are coated with a granular material before the bars are completely cured. These granular particles in-crease bond transfer through friction between the bars and concrete. Another way of increasing the bond strength of the bars is through the formation of indentations or deformations on the bar before full curing. The V-ROD FRP bars; which have sand-coated surface and are produced by Pultrall Inc., Quebec, Canada, stand as example of the bars of first category, whereas LeadlineTM CFRP bars; which have indented surface and are produced by Mitsubishi Chemical Cooperation, Japan, stand as example of the bars of second category. In addition, both methods may be combined, whereas the surface of the Aslan FRP bars produced by the Hughes Brothers Inc., USA, contains indentations as well as a granular coating. Figure (2.1-b) shows different surfaces types of sand-coated and deformed FRP bars. Further information concerning the physical and mechanical prop-erties, time dependent behavior, and durability of FRP reinforcement, can be found in the follow-ing: (JSCE, 1997; ACI 440.1R, 2015; ISIS design manual No. 3, 2007; CSA S806-12; CSA S807-10; and CSA S6-14).

2.4　Characteristics of Carbon-Fiber Cables

2.4.1　Advantages of CFRP

The CFRP cables have general properties of CFRP (carbon-fiber reinforced polymer) and also configuration properties of stranded wire. Therefore, CFRP cables have the following advantages over conventional steel strands or other FRP (fiber reinforced polymer) rods (JSCE 1997) (Enomoto and Ushijima 2012).

- Excellent corrosion resistance: High acid resistance and alkali resistance.
- Lightweight: About 1/5th of the weight of steel with specific gravity of 1.5.
- Low relaxation loss: Relaxation performance of CFRP is nearly same as low relaxation steel strands.
- High tensile strength: Equal to that of steel strand.
- High tensile elastic modulus.
- High tensile fatigue performance: Fatigue performance of CFRP is superior to that of the steel strands.
- Low linear expansion: Coefficient of linear expansion is about 1/20 of that of steel.
- Nonmagnetic interact: No magnetic effect.
- Flexibility: Stranded configuration of the cables allows them to be easily coiled. In addition, CFRP strands can be wound on a reel for easy transportation even if the material is CFRP and the length exceeds 1,000 m.

2.4.2　Mechanical properties of CFRP

The following section provides a brief description of the basic mechanical properties when CFRP is used for tendons and reinforcing components in prestressed concrete bridges. It is believed that CFRP with these characteristics is most suitable for the tendons and reinforcement materials of prestressed concrete bridges than any other types of FRP.

2.4.2.1　Load–elongation curve

The relation between tensile load and elongation of CFRP is shown in Figure 2.4. For comparison, cases of steel strands and aramid FRP (AFRP) rod of almost same diameter (0.5 in.) are also presented in Figure 2.4. FRP material in CFRP indicates an elastic behavior in all sections up to the point of breakage, and almost no plastic region was observed. It can be noticed from the figure that elastic modulus of CFRP is high as compared with an AFRP rod, rather close to steel materials (Enomoto and Ushijima 2012).
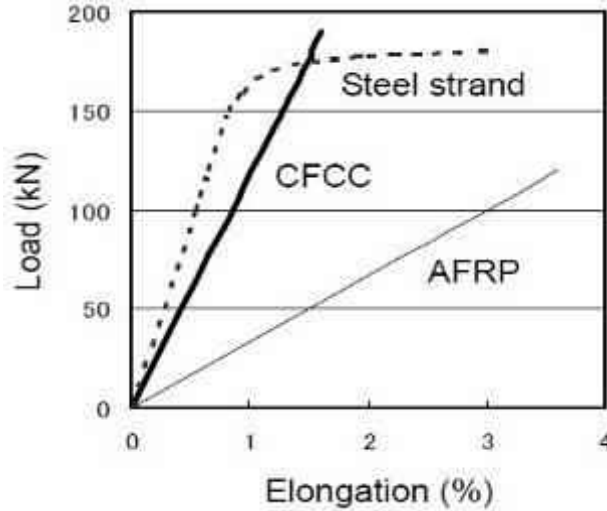
Figure 2.4: Load-Elongation curve (Enomoto and Ushijima 2012)

2.4.2.2 Relaxation

Results given by Enomoto et al. (2009) for relaxation testing of CFRP 1x7 (12.5 mm) are shown in Figure 2.5. It was observed that the relaxation property of CFRP is almost the same as that of steel strands. Figure 2.5 shows relaxation rate up to 33,000 hr when initial load of 70% of tensile product standard load was applied. Plot gives details of the relation between time and relaxation rate. Relaxation was estimated by the following formula.

$$Y = 0.056 + 0.396 \, log \, T \tag{2.1}$$

2.4.2.3 Development length

Transfer length of CFRP is the length required to achieve anchoring bond between the CFRP tendon and concrete in prestressed member. It is defined in the "Recommended Guidelines for Design and Construction of Prestressed Concrete Highway Bridge using FRP Tendons" (Enomoto and Ushijima 2012), as 65 times the nominal diameter of the CFRP. Bond strength of CFRP is similar to or greater than that of prestressing steel strands, and several reports have indicated that the required length for bonding is 50 times the nominal diameter or less.
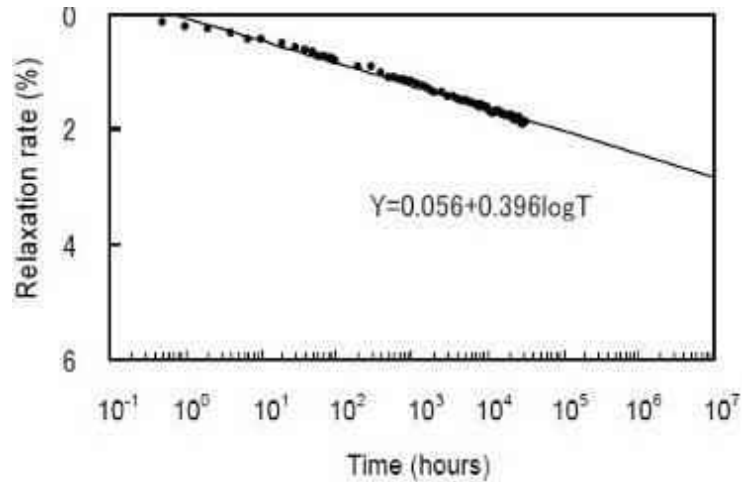
Figure 2.5: Relaxation curve of th0e 33,000 hr (Enomoto and Ushijima 2012)

2.4.2.4 Bond strength with concrete

Results from the testing of three specimens confirmed that CFRP had sufficient bond strength, with 7-strand 12.5 mm in diameter as reported by Enomoto and Ushijima 2012. These CFRP strands had a pullout load of 723 N/cm^2. A graphic representation of the test setup for bond strength was used as shown in Figure 2.6.

2.5 Durability of GFRP Reinforcing Bars

The corrosion of steel has cost billions of dollars in infrastructure repair in North America. It is estimated that $3.6 trillion are needed by 2020 to alleviate potential problems in civil infrastructure. Approximately one in nine bridges in the United States are rated as structurally deficient, requiring about $20.5 billion annually to eliminate the bridge deficient backlog by 2028 (Tavassoli et al. 2015). As a relatively new material with excellent corrosion resistance and a high strength-weight ratio, internal glass fiber-reinforced polymer (GFRP) reinforcement is considered a feasible and sustainable alternative to steel reinforcement for future infrastructure (Tavassoli et al. 2015). Despite the resistance of FRP to electrochemical corrosion, the performance of FRP may deteriorate due to environmental, physical, or chemical conditions, leading to loss of strength and stiffness. The literature (Chu and Karbhari, 2005, Chen et al., 2006; Chen et al., 2007; Riebel and Keller, 2007) indicates that the performance of FRPs deteriorates due to certain physical (e.g., cyclic or sustained loading, moisture diffusion, extreme temperature variation) or chemical (e.g., alkalinity) exposure. The degree of deterioration depends on a variety of factors such as the type and volume of fibers and resin matrix, the exposed environment, and the manufacturing process. Furthermore, due to the addition of FRP composites to concrete structures, the durability performance of FRP reinforced concrete structures becomes more complex due to the combined effect of FRP composites, interface, concrete, and various environmental and mechanical conditions. Therefore, assessing the durability of FRP composites, in association with concrete structures and

38

as an individual material, is a very complex task. The literature indicated several durability influence factors: fluids (moisture; chemical solutions); alkalinity; and creep/relaxation.
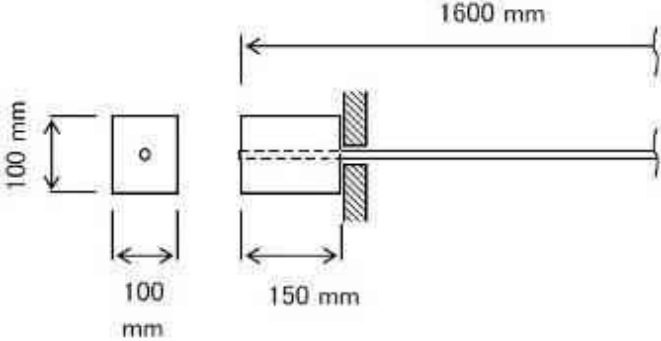
Figure 2.6: Test method for bond strength (Enomoto and Ushijima 2012)

Figure 2.7: Concrete structure deteriorated by the corrosion of steel reinforcemen-t

The degree of damage/deterioration of internal FRP reinforcement depends on fundamental factors such as the type and volume fraction of fibers, type of resin, morphology, and strength of the fiber-matrix interface, severity of the exposure environments and the process of fabrication. The E-glass fibers are the most susceptible to degradation due to the moisture and alkalinity while carbon fibers are relatively inert to such environments. Aramid fibers, on the other hand, are highly resistant to abrasion and impact, but are sensitive to creep, moisture, and ultraviolet light. To achieve appropriate performance, a suitable type of resin must protect the fibers. The durability of the resin system is dependent on several factors such as the resin components, their individual properties and proportions, as well as curing time and conditions.

2.5.1   Effect of moisture

Concrete with internal FRP reinforcement is generally exposed to alternating wet/dry cycles, natural weathering, and corrosive media. Even if concrete provides an excellent first line of defense, the permeability could eventually transmit moisture and other corrosive elements to the internal reinforcement. The effect of fluids on the performance of FRP composites has been one of the most studied subjects related to durability of composites during the past decades. In general, the sorption behavior of fluid into FRPs depends on types of fluid (water, acid, base), fluid concentration, temperature, external applied stress, type of fiber and resin, interface, process of molding and state of material (damage, curing condition). (Ben Daly et al., 2007) showed that moisture diffusion took place in pultruded composites. The maximum saturation level could be related to the presence of fillers and additives in the polymer matrix. The literature indicated that the rate of sorption is controlled by the chemical structure of the matrix (degree and type of cross-linking, presence of void), interface/interphase, and manufacturing process. Researchers have attempted to control diffusion process by using resin matrix with lower permeability (Benmokrane 2000), modifying interphase region by using suitable sizing chemistry or select appropriate process of molding to reduce void content. In addition, moisture ingress can degrade resin by chemical attack (hydrolysis) or drop in glass transition temperature (Chin et al., 2001). For this reason, fluids affect matrix dominant properties such as transverse and shear strengths of FRP composites and decreases of these properties become more important with increased exposure time and temperature (Liao et al. 1998, Ali et al. 2015).

Glass fibers are particularly sensitive to fluids ingress, due to their susceptibility to chemical and physical attack. The level of degradation depends on composition of fibers, fluid type and concentration and exposed temperature. Extensive studies have been conducted in this research area (Chin et al. 2001; Al-Zahrani 2005; Chu and Karbhari 2002 and 2004; Chen et al. 2006). Typically, the tensile strength of E-glass/vinylester composites would decrease by 40% in 100% relative humidity environment at 93°C. In general, (Al-Zahrani, 2005) has shown that the modulus of elasticity was less affected by all the exposure conditions than the tensile strength. Carbon fibers are not affected by fluids ingress, but resin matrix is usually affected. Consequently, the performance of composites is also affected in the case of CFRP. For unidirectional carbon composites, this usually leads to reduction in the compressive strength and shear strength, but only a small effect on the tensile strength since this property is especially dominated by fibers which are not affected by fluids (Dejke and Tepfers 2001). (Hancox and Mayer 1994) reported minimal weight gain and strength loss for carbon/epoxy specimen exposure to 65% humidity for over four months and to boiling water for over three weeks. Aramid fibers are affected by fluids, mostly at higher temperatures. AFRP composites saturated in water have been reported to lose 35% of their flexural strength at room temperature (Allred 1984), and up to 55% if stressed and under wet/dry thermal cycles (Sen et al. 1996). On the other hand, Technora and Kevlar fibers, also categorized as Aramid fibers, show different behavior under combined effects of fluids and temperatures. For Technora fibers, no degradation was observed in distilled water at any temperature; however, the decreases

in strength were reported for specimens immersed in acid and alkali solutions and the reduction was increased with time and temperature.

2.5.2   Effect of alkaline environments

The concrete environment has high alkalinity, with pH between 12 and 13 depending on the concrete mixture design and the type of cement used, (Benmokrane et al. 2006). This alkaline environment damages glass fibers through loss in toughness, strength, and embrittlement. In general, carbon fibers are known to exhibit the best alkaline resistance followed by Aramid then glass fibers. Glass fibers are damaged due to the combination of two processes (1) chemical attack on the glass fibers by the alkaline cement environment, and (2) concentration and growth of hydration products between individual filaments (Murphy et al. 1999). The embrittlement of fibers is due to the nucleation of calcium hydroxide on the fiber surface. The hydroxylation can cause fiber surface pitting and roughness, which act as flaws severely reducing fibers properties in the presence of moisture. In addition, calcium, sodium, and potassium ions found in the concrete pore solution are highly aggressive towards glass fibers. Therefore, the degradation of glass fibers not only depends on the high pH level, but also due to the combination of alkali salts, pH, and moisture. Aramid fibers show strength degradation in an alkaline environment. Kevlar 29 exposed to 10% sodium hydroxide solution for 1,000 hr loses 74% of its strength. High modulus Aramids such as Kevlar 49 demonstrates better alkaline resistance (Malvar 1998). Carbon fibers are commonly believed not to be affected by alkaline environment. (Judd 1971) reported that carbon fibers were resistant to alkaline solutions at all concentrations and all temperatures up to boiling. Carbon tows immersed for 257 days in a very basic 50% sodium hydroxide solution showed variations in strength and elastic modulus only around 15%. Although an appropriate resin matrix (vinylester, epoxy) provides certain level of protection to fibers from alkaline degradation, migration of high pH solutions and alkali salts through resin (or through void, crack, interface between fiber/matrix) to the fiber surface is possible. Katsuki and Uomoto (Katsuki and Uomoto, 1995) used Electron Probe Microscopy to track ingress of alkali ions (sodium ions) into Aramid, carbon and glass reinforced vinyl ester rods. Sodium ions penetrated into GFRP in radial direction with time. No degradation was noticed in AFRP, or CFRP rods immersed for 60 days compared to GFRP rods. Chin et al. (Chin et al. 2001) observed, by Energy Dispersive X-Ray Analysis, that appreciable amounts of sodium, potassium and calcium were found in the interior of isopolyester specimens exposed to 60°C [140°F] pore solution for 60 days. However, the authors also noticed that no evidence for the ingress of ions was found for the vinylester specimen. Hojo et al. (Hojo et al. 1991) studied the corrosion behavior of resins in aqueous solutions, and compared it with that of the metal. Three forms of corrosion mechanisms were found namely surface reaction, corrosion layer forming, and penetration type. By using corrosion depth, with immersion time, the authors found that the concept of corrosion rate could be applied even in polymeric materials. The corrosion rates were dependent on the chemical structure and reactivity between resin and environments. Resin cracking and fiber delamination creating a pathway for moisture and ionic species, may also be observed (Benmokrane et al. 2006).

A recent study on the durability of GFRP bars in moist concrete was conducted (Robert et al. 2009). Sand-coated GFRP bars with a nominal diameter of 12.7 mm were embedded in concrete and exposed to tap water at 23, 40, and 50°C for periods of 60–240 days. The tensile test results showed that at 40 and 50°C, the decrease of the tensile strength was 10% and 16%, respectively, of the original tensile strength after 240 days of exposure. In a field study (Mufti et al. 2005), concrete cores were taken from five in-service concrete bridge structures of 6–8 years age across Canada, reinforced with GFRP bars. On the basis on microscopic and chemical analysis, they concluded that the concerns about the durability of GFRP in alkaline concrete, based on simulated laboratory studies in alkaline solutions, are unfounded. The performance of the glass fiber-reinforced polymer bars was evaluated by conducting tensile tests on the bars extracted out from the concrete prisms after exposure to different conditions. In addition, scanning electron microscopy was used to investigate the degradation mechanism of the bars. After 18 months of exposure, test results showed that both the tap water at 50°C and the alkaline solution at 50°C had the maximum harmful effect on the tensile strength of glass fiber-reinforced polymer bars. The two field conditions showed almost no degradation (1% - 2%) in the tensile properties of the tested bars, (Al-musallam et al. 2013).

Caceres et al. (2002) has been investigated the durability under accelerated salt-fog exposure of six commercially available composites. These composites included glass-reinforced vinylesters, polyesters, phenolics, and an epoxy. Durability was measured mainly in terms of the loss of elastic modulus and flexural strength after exposure. In order to accelerate aging, the specimens were subjected to temperatures of 95°F (35°C), 120°F (49°C), and 160°F (71°C) for one, two and three months each while exposed to a salt-fog spray. A previous project had determined that among the common marine exposures, salt-fog was a major cause for degradation of composites used in the retrofit of the Navy's waterfront infrastructure. Flexural tests were performed, along with Dynamic Mechanic Analyses and Scanning Electron Microscopy. Once the aging effects were determined, a time-temperature superposition analysis was performed in order to extrapolate the results and estimate the degradation over longer time periods. Analysis predictions indicate losses of 35% or more in flexural strength over a 5-year period. Wang et al. (2010) studied degradation of tensile properties of basalt FRP and the related hybrid FRP tendons under salt solution. The results show that 1) the degradation of tensile strength of BFRP tendons is proportional to the increase of stress level, whereas the corresponding modulus is relatively constant; 2) the BFRP tendons under the stress level of 0.6fu after 63 days aging maintain the tensile strength of more than 90%, which shows a good resistance to salts corrosion; 3) hybrid B/CFRP tendons shows even better resistance to salt corrosion in comparison to BFRP but the positive hybrid effect is only observed for the tendons under low stress level ($0.3f_u$); 4) the degradation of hybrid B/SFRP tendons is larger than that of the other FRP tendons, which is mainly caused by the corrosion of inside steel wires. Robert et al. (2013) has presented the mechanical, durability, and micro–structural characterization of unstressed glass fiber–reinforced–polymer (GFRP) reinforcing bars exposed to concrete environment and saline solutions under accelerating conditions. These conditionings were used to simulate the effect of seawater or deicing salts on GFRP bars. The pre– and post–exposure tensile strengths

of the bars were used for long-term property predictions based on the Arrhenius theory. The results revealed no significant differences in the durability of the concrete-wrapped GFRP bars whether immersed in salt solution or tap water and the very high long–term durability of the GFRP bars in salt solution. According to the predictions, even after a service life of 100 years, the tensile strength retention of the tested GFRP bar would still be 70% and 77% for mean annual temperatures of 50°C (the mean annual temperature and the marine environment of the Middle East and warm regions) and 10°C (mean average temperature of northern regions), respectively. That is higher than the design tensile strength according to the ACI 440.1R.

Recently, Benmokrane et al. 2017 and Ali et al. 2017 assessed the physical and mechanical properties of GFRP bars made with three types of reins such as vinyl-ester, isophthalic polyester, or epoxy resin. The alkaline exposure consisted in immersing the bars in an alkaline solution for 1000, 3000 and 5000 hr at elevated temperature (60°C [140°F]) to accelerate the effects. Subsequently, the bar properties were assessed and compared with the values obtained on unconditioned reference specimens. The test results reveal that the vinyl-ester and epoxy GFRP bars had the best physical and mechanical properties and lowest degradation rate after conditioning in alkaline solution, while the polyester GFRP bars evidenced the lowest physical and mechanical properties and exhibited significant degradation of physical and mechanical properties after conditioning.

2.5.3   Creep and relaxation

Polymer resins generally exhibit creep and relaxation behavior. Since glass and carbon fibers are linear elastic to failure, the addition of these fibers increases the creep resistance of the resins. Moreover, creep behavior of FRP composites strongly depends on the structure of material and load condition of the material. Consequently, creep and relaxation behaviors are more pronounced when load is applied transverse to fibers or when the composite has a low fiber volume fraction. For these reasons, for unidirectional FRP composites, the creep compliance is less affected by the creep behavior of the polymer matrix when the material is loaded along fiber direction. For off-axis loading, the creep behavior is strongly dependent on the creep of the matrix. FRP composites are reinforced with discontinuous randomly oriented or with continuous bi-directional woven fibers. The properties of the material is matrix dominated, therefore creep of polymer matrix is the main reason for creep behavior of FRP composites. Typically, thermosetting resins (unsaturated polyesters, vinylesters, epoxies, and phenolics) are more resistant to creep than are thermoplastics (polypropylene, nylon, polycarbonates, etc.). Under-cured resins are susceptible to creep during the early stages of service but this susceptibility diminishes with time. In addition, physical aging, temperature, moisture and stress level could affect creep behavior of FRP composites. Some data related to these influencing parameters could be found from recent review (Weitsman and Elahi 2000). The data on the effect of moisture absorption to creep behavior is rare. Fluids and time often can affect creep behavior of FRP composites in a manner similar to the effect of temperature and time. Fluid absorption in FRP composites will lead to developing residual stress and plasticizing of the resin, which can accelerate time-dependent behavior of FRP composites. (Liao et al.

1998) schematically described the effect of time, temperature, and fluids on creep behavior of FRP composites. The author concluded that creep compliance increased with the increase in fluid content and temperature over time.

In general, carbon fibers are the least susceptible to creep-rupture, Aramid fibers are moderately susceptible, and glass fibers are the most susceptible to creep-rupture. Creep-rupture tests have been conducted on GFRP, CFRP, and AFRP bars with 0.25 in (6.35 mm) diameter. The bars were tested at different load levels at room temperature. The results indicated that a linear relationship exists between creep-rupture strength and the logarithm of time for all load levels. Extrapolation of short term creep data to longer service lifetimes at room temperature air suggest rupture strengths of 29-55%, 47-66% and 79-93% of the initial strength for essentially unidirectional GFRP, AFRP and CFRP bars, respectively (Greenwood 2002). Benmokrane 2000 studied stress rupture mechanism of GFRP bars in various alkaline environments (NaOH, simulated pore water, moist concrete) under different stress levels of 22 to 68% of ultimate strength (Benmokrane and Mohamed 2013; Benmokrane 2000). The results obtained indicate that stress rupture mechanism of GFRP bars depends on the environment and stress level. Under a stress level of about 20-30% of the ultimate strength, in NaOH solution, the stress rupture mechanism mainly involves the damage of fibers. While in simulated pore water solution and concrete environment, the stress-rupture is caused by interface damage. At high stress levels, above 55%, matrix and fiber cracking are the most dominant mechanisms. Nkurunziza et al. 2005 conducted stress rupture tests on GFRP bars. Two test series; with 9.5 mm diameter, sand coated bars were investigated under two different stress corrosion environmental conditions. The first series consisted of 10 specimens immersed in de-ionized water (pH 7.0), stressed of 25 and 38% of ultimate, and subjected to ambient temperature. The other series consisted of 10 specimens immersed in alkaline solution (pH 12.8), subjected to the same temperature and stress level. After 417 days of exposure, the average residual tensile strength was found to be 139 and 144% of the design tensile strength for bars conditioned in de-ionized water at 25 and 38% stress level respectively. In alkaline solution, this range was 126 to 97%. These results showed that the testes GFRP bars performed very well under these extreme loading and environmental conditions. More important, no significant change in the elastic modulus was observed under the stress levels and environmental conditions used (Nkurunziza et al. 2005). Budelman et al. (1993) experimentally observed that creep rupture does not occur if sustained stress is lower than 60% of the short-term strength. Therefore, this phenomenon is relevant for prestressed element, while in the RC elements the low level of stress in FRP rebars at serviceability loads does not cause the possibility of creep rupture.

Experimental results on GFRP, AFRP, and CFRP bars, by Yamaguchi et al. (1997), proved a linear relationship between creep rupture strength and the logarithm of time, for period up to 100 hr. By extrapolating, the results to 500,000 hr (57 years) the ratios of creep strength rupture to the short-term strength of bars were linearly extrapolated to be 0.29, 0.47 and 0.93 for GFRP, AFRP, and CFRP, respectively. Ando (1997) did tests on commercial twisted CFRP bars and AFRP bars with an epoxy matrix at room temperature to determine the endurance time showed that the estimated

retained percentage of short-term strength after 50 years was 79% for CFRP and 66% for AFRP. Seki et al (1997) did tests on GFRP bars with vinylester matrix at room temperature evidenced a creep strength rupture equal to 55% of the short-term strength for an extrapolated endurance time of 50 year. CFRP shows excellent behaviour with regard to the strains due creep. It can be stated that creep strain of CFRP, at room temperature and humidity, remains under 0.01% after 3000 hr at a tensile stress of even 80% of the tensile strength (Machida et al. 1993; Saadatmanesh et al. 1999; Tokyo Rope 1993). AFRP and GFRP give much higher creep strain than CFRP: 0.15–1.0% for AFRP and 0.3–1.0% for GFRP at the same conditions above described (Gerritse 1998; Machida 1993; Piggott et al 1980).

Ando et al. (1997) experimentally studies performances of different FRP products considering various load durations. Test results indicate that at increasing the temperature, the relaxation rate becomes greater and this tendency is stronger for AFRP bars. Balazs et al. (2001) concluded that relaxation after 1000 hr can be estimated as 1.8–2.0% for GFRP tendons, 0.5–1.0% for CFRP tendons and 5.0–8.0% for AFRP tendons, while relaxation of GFRP, CFRP and AFRP tendons after 50 years of loading can be estimated as 4.0–14.0%, 2.0–10.0% and 11.0–25.0%, respectively, depending on the initial tensile stress. A summary of time-depending phenomena described in Table 2.2.

Nkurunziza et al. (2005) have been focused on the durability of E-glass/vinylester FRP bars in alkaline and de-ionized water under sustained tensile stress (or no stress) at ambient and elevated temperatures up to 60ºC [140ºF] for periods of up to 14 months evidenced that the creep strain in the 9.5 mm bars was less than 5% of the initial value after 10,000 hr of sustained tensile loading. This value was obtained under high tensile stress of 38% of the guaranteed tensile strength. Yousef et al. (2006) investigated the effect of different environmental conditions on the creep behavior of concrete beams reinforced with GFRP bars under sustained loads. This was achieved through testing concrete beams reinforced with GFRP bars and subjected to a stress level of about 20–25% of the ultimate stress of the GFRP bars. Reference beams were loaded in the temperature-controlled laboratory (24±3ºC). Other test beams were either completely or partially immersed in different environments (tap water and seawater) at elevated temperature (40±2ºC) to accelerate the reaction. During the exposure period, which lasted for ten months, strains in concrete and GFRP bars as well as the mid-span deflections were recorded for all considered environmental conditions. The results show that the creep effect due to sustained loads was significant for all environments considered in the study and the highest effect was on beams subjected to wet/dry cycles of sea-water at 40±2ºC (Beam T3), as shown in Figure 2.8. Robert et al. (2013) studied the creep-rupture on GFRP bars of size 8-mm subjected to different levels of sustained axial load using MTS 810 hydraulic machine, as shown in Figure 2.9. The tested specimens were loaded with different load levels start from 65 to 90% of the bars' tensile capacity until their rupture. The applied strain and time to rupture of each specimen were recorded in order to plot the required graph. Figure 2.10 presents the logarithmic time to failure (stress rupture) curve for GFRP bars. Logarithmic trend lines were drawn and extrapolated to the point of 1,000,000 hr (114 years). It was concluded that

the creep rupture stress of tested GFRP bars was around 48.8% of ultimate tensile stress. This value is well above the specified limit value of 35% of ultimate tensile strength for GFRP bars according to CAN/CSA-S807.

Table 2.2: Ranges of time-depending effects; Balazs et al. (2001)

Phenomenon	Aramid (%)	Carbon (%)	Glass (%)	Influencing parameters
Creep strain under sustained load (i.e. 80% tensile strength after 3000h)	0.15-1.0	<0.01	0.3-1.0	Temperature, humidity
Creep failure strength after about 50 years	47-66	79-93	29-55	Resin type, volume fraction and orientation of fibers and environmental conditions
Relaxation after 1000h	5.0-8.0	0.5-1.0	1.8-2.0	Temperature and initial tensile stress
Relaxation after 50 year	11-25	2.0-10	4.0-14	
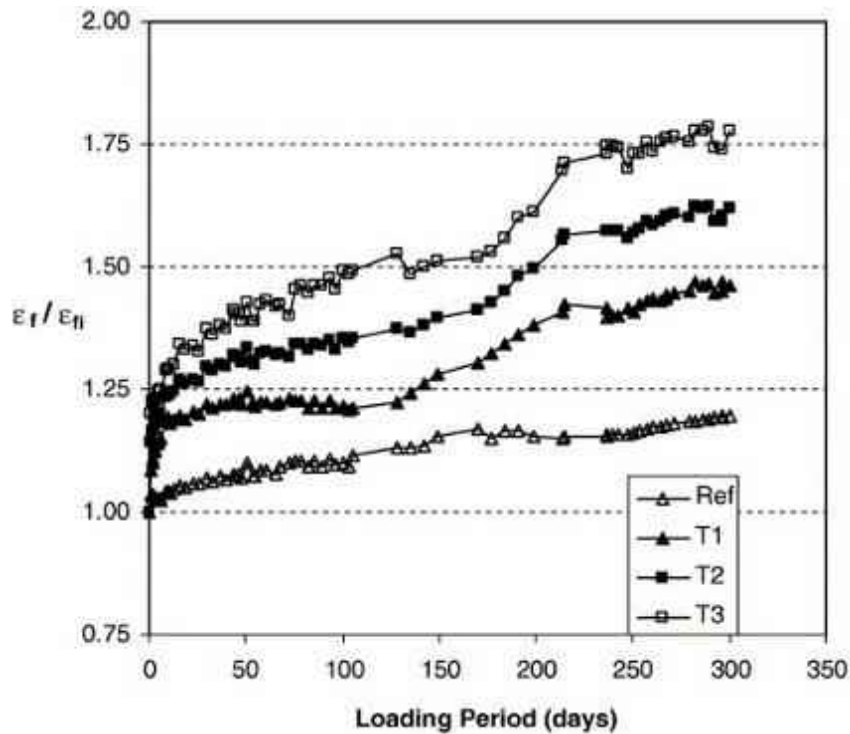
Figure 2.8: The normalized strain in GFRP bars versus time for tested beam (Yousef et al. 2006)

Figure 2.9: MTS 810 hydraulic machine for creep rupture test
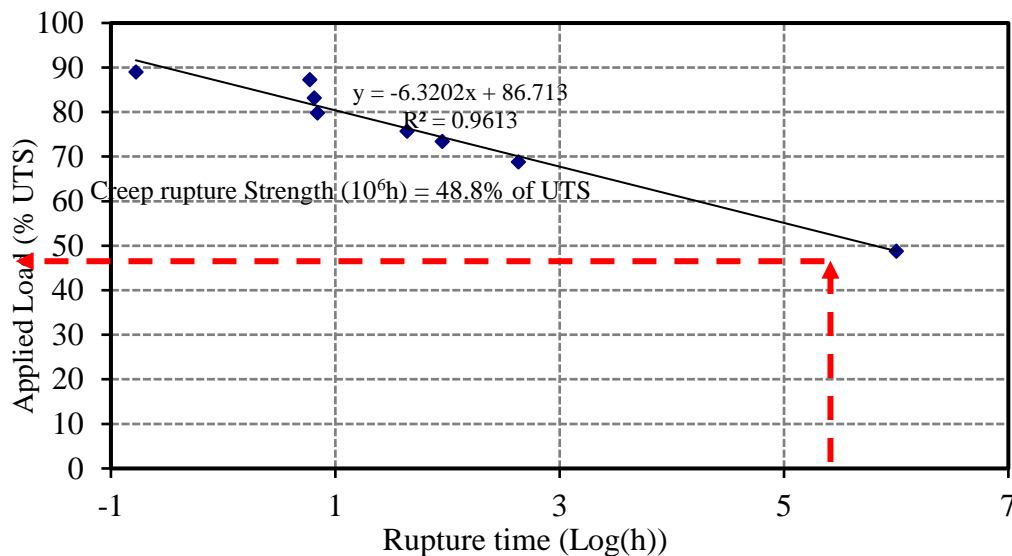
Figure 2.10: Logarithmic Time to Failure (Stress Rupture) Curve for GFRP bars bars (Robert et al. 2013).

Wang et al. (2014) studied the degradation of tensile properties of basalt FRP and the related hybrid FRP tendons under salt solution. Test specimens consisted of basalt FRP (BFRP), carbon FRP (CFRP), hybrid basalt and carbon FRP (B/CFRP), hybrid basalt and steel wire FRP (B/SFRP). The salt solution was prepared according to ASTM D1141-98. Two levels of prestressing toward typical prestressing applications were applied in the experiment. To apply prestressing loads on the specimens, a set of reaction equipment was designed and manufactured and a polyvinyl chloride (PVC) tee-shaped tube with an internal diameter of 16 mm was installed at the central part of the specimen, as shown in Figure 2.11.The variations of tensile strength, elastic modulus and the relevant coefficient of variation (CV) were investigated. The parameters in this study comprised the

stress levels and the aging days. The tensile strength, elastic modulus, the corresponding coefficient of variation and the hybrid effect were analyzed. Moreover, a prediction model with different levels of prestressing in a marine environment was proposed to predict the service-life of BFRP. The results show that 1) the degradation of tensile strength of BFRP tendons is proportional to the increase of stress level, whereas the corresponding modulus is relatively constant; 2) the BFRP tendons under the stress level of $0.6f_u$ after 63 days aging maintain the tensile strength of more than 90%, which shows a good resistance to salt corrosion; 3) hybrid B/CFRP tendons show even better resistance to salt corrosion in comparison to BFRP but the positive hybrid effect is only observed for the tendons under low stress level ($0.3f_u$); 4) the degradation of hybrid B/SFRP tendons is larger than that of the other FRP tendons, which is mainly caused by the corrosion of steel wires inside. The proposed model by the Napierian logarithm equation well represented the degradation trend of BFRP tendons under different levels of prestressing.
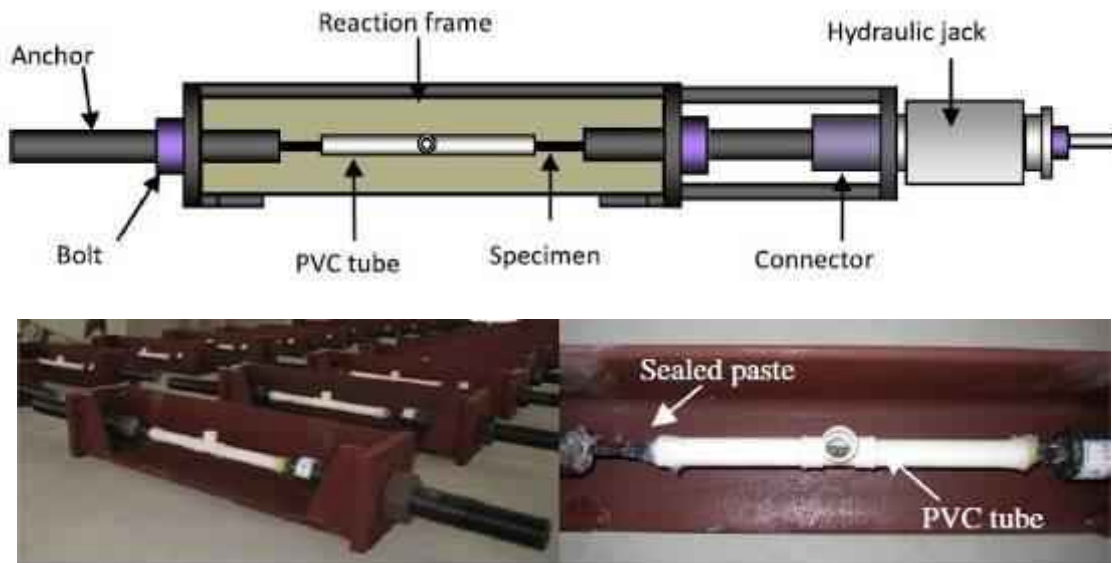
Figure 2.11: Prestressing equipment and salt solution container (Wang et al. 2014).

2.6 Durability of Carbon-Fiber Cables

2.6.1 Possible degradation mechanisms of CFRP tendons in moist and alkaline environments

The degree or rate of damage/deterioration of FRP reinforcement—and its reduced strength, stiffness, and durability—depends on many factors such as fiber type and volume, resin matrix, fiber–matrix interface, manufacturing process (curing rate, void content), and exposure environments (Benmokrane and Mohamed, 2013). Degradation processes in FRPs are typically denoted as fiber dominated, matrix dominated, and interface dominated, as shown in Figures 2.12(a), 1(b), and 1(c), respectively, (Benmokrane and Mohamed, 2013). The carbon-fiber composite cables (CFRPs) manufactured by Tokyo Rope Manufacturing Co. Ltd are made of polyacrylonitrile-based (PAN) carbon fibers impregnated in thermosetting epoxy resin. The following section

briefly reviews the possible mechanisms of degradation to carbon–fiber/epoxy composites (such as Tokyo Rope CFRP) caused by moisture and alkalis (conditioning environment considered in this study) (Benmokrane et al. 2016).

2.6.1.1 Aging in wet environment: (effect of moisture)

Effect on Epoxy Resin

Epoxy resins absorb a certain amount of water, depending on their type and epoxide number (Dell'Anno and Lees, 2011; Benzarti and Colin, 2013). When moisture penetrates epoxy resins, the following mechanisms may occur:

(a) Plasticization: Plasticization (or softening) is the result of the interaction of water molecules with weak bonding (polar, Van der Walls, dipole-dipole, H-bonds) between polymer chains. When the interaction between water molecules and some chemical groups in the epoxy resin is stronger than the interaction between these groups, the mobility of polymer chains increases and Tg decreases. This can reduce the epoxy resin's strength, modulus, strain at failure, and toughness, causing subsequent reductions ion-matrix-dominated (off-axis) properties such as bond, shear, and flexural strength, and stiffness. In some cases, this may also affect the longitudinal tensile strength and stiffness of the carbon-fiber / epoxy composites. Plasticization is, however, a reversible phenomenon: once dried, the material recovers its original properties. Some epoxies that absorb large amounts of water may be highly affected by plasticization; drops in Tg of up to 50°C and even 80°C have already been recorded (McKague et al. 1978; Browning 1978).

(b) Chemical degradation (hydrolysis): Epoxy resins can be hydrolyzed by water (Xiao and Shanahan, 1997; DéNève and Shanahan, 1995) and alkalis even exacerbate the degradation. Yet epoxy resins are not significantly degraded by water at low temperatures (Benzarti and Colin, 2013).

Effect on Carbon Fiber

Carbon fiber is inert and insensitive to moisture (Banthia et al., 2006).

Effect on the Carbon-Fiber–Epoxy Interface

The interface is considered as the "weak point" of any FRP composite materials, since it bonds materials with very different natures. To maintain performance and durability, the interfacial adhesion between the fibers and resin must remain strong enough to properly transfer the stress and load through the material's two phases and maintain its cohesion. Two different mechanisms can affect the carbon–fiber / epoxy–resin interface:

(a) Physical degradation: Water molecules diffusing along carbon-fiber / epoxy composites may concentrate in less dense areas, such as pores, microcracks, or free gaps located between the carbon fibers and the epoxy resin. In this case, the interfacial adhesion between the two phases may be weakened, especially at elevated temperature, which increases the effect of differential expansion/swelling and interfacial debonding.

(b) Chemical degradation: The epoxy resin and carbon fibers are bonded together with specific coupling agents (e.g., silanes) previously applied to the fiber surface, which create strong chemical (covalent) bonds between polymeric chains and the fiber surface. Moisture can diffuse along the carbon–fiber surface and could react, via hydrolysis or condensation, with the chemical bond created by the reaction between the coupling agent and epoxy resin. In this case, the interface's cohesive properties are affected and the mechanical performance reduced (Benmokrane et al. 2016).
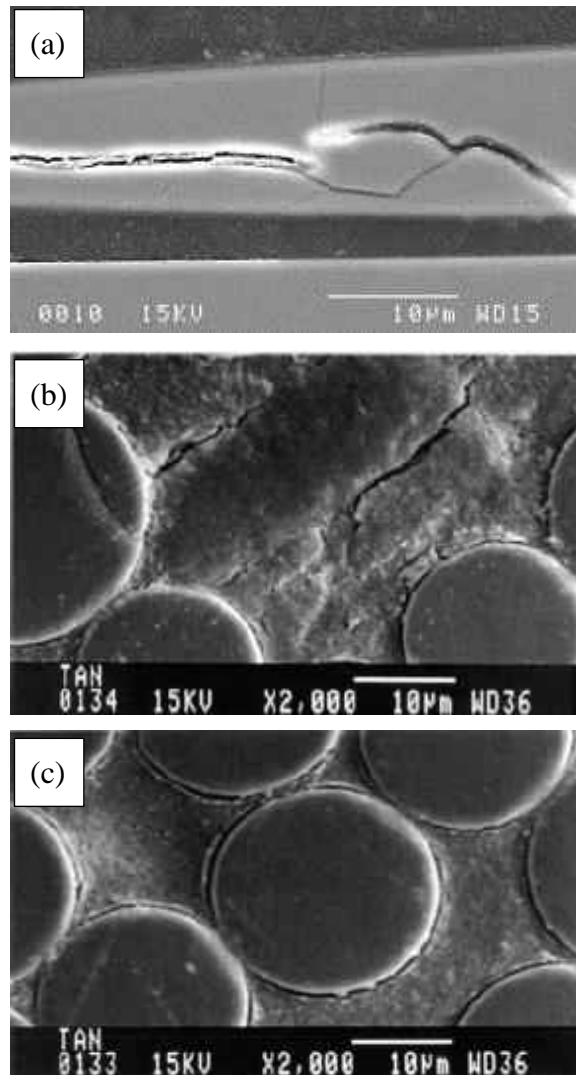
Figure 2.12: Degradation processes in FRP's: (a) Fiber dominated (e.g.,microcracks in the fiber); (b)matrix dominated (e.g.,microcracks in the matrix); (c) interface dominated (e.g., debonding at the interface fiber/matrix)

(c) Other effects: Epoxy will permit small quantities of water to pass through it in vapor or liquid form. On its passage, this water may react with sensitive components in the resin (additives, filler, etc.) to form tiny cells of concentrated solution. Under the osmotic pressure generated, more water

is then drawn in in an attempt to dilute this solution. This water increases the fluid pressure in the cell and, eventually, the pressure modifies the resin's microstructure and can sometimes affect the properties of the carbon-fiber / epoxy composites (Perez-Pachero et al. 2013). The onset of osmosis can be delayed by using a resin with a low water-transmission rate.

2.6.1.2   Aging in alkaline environment:

The alkaline solution used in this study contained concentrations of calcium, sodium, and potassium hydroxides (such as present in concrete environments). These hydroxides, borne by water diffusing through the carbon-fiber / epoxy composites, may come into contact with and affect the various components.

Effect on Epoxy Matrix

Chemical degradation occurs when strong bonds (covalent) of polymer chains are ruptured by contaminants. Particularly, the ester groups in a polymer material can be strongly affected by hydrolysis in alkaline environment. Epoxy resin that has not been cured with anhydrides contains no ester groups and is therefore highly resistant to alkali attack. That notwithstanding, not all types of epoxy resin offer the same chemical performance. Epoxy resins that absorb large amounts of water are more sensitive to chemical degradation in spite of their inherent resistance. The properties of epoxy polymers can be varied so as to produce epoxy polymers resistant to most chemicals. In general, epoxy resins are highly resistant to alkalis.

Effect on Carbon Fiber

Carbon fibers are not supposed to be affected by alkaline solution at any concentration or by temperatures up to boiling of water (Judd 1971; Santoh 1993; Santoh et al. 1993).

Effect on the Carbon-Fiber–Epoxy Interface

Physical and chemical degradation occurring at the carbon–fiber–epoxy interface in the presence of water may be considerably enhanced at higher pH levels. More specifically, chemical bonds formed by coupling agents (e.g., silanes) may be destroyed when in contact with high concentrations of hydroxyls (Liao 1989). Silane coupling agents have been commonly used with glass fibers (Suzuki et al. 1992), whereas methods such as surface oxidation, electrochemical deposition, plasma etching, plasma polymerization, cryogenic treatments, and polymer coatings have been employed to modify carbon fibers (Kang et al. 2001). The manufacturer has not disclosed the coupling agent used in Tokyo Rope CFRP tendons. Lastly, the resistance of carbon–fiber / epoxy composites to water and alkaline solutions is also affected by other parameters such as sustained load, creep, and fatigue, which might create cracks in the epoxy matrix. Elevated temperatures will accelerate chemical degradation (Benmokrane et al. 2016).

2.6.2 Durability performance of Tokyo Rope CFRP tendons exposed to elevated temperature and alkaline environment

The physical, mechanical, and durability characterization of Tokyo Rope CFRPs have been investigated by Benmokrane et al. 2016. A total of 53 unstressed Tokyo Rope CFRP tendon specimens (7.5 mm in diameter and 1600 mm in length) were tested under tension according to ASTM D7205. Figure 2.13 shows the cross-section of 7.5 mm CFRP tendon specimens and CFRP cable as received. The conditioned CFRP specimens were exposed to alkaline solution (12.8 pH) for 1,000, 3,000, 5,000, and 7,000 hr and subjected to different elevated exposure temperatures at 22°C, 40°C, 50°C, and 60°C (Figure 2.14) to simulate the alkaline effect of concrete. The pre- and post–exposure tensile strengths of the tendons were deemed indicative of specimen durability and were used for long–term property predictions based on the Arrhenius theory. In addition, differential scanning calorimetry (DSC) and scanning electron microscopy (SEM) were used to characterize the physical properties of the CFRP specimens (as received and conditioned). Chemical degradation of the reference and conditioned specimens was also assessed with Fourier transform infrared spectroscopy (FTIR). The test result indicated that the carbon-fiber content was 82% by weight and the water uptake at saturation was equal to 1.1%. The cure ratio of the material was very high (close to 100%). The polymer matrix was not affected by alkaline solution at high temperatures: no changes in the glass transition temperature occurred, as observed by differential scanning calorimetry (Benmokrane et al. 2016).

Optical microscopy and scanning electronic microscopy analysis of as-received CFRP samples showed that the strands presented various levels of defects as porosities, air bubbles, and poor fiber wetting due to an inadequate consolidation during the manufacturing processes, as shown Figure 2.15 (a) and (b). It was recommended that the manufacturer reduce these defects, which make the material more sensitive to moisture and corrosive-fluid ingress (as alkaline solution). The moisture and corrosive-fluid ingress could be aggravated in presence of elevated temperature and also when tensile stress is applied to the material.

The test result of FTIR analysis also confirms that the epoxy resin of the CFRP specimens did not degrade chemically during the immersion in the alkaline solution at 60°C for 7,000 hr. Microcracks did develop in the epoxy resin.

Figure 2.13: (a) Overview of cross-section of 7.5 mm CFRP tendon specimens; (b) CFRP cable as received (Benmokrane et al. 2016)

(a) Environmental chambers

(b) PVC tubes included CFRP specimens and filled with alkaline solution inside the chamber

Figure 2.14: CFRP Environmental conditioning
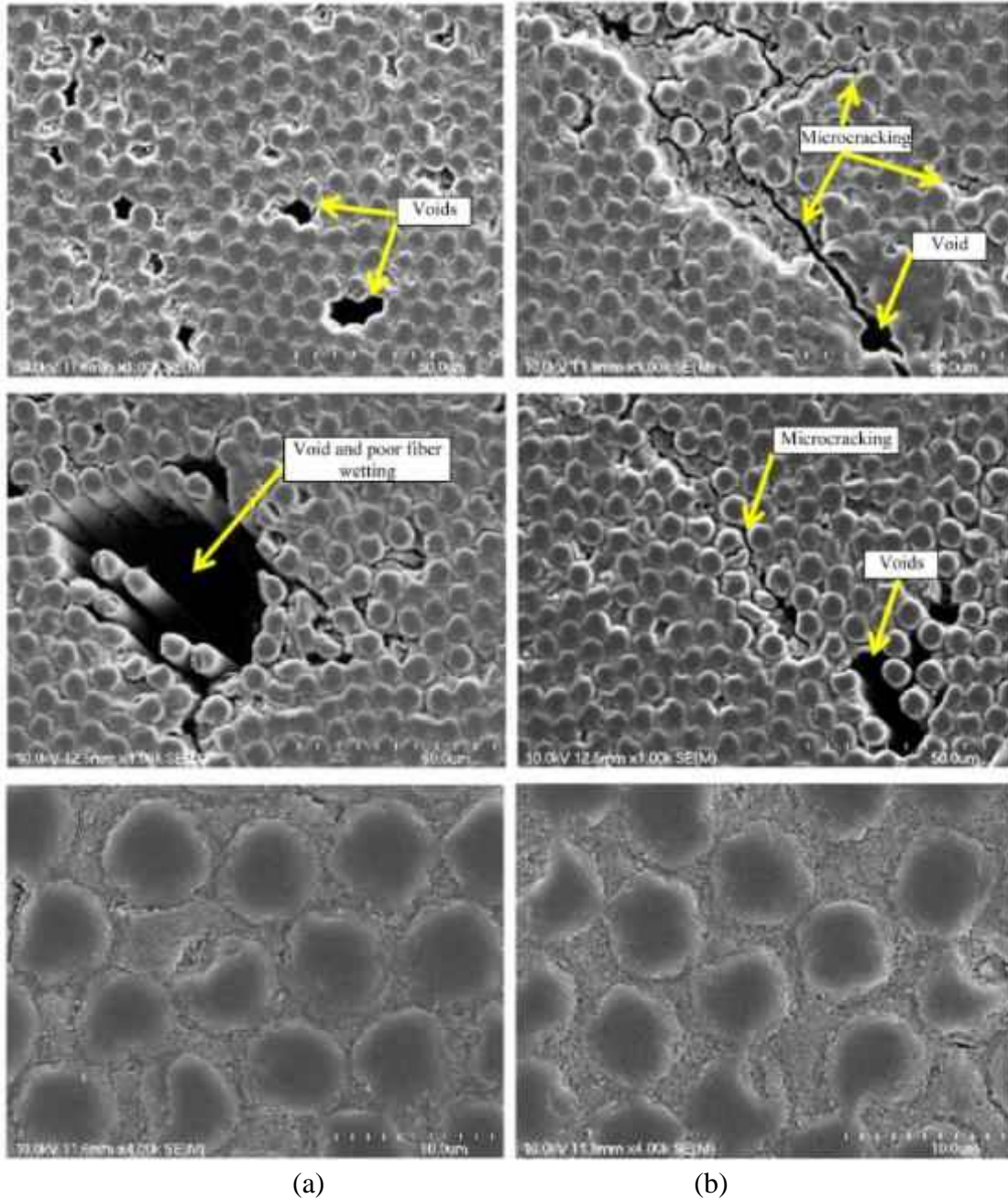
Figure 2.15: Micrographs of the fiber/matrix interface of CFRP tendon before and after conditioning: (a) before conditioning; (b) after conditioning for 7,000 hr at 60°C (Benmokrane et al. 2016)

In addition, the results indicate that specimen strength was affected by increased immersion time at higher temperatures. The test results after 7,000 hr of immersion in the alkaline solution at 60°C [140°F] reveal a 7.17 % reduction in tensile strength. The tensile-strength reduction was attributed to the development of microcracks in the epoxy resin, resulting essentially from the existing defects in the material (as seen in SEM micrographs). Diffusion of water along these microcracks

and the fibers might also have weakened the interfacial adhesion between the carbon fibers and epoxy resin, which reduces the stress transfer between carbon fibers and, consequently, the composite's tensile strength (Benmokrane et al. 2016).

2.6.3 Durability performance of CFRP tendons under sustained loading and environmental conditioning

Regarding the durability of CFRP tendons, the CFRP tendons are exposed to alkali in concrete under tensile loading condition in prestressed concrete applications. Saadatmanesh and Tannous (1999) conducted relaxation, creep, and tension-tension fatigue tests on two CFRP tendons namely, Leadline PC-D8-(8 mm) and 1x7-(7.5 mm) carbon fiber composite cable (CFRP) (Figure 2.16). Twelve Leadline and 12 CFRP tendon specimens were tested in air at temperatures of –30, 25, and 60ºC [140ºF] to determine their relaxation behavior. In addition, the relaxation behavior of 24 Leadline and 24 CFRP samples was examined in chemical solutions simulating aggressive field conditions. The loss of tensile force, for the 3000 hr test duration at stress ratios of 0.4 and 0.6, was generally less than 10 % and it depended primarily on the initial stress level and the type and temperature of the environment. Moreover, preliminary investigation on the creep behavior of Leadline and CFRP in air and in chemical solutions was also conducted. Six samples of Leadline and CFRP were subjected to sustained load at room temperature in air, alkaline, and acidic solutions, for a period of 3,000 hr. Creep behavior of both tendons was good; however, the creep strains were higher in solutions than in air. Furthermore, 190 samples of Leadline and CFRP were tested in tension-tension fatigue to examine the effect of repeated loading on the modulus of elasticity, Poisson's ratio, and the tensile strength of these types of tendons. Fatigue strength was generally good and depended on the stress range and initial stress level.

In 2015, Sasaki and Nishizaki have carried out outdoor exposure tests for 17 years to verify the long-term durability. FRP cables, carbon, aramid, glass, and vinylon fibers were exposed in various conditions, such as initial prestressing tensile load, with/without direct sunlight radiation (Figure 2.17). After 3.5, 15, 17 years exposure, the specimens were retrieved and investigated with residual prestressing tensile load, strength, and material degradation. The results suggested that practical durability of carbon and aramid FRP cables seems to be still good, but initial loading level should be carefully considered for glass and vinylon FRP cables. The cables were also evaluated with chemical analysis such as SEM and FTIR microscopy. Loss of surface resin was observed for all the tested FRP cables; however, the deterioration between fiber and matrix resin was not found. Observation with FT-IR microscopy detected the deterioration in the surface of AFRP cables.
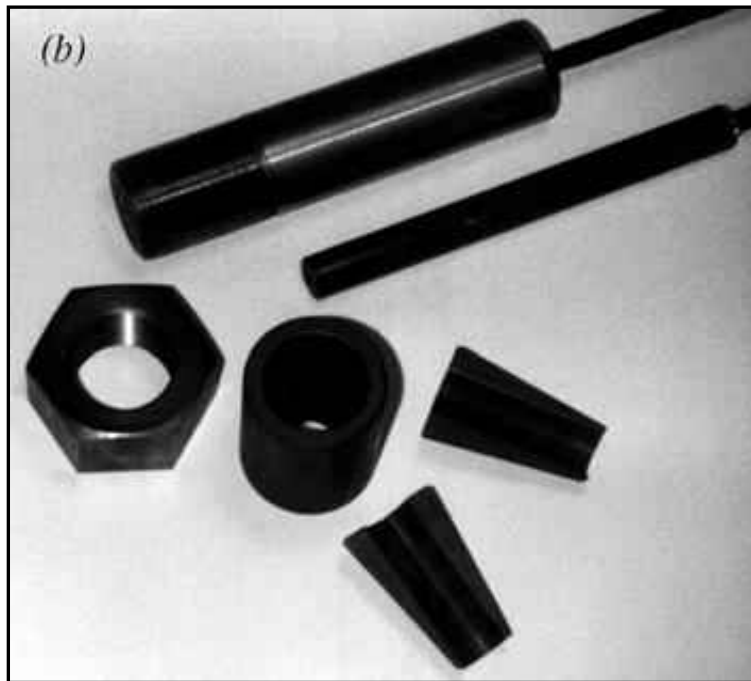
Figure 2.16: (a) Leadline PC-D8 tendon; (b) 1 x 7 CFRP and their respective grips (Saadat-manesh and Tannous 1999).

Figure 2.17: FRP cables (Sasaki and Nishizaki 2015)

Figure 2.18: FRP cables pre-stressed in SUS flames (Sasaki and Nishizaki 2015)

Abdelrahman et al. (1996) tested four prestressed concrete T–beams pretensioned with two types of CFRP tendons such as Leadline and CFRP. The beams were 1: 3.3 scale models of girders of the first Canadian smart highway bridge built in Calgary, Alberta. The main objective was to study the limit state behavior, ultimate capacities and failure modes of the beams. Two beams were monotonically loaded to failure at the start, while the other two were subjected to 2 million cycles of loading before being monotonically loaded to failure. All beams failed by rupture of cables at a higher load than expected, due to underestimation of the ultimate strength of cables. Load-deflection behavior was bilinear and elastic up to failure. The beams showed large cracks over an extensive region and large deflections before failure, which were good warning signs of impending failure. The beams exposed to cyclic loading survived 2 million cycles between cracking and 70% of cracking load with no significant effect on beam stiffness. The ultimate capacity of beams subjected to cyclic loading and the strains in CFRP tendons were very similar to the beams that did not undergo cyclic loading. Overall, the fatigue strength of beams pretensioned by FRP tendons was judged as excellent.

Braimah et al. (2003) and Braimah (2000) investigated the long-term behavior of CFRP pretensioned concrete beams under sustained load at room temperature. A total of 4 CFRP beams comprised three prestressed beams with Leadline CFRP tendons and one with seven-wire steel strands were constructed and tested. The beams were subjected to a sustained load of 29% of their flexural capacity for 651 days. An analytical model was developed to predict the time-dependent behavior of the beams. Test results indicated that the CFRP-prestressed beams had comparable or superior

performance in comparison to the steel-prestressed beam. Also, the ratio of long-term to instanta-neous deflection increased with prestressing force. Prestressing strain was found to decrease with time in cracked sections and remain unchanged in uncracked sections. ACI recommendations and the CEB Model Code over-estimated the measured deflections by an average of 28% and 42%, respectively.

Zou (2003) tested three series of pretensioned concrete beams, using Leadline CFRP tendons or steel strands as prestressing reinforcement. The beams were subjected to sustained loading below and above cracking load. Prestress level, sustained load and concrete strength were varied between pairs. The study concluded that beams prestressed with CFRP met serviceability criteria for deflection and cracking. It was shown that this performance improved with increasing concrete strength. Also, CFRP-prestressed and steel-prestressed beams were similar in long-term deflections in both uncracked and cracked states. Cracks were slightly wider for beams with CFRP compared to those with steel prestressing.

Mertol et al. (2007) investigated the durability of concrete beams prestressed with CFRP tendons compared to those prestressed with steel wires. Fifteen beams were exposed to different mechanical and environmental conditions. The parameters included in the program were the level of sustained stress in the bars and wires (55 and 70 percent of the ultimate bar or wire strength), the environmental exposure condition (air exposure and continuous exposure to 15 percent by mass salt water spray at 54°C temperature), the length of time under sustained load (9 and 18 months) and the method of testing (with or without application of cyclical loading prior to static testing to failure). The experimental program illustrates that CFRP prestressed concrete beams exhibit comparable ultimate strength and fatigue strength properties in comparison to equivalent steel prestressed concrete beams. Furthermore, test results show that the beams prestressed with steel wires did not survive the environmental exposure over 12 months whereas the beams prestressed with CFRP bars survived up to the end of the 18-month long extreme environmental exposure, indicating the excellent durability of CFRP in the marine environment. Provided that provision is made for the lack of CFRP ductility in comparison to steel, the research undertaken has indicated that CFRP prestressed concrete is a durable and appropriate option when designing structures for use in offshore environments. Figure 2.20 shows a schematic view of test setup for the beams under sustained loading. The test setup and beams were kept in an environmental chamber for conditioning as shown in Figure 2.21.

Grace et al. 2003 investigated the flexural behavior of full-scale double-tee (DT) beams, pre-stressed using bonded pretensioned CFRP LeadlineTM tendons and unbonded carbon fiber composite cable (CFRP) post-tensioning strands (Figure 2.23). The beams were designed to simulate the performance of the DT beams used for the construction of the three-span Bridge Street Bridge, the first vehicular concrete bridge ever built in the United States that used CFRP material as the principal structural reinforcement. Testing focused on measurement of strain distributions along the length and depth of the beam, transfer length, camber/deflection, cracking load, forces in post–

tensioning strands, ultimate load-carrying capacity, and mode of failure. In addition, an analysis approach is presented to theoretically evaluate the response of the tested beam. It was observed that the ultimate failure of the beam was initiated by partial separation between the topping and the beam flange, which led to the crushing of the concrete topping followed by rupture of bottom tendons, as shown in Figure 2.24.
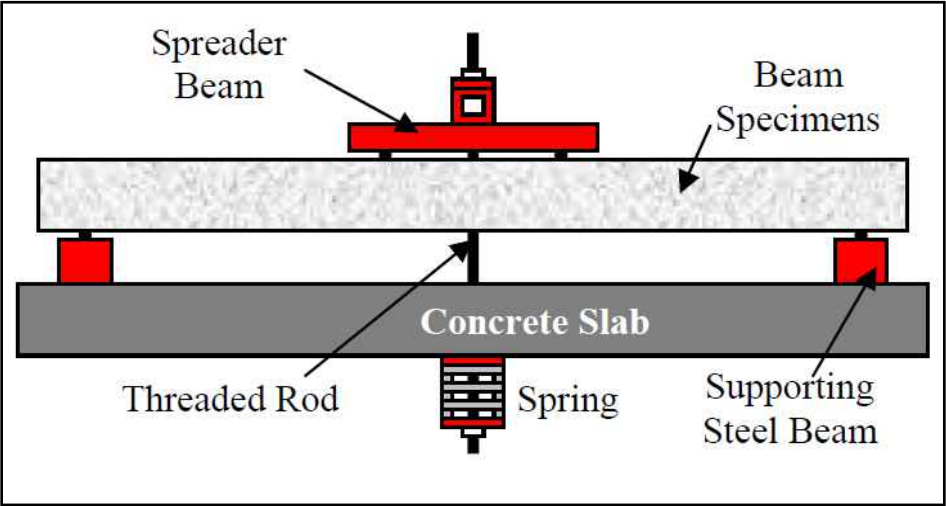
Figure 2.19: Test set-up for sustained loading (environmental exposure) (Mertol et al. 2007)

Figure 2.20: Test set-up for sustained loading (environmental exposure) (Mertol et al. 2007).

The tested beam was found to have significant reserve strength beyond the service load. Theoretical calculations were similar in value to the corresponding experimental results — especially under the service load condition.

Figure 2.21: Instrumentation and CFRP reinforcing cage of one web (Grace et al. 2003).

Figure 2.22: Test setup for flexural loading of DT girder (Grace et al. 2003).

Figure 2.23: Failure of DT girder due to separation of concrete topping and crushing of concrete (Grace et al. 2003).

2.7 CFRP Field Applications

2.7.1 Shinmiya bridge

Shinmiya Bridge is the first instance where CFRP was used as tendons, and also the first instance in the world of CFRP being used as tendons in a prestressed concrete bridge (Hosotani et al.1993). In this bridge, CFRP, being high-strength, corrosion-resistant and capable of being handled similarly to conventional prestressing steel, was adopted as a means of combating salt damage in concrete structure. In addition, out of 24 main girders of the bridge, two test girders were erected on either side of the bridge for long-term observation. Loading tests were conducted on the test girders six years after construction, and durability of the bridge was confirmed. This bridge is a pre-tensioned prestressed concrete slab bridge system. Comparison of the former and new Shinmiya Bridge has been passed 20 years after the beginning of using of each bridge, respectively is shown in Figure 2.24. No change had been observed in the property of the prestressed concrete bridge after 20 years.

In 2011, MDOT built the Pembroke bridge to replace a deteriorated steel bridge over Southfield Highway M 39 in Detroit. The two-span bridge is 32.51 m (106.7 ft) long. Each span comprises 16 box beams with 150 mm (6.0 in.) composite deck. Each beam is 686 mm (27.0 in.) deep and

1220 mm (48.0 in.) wide and is prestressed with low-relaxation steel strands. Each span has six transverse diaphragms. One 37-wire 40 mm (1.6 in.) diameter CFRP was used for transverse post-tensioning to integrate the adjacent box beams.

In addition, the MDOT replaced an existing earth-filled arch culvert on M 102 (8 Mile Road) with a CFRP prestressed spread box-beam structure (2013 and 2014). M 102 is a major urban route in the Detroit metropolitan area with four lanes of traffic in each direction. CFRP was thooughly applied for the new precast concrete bridge as noncorrosive tendons, stirrups, and reinforcing bars. Each bridge was constructed with a skew angle of 45 degrees, a span of 20.7 m (67.9 ft), and a deck width of 18.8 m (61.7 ft). Each bridge superstructure comprises eight spread box beams supporting a 230 mm (9.1 in.) thick reinforced concrete deck slab. Each box beam has a width of 1220 mm (48.0 in.) and a depth of 840 mm (33 in.) and is prestressed by a total of 37 CFRP 15.2 mm (0.6 in.) diameter prestressing strands with an initial prestressing force of 146 kN (32.8 kip) per strand. The constructed beams were shipped to the site, and after the beams were placed the crew fabricated the formwork for the deck slab, which was also reinforced with two lattices of CFRP reinforcement. Two side-by-side box-beam bridges were constructed to carry the east- and west-bound Interstate 94 over Lapeer Road in Port Huron, Mich. The eastbound and westbound bridges were completed in 2014 and 2015, respectively. Each bridge consists of three spans with total length of 50 m (164 ft). The eastbound bridge, with a width of 17.6 m (57.7 ft), is composed of 14 beams and is posttensioned using 20 CFRPs with a 40 mm (1.6 in.) diameter and a transverse posttensioning force of 623 kN (140 kip) per diaphragm. The westbound bridge, with a width of 18.8 m (61.7 ft), comprises 15 beams and is posttensioned using 20 CFRPs with a 40 mm diameter and transverse posttensioning force of 667 kN (150 kip) per diaphragm. The box beams in both bridges have a depth of 840 mm (33 in.) and a width of 1220 mm (48.0 in.).

After the successful deployment of CFRP in Little Pond Bridge, where CFRP was used as transverse posttensioning cables, Maine Department of Transportation (MaineDOT) built its first precast, prestressed CFRP bridge in 2014. This 19.2 m (63.0 ft) simply supported bridge comprises eight precast concrete double-tee beams, called northeast extreme tee (NEXT) beams. Each beam has a deck width of 2655 mm (104.5 in.), depth of 915 mm (36.0 in.), and span of 18.9 m (62.0 ft). Each beam was prestressed with 40 CFRPs with a diameter of 15.2 mm (0.6 in.). The initial jacking force was 176 kN (39.5 kip) per strand. VDOT built its first bridge with CFRP reinforcement in 2014. This is a two-span bridge with a total deck width of 9.85 mm (32.3 ft). Each span has a length of 25.46 m (83.53 ft). The span comprises four 1143 mm (3.75 ft) deep bulb-tee girders. Each bulb-tee girder was prestressed with forty-four 15.2 mm (0.6 in.) diameter CFRPs. Each strand was prestressed with an initial prestressing force of 147 kN (33 kip). The stirrups were also made of CFRP and had 15.2 mm (0.6 in.) and 17.2 mm (0.68 in.) diameter.

Former Bridge

New Shinmiya Bridge
Figure 2.24: Shinmiya Bridge

2.7.2   Haranomachi thermal power plant outfall bridge

Two-span post-tensioned/pre-tensioned concrete simple girder bridge links breakwater to marine facility. These post-tensioned girders were constructed by 3-part precast block method reinforced with CFRP tendons. The outline of this bridge is shown in Figure 2.25.

Figure 2.25: Haranomachi thermal power plant outfall Bridge

2.7.3 Cantilever erection using cable systems (Hisho Bridge: Tsukude C.C.)

The Hisho Bridge was the first application of CFRP in a cantilevered construction. CFRPs were used for all 108 internal (cantilever) and external (span) cables in this post-tensioned structure (Hosotani et al.1993). Post-tensioning and anchoring methods for 6 strands CFRP multi-cables were developed and applied separately for internal and external cables. Grouting was used for the internal cables, while unbonded CFRP were used for the external cables. Long-term load monitoring for the bridge is in progress. The side view and cross section of this bridge is shown in Figure 2.26.
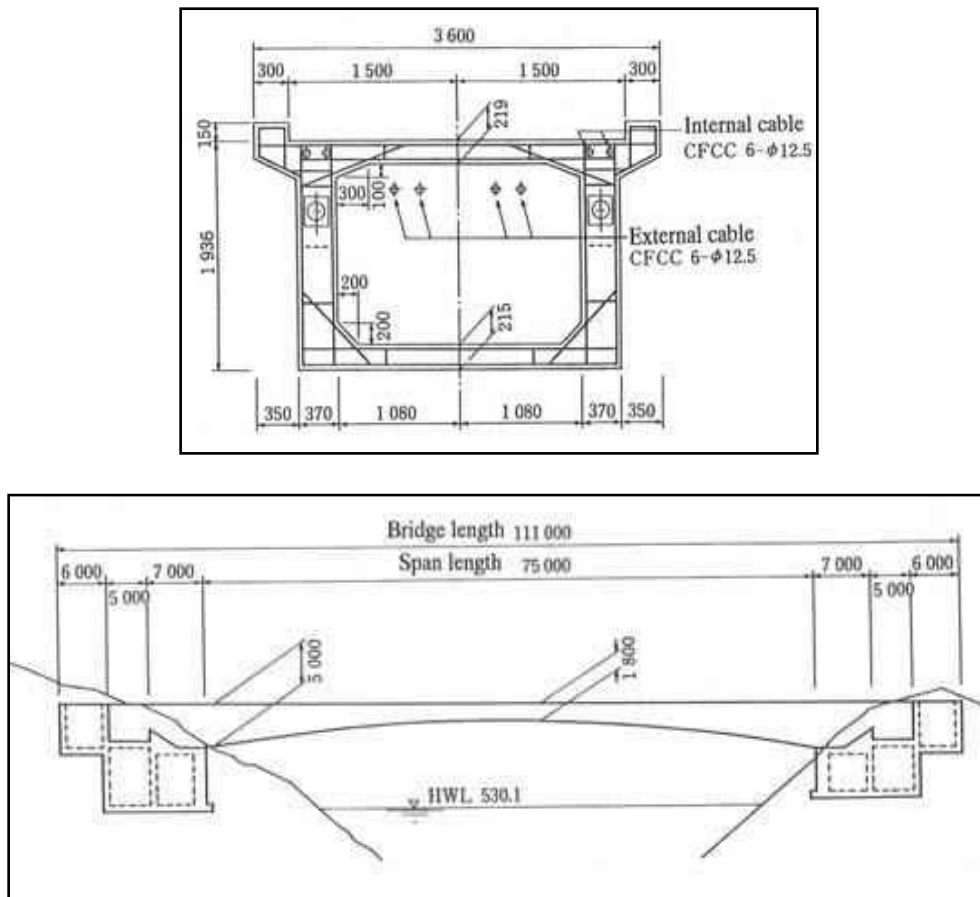
Figure 2.26: Hisho bridge (Hosotani et al.1993).

2.7.4 Cable stayed PC bridge (Herning Footbridge)

In Denmark, a large amount of money is being spent to prevent steel reinforcement corrosion caused by agents that are spread on the road to melt down the snow in winter. Designers wanted to reduce the life cycle cost of prestressed concrete bridge beams by using the CFRP stay cables in large-sized bridge beams. CFRP materials were used for all the stay cables, tendons and also as reinforcement in PC cable stayed bridge. Cross section of this bridge is shown in Figure 2.27 (Enomoto and Ushijima 2012).
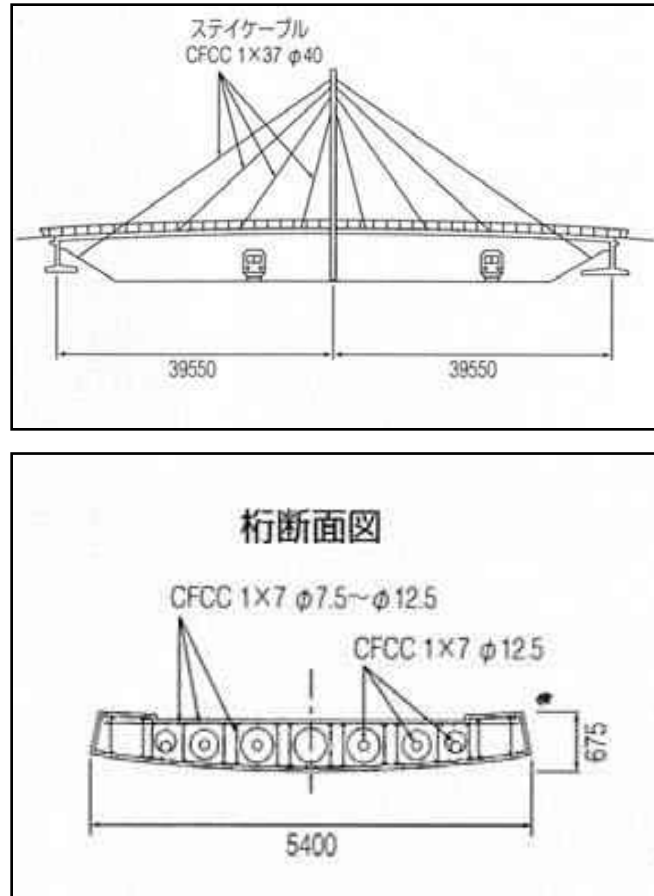
Figure 2.27: Herning footbridge

2.7.5 Beddington Trail Bridge

In 1993, the Beddington Trail Bridge was built in Calgary, Alberta, Canada (Figure 2.28). It consists of two continuous spans. Each span consists of 13 precast, pretensioned concrete girders. Four girders were prestressed using CFRP cables, while two other girders were prestressed using two Leadline tendons. The girders were instrumented with fiber optic sensors and are being monitored by ISIS Canada (2009).

2.7.6 Bridge street bridge deployment project Southfield, Michigan

The Bridge Street Bridge Deployment Project consisted of the replacement of a failing bridge over the Rouge River in the City of Southfield, Michigan, with two parallel concrete bridges (Figure 2.29). Each bridge contains 3 spans over a 62 m length and carries traffic in a boulevard configuration. While the first bridge constructed, Structure A, used standard AASHTO precast concrete girders and steel reinforcement, the second bridge, Structure B, was constructed of precast concrete double tee (DT) beams that were reinforced, pre-stressed and post-tensioned with rods, tendons, and strands produced from carbon fiber reinforced polymer (CFRP) (Grace et al. 2001).

Figure 2.28: Beddington Trail Bridge, Calgary, Canada (ISIS Canada, 2009)

2.7.7   Taylor bridge in headingly, Manitoba, Canada

Taylor Bridge is located on Provincial Road No. 334 over the Assiniboine River in the Parish of Headingley, Manitoba, and was opened to traffic in October 1997. The 165m-long bridge consists of 40 prestressed concrete AASTO type girders, as shown in Figure 2.30. Four girders of the Taylor Bridge were prestressed by two different types of carbon fibre reinforced polymer (CFRP) material using straight and draped tendons. The girders were also reinforced by CFRP stirrups protruded from the AASHTO type girders to act in composite action with the bridge deck. A portion of the deck slab is reinforced by CFRP reinforcement. Glass fiber reinforced polymer (GFRP) was also used to reinforce the barrier wall. The barrier wall was connected to the deck slab with double-headed stainless steel bars. To obtain continuous information on the behavior of the bridge and the performance of FRP as reinforcement and prestessing tendons, the bridge was monitored to provide data to evaluate the long-term behavior and durability of the FRP materials used (Shehata et al. 1999).

a) Leadline tendons and CFRP *strands in reinforcement cage of double-T girders*

b) Installed double-T girders with external CFRP *post-tensioning strands in place*

Figure 2.29: Bridge Street Bridge, Southfield, Michigan, USA (Grace et al. 2002)

Figure 2.30: Taylor Bridge, Manitoba, Canada (ISIS Canada, 2009)

2.8 GFRP Field Applications

2.8.1 Highway bridge structures

The corrosion of steel reinforcing bars in concrete bridge decks leads to excessive cracking, spalling, reduced strength, and loss of structural integrity. That represents a major problem in terms of rehabilitation costs and traffic disruption. Concrete bridge decks deteriorate faster than any other bridge components because of direct exposure to the environment, de-icing chemicals and ever-increasing traffic load. In North America, around half of the maintenance budget of the Ministry of Transportation (MT) is spent on concrete structures damaged by corrosion of steel. Therefore, since the late 1990s, the Structures Division of the MT at different provinces has been interested in building more durable bridges with an extended service life of 75 to 150 years. For example, the MT at Québec (MTQ), Canada has carried out, in collaboration with the University of Sherbrooke (Sherbrooke, Québec), several research projects utilizing the straight and bent non-corrodible FRP bar in concrete deck slabs and bridge barriers (El-Salakawy et al. 2003; Mohamed and Benmokrane 2012). The use of FRP bars as reinforcement for concrete bridge provides a potential for increased service life and economic and environmental benefits.

In the last ten years, the FRP bars have been used in hundreds of bridge structures across Canada and USA. These bridges were designed using the Canadian Highway Bridge Design Code or the AASHTO LRFD Bridge Design Guide Specifications for GFRP-Reinforced Concrete Bridge Decks and Traffic Railings. Straight and bent FRP bars (carbon or glass) were used mainly as internal reinforcement for the deck slab and/or for the concrete barriers and girders of these bridges. In general, all the bridges that included with FRP reinforcements though the ten years ago are girder-type with main girders made of either steel or prestressed concrete. The main girders are simply supported over spans ranging from 20.0 to 90.0 m. The deck is a 200 to 260 mm thickness concrete slab continuous over spans of 2.30 to 4.0 m. Most of these bridges have been reinforced with the glass FRP bars as a result of their relatively low cost compared to other types of FRPs (carbon and Aramid). The FRP bars were used mainly as reinforcement to the deck slabs, barriers, and girders. Figure 2.30 shows some field application of FRP in highway bridge decks.

2.8.2 Water tanks

Reinforced concrete (RC) tanks have been used for water and wastewater storage and treatment for decades. Design of these tanks requires attention to not only strength requirements, but also crack control and durability. RC water treatment plant structures are subject to severely corrosive environments as a result of using the chlorine to treat the wastewater before it is released. Therefore, the challenge for the structural engineer and municipalities is to design these structures using noncorrosive fiber-reinforced polymers (FRP) reinforcing bars. The first worldwide concrete chlorination water treatment tank totally reinforced with FRP bars was designed in 2010 and the con-

struction started and finished in 2012. The project is located in Thetford Mines city, Quebec, Canada, and it is considered as one component of the water treatment plant for the municipality. The volume capacity of the tank is 4500 m^3, and it has the dimensions 30.0 m wide, 30.0 m long and 5.0 m high. The structural system of the tank is a rectangular underground tank resting on a raft foundation that supports the vertical walls and top slab. The design of the tank was made according to CAN/CSA-S806-12, Design and Construction of Building Components with Fiber-Reinforced-Polymers. This included the use of High Modulus GFRP reinforcing bars (Grade III, CSA S807-10) as main reinforcement for the foundation, walls and top slab. The tank is well instrumented at critical locations for strain data collection with fiber-optic sensors. Figure 2.32 shows the FRP bar reinforcements in the vertical walls and overview of the complemented FRP tank. The field test results under actual service conditions for the strain behavior in the FRP bars at different location in the tank are indicated by a significant value less the 1.0 % of the ultimate strain. In conclusion, the construction procedure, serviceability performance under real service conditions (water and earth pressure), and monitoring results of the FRP-reinforced walls and slabs of the tank, in terms of strain, cracking and deflection were very conservative and satisfactory when compared with the serviceability requirements and strength needed (Mohamed and Benmokrane 2014).

2.8.3　GFRP soft eyes in tunnels

Building tunnels with tunnel boring machines (TBM) is today state of the art in different ground conditions. Launching and receiving the TBM in shafts and station boxes has recently required a considerable construction effort. Breaking through the steel reinforced walls of the excavation shaft with a TBM required extensive measurements and preparation works (Schürch and Jost 2006). FRP is an anisotropic composite material with a high tensile strength in axial direction and a high resistance against corrosion. The anisotropy of the material is quite advantageous at excavation pits for the starting and finishing processes at automated excavation like tunnel boring machine (TBM) and Pipe jacking (Figure 2.33). Therefore, using FRP bars in reinforced walls and piles of the excavation shaft allows the designer and contractor today to find innovative solutions for the well-known situation and save time and costs on site. Soft eyes consist usually of bore piles or diaphragm walls that are locally reinforced with GFRP bars and stirrups (Figure 2.34). The sections below and above the tunnel opening are reinforced steel bars. Depending on the designer and contractors' preferences, full rectangular sections are built out of GFRP bars or the fiber reinforcement follows the tunnel section more closely, resulting in a circular arrangement of the GFRP links and similar adjustments for the vertical bars. Building the corresponding reinforcement cages out of GFRP bars on site requires the same working procedures as for an equal steel cage. The necessary bars are tailor made and delivered to the site where the assembly takes place. The bars are fixed together with binding wire, cable binders or similar products. U-bolts are used for clamping bars together when high loads have to be transferred over a connection. This is the case for example in the connection between vertical GFRP bars and the corresponding steel bars which have to carry the dead load of the reinforcement cage during the lifting process and lowering of

the cage into the trench. Welding as is commonly done with steel reinforcement in such situations is not possible with GFRP bars (Schürch and Jost, 2006).

2.8.4 Parking garages

The need for sustainable structures has motivated the Public Works and Government Services Canada (PWGSC) in the use of FRP bar as internal reinforcement in concrete infrastructure applications. One of the most important successful applications is using FRP bar to reinforce parking garages. An agreement between PWGSC and the University of Sherbrooke was reached to reconstruct the interior structural slabs of the Laurier–Taché parking garage (Hull, Quebec) using carbon and glass FRP bar, (Figure 2.35). The design was made according to (CAN/CSA-S806, 2012). This project allowed direct field assessment and long-term monitoring of FRP composite bars in a structure subjected to harsh environmental and loading conditions. In 2010, the new large parking garage (La Chancelière parking garage, area 3,000 m^2) in Quebec City was designed and constructed using the FRP bar, (Figure 2.35). This design was made according to the (CAN/CSA-S413-07) for parking structures and (CAN/CSA-S806-12) for design and construction of building components with fiber reinforced polymers. The two-way flat slabs of La Chancelière had a maximum span of about 9.0 m. The thickness of the slabs was 250 mm, which increased to 355 mm over the columns through the drop panels, (Figure 2.36). The increased thickness over the columns was required to satisfy the punching stresses around the columns' area. The punching strength of the two way slabs was verified using the new punching equations that are being incorporated in the new version of the S806 Standards (2012), (Benmokrane et al. 2012).

(a) FRP decks/app slabs/ barriers – Skagit River – BC MOT (2009)

(b) FRP decks and barriers – Gateway Blvd/23rd Ave – Alberta (2009)

(c) Reinforcement of the bridge deck, 410 overpass bridge Quebec, Canada

Figure 2.31: Recent FRP-reinforced concrete bridges

(a) FRP reinforcement bars of the vertical wall

(b) Over view of the tank

Figure 2.32: FRP-reinforced concrete tank, Quebec, Canada

Figure 2.33: TBM cutting through FRP-reinforced concrete drilled shaft wall

(a) Overview of the GFRP soft eyes

(b) Handling and lifting the GFRP soft eyes

Figure 2.34: GFRP reinforcement for soft eyes

Figure 2.35: Laurier-Taché Parking Garage

Figure 2.36: La Chancelière Parking Garage

2.9 Long-Term Predictions

In endeavoring to assess the long-term durability performance of FRP in harsh environments, extensive studies have been conducted to develop accelerated aging procedures and predictive models for long—term strength estimates, especially for FRP bars (Davalos et al. 2012; Chen et al. 2006; Bank et al. 2003; Dejke 2001; Porter et al. 1997). These models are based on the Arrhenius model (Litherland et al. 1981). Research on the effects of temperature on the durability of FRP bars in concrete alkaline environments indicated that an accelerated factor for each temperature difference can be defined using Arrhenius laws. These factors differ for each product, depending on fiber and resin types and bar size. In addition, these factors are affected by environmental conditions, such as surrounding solution media, temperature, pH, moisture, and freeze–thaw conditions. Predictive models based on Arrhenius laws make the implicit assumption that the elevated temperature will only increase the rate of degradation without affecting the degradation mechanism or introducing other mechanisms. Gerritse 1998 indicated that at least three elevated temperatures were necessary to perform an accurate predication based on Arrhenius laws.

Eq. 2.2 expresses the Arrhenius relation in terms of the degradation rate (Nelson 1990):

$$k = A \exp\left(\frac{-E_a}{RT}\right) \tag{2.2}$$

where k = degradation rate (1/time); A = constant relative to the material and degradation process; E_a = activation energy of the reaction; R = universal gas constant; and T = temperature in Kelvin. The primary assumption of this model is that only one dominant degradation mechanism of the material operates during the reaction and that this mechanism will not change with time and temperature during the exposure (Chen et al. 2006). Only the rate of degradation accelerated with the temperature will increase. Eq. 2.2 can be transformed into:

$$\frac{1}{k} = \frac{1}{A} \exp\left(\frac{E_a}{RT}\right) \tag{2.3}$$

$$\ln\left(\frac{1}{k}\right) = \frac{E_a}{R}\frac{1}{T} - \ln(A) \tag{2.4}$$

From Equation (1-4), the degradation rate k can be expressed as the inverse of time needed for a material property to reach a given value (Chen et al. 2006). Eq. 2.4 further shows that the logarithm of time needed for a material property to reach a given value is a linear function of $1/T$ with a slope of E_a/R (Chen et al. 2006). E_a and A can be easily calculated with the slope of the regression and the point of intersection between the regression and the y-axis, respectively. More details on using the Arrhenius model and long-term-durability prediction models of FRP reinforcement can be found in Davalos et al. (2012).

Predictions of the service life of the CFRP at mean annual temperatures (MAT) of 10°C and 50°C were performed by Benmokrane et al. 2016.The temperature of 10°C is a close approximation of

the mean average temperature of northern regions, where deicing salts are often used. The temperature of 50°C exacerbates the combined effect of the mean annual temperature and the marine environment of the Middle East, Caribbean, and Florida. The Arrhenius plot can be used to extrapolate the service life necessary to reach the established tensile-strength retention levels (PR) for any temperature. Consequently, predictions were made for tensile-strength retention as a function of time for immersions at 10°C and 50°C. Figure 2.37 provides the general relationship between the PR and the predicted service life at the two MATs. This figure shows that the predicted strength-property retention level (PR) for the specimens immersed at an isotherm temperature of 10°C would be slightly affected over 200 years. For the same specimen immersed at an isotherm temperature of 50°C, the service-life predictions are approximately 10 and 200 years for a PR of 94.2% and 91.6%, respectively. As expected, these results show that the long-term tensile strength of the CFRP was more affected by the alkaline environment in a warm climate. The predicted service life of CFRP embedded in an alkaline environment or aged in alkaline solution at an isotherm temperature of 10°C to reach a PR of less than 95% can be estimated at more than 200 years. Figure 2.37 indicates that, even after a service life of 150 years—which corresponds to the longest design service life—the tensile-strength retention was still over 95% and 90% for MATs of 10°C and 50°C, respectively. These predictions show that the CFRP are durable with respect to the concrete environment, as simulated in this study (Benmokrane et al. 2016).
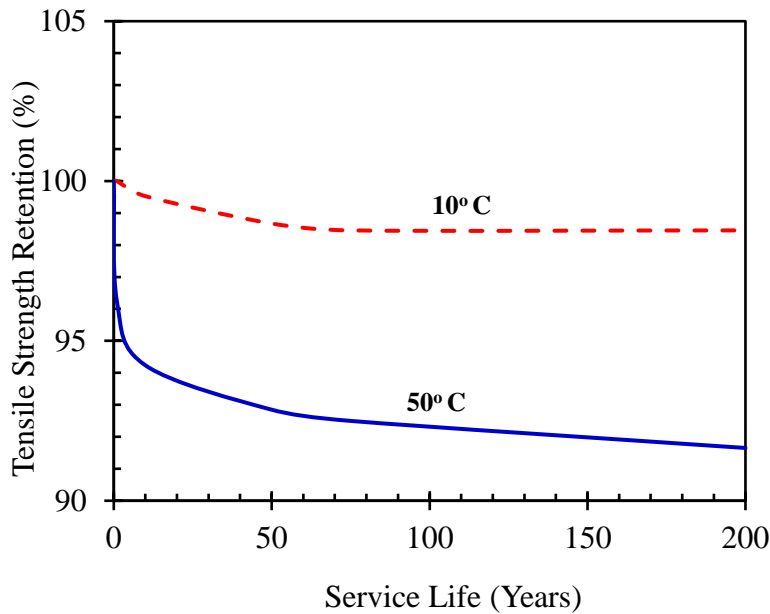
Figure 2.37: General relation between the PR and the predicted service life at mean annual temperatures of 10 and 50°C (Benmokrane et al. 2016)

CHAPTER 3
CHARACTERIZATION AND DURABILITY OF CFRP TENDONS UNDER SUSTAINED LOAD IN HIGH ALKALI ENVIRONMENT AND ELEVATED TEMPERATURES

3.1 Introduction

Recent years have witnessed valuable research work on FRP and widespread applications of carbon-fiber-reinforced polymer (CFRP) tendons and stirrups as flexural and shear reinforcement for concrete bridges. Grace et al. 2014 indicated that the performance of CFRP stirrups was analogous to that of steel stirrups with the exception that steel stirrups demonstrated a yield plateau before concrete failure in decked bulb T-beams. In another study, it was concluded that the flexural performance of beams reinforced with CFRP tendons were comparable with the performance of a control beam at both service and ultimate limit states (Grace et al. 2012). Moreover, the study showed that corrosion-free FRP-reinforced decked bulb T-beams can be safely deployed in construction to enhance the performance and extend the life span of bridge superstructures. Nonetheless, no experimental research on the durability behavior of CFRP tendons, under sustained load at elevated temperatures, has yet been reported. Only, an experimental investigation on the durability behavior of CFRP tendons has previously been reported under no stress (no sustained load) and exposed to alkaline solution at different elevated temperatures (Benmokrane et al. 2016). The previous investigation conducted by the research team presented one phase of a multitask FDOT project dedicated to establish a comprehensive durability database for Tokyo Rope CFRP tendons with different parameters such as temperature exposures, type of environment (alkaline solution), and sustained tensile-load levels. The previous test results indicated that the strengths of the CFRP specimens were slightly affected by increasing the immersion duration at higher temperature levels.

This chapter focuses on studying the possible degradation of CFRP prestressing tendons due to exposure to simultaneous high alkali environment and sustained loading at an elevated temperature of 130 ºF (60 ºC) for durations up to 7,000 hr. The high alkali environment simulated the concrete pore solution and the elevated temperature was used to accelerate the aging process. The applied sustained load on the CFRP tendons were equivalent to 40% and 65% of their guaranteed strength. Upon completion of the exposure duration, the CFRP tendons were tested in tension and shear to evaluate their mechanical properties. The CFRP tendons were exposed to the environmental conditions and sustained loading using two different test setups one at Sherbrooke University and the other at North Carolina State University. This research is critical in order to establish the critical

stress (allowable) and safety factors for the use of CFRP tendons as corrosion-resistant reinforcing material for prestressed precast-concrete applications in Florida's marine environment.

3.2 Experimental Program

3.2.1 Tensile test specimens of CFRP

Carbon-fiber reinforced polymers (CFRPs) manufactured by Tokyo Rope Manufacturing Co. Ltd., Japan, are used in this study, as shown in Figure 3.1. This type of reinforcement is of interest to the Florida Department of Transportation and other DOTs for its use as corrosion-resistant reinforcing material for prestressed precast-concrete bridge beams. The Tokyo Rope CFRP is a stranded cable comprising a number of individual strands. In this study, the CFRPs Cables are made with 7 twisted carbon strands, with nominal diameters 7.5 mm and cross section area 31.1 mm^2 (0.048 in^2), as shown in Figure 3.2. Individual strands of Tokyo Rope CFRPs consist of carbon fibers impregnated with thermosetting epoxy resin; in addition, each strand is protected with wrapping material (polyester fiber).

(a)Test specimens without load: A total of 60 CFRP specimens were cut in length 1,600 mm (63 inch) as specified in ASTM D7205 (specimens without load). The specimens were divided into two series: (1) 24 unconditioned samples; and (2) 36 conditioned samples immersed in alkaline solution.

(b) Test specimens with load: A total of 144 CFRP specimens were cut in length 2,030 mm (80 inch) to be subjected to sustained tensile load corresponding to 40 % and 65 % of their guaranteed strength. Table 3.1 provides a summary of the environmental conditioning, the number of CFRP samples, and level of sustained load.

Figure 3.1: CFRP coil as received

78

Figure 3.2: Overview of the cross section of CFRP tendon specimens (7.5 mm, 31.1mm^2)

Table 3.1: Tensile and Shear testing matrix for accelerated aging of CFRP

Sustained Load	Alkaline Solution	Duration of exposure (hr)	Temp. (^{o}F)
	As received		
	No	3000	72
	No	5000	72
0%	No	7000	72
	Yes	3000	72, 140
	Yes	5000	72, 140
	Yes	7000	72, 140
	No	3000	72, 140
	No	5000	72, 140
40%	No	7000	72, 140
	Yes	3000	72, 140
	Yes	5000	72, 140
	Yes	7000	72, 140
	No	3000	72, 140
	No	5000	72, 140
65%	No	7000	72, 140
	Yes	3000	72, 140
	Yes	5000	72, 140
	Yes	7000	72, 140

* The alkaline solution includes calcium hydroxide, potassium hydroxide, and sodium hydroxide (118.5 g of Ca(OH)$_2$ + 0.9 g of NaOH + 4.2 g of KOH in 1 L of deionized water) according to CSA S806 and ACI 440.3R.

** A total of five specimens will be used for mechanical testing and one specimen, at each temperature, will be used for SEM/EDS and DSC testing.

3.2.2　Tensile test setup and environmental conditioning

CFRP specimens were tested for their residual tensile capacity upon completion of the exposure durations of 3000, 5000 and 7000 hr. The CFRP specimens were anchored at both ends in order to achieve the full tensile capacity without any slippage throughout the length of the anchor during the test. The CFRP specimens tested at Sherbrooke University had two different dimensions. The first dimension was for the specimens exposed to alkaline solution and/or high temperature. The CFRP specimens were 63 inches (1600 mm) long with anchor length of 20 inches (510 mm) at each end and clear length of 23 inches (580 mm) as shown in Figure 3.3. The second dimension was for the specimens subjected to sustained loading. The CFRP specimens were 81 inches long with anchor length of 20 inches at each end and clear length of 41 inches (1030 mm) as shown in Figure 3.4. Steel pipes filled with cement grout were used as anchors for the CFRP specimens. Figure 3.5 shows the preparation process of the cement grout and the placement of plastic rings to seal the ends of the pipes. The tensile tests were carried out using Baldwin testing machine at Sherbrooke University as shown in Figure 3.6. The test specimens were instrumented with an extensometer of 200 mm length to capture elongation during testing. For each tensile test, the specimen was mounted in the tensile machine with the steel-pipe anchors gripped by the wedges of the machine's upper and lower jaws. The loading rate was around 27 kN/min. The applied load and bar elongation were recorded with a computer data-acquisition system. Figure 3.7 shows an example for the mode of failure for some tested specimens.

Steel pipe

510 mm (20.1inch)　　580 mm (22.8 inch)　　510 mm (20.1inch)

1600 mm (63 inch)
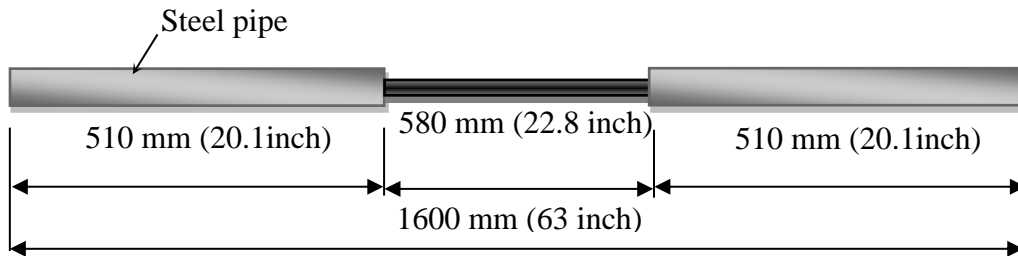
Figure 3.3: Dimensions of CFRP specimens not subjected to sustained load at Sherbrooke University

Steel pipe

510 mm (20.1inch)　　1030 mm (40.55 inch)　　510 mm (20.1inch)

2060 mm (81.1 inch)
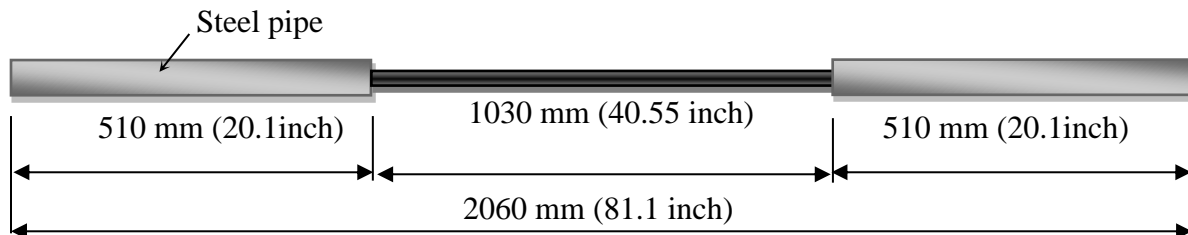
Figure 3.4: Dimensions of CFRP specimens subjected to sustained load at Sherbrooke University

Steel tube dia. 3/4 inch schedule 80:
ID= 0.742 in. OD = 1.05 in.
Wall thickness 0.145 in.
Length of the tubes 510 mm

Figure 3.5: Anchorage preparation at Sherbrooke University

Figure 3.6: Typical tensile test setup at Sherbrooke University

Figure 3.7: Typical mode of failure of CFRP tension specimens (Sherbrooke University)

CFRP specimens tested at North Carolina State University were anchored at both ends using steel tubes and epoxy with anchorage length of 18 inches (457 mm) to provide a clear length of 15 inches (381 mm) in between as shown in Figure 3.8 and specified by ASTM D7205. All prepared anchors were left to cure for 7 days. Figure 3.9 shows the preparation and curing process of the anchors. A 200 kips MTS machine was used for the tensile testing of the CFRP specimens at North Carolina State University. The tests were conducted using a strain control manner with a

loading rate of 0.05 in/min. Due to the vicious failure nature of the specimens, an acrylic tube was placed around the specimen as shown in Figure 3.10. The tube had an opening to allow the placement of an extensometer to measure the strain. The extensometer was removed approximately at 70% of the guaranteed breaking load. Figure 3.11 shows an example of the tested specimens after failure.
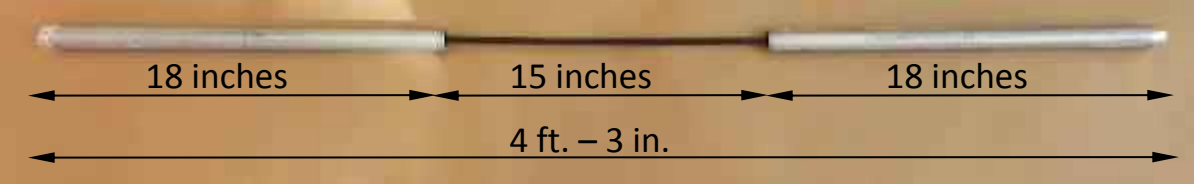
Figure 3.8: Dimensions of CFRP specimen at NCSU

Figure 3.9: Preparation and curing of anchorages at NCSU

Figure 3.10: Tensile test of CFRP specimen at NCSU

Figure 3.11: Typical failure mode of CFRP tension specimens (NCSU)

Two different test setups were used to expose the CFRP strands to environmental conditions. The first test setup, used at Sherbrooke University, consisted of 6 PVC tubes to immerse 36 CFRP specimens in alkaline environment for three different exposure periods (3,000, 5,000, and 7,000 hr) at two temperatures 30 and 60°C. Each PVC tube was 4 in. (100 mm) diameter and 67 in. (1,700 mm) long as shown in Figure 3.12. Both ends of the PVC tubes were sealed using PVC caps and PVC adhesives. For the CFRP specimens subjected to simultaneous sustained tensile load (40 and 65%) and exposed to alkaline solution, a total of 72 PVC tubes were prepared. Each tube was 1.57 in. (40 mm) diameter and 20 in. (500 mm) long as shown in Figure 3.13. New steel frames were fabricated to install 144 CFRP specimens subjected to sustained tensile loading at

40% and 65 % of their guaranteed strength. Figure 3.14 shows a schematic view of the one frame with six specimens placed in it. Figures 3.15 and 3.16 show the actual steel frame and a close up view of the anchors used to apply the sustained load. The alkaline solution was prepared using calcium hydroxide, potassium hydroxide, and sodium hydroxide (118.5 g of Ca(OH)2 + 0.9 g of NaOH + 4.2 g of KOH in 1 L of deionized water) according to CSA S806 and ACI 440.3R. The pH of the alkali solution was 12.8.

6 PVC tubes with 1,700 mm length and 100 mm diameter to keep the 36 CFRP specimens in

12 PVC cap with 100 mm di-

Figure 3.12: The CFRP specimens exposed to alkaline solution inside PVC tubes

Figure 3.13: The PVC tubes used for CFRP specimens subjected to sustained load and alkaline solution
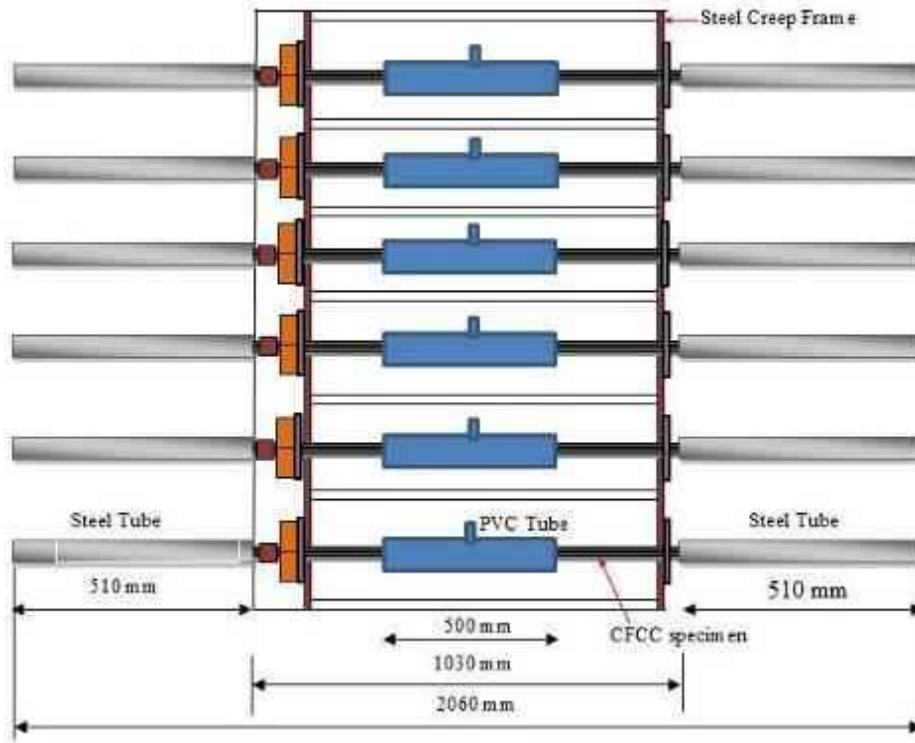
Figure 3.14: Schematic view of steel frame used to apply sustained load to CFRP specimens

The second test setup used at North Carolina State University was designed to subject the CFRP strands to sustained loading equivalent to 65% of their guaranteed capacity. The test setup consisted of four steel trusses in which the CFRP specimens were subjected to tension. Each steel truss was 21 feet long, 7 inches wide and 4 feet high. Four 20 feet long CFRP tendons were tensioned in each truss, two strands were subjected to sustained load, and two strands were subjected to the same sustained loading and exposed to alkaline solution. In addition, two steel trusses were thermally isolated using insulating foam and four heating mats were placed along the length of the trusses to increase the temperature to 60 ℃ (130 ℉). The strands were anchored from the ends using threaded steel pipes. The anchors had a total length of 24 inches with 18 inches of threaded length. Plastic caps and aluminum tape were used to seal one end of the anchor pipes. Sikadur 35 epoxy grout was used to bond the strands to the anchors. The epoxy was cured for 7 days before mounting the strands in the loading frame and applying the sustained load. The sustained tensile load was applied to the CFRP tendons from one end, the live end, and the load level was monitored using a load cell during the application of the load as shown in Figure 3.17. Another load cell was manufactured and placed at the other end, the dead end, to monitor the load throughout the exposure duration. The manufactured load cells were connected to a Vishay SB-10 system which was wired into a Vishay P3 Strain Indicator System. Spring washers were placed at the dead end of the strand to allow for the deformation of the CFRP as shown in Figure 3.18. Figure 3.19 shows a close up view of the manufactured load cell used to monitor the load during the exposure duration. A fabricated steel truss with 4 loaded strands undergoing conditioning is shown in Figure 3.20.

Figure 3.21 shows the four steel trusses with the heating mats placed in the middle between the last two trusses and before placing the insulating foam. For the strands that were not subjected to sustained load, the strands were placed in 20 ft. PVC tubes and filled with alkaline solution. Upon completion of the exposure duration, the sustained load was released and each CFRP tendon was cut into 4.25 feet (1.3-m) long specimens and anchored from both ends using steel tubes and epoxy to test their residual tensile capacity. This test setup was designed so that all the replicates for a given condition were prepared from the same CFRP tendon, ensuring that they are subjected to the same environmental and mechanical loading.

Figure 3.15: Steel frame used to subject CFRP tendons to sustained load

Figure 3.16: Sustained creep load frame during fixing the CFRP specimens with and without alkaline solution: (a) T=22ºC [72]; (b) T=60ºC [140ºC]
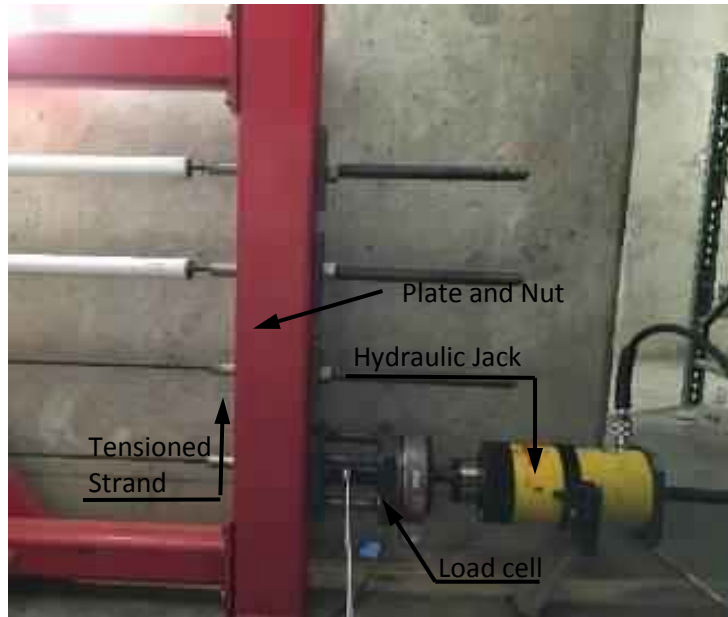
Figure 3.17: Applying sustained load on CFRP tendon using a hydraulic jack at the live end of tensioning
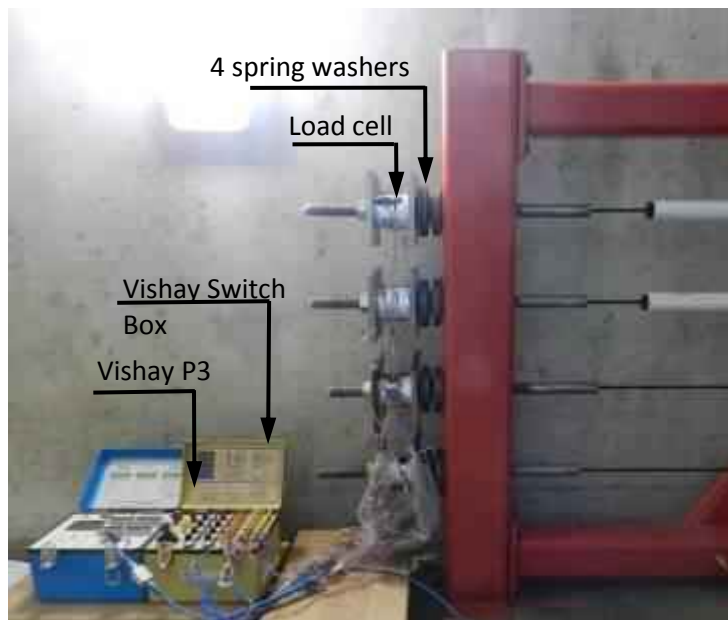
Figure 3.18: Load cells and spring washers placed at the dead end of tensioning

Figure 3.19: Manufactured load cell used at dead end of tensioning

Figure 3.20: Steel truss with 4 tensioned CFRP tendons

Figure 3.21: Four steel trusses with 16 CFRP tendons under sustained load and environmental exposure

3.2.3 Transverse shear test

A total of 65 specimens of Tokyo Rope CFRP specimens were tested, with and without sustained load, as reference, 3,000; 5,000; and 7,000 hr conditioned specimens in transverse shear test till failure and the shear strengths were determined. The specimens were cut at approximate length of 250 mm (see Figure 3.22), regardless of the nominal diameter of the FRP rods, according to CSA-S806-12 (2012), Annex L–"Test Method for Shear Properties of FRP Rods". The specimens were tested by direct application of double shear till failure and shear strength was determined. Figures 3.23 and 3.24 show the test setup and a specimen during testing.

Figure 3.22: Test specimens

Figure 3.23: Typical test setup

Figure 3.24: Specimen during loading

The tests were carried out using MTS 810 testing machine equipped with 500 kN (112.4 kip) load cell. The distance between the shear planes was set to 25 mm (0.98 in.) The typical test setup used to perform the test is shown in Figure 3.24. The rate of loading (1.3 mm/ min) was chosen to allow an increase of 30 to 60 MPa/min of the shearing stress and the load was applied without subjecting the test specimen to any shock. The applied load was recorded during the test using a data acquisition system monitored by a computer. The transverse shear strength, τ, of CFRP specimens was calculated according to the following equation:

$$\tau = \frac{P}{2A}$$

(3.1)

where:

τ = Transverse shear strength (MPa or ksi);

P = Shear failure load (N or kip); and

A = Cross-sectional area of the test specimen ($31.1 mm^2 = 0.0482 in^2$).

3.2.4   Physical characteristics

This section presents physical characteristics of Tokyo Rope CFRP specimens 1X7 (ϕ7.5mm). The test procedures and experimental test results of carbon fiber content, water absorption, cure ratio and glass transition temperature were carried out according to the specification of the (ACI-440.6M, 2008) and (CSA-S807, 2010). Moreover, Optical and Scanning Electronic Microscopy (SEM) analyses were performed to investigate the microstructure of the material.

3.2.4.1 Fiber content

Carbon fiber content was determined by thermogravimetry according to (ASTM E 1131, 2008) – "Standard Test Method for Compositional Analysis by Thermogravimetry". A very small piece of material (a few tenths milligrams) was cut from the center of the cable, placed in a platinum crucible, and then heated up to 550°C under inert atmosphere. The weight loss was recorded as a function of temperature while the weight loss at 550°C (W_L) was measured. Since the material only contains carbon fibers and resin, fiber content by weight was calculated according to the following equation:

$$\text{Fiber Content by weight} = 100 \cdot (W_T - W_L)/W_T \qquad (3.2)$$

3.2.4.2 Water absorption

The water absorbtion was determinted according to the (ASTM D 570, 2010) – "Water Absorption of Plastics". The water content percentage in weight was obtained from three 1-inch long specimens, which were cut, dried, and weighed. After 24 hr, the specimens were immersed in water at 50°C. Then, the specimens were removed from water until the surface was dried and weighed again. Therafter, the specimens were immersed again and periodically removed from water until the surface was dried and weighed until full saturation. The specimens were considered as saturated when the weight became constant. The water content percentage in weight, W, was calculated from Eqn. 3.3.

$$W = 100 \cdot (P_i - P_d)/P_d \qquad (3.3)$$
where P_i and P_d are the weights of the sample after immersion and in dry state, respectively.

3.2.4.3 Cure ratio

The cure ratio was detearminted according to (ASTM D 5028, 1990) – "Curing Properties of Pultrusion Resin by Thermal Analysis". The measurements were carried out on three specimens. The enthalpy of polymerization of the samples were measured by Differential Scanning Calorimetry (DSC). Therafter, the measurements were compared to the enthalpy of polymerization of pure resin, taking into accounts the weight percentage of resin in the matrix. Thirty to fifty milligrams of sample were accurately weighed and placed in aluminum crucible. The samples were heated from the room temperature to 200°C at 20°C/min and the peak area of polymerization was calculated.

3.2.4.4 Glass transition temperature

The Glass transition temperature, *Tg*, was determined by (DSC) using (ASTM D 3418, 2012) – "Transition Temperatures of Polymers by Thermal Analysis". Three specimens were used to meas-

ure the *Tg*. Thirty to forty milligrams of composite sample were weighed and placed in an aluminum pan. Then, the sample was heated up to 200°C under nitrogen at a heating rate of 20°C/min. The value of T_g was taken at the mid-height of the C_p jump.

3.2.4.5 Scanning electronic microscopy (SEM)

Longitudinal and transverse sections of cable sample (one-inch-long) were cut and placed in cylindrical molds, where epoxy resin was cast. After 24 hour of curing at room temperature, the samples were removed and cut using a low speed saw equipped with a diamond blade. Therafter, the specimens were polished using a polishing machine with three diamond pastes (15, 3, and 1 micron) before sputtering them with palladium. Thus, the specimens were ready for analysis with a Hitachi SEM.

3.3 Results

3.3.1 Physical properties

3.3.1.1 Fiber content

The carbon fiber content in weight of Tokyo Rope CFRP cables is 82.5 %.

3.3.1.2 Water absorption

The mass percentage of water uptaked after 24 hr, 7 days, and at saturation was reported in Table 3.2. At saturation, the material absorbed 1.1% water.

Table 3.2: Water absorption after 24 hr, 7 days, and at saturation (%)

Specimen	No conditioning	After 7,000hr
Average	@ 24 hr	
	2.7	9.8
	@ 7 days	
	3.1	10.9
	@ saturation	
	3.5	11.6

3.3.1.3 Cure ratio

The enthalpy of polymerization of the sample was measured by DSC and compared to the enthalpy of polymerization of the resin matrix, taking into account the weight percentage of resin in the material. Fifty to ninety milligrams specimens were accurately weighed and placed in aluminum pans. The sample are fully cured (Table 3.3).

Table 3.3: Cure ratio of the tested FRP bar (%)

Sample	Cure ratio %
1	100
2	100
3	100
4	100
5	100
Average	**100**

3.3.1.4   Glass transition temperature

The values of the glass transition temperatures determined by DSC are presented in Table 3.4. Since the material as received was not fully cured, the conditioning at elevated temperature has increased the cure ratio, which leads to a shift of Tg from 118 to 126°C.

Table 3.4: Glass transition temperature, Tg, in °C

Specimen	No conditioning	After 7,000h at 60ºC [140ºF]
1	120	124
2	117	125
3	116	128
Average	**118**	**126**

Figure 3.25 shows the glass transition temperatures Tg with different temperatures. The DMA measurements show a slight increase of Tg after conditioning at 60°C. At 22°C, the increase is insignificant since the temperature is too low to post-cured/consolidate the material.
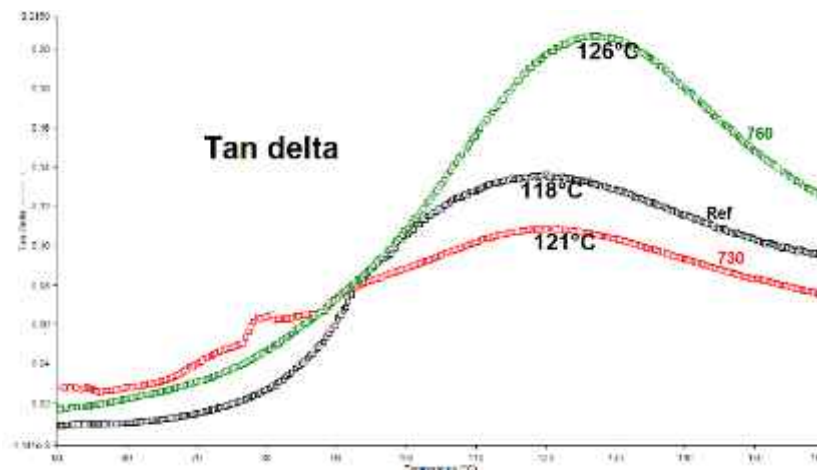
Figure 3.25: The glass transition temperatures Tg with different temperatures.

3.3.1.5 Optical microscopy

Figure 3.26 presented the optical micrographs of the cross-section of reference and conditioned CFRP sample. The figure showed a general view of the seven strands. Each strand was covered with a layer of carbon fibers. The intersection between the central and outer strands creates six voids along the cable. Some pores were visible at various degrees. Voids generally were occured at the interface between carbon fiber bundles, which corresponded to the white lines clearly visible in strand. Figure 3.27 was a close-up of the intersection between two strands. A few voids were visible in the coating.

3.3.1.6 SEM analysis

SEM observations were performed to investigate CFRP specimen microstructural changes before and after 7,000 hr of conditioning. Figure 3.28 to 3.30 display the micrographs of a strand before and after 7000 hr conditioning at 22° and 60°C. It can be seen that the SEM analysis shows a degradation of the surface of the material due to the dissolution of the coating resin. Figure 3.28 shows the SEM micrographs of the cross section of the reference CFRP tendons. SEM analysis of the reference and conditioned specimens indicates that the polyester coating resin is highly degraded, the epoxy core resin is not attacked and the bonding with the carbon fiber has not been changed.

3.3.1.7 FTIR measurement

FTIR spectra of the surface and core of the material specimens were recorded using a Jasco 4600 spectrometer equipped with an attenuated total-reflectance device. Five hundred and twelve scans were routinely acquired at a resolution of 4 cm–1. Chemical degradation in the alkaline solution is mainly due to a hydrolysis reaction, which forms new hydroxyl (-OH) groups from sensitive units, such as ester groups. Hydroxyl groups appeared as a broad peak between 3200 and 3650 cm–1, which corresponds to the stretching mode of the hydroxyl groups in the polyester, vinylester, and epoxy resins. Figure 3.31 shows the FTIR spectra of the unconditioned and conditioned CFRP specimens in the alkaline solution for 3,000; 5,000; and 7,000 hr at 60–C. For each specimen reference and conditioned, spectra of the surface of the specimen were recorded as presented in Figure 3.31. The FTIR analysis of a CFRP tendon surface shows a degradation (hydrolysis) of the coating resin.
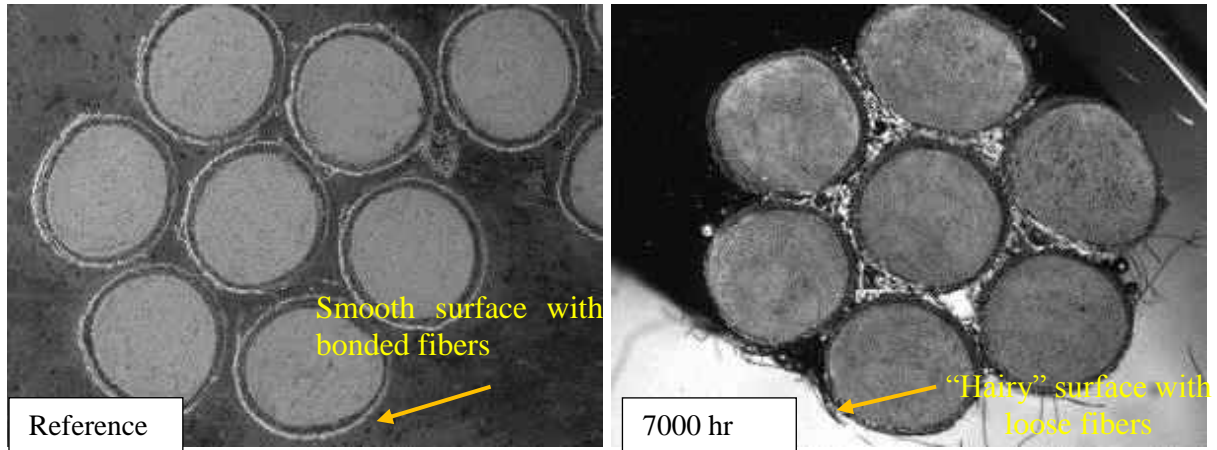
Figure 3.26: General view of carbon Rope cross-section by optical microscopy of reference and conditioning specimens
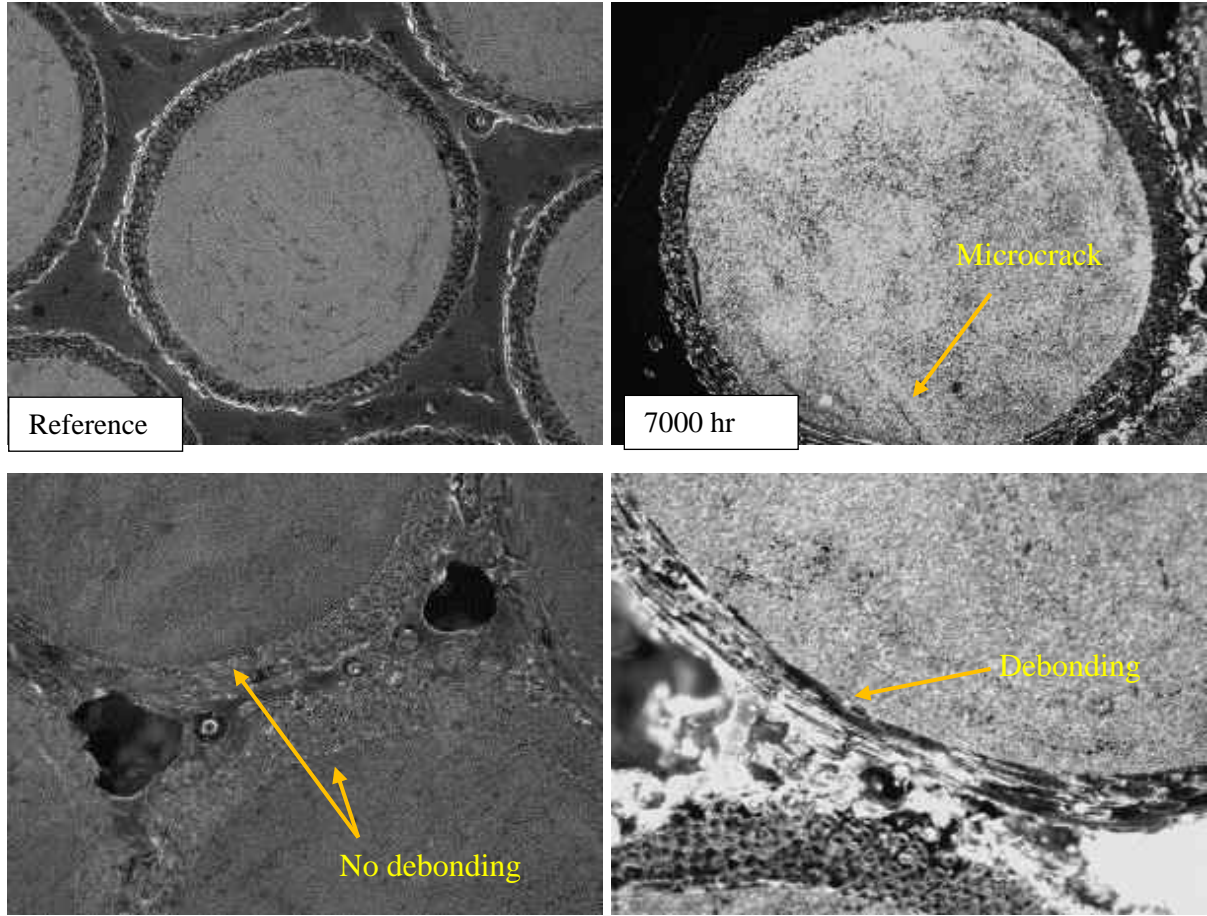
Figure 3.27: View of strand and Intersection between two strands
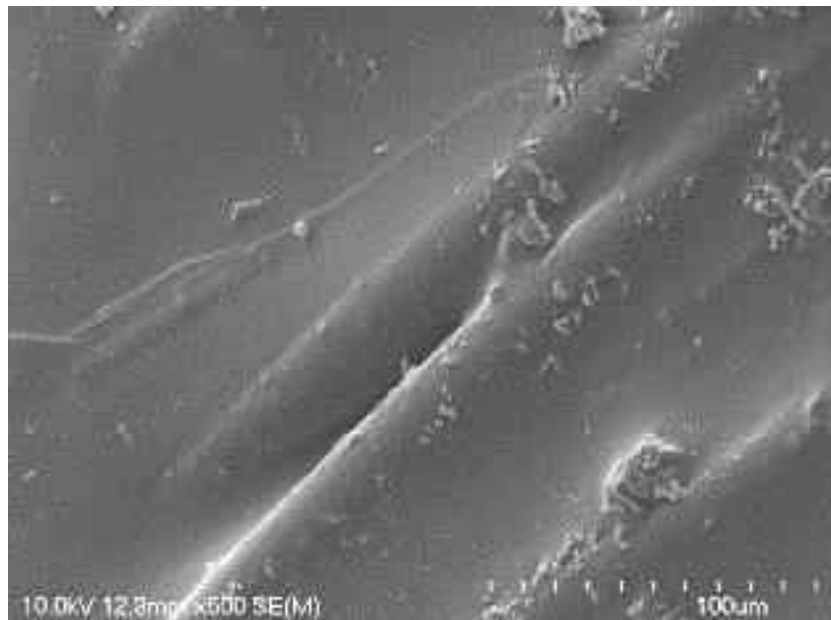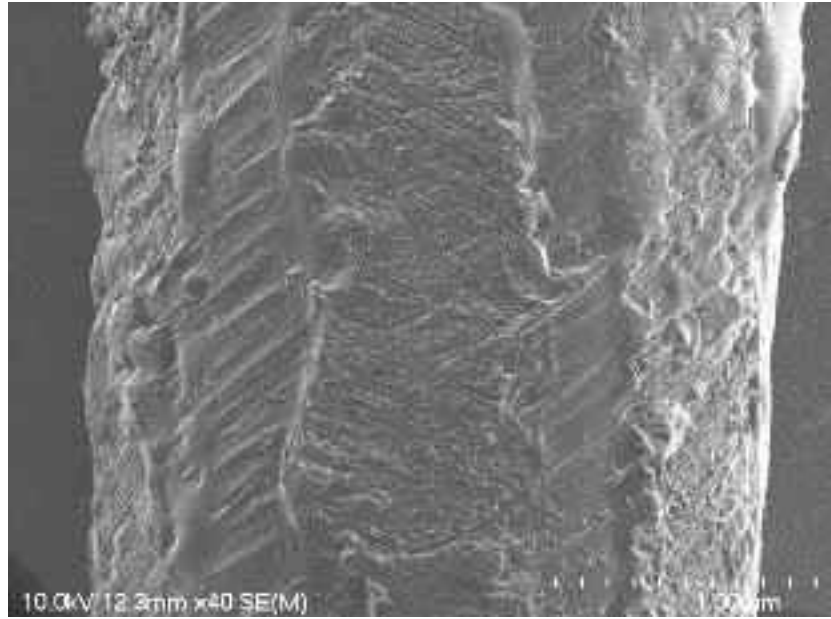
Figure 3.28: Micrographs of CFRP tendons before conditioning (reference speciemns)
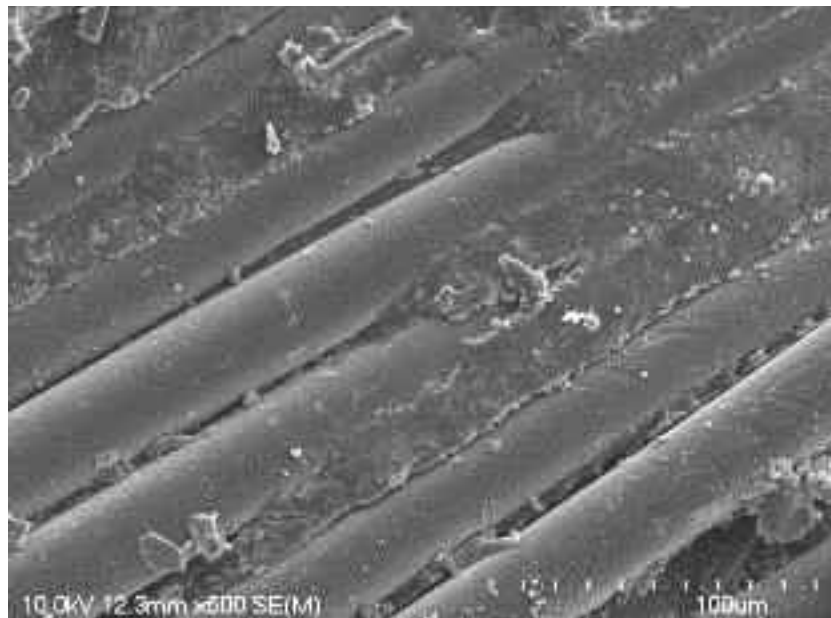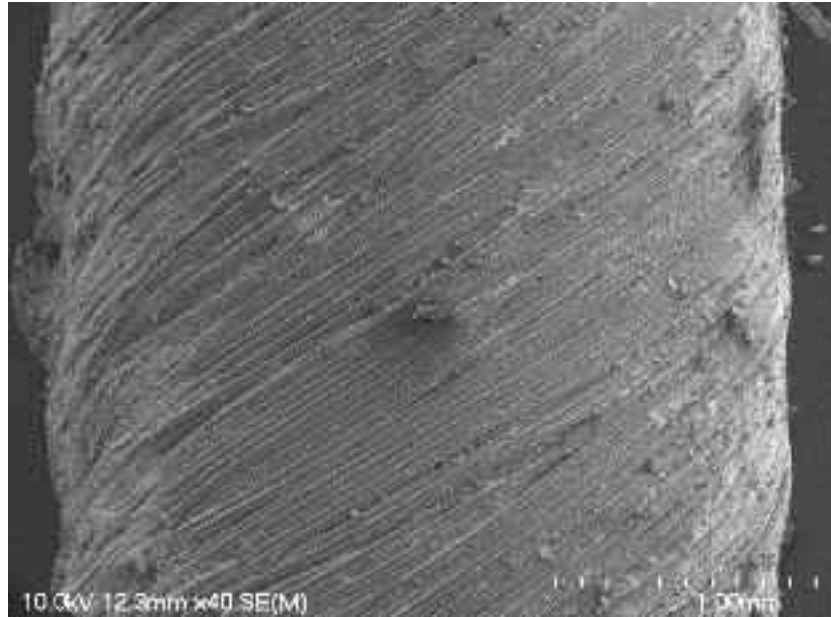
Figure 3.29: Micrographs of CFRP tendons at 22°C [72°F] after 7000 hr of conditioning
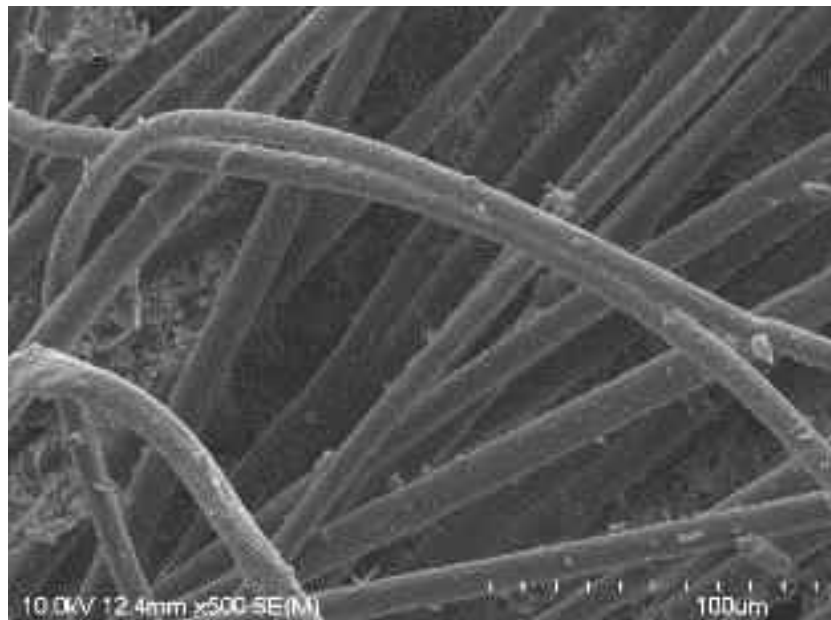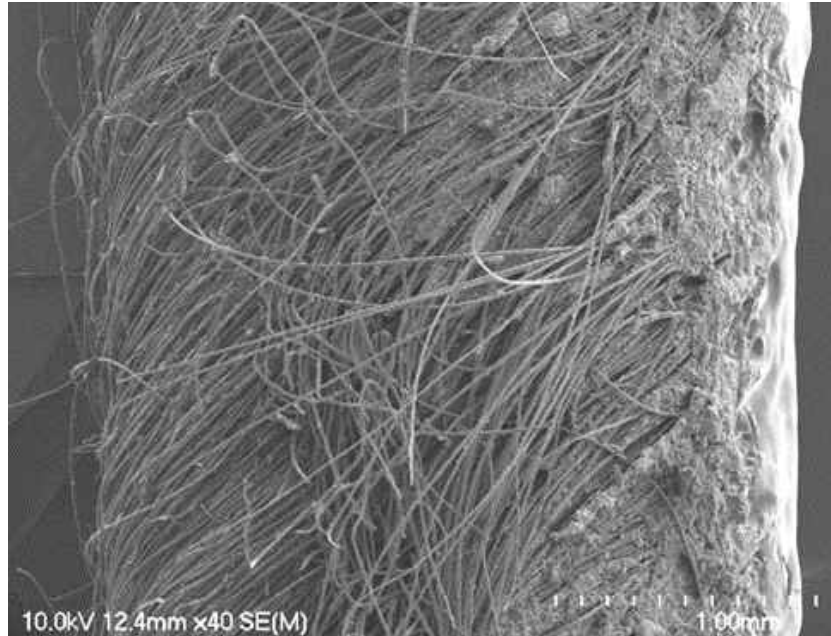
Figure 3.30: Micrographs of CFRP tendons at 60°C [140°F] after 7000 hr of conditioning
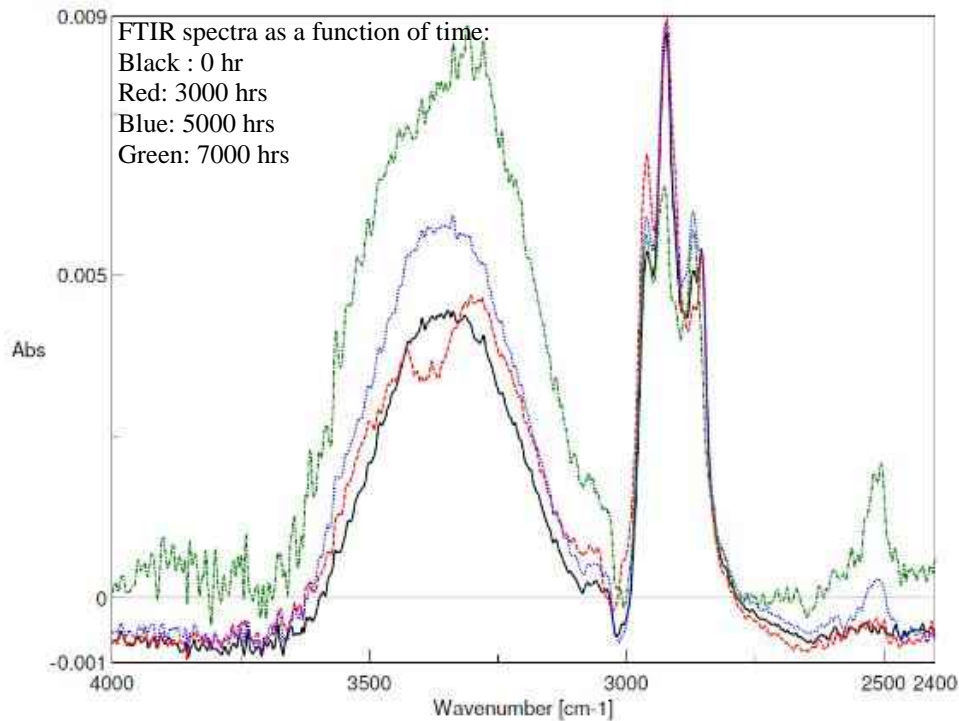
Figure 3.31: FTIR spectra of reference and specimens conditioned for 3,000; 5,000; and 7,000 hr.

3.3.2 Tensile properties of long-term durability of carbon fiber (CFRP) tendons

3.3.2.1 Tensile tests results and discussion

The average immersion-based cross-sectional area (40.8 mm^2) for three samples was measured according to ASTM. The nominal cross-sectional area (31.1 mm^2) as provided by the manufacturer was, however, considered in the calculation. The difference between the nominal and immersion-based cross-sectional areas can be attributed to the polyester wrapping material layer on each strand of the Tokyo Rope CFRP. The following section presents the test results of the tensile testing of CFRP specimens at 72ºF [22 ºC] and 140ºF [60ºC], after an aging duration of 3000, 5000, and 7000 hours.

Calculation of mechanical properties

The tensile strength, f_u, was calculated according to the following equation:

$$f_u = \frac{F_u}{A}$$

(3.4)

Where,

f_u = Tensile strength (MPa or Ksi);

F_u = Tensile capacity (kN or kips); and

101

A = Cross-sectional area of the CFRP test tendon (31.1 mm^2 = 0.0482 in^2).

The tensile modulus of elasticity, E_L, was calculated from the difference between the stress/strain values at 25 and 50% of the tensile capacity according to the following equation:

$$E_L = \frac{F_1 - F_2}{(\varepsilon_1 - \varepsilon_2)A}$$

(3.5)

Where,

E_L = Longitudinal modulus of elasticity.

A = Cross-sectional area of the test bar.

F_1 and ε_1 = Load and corresponding strain, respectively, at approximately 50% of the ultimate tensile capacity; and F_2 and ε_2 = Load and corresponding strain, respectively, at approximately 25% of the ultimate tensile capacity, (N and dimensionless, respectively).

The ultimate strain calculated according to the following equation:

$$\varepsilon_u = \frac{f_u}{E_f} \text{x} 100$$

(3.6)

Guaranteed tensile strength and strain

The "Guaranteed Tensile Strength", (f_u^*) was calculated as defined by ACI 440.1R-15 as the mean tensile strength of a given production lot, minus three times the standard deviation (SD).

$$f_u^* = f_{uav} - 3\, SD.$$

(3.7)

The "Design or Guaranteed Modulus of Elasticity is defined by ACI 440.1R-15 as the mean modulus of elasticity of a production lot or as follows:

$E*f = E f_{ave}.$

(3.8)

Usually, a normal (Gaussian) distribution is assumed to represent the strength of a population of bar specimens (ACI-440.1R (2015). ACI 440.1R (2015) stated that the manufacturers should report the guaranteed tensile properties of FRP reinforcement as mentioned in Equations (3.4, 3.5 and 3.6) for strength, modulus, and strain, respectively, to be used in any design calculation. These guaranteed values of strength and strain provide a 99.87% probability that the indicated values are exceeded by similar FRP bars, provided that at least 25 specimens are tested (ACI-440.1R (2015). Also, ACI 440.1R (2015) stated that the material properties provided for FRP reinforce-ment, such as the guaranteed tensile strength, should be considered as initial properties that do not include the effects of long-term exposure to the environment. Because long-term exposure to various types of environments can reduce the tensile strength and creep rupture and fatigue en-durance of FRP bars, the material properties used in design equations should be reduced based on the type and level of environmental exposure. Therefore, one of the main objectives of this report is to determine the

effect of sustained load, different elevated temperature, and alkaline conditioning on the guaranteed tensile strength of the investigated CFRP Tokyo Rope cables to be used as reinforcement for prestressed concrete structures.

3.3.2.2 Test results

Tensile testing of the reference and conditioned CFRP specimens (7.5 mm in diameter) revealed an approximately linear behavior up to failure. Figure 3.7 and Figure 3.11 show the typical failure mode of both types as tested at Sherbrooke and NCSU University, respectively. Test observations indicate that both the reference and conditioned specimens experienced the same failure mode. Test results of all the specimens as received from Tokyo Rope Co. indicated that the measured average tensile strength was 469.3 ksi (3235.4 MPa), the average modulus of elasticity was 22.1 ksi (152.8 GPa) and the average ultimate strain was 2.12%, as reported in Table 3.5. It should be noted that the measured guaranteed tensile strength was 451.4 ksi (3112.3 MPa). However, the manufacturer set the guaranteed tensile strength of the CFRP specimens as 354.4 ksi (2,444 MPa) with a modulus of elasticity of 22480.8 ksi (155 GPa) and ultimate strain of 1.58% (Tokyo Rope 2015). Table 3.5 gives the average vaules and standard deviation (SD) for the tensile strength, modulus of elasticity, and strain of the tested CFRP specimens as received.

To assess the long-term durability behavior of Tokyo Rope CFRP cables, four parameters were considered in the experimental program, which were aging the CFRP specimens in alkaline solution, subjecting specimens to sustained load, exposure to high temperature, and the duration time of aging. The effect of each parameter was investigated separately and combined with the other parameters. The following sections discuss the effect of all parameters on degradation of CFRP speciemns.

Effect of alkaline solution

CFRP specimens were exposed in an alkaline solution with pH value of 12.8, which simulates typical concrete environment, for a duration of 3000, 5000 and 7000 hr. The effect of alkaline solution on the degradation of CFRP was studied by the tensile strength of the as received specimens with the specimens exposed in alkaline solution only without any sustained load or high temperature. Test results indicated that exposing the CFRP to alkaline solution resulted in a reduction in the average tensile strength by 2.1% after 3000 hr, 2.2% after 5000 hr and 4.5% after 7000 hr of exposure. Table 3.5 provides the detailed results of all the tests conducted on CFRP speciemns at room temperature for a duration of 3000, 5000 and 7000 hr. While, Table 3.6 presents the guaranteed properties of the CFRP tendons as well as the tensile strength and modulus of elasticity retentions of the conditioned CFRP tendons. Table 3.5 and 3.6 present a comparison between the CFRP as received specimens and the specimens exposed to alkaline solution for the three specified durations (3000, 5000, 7000 hr).

Effect of sustained load

Gernally, under sustained load, the FRP bars suffer plastic (permanent) deformation, typically occurring under unfavourable environments over a long time. The mechanism by which sustained stress might affect the properties of the FRP bars is a function of the constituents of the bars themselves (fibers, and resin matrix) and manufacturing process (rate and thoroughness of curing, and fillers). The resin matrix has a larger ultimate tensile strain than the fiber. When fibers are impregnated with resin during the manufacturing process, however, pores in the resin matrix cannot be avoided. These pores give rise to stress concentrations in the resin matrix which, when the bars are subject to sustained tensile stress, initiates microcracks. These microcracks may result in invasion of the matrix by the surrounding mediums (alkaline and water) which in turn may reach and attack the fibers (Nkurunziza et al. 2005, Benmokrane et al. 2017). In the current study, the CFRP specimens were subjected to a sustained load equivalent to 65 percent of their guaranteed capacity specified by the manufacturer, for 3000, 5000 and 7000 hr. The effect of sustained load was studied by comparing the as received specimens to the specimens subjected to sustained load only for the specified durations (no alkaline solution and no elevated temperature). Test results indicated that subjecting the CFRP specimens to a sustained load equivalent to 65% of their guaranteed capacity, for a duration up to 7000 hr of sustained load, had an insignificant effect (~2.0% reduction) on their tensile strength. Table 3.7 and 3.8 present a comparison between the as received specimens and the specimens subjected to sustained load for the three specified durations. Based on the above results, it can be concluded that subjecting the CFRP specimens to sustained load only equivalent to 65% of their guaranteed strength did not affect their ultimate tensile strength. It is worth mentioning that, this reduction of the tensile strength (~2.0% reduction) was observed for the CFRP speciemns without alkaline solution and elevated temperature, it was only under sustained load.

Effect of high temperature

CFRP specimens were subjected to high temperature of 130 ºF (60ºC) for a duration of 3000, 5000 and 7000 hr. The effect of high temperature was studied by comparing the tensile strength of as received CFRP specimens to the tensile strength of CFRP specimens exposed to high temperature only for the specified durations. Table 3.5 provides all the test results conducted on CFRP tendons without sustained load, while Table 3.7 and Table 3.9 present the test results conducted on the CFRP specimens subjecting to a sustained load equivalent to 65% and 40% of their guaranteed capacity, respectively. Test results indicated that exposing CFRP to an elevated temperature of 130 ºF (60ºC [140ºF]), for a sustained load equivalent to 40% and 65% of their guaranteed capacity, had a reduction of only ~3.2% and ~4% after 7000 hr of exposure. Exposing CFRP speciemns to an elevated temperature of 130 ºF (60ºC [140ºF]) for a duration of 7000 hr, without alkine solution and sustained load, had 2.1% reduction on tensile strength. It is worth mentioning that, the above results were observed on the CFRP specimens with only a high temperature, which were without alakine solution.

Combined effect of alkaline solution and high temperature

In the case of simultaneously exposing the CFRP specimens to alkaline solution and high temperature of 140ºF (60ºC) and without sustained load, a reduction of approximately 10.5% was measured in the ultimate tensile strength after 7000 hr of exposure as reported in Tables 3.5 and 3.6.

Combined effect of sustained load, alkaline solution and high temperature

The most severe case of exposure was considered in this research by combining all the parameters together. The CFRP specimens were subjected to sustained load (65% of their guaranteed capacity), exposed to alkaline solution and high temperature for durations of 3000, 5000, and 7000 hr. As reported in Tables 3.7 and 3.8, the test results indicated that the tensile-strength reduction of CFRP speciemns subjected to a sustained load equivalent to 65% of their guaranteed capacity was about 12.4% after 7,000 hr of immersion in alkaline solution at high temperature 140ºF (60°C). These results indicate that longer immersions in alkaline solution, under suatained load, and higher temperatures affected CFRP specimen strength. This phenomenon could be due to a higher solution diffusion rate within the sample and to the immersion temperature accelerating the chemical reaction of degradation, leading to a higher absorption rate for the same immersion time and accelerated degradation reaction. Solution absorption can lead to degradation of the fiber–matrix interface, resulting in a loss in ultimate tensile strength (Bank and Gentry 1995).
Table 3.10 presents the guaranteed strength of CFRP speciemns subjected to a sustained load equivalent to 40% of their guaranteed capacity after 3,000, 5000 and 7000 hrs.

3.3.3   Transverse shear-strength results

Figure 3.32 shows the typical failure mode of the exposed CFRP specimens. Test observations indicate that the reference and exposed specimens experienced the same failure mode.

Figure 3.32: Typical shear failure of CFRP specimens

Figure 3.33 presents the shear strength retention of exposed CFRP specimens, without load and with sustained load equivalent to 65% of their guaranteed capacity, after aging period (up to 7,000

hr) at different exposure temperatures (30 and 60°C [140°F]). It can be indicated that the unstressed CFRP specimens were affected by accelerated aging with a transverse-shear strength reduction of 16.5 % at 60°C [140°F] after 7,000 hr of immersion, while the 65% stressed CFRP specimens had transverse-shear strength reductions of 22.5%.
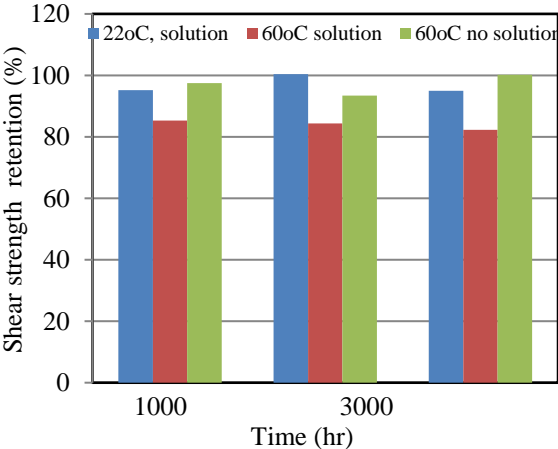
(a) Unstressed CFRP strands   (b) Stressed CFRP strands (65% loading)
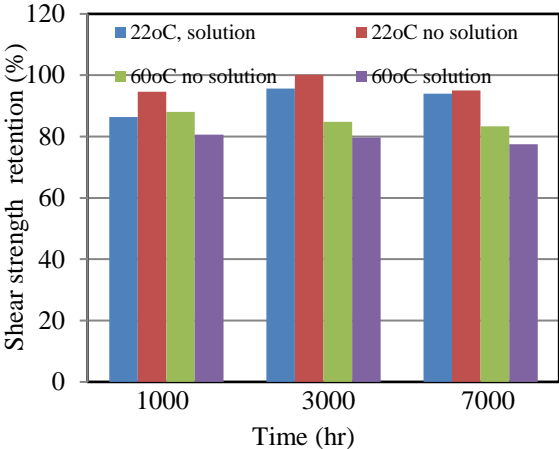
Figure 3.33: Transverse shear strength retention of unstressed and stressed CFRP strands vs duration of exposure

Table 3.5: Average tensile properties of Tokyo Rope CFRP tendons (reference and conditioned at 30 and 60°C [140°F]) for 3000, 5000, and 7000 hrs (Without sustained load)

Bar Status	Elastic tensile modulus, E_f (GPa)				Ultimate Tensile Strength, f_{fu} (MPa)				Ultimate Tensile Elongation, ε_u (%)			
	0 hrs	3000 hrs	5000 hrs	7000 hrs	0 hrs	3000 hrs	5000 hrs	7000 hrs	0 hrs	3000 hrs	5000 hrs	7000 hrs
Reference	152.8 ±1.9	-	-	-	3235 ±41	-	-	-	2.12 ±0.02	-	-	-
No Conditioned at 60°C	-	150.9 ±0.7	151.1 ±1.4	150.7 ±1.2	-	3201 ±31	3170 ±15.8	3166 ±48	-	2.12 ±0.02	2.09 ±0.09	2.10 ±0.04
Conditioned at 22°C	-	152.7 ±1.2	150.6 ±1.1	150.9 ±0.7	-	3167 ±92	3162 ±94	3133 ±33	-	2.07 ±0.06	2.10 ±0.06	2.1 ±0.0
Conditioned at 60°C	-	147.8 ±0.5	147.8 ±2.4	147.0 ±0.8	-	3045 ±68	2873 ±43	2895 ±74	-	2.06 ±0.04	1.94 ±0.06	1.97 ±0.05

Table 3.6: Guaranteed tensile strength and modulus of elasticity retentions of the conditioned Tokyo Rope CFRP tendons after 3,000, 5000 and 7000 hrs (without sustained load)

Bar Status	Elastic tensile modulus, E_f (GPa)			Guaranteed Tensile Strength, f_{fu}*(MPa)			Tensile Capacity Retention (%)			Elastic Modulus Retention (%)		
	3000 hrs	5000 hrs	7000 hrs	3000 hrs	5000 hrs	7000 hrs	3000 hrs	5000 hrs	7000 hrs	3000 hrs	5000 hrs	7000 hrs
No Conditioned at 60°C	148.8	146.9	147.1	3108	3122	3022	98.9	97.9	97.8	98.7	98.8	98.6
Conditioned at 22°C	149.1	147.3	148.8	2891	2880	3034	97.9	97.7	96.8	99.9	98.5	98.7
Conditioned at 60°C	146.3	140.6	144.6	2841	2744	2673	94.1	88.8	89.5	96.7	96.7	96.2

Table 3.7: Average tensile properties of Tokyo Rope CFRP tendons (conditioned at 22°C [72°F] and 60° C [140°F]) for 3000, 5000, and 7000 hrs (with sustained loading equivalent to **65%** of their guaranteed capacity)

Bar Status	Elastic tensile modulus, E_f (GPa)			Ultimate Tensile Strength, f_{fu} (MPa)			Ultimate Tensile Elongation, ε_u (%)		
	3000 hrs	5000 hrs	7000 hrs	3000 hrs	5000 hrs	7000 hrs	3000 hrs	5000 hrs	7000 hrs
No Conditioned at 22° C	150.6 ±1.3	152.9 ±0.7	152.3 ±0.8	3190 ±75	3202 ±57	3187 ±30	2.12 ±0.06	2.09 ±0.04	2.09 ±0.02
No Conditioned at 60° C	151.4 ±1.2	153.4 ±1.3	152.1 ±1.8	3151 ±36	3130 ±41	3117 ±30	2.08 ±0.03	2.04 ±0.03	2.05 ±0.02
Conditioned at 22 ° C	151.4 ±1.3	152.3 ±1.4	152.0 ±1.5	3136 ±43	3118 ±56	2930 ±74	2.07 ±0.03	2.11 ±0.03	1.94 ±0.06
Conditioned at 60 ° C	150.7 ±1.9	151.3 ±1.6	151.1 ±1.5	3018 ±45	2853 ±23.2	2834 ±82	2.0 ±0.06	1.88 ±0.14	1.89 ±0.07

Table 3.8: Guaranteed tensile strength and modulus of elasticity retentions of the conditioned Tokyo Rope CFRP tendons after 3,000, 5000 and 7000 hrs (with sustained loading equivalent to **65%** of their guaranteed capacity)

Bar Status	Elastic tensile modulus, E_f (GPa)			Guaranteed Tensile Strength, $f_{fu}*$(MPa)			Tensile Capacity Retention (%)			Elastic Modulus Retention (%)		
	3000 hrs	5000 hrs	7000 hrs	3000 hrs	5000 hrs	7000 hrs	3000 hrs	5000 hrs	7000 hrs	3000 hrs	5000 hrs	7000 hrs
No Conditioned at 22° C	146.7	150.8	149.9	2965	3031	3097	98.6	98.9	98.5	98.5	100.0	99.1
No Conditioned at 60° C	147.8	149.5	146.7	3043	3007	3027	97.4	96.7	96.3	99.1	100.3	99.5
Conditioned at 22° C	147.5	148.1	147.5	3007	2950	2708	96.9	96.4	90.5	99.1	99.6	99.4
Conditioned at 60 ° C	145.0	146.5	146.6	2883	2783	2588	88.2	88.1	87.6	98.6	99.0	98.9

Table 3.9: Average tensile properties of Tokyo Rope CFRP tendons (conditioned at 22°C [72°F] and 60°C [140°F]) for 3000, 5000, and 7000 hrs (with sustained loading equivalent to **40%** of their guaranteed capacity)

Bar Status	Elastic tensile modulus, E_f (GPa)			Ultimate Tensile Strength, f_{fu} (MPa)			Ultimate Tensile Elongation, ε_u (%)		
	3000 hrs	5000 hrs	7000 hrs	3000 hrs	5000 hrs	7000 hrs	3000 hrs	5000 hrs	7000 hrs
No Conditioned at 22° C	152.0 ±1.2	151.4 ±1.1	151.0 ±1.1	3199 ±27	3196 ±37	3191 ±46	2.10 ±0.03	2.11 ±0.04	2.11 ±0.02
No Conditioned at 60° C	151.7 ±0.7	151.2 ±1.6	150.1 ±1.2	3154 ±21	3146 ±51	3133 ±32	2.08 ±0.01	2.08 ±0.04	2.09 ±0.03
Conditioned at 22° C	151.5 ±0.8	151.5 ±1.3	150.2 ±1.4	3150 ±18	3129 ±57	3035 ±87	2.08 ±0.02	2.07 ±0.03	2.02 ±0.08
Conditioned at 60° C	151.1 ±1.0	151.3 ±1.5	151.1 ±1.0	3032 ±55	2957 ±16	2929 ±29	2.01 ±0.04	1.95 ±0.02	1.94 ±0.01

Table 3.10: Guaranteed tensile strength and modulus of elasticity retentions of the conditioned Tokyo Rope CFRP tendons after 3,000, 5000 and 7000 hrs (with sustained loading equivalent to **40%** of their guaranteed capacity)

Bar Status	Elastic tensile modulus, E_f (GPa)			Guaranteed Tensile Strength, f_{fu}*(MPa)			Tensile Capacity Retention (%)			Elastic Modulus Retention (%)		
	3000 hrs	5000 hrs	7000 hrs	3000 hrs	5000 hrs	7000 hrs	3000 hrs	5000 hrs	7000 hrs	3000 hrs	5000 hrs	7000 hrs
No Conditioned at 22° C	148.4	148.1	147.7	3118	3085	3053	98.8	98.7	98.6	99.5	99.1	98.8
No Conditioned at 60° C	149.6	146.4	146.5	3091	2993	3037	97.5	97.2	96.8	99.3	98.9	98.2
Conditioned at 22° C	149.1	147.9	146.0	3096	2958	2861	97.3	96.7	93.8	99.1	99.1	98.2
Conditioned at 60° C	148.1	146.8	146.8	2867	2909	2842	93.7	91.4	90.5	98.8	99.0	98.8

3.4   Other Testing of CFRP

To verify the expereminat results of the CFRP tested at Sherbrooke University, an experimental work was also conducted at the North Carolina State University. The measurements of tensile strength performed at both institutions were consistent. Although slight differences in the tensile strength values are observed. The difference percentages are small and were within the same order of magnitude as the observed standard deviation of the measurement. It should also be noted that the measured strength of the CFRP composite might be slightly influenced by the type of grip, bonding materials and grouts used in the grip, alignment of the CFRP within the grip, length of test specimen, test equipment, and other factors that cannot be precisely controlled.

In the other set of tests, although a maximum reduction of 11.8% is observed in one of the test results, this observed change should be interpreted in the light of the observed scatter of the data standard deviation and coefficient of variation which in this case was 33.7 ksi and 8.1% respectively. Overall, given the coefficient of variations and insignificant changes of the tensile strength, it can be concluded that, conditioning/aging of the materials, up to 7000 hr, does not degrade the tensile strength of the composite. It should also be noted that the changes in tensile strength reflect the changes in the ultimate strength of the material rather than the guaranteed strength of the material which the latter is used in the design process. The ultimate strength of the material is approximately 30% higher than the guaranteed strength reported by the manufacturer. Therefore, the guaranteed strength of the material, which is used in design, is not affected by the conditioning.

3.5   Prediction of Long-Term Performance of CFRP Tendon

3.5.1   Arrhenius model

Accelerated aging tests are used to accelerate the aging process by exposing the samples to di ferent conditions at elevated temperatures. Based on the short-term data from accelerated aging tests, the popular Arrhenius model was adopted to predict the long-term behavior of the GFRP bars. In the Arrhenius relation, the degradation rate is expressed as Eq. 3.9 (Nelson 1990).

$$k = A\exp\left(\frac{-E_a}{RT}\right) \tag{3.9}$$

where k=degradation rate (1/time); A=constant of the material and degradation process; E_a=activation energy; R=universal gas constant; and T=temperature in kelvin. The primary assumption of this model is that the single dominant degradation mechanism of the material will not change with time and temperature during the exposure, but the rate of degradation is accelerated with the increase in temperature (Benmokrane et al. 2016; Bank et al. 2003; Chen et al. 2007).

Based on the Arrhenius model, Bank et al. (2003) proposed a service-life prediction procedure for FRP materials that the accelerated aging data could be calculated and plotted with the percentage of property retention in linear scale versus time in logarithmic scale (Figure 3.34). By using linear regression, a regression line can be fit through each set of data (one for each aging temperature) of which an acceptable regression line must have an R^2 of at least 0.80 (Bank et al. 2003). The data plot can be constructed in one of the two ways: time may be plotted as a function of inverse absolute temperature for various percentages of property retention or property retention may be plotted as a function of inverse absolute temperature for various chosen lifetimes (Bank et al. 2003). Thus, the relationship among service life, temperature, and strength retention in CFRP tendon can be obtained. This approach provided a good procedure for the prediction of longterm performance of FRP materials.

3.5.2 Prediction method based on Fick's law

Fick's law has been used to predict the residual strength of FRP bars embedded in concrete. The prediction method in Fick's law depends on the diffusion coefficient; where the rate of diffusion of elements or compounds has a significant impact on the FRP bars' residual strength. Shen and Springer (1976) recommended that the diffusion coefficient (required in Fick's law) be obtained using Eq. (3.10). In 1995, Katsuki and Uomoto proposed also a prediction model based on Fick's first law. They assumed that the tensile strength of FRP bar can be determined quantitatively by the amount of alkali penetration area into the bars and recommended that the depth of penetration be calculated using Eq. (3.11)

$$D = \frac{\pi r^2}{16} \left[\frac{M_2 - M_1}{M_m} \right]^2 \left[\frac{1}{\sqrt{t_2 - t_1}} \right]^2$$

(3.10)

where, M_1, M_2, and Mm are the moisture contents of the bar (in percent) at time t_1, t_2, and at saturation, respectively.

$$X = \sqrt{2.D.C.t}$$

(3.11)

Where, X is the depth of penetration from the surface, C is the alkaline concentration (percent), t is the curing time, and D is the diffusion coefficient. It should be noted that various units can be used in this equation and the units of the square root of the product should result in a length unit. Katsuki and Uomoto (1995) assumed that as glass fibers were exposed to the diffusing solution, these fibers exhibited complete failure and no longer contributed to the bars' capacity. Using this assumption, the authors proposed the following equation for estimating the residual strength (Eq. 3.12).

$$f_t = \left[1 - \frac{X}{R_O} \right]^2 \cdot f_0$$

(3.12)

where, f_0 and f_t are the transverse shear-strengths before and after exposure (MPa), respectively,

and R_0 is the radius of CFRP tendon. A similar approach was proposed by Tannous and Saadat-manesh (1998). Using results from moisture absorption and tensile strength tests, the authors recommended that Fick's law be used to predict the residual strength.

3.5.3   Fib Bulletin (40) model

Predications of the long-term tensile strength retention of the CFRP tendons were performed according to the method in fib Bulletin 40 (2007). The method includes a safety factor for tensile strength that takes into account tensile deterioration with time. The tensile strength should be reduced by $\eta_{env,b}$ determined according to the equation below.

$$\eta_{env,t} = \frac{1}{[(100 - R_{10})/100]^n} \tag{3.14}$$

$$n = n_{mo} + n_T + n_{SL} + n_d \tag{3.15}$$

where n_{mo}, n_T, and n_{SL} are the influence terms for moisture condition, temperature, and desired service life, respectively. R_{10} is the standard reduction in tensile strength in percent per decade (logarithmic decade) due to environmental effects, which can be extrapolated from each individual degradation line (see Figure 3.36).

3.5.4   New life prediction model for CFRP tendons

In order to achieve more refined design of CFRP tendons reinforced concrete under service, environmental RFs need to be developed by taking all the effects of service temperature, RH, and design life into account. Several publications revealed that the degradation behavior of FRP bar subjected to solutions or moisture saturated concrete would follow Arrhenius empirical model (Bank et al. 2003; Dejke and Tepfers 2001; FIB 2007). In this study, based on the new model first proposed by Huang and Aboutaha (2010), that incorporates the effects of temperature, design life, and relative humidity (RH) of exposure into the environmental reduction factor (RF) for the FRP bars will be presented. Eq. (6) expresses the strength retention of FRP bar for specific design service life and service temperature [Huang and Aboutaha (2010)].

$$f_d = f_u \cdot [1 - \Delta_1 - (\Delta_2 + \Delta_3)] \tag{3.16}$$

where f_d = design value or predicted value for tensile strength and f_u = characteristic value for tensile strength. The Δ_1 strength reduction value can be obtained by the experimental result as shown in Figure 3.34. Δ_2 can be obtained by the triangular relationship from Figure 3.34 as presented in Eq. 3.17:

$$\Delta_2 = (tg\alpha) \cdot [\log(t_D) - \log(292)] = (-\phi) \cdot \log(t_D/292) = (-\phi) \cdot \log(DL) \tag{3.17}$$

where ϕ = slope of the regression line as can be obtained by linear regression also; t_D = design lifetime in days; and DL = design life in years. Similarly, Δ_3 value can be obtained from Eq. 3.18:

$$\Delta_3 = (tg\alpha) \,.\, [\log(ts) - \log(t_D)] = (-\phi) \,.\, \log(ts\,/\,t_D) = (-\phi) \,.\, \log(TSF) \tag{3.18}$$

where t_S = lifetime in days by time temperature shift from T to T_1; and TSF is the time shift factor for temperature T and temperature T_1, which can be calculate based on proposed approach by Dejke and Tepfers (2001) as follows in Eq. 3.19.

$$TSF = \mathrm{e}^{[B/(T1+273.15)] - [B/(T2+273.15)]} \tag{3.19}$$

By substituting the values of $\Delta 2$ and $\Delta 3$ into Eq. (3.16), f_d can be rewritten as Eq. (3.20)

$$f_d = f_u \,.\, [1 - \Delta_1 + \phi \,.\, \log(DL \,.\, TSF)] \tag{3.20}$$

It is known that the contained water in concrete can be classified as capillary water, adsorbed water, interlayer water and chemically combined water. Huang and Aboutaha (2010) noted that the transportation of OH- can only occur in capillary water and some adsorbed water, which could be easily affected by the environmental relative humidity (RH). In moisture-saturated concrete, the degradation rate of FRP bars is the highest, and the degradation rate under less humidity can be adjusted using a correction factor (nH), which is closely related to the RH. The correction factor (n_H) was assumed to be the same as the ratio of capillary and adsorbed water in the water content in concrete, as shown in Figure 3.38. The data presented in Fig. 3.38 are adapted from Huang and Aboutaha (2010). Thus the design tensile strength or predicted strength of GFRP bars in both saturated and unsaturated concretes can be written as Eq. (3.21)

$$f_d = f_u \,.\, [1 - \Delta 1 + \phi \,.\, \log(DL \,.\, TSF) \,.\, n_H] = f_u \,.\, RF \tag{3.21}$$

where RF = reduction factor of tensile strength for the effects of service lifetime, temperature, and RH; n_H would be equal to the ratio of mobile water in concrete under different RHs as shown in Figure 3.36. Δ_1, ϕ can be obtained by the accelerated aging data through linear regression. In this study, the residual tensile strength of stressed GFRP bars (under sustained load of 30%) exposed to alkaline solution was used for long-term performance prediction based on the Arrhenius model and new model that incorporates the effects of temperature, design life, and relative humidity (RH) of exposure into the environmental reduction factor (RF) for the FRP bars used as concrete reinforcement. The prediction results and discussion are presented in the following section.

3.6   Results and Discussion for the Prediction of Long-Term Behavior and Service Life of CFRP Tendons

3.6.1. Arrhenius model for CFRP tendons under sustained load (65% of loading)

Predictions of the service life of the CFRP tendons, at mean annual temperatures (MAT) of 10°C [50°F] and 50°C [122°F] were performed according to the procedure based on previous work performed by Bank et al. (2003). In addition annual temperature (MAT) of 27°C [81°F] was performed according to weather condition of Florida State. The temperature of 10°C [50°F] is a close approximation of the mean average temperature of northern regions, where deicing salts are often used. The

temperature of 50°C [122°F] exacerbates the combined effect of the mean annual temperature and the marine environment of the Middle East, Caribbean, and Florida (Robert and Benmokrane 2013). The Arrhenius plot can be used to extrapolate the service life necessary to reach the established tensile-strength retention levels (PR) for any temperature. Consequently, predictions were made for tensile-strength retention as a function of time for immersions at 10°C [50°F], 27°C [81°F], and 50°C [122°F]. Figure 3.35 provides the general relationship between the PR and the predicted service life at the two MATs for CFRP tendons, respectively. This figure shows that the predicted strength-property retention level (PR) for the CFRP specimens immersed at an isotherm temperature of 10°C [50°F] would be slightly affected over 150 or 200 years. For the same specimen immersed at an isotherm temperature of 50°C [122°F], the service-life predictions are approximately 10 and 200 years for a PR of 90% and 84%. For the same specimen immersed at an isotherm temperature of 27°C [81°F], the service-life predictions are approximately 10 and 200 years for a PR of 91% and 86%. As expected, these results show that the long-term tensile strength of the CFRP was more affected by the alkaline environment in a warm climate cpmpared to the cold climate. The predicted service life of CFRP embedded in an alkaline environment or aged in alkaline solution at an isotherm temperature of 10°C to reach a PR of less than 88% can be estimated at more than 200 years. Figure 3.35 indicates that, even after a service life of 150 years—which corresponds to the longest design service life—the tensile-strength retention was still over 88%, 86.9% and 84% for MATs of 10°C [50°F], 27oC [81°F] and 50°C [122°F], respectively.
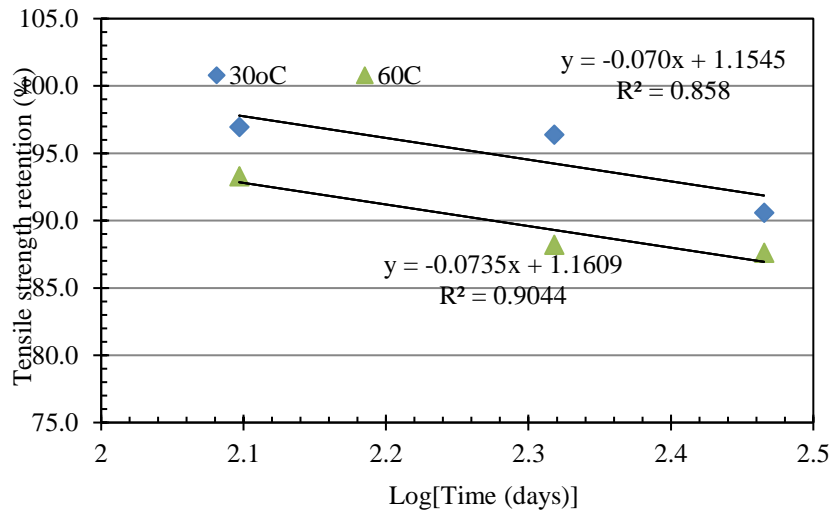
Figure 3.34: Strength retention versus log(time) for CFRP tendons after being embedded in solution at 30 and 60°C
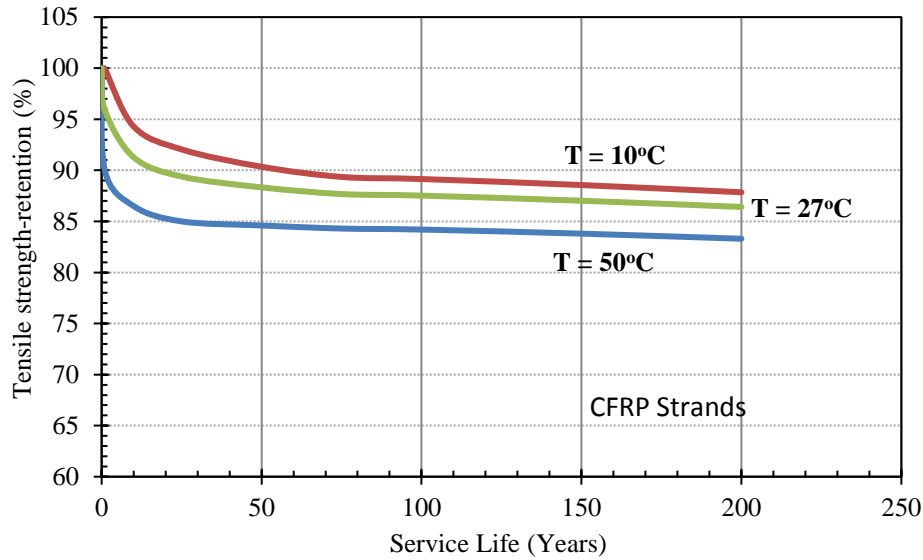
Figure 3.35: General relation between the PR and the predicted service life for CFRP tendons under sustained load (65% of loading), at mean annual temperatures of (10°C, 27°C and 50°C).

3.6.2. Prediction results based on Fick's law

The moisture contents of the CFRP tendons were 9.8, 10.9, and 11.6% at 24 hr, 7 days, and saturation, respectively. The the depth of penetration from the surface X was 0.214, 0.303, and 0.372 after 50, 100, and 150 years. The results showed that the predicted service life of CFRP embedded in an alkaline environment or aged in alkaline solution at temperature of 50°C was 89%, 85%, and 82% at 50, 100, and 150 years, respectively.

3.6.3. Fib Bulletin (40) results

The values of the environmental influence parameter R_{10} of the CFRP specimens conditioned at 30°C and 60°C were 3.3% and 3.8%. From the curve fitting, the shear-strength retentions after 100 years were 86% and 83% at 30°C and 60°C, respectively. According to fib Bulletin 40 (2007), for instance, $n_{mo}= 1$ and $n_{SL} = 3.0$ at a service life of 100 years, assuming a moisture-saturated condition. As adopted by Serbescu et al. (2014), n_T is equal to 1.0 and 2.5 at 30°C and 60°C, respectively. The value R_{10} for all the environments tested can be determined by using the average slope of the individual degradation lines, assuming that the degradation rate is similar regardless of environment (Serbescu et al. 2014). Thus, R_{10} is equal to 3.55%. The estimated tensile-strength retention ($1/ \eta_{env,b}$) is equal 84% and 80% at 30°C and 60°C, respectively. Noticeable differences between the two methods were observed for each environmental conditioning. The differences might be attributed to increased concrete strength resulting from immersion. This is not considered in the equation, nor are the effects of moisture diffusion on the degradation mechanism. Table 3.11 reports the ($1/\eta_{env,b}$) predications at different moisture-saturated conditions and mean annual temperatures (MATs) after 100 years of service life.
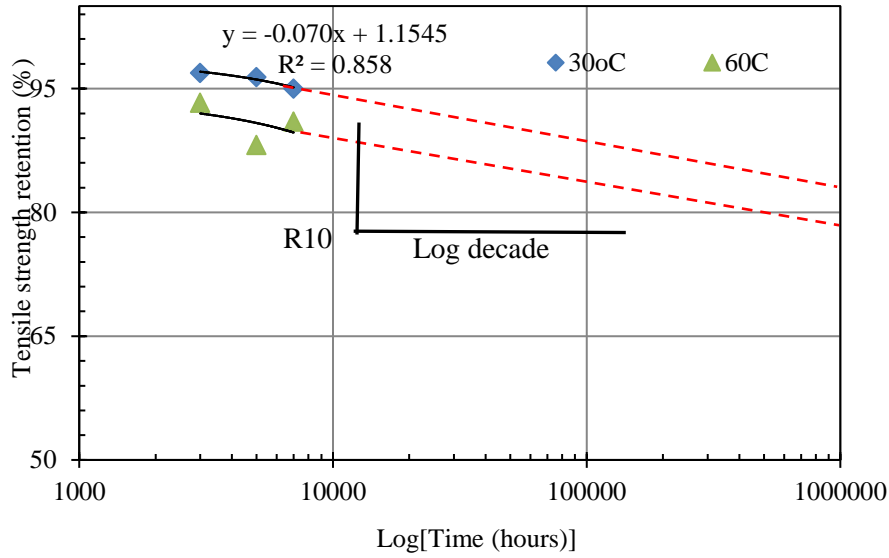
Figure 3.36: Experimental tensile strength-retention curves of CFRP tendons

Table 3.11: Tensile-strength-retention predications after service life of 100 years based on the method in fib Bulletin 40

Material	Moisture Condition	n_{mo}	MAT (oC)	n_T	n	$\eta_{env,b}$	1/ $\eta_{env,b}$
CFRP tendons	Dry (RH = 50%)	-1	<5	-0.5	1.5	1.0557149	0.94722543
			5~15	0	2	1.074968	0.93026025
			15~25	0.5	2.5	1.09457222	0.91359893
			25~35	1	3	1.11453395	0.89723601
	Moist (RH = 80%)	0	<5	-0.5	2.5	1.09457222	0.91359893
			5~15	0	3	1.11453395	0.89723601
			15~25	0.5	3.5	1.13485974	0.88116616
			25~35	1	4	1.1555562	0.86538413
	Moisture saturated (RH = 100%)	1	<5	-0.5	3.5	1.13485974	0.88116616
			5~15	0	4	1.1555562	0.86538413
			15~25	0.5	4.5	1.17663011	0.84988476
			25~35	1	5	1.19808834	0.834663

116

3.6.4. Results of the the new life prediction model for CFRP tendons

Based on the reported data of the current study, the property tensile retention value for specimens tested at each temperature (22°C [72°F] and 60°C [140°F]) and conditioning time (3,000, 5,000, and 7,000 hr) were calculated as the average property value at the time of testing (t) divided by the average property value for the reference specimen ($t=0$). These data were then plotted on a graph with time on the x-axis using a logarithmic scale (log-time), and the property retention value on the y-axis using a linear scale (Figure 3.34). Using linear regression, a line was fit through each data set (one for each conditioning temperature). The figure indicated that the slopes (ϕ) of the two regression lines are nearly the same, which is approximately equal to 16.0. The regression line must have a minimum r^2 of 0.80. In our case, the property tensile retention values used for the linear regression were chosen in the standard-deviation range to accommodate r^2 and all the r^2 values for regression lines at 22°C [72°F] and 60°C [140°F] were greater than 0.80. Meanwhile, by substituting log[7000h (292 days)] as the value of x in the equation of y=$-0.07x$ +1.1545, Δ_1 for T_1 (22°C) can be obtained as a value equal to 0.01805. The TSF value at each of the conditioning temperatures (60°C [140°F] and 22°C [22°F]) was obtained as of approximately 7.10. Then by Then by substituting the value (7.10) into Eq. (3.22) as the TSF value, the constant B can be obtained as a value of 5,059. Thus, the TSF value between the reference temperature (22°C [72°F]) and other selected temperature T can be obtained using Eq. (3.23). Figure 3.37 shows the TSF values versus temperatures.

$$TSF=e[B/(22+273.15)]–[B/(T+273.15)] \tag{3.22}$$

$$TSF=e[1,794/(22+273.15)]–[1,794/(T+273.15)] \tag{3.23}$$

By substituting DL=100 years, values of TSF from Figure 3.37 and values of n_H from Figure 3.38 into Eq. (3.21), the reduction factor (RF) can be obtained, as shown in Table 3.12, which presents the retention factor for tensile strength of CFRP tendons for some typical application temperature and RH with 100-year design life. Table 3.12 indicated that, for an environment with an RH of 100%, the values of the RFs of tensile strength are ranged between 0.79 and 0.90, in which the lower temperature, the greater RF value. It can be also observed that CFRP tendons have much better durability resistance in dry concrete than in moist concrete. For cases where RH<90% the values of the RFs, for the CFRP tendons, can retain over 94 % of its original tensile strength after 100 years service in concrete environment. While, these values were ranged between 91% and 95% for the RH=80%. As long as RH is under 80%, the RFs are greater than 90% (ACI 440.1R-15), even with elevated temperatures (up to 60°C). Therefore, in most case, CFRP tendons can provide excellent long-term performance in field concrete having lower exposure to temperature and humidity. Benmokrane et al. (2016) reported a study on experimental and analytical research to investigate the durability of Tokyo Rope CFRP tendons (without sustained load) for use as a corrosion-resistant reinforcing material for prestressed precast-concrete bridge-deck and pile applications. In such study, the tensile strength retention after 100 years is greater than 90% with the RH less than 100%.
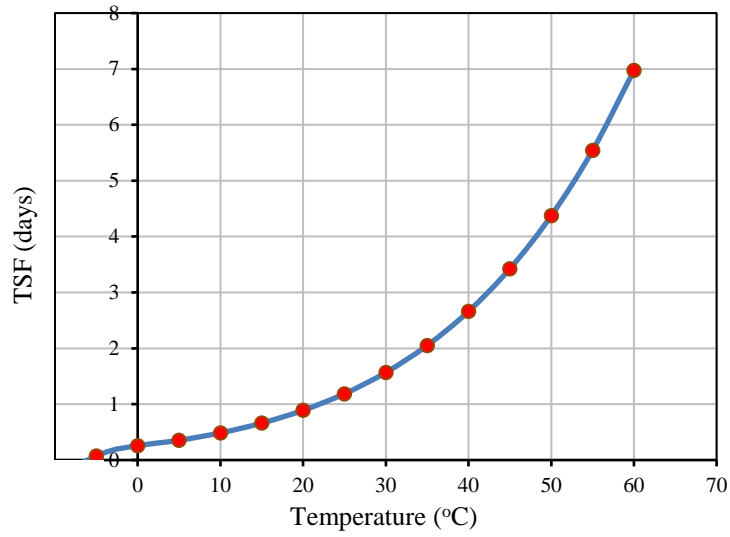
Figure 3.37: TSF versus temperature
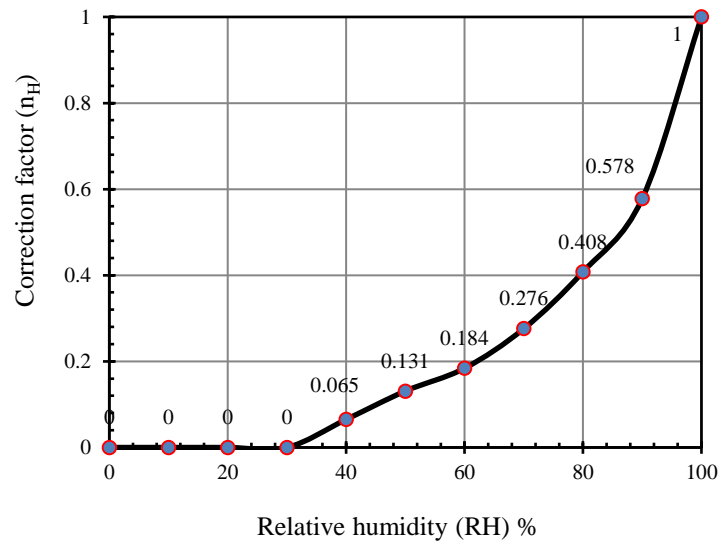
Figure 3.38: Relationship between the correction factor and the relative humidity (Adapted from Huang and Aboutaha 2010)

Table 3.12: Strength retention factor (RF) under different temperatures and RH for 100-years design life

T ºC	Tensile Retention Factor (RF)							
	100% RH	90% RH	80% RH	70% RH	60% RH	50% RH	40% RH	Less than 30 % RH
0	0.90	0.932	0.953	0.968	0.979	0.985	0.992	1
5	0.89	0.926	0.950	0.965	0.977	0.983	0.992	1
10	0.88	0.921	0.944	0.962	0.975	0.982	0.991	1
15	0.86	0.916	0.940	0.960	0.973	0.981	0.991	1
20	0.85	0.911	0.937	0.957	0.971	0.980	0.990	1
25	0.84	0.906	0.933	0.955	0.970	0.979	0.989	1
30	0.83	0.901	0.930	0.953	0.968	0.978	0.989	1
35	0.82	0.896	0.927	0.950	0.967	0.976	0.988	1
40	0.81	0.891	0.923	0.948	0.965	0.975	0.988	1
45	0.81	0.887	0.920	0.946	0.964	0.974	0.987	1
50	0.80	0.883	0.917	0.944	0.963	0.973	0.987	1
55	0.80	0.879	0.914	0.942	0.961	0.972	0.986	1
60	0.80	0.875	0.911	0.940	0.960	0.972	0.985	1

3.7   Test Protocol to Evaluate the Service Life and Degradation of CFRP Reinforcements

The research team conducted an extensive number of tests (mechanical, physical, durability characterization, and microstructure analysis) on FRP reinforcements. Based on the test results, the research team concluded that the most sensitive test method is the "Tensile Test under sustained load, elevated temperature of 140ºF (60ºC), alkaline solution of pH=12.8, and exposure duration of 3 months). The reason for choosing this tensile test and its associated factors as the most dominant effects (sustained load, elevated temperature, and alkaline exposure) is that the conditioned FRP reinforcements that performed properly in tensile test meeting the threshold (80% guaranteed tensile strength under un-sustained loading and 70% guaranteed tensile strength under sustained loading) also performed well under shear tests. In addition, the FRP reinforcement with acceptable tensile capacity retention did not reveal remarkable defects in the interface between the resin and fibers under microstructural analysis. In conclusion, the shear capacity retention and microstructure analysis were related to and consistent with the recommended tensile capacity retention. This recommended test was based on the reported results for CFRP on the tensile capacity, shear capacity, and microstructural analysis. Therefore, based on the observed degradation mechanisms and test results, a test protocol is recommended for rapid assessment of the durability and service life performance of FRP materials; which is the "Tensile Test for conditioned CFRP strands". The recommended test protocol is detailed for CFRP and listed in the following section.

Recommended Test Protocol: Tensile Test for Conditioned CFRP Bars:

1. **Specimen preparation should be conducted according to ASTM D7205 as follows:**

1.1 Specimens should be representative of the lot or batch being tested.

1.2 During the sampling and preparation of test specimens, all deformation, heating, outdoor exposure to ultraviolet light, and other factors possibly causing changes to the material properties of the specimen should be avoided.

1.3 The length of the specimen should be the sum of the length of the test section and the lengths of the anchoring sections. The length of the test section should not be less than 100 mm, nor should it be less than 40 times the diameter of the FRP bar.

1.4 The number of test specimens should not be less than five. If the specimen fails at or slips out of an anchoring section, an additional test should be performed on a separate specimen taken from the same lot as the failed specimen.

2. **Conditioning**

2.1 Standard conditioning procedure—Conditioning according to Procedure A of ASTM D 618 is recommended. Store and test specimens at the standard laboratory atmosphere ($23 \pm 3°C$ [73°F] and $60 \pm 10\%$ [140°F] relative humidity) and sustained load.

2.2 As a minimum time, FRP samples should be immersed in the alkaline solution at $60 \pm 3°C$ [140°F] for exposure times of 3 months.

2.3 Sustained load should be 65% for CFRP bars.

3. **Test method:**

3.1 When mounting the specimen on the testing machine, care should be taken to ensure that the longitudinal axis of the specimen coincides with the line joining the two anchorages fitted to the testing machine.

3.2 The load should be increased until tensile failure occurs. Strain measurements should be recorded until the load reaches at least 50% of the tensile capacity or the guaranteed tensile capacity, whichever is higher.

4. **Specified limits:**

4.1 Alkali resistance in high at least pH of 12.8 a solution (without load): Tensile capacity retention should be greater than 80% guaranteed tensile strength for FRP bars.

4.2 Alkali resistance in high pH solution (with sustained load): Tensile capacity retention should be greater than 70% guaranteed tensile strength for FRP bars.

In this testing protocol, the tensile test for conditioned CFRP (under 65% sustained load, elevated temperature of 140ºF (60ºC), alkaline solution of pH=12.8, and exposure duration of 3 months) is the most sensitive test method that also includes the most dominating effects (elevated temperature and alkaline solution) to material degradation.

The minimum exposure duration is specified to be 3 months and that is consistent with the CAN/CSA 806-12 and ACI 440.3R-4. The research team took into consideration the test

results reported for the 3-months exposure (for CFRP) and the available test results in the literature (Ali et al. 2018). The research team concluded that the minimum exposure duration of 3 months is representative of the degradation and can predict the long-term degradation of FRP reinforcements and the service life of FRP.

3.8 Conclusions

Physical characteristics:

Physical and microstructural analyses were conducted on Tokyo Rope CFRP tendons (diameter: 7.5 mm). The carbon fiber content was 82.5% by weight, and the water uptake at saturation is equal to 11.6%. The cure ratio of the material was very high (close to 100%). The DMA measurements show a slight increase of Tg after conditioning at 60°C. At 22°C, the increase is insignificant since the temperature is too low to post-cured/consolidate the material. Optical and electronic scanning microscopy analysis showed that a few voids were visible in the coating.

Tensile and transverse shear strength:

This research focuses on studying the possible degradation of CFRP prestressing strands due to exposure to simultaneous high alkali environment and sustained loading at an elevated temperature of 130 ºF (60 ºC) for durations up to 7,000 hr. The high alkali environment simulated the concrete pore solution and the elevated temperature was used to accelerate the aging process. The applied sustained load on the CFRP tendons was equivalent to 40% and 65% of their strength. Based on the results of this research, the following conclusions may be drawn:

a) For specimens without load:

1- The results indicate that specimen strength was affected by increased immersion time at higher temperatures. The test results after 7,000 hr of immersion in the alkaline solution at 60ºC [140ºF] reveal a 10.5 % reduction in tensile strength. The tensile-strength reduction was attributed to the development of microcracks in the epoxy resin, resulting essentially from the existing defects in the material. Diffusion of water along these microcracks and the fibers might also have weakened the interfacial adhesion between the carbon fibers and epoxy resin, which reduces the stress transfer between carbon fibers and, consequently, the composite's tensile strength.

2- The transverse-shear strength of the Tokyo Rope CFRP tendons was significantly affected by accelerated aging (16.5 % reduction after 7,000 hr).

b) For specimens with load = 65%:

3- The results indicate that specimen strength was affected by increased immersion time at higher temperatures. The test results after 7,000 hr of immersion in the alkaline solution at 60ºC reveal a 12.3 % reduction in tensile strength.

c) For specimens with load = 40%:

4- The test results after 7,000 hr of immersion in the alkaline solution at 60°C [140°F] reveal a 9.4 % reduction in tensile strength.

Conclusions on Models

Based on the results of this research, the following conclusions may be drawn:

1- Long-term-behavior predictions of the conditioned CFRP and GFRP specimens were made with a method based on the Arrhenius theory. Accordingly, the CFRP specimen immersed at an iso-therm temperature of 50°C, the service-life predictions are approximately 10 and 200 years for a PR of 90% and 84% (CFRP). As expected, these results show that the long-term tensile strength of the CFRP was more affected by the alkaline environment in a warm climate compared to the cold climate. While, the predicted service life of CFRP embedded in an alkaline environment or aged in alkaline solution at an isotherm temperature of 10°C to reach a PR of less than 88% (CFRP) can be estimated at more than 200 years.

2- According to Fib Bulletin (40) model, the tensile-strength retention predications of CFRP strands after 100 years of service life in dry, moist, and moisture-saturated environments with mean annual temperatures between 5°C and 35°C ranged from 84% to 95%.

3- Based on the test results and proposed service life prediction model, the tensile strength reten-tions (RF) for CFRP strands under sustained load, were predicted to be 91% and 82% (for CFRP) at a relative humidity (RH <90%) and a moisture saturated environment (RH=100%), respectively.

3.9   Recommendations

1- Based on the test results, the research team concluded that the most sensitive test method is the "Tensile Test under sustained load, elevated temperature of 140°F (60°C), alkaline solution of pH=12.8, and exposure duration of 3 months.
2- The Recommended test protocol of tensile test for conditioned FRP bars should be conducted in according with ASTM specifications.
3- The sustained load should be applied as 65% for CFRP.
4- Based on results of different performed tests, the tensile test for conditioned CFRP (under 65% sustained load, elevated temperature of 140°F (60°C), alkaline solution of pH=12.8, and exposure duration of 3 months) is the most sensitive test method that also includes the most dominating effects (elevated temperature and alkaline solution) to material degradation.
5- Based on the test results conducted on FRP reinforcements in this study, considering the rec-ommendation of the CAN/CSA 806-12 and ACI 440.3R-4, the minimum exposure duration is specified to be 3 months.

6- The new proposed service life prediction models (detailed in the previous sections 3.5.4) incorporate the effects of temperature, design life, and RH of exposure into the environmental reduction factor for the FRP bars. Based on the service-life prediction models, the tensile-strength retention is predicted to retain over 82% of guaranteed tensile strength (CFRP), after 100 years of service life in moist alkaline environment with elevated temperatures and under sustained load.

CHAPTER 4
DEGRADATION OF GFRP BARS UNDER SUSTAINED TENSILE LOADING IN HIGH ALKALI ENVIRONMENT AND ELEVATED TEMPERATURE

4.1 Introduction

In recent years, fiber-reinforced polymer (FRP) materials have emerged as an acceptable construction material for both new constructions and for the rehabilitation and strengthening of existing structures (Benmokrane et al. 2016; Ali et al. 2018). Fiber-reinforced composites offer better resistance to environmental agents as well as high stiffness-to-weight and strength-to-weight ratios when compared with conventional construction materials. Unfortunately, the long-term performance of GFRP under some special harsh environmental conditions such as in a high alkalinity environment, seawater, or deicing salts remains unresolved. The strength of the glass fibers and resin matrix, two constituents of the GFRP materials, can decrease when subjected to a wet alkaline environment. Therefore, the durability of GFRP bars is not straightforward topic. It tends to be more complex than corrosion of steel reinforcement because the durability of the FRPs is related not only to the strength of its constitutive materials (fibers and matrix) but also to the integrity of the interface between these two components while aging. Numerous studies have been conducted on the durability of FRP bars in simulated corrosive solutions. Immersion of the FRP reinforcements in various simulated corrosive solutions and acceleration of the associated processes with elevated temperatures represent the most commonly adopted research technique found in the literature (Micelli and Nanni 2004; Chen et al. 2007; Robert et al. 2010; Kamal and Boulfiza 2011; Al-Salloum et al. 2013). Furthermore, tests on FRP bars enveloped in concrete during environmental exposure were conducted by other researchers [e.g., Robert et al. (2009) and Robert and Benmokrane (2013)]. However, these studies were all conducted without sustained loading, which is different from the actual service conditions. Indeed, the micropores in the resin matrix give rise to stress concentrations when the bars are subjected to tensile stress, which accelerates the production of microcracks. These microcracks provide additional channels for the invasion of surrounding media and have an adverse effect on the durability of FRP bars.

This chapter presents the physical and mechanical properties of two different types of GFRP bars, named Pultrall GFRP (No. 5) and Aslan GFRP bars (No. 6), under sustained tensile loading (0 % and 30%) in high alkali environment at different temperature exposures (see Figure 4.1 and 4.2) . In addition, an investigation on the durability of GFRP bars made with three different types of resin suc as vinyl-ester, isophthalic polyester, or epoxy resins were evaluated and presented in this chapter.

Figure 4.1: Pultrall GFRP bars as received (GFRP #5)

Figure 4.2: Aslan GFRP bars as received (GFRP #6)

4.2 Procedures

4.2.1 Physical properties

The physical properties of the GFRP bars were determined according to the (ACI-440.6M, 2008) "Specification for Carbon and Glass Fiber-reinforced Polymer Bar Materials for Concrete Reinforcement" (when applicable) and (CSA-S807, 2010) "Specifications for Fiber Reinforced Polymer". Cross section area, fiber content, transverse coefficient of thermal expansion, void content, water absopaion, cure ratio, wicking, and glass transition temperature (T_g) were determined. Table**Error! Reference source not found.** 4.1 shows test method, number of specimens and specified limits of the each property.

4.2.1.1 Cross section area

Three specimens have been cut. Their length, L, and weight were then determined to calculate the linear mass. Their density has been measured by water displacement using a glass cylinder filled with water to the top, taking care that no air bubbles were entrapped. The cylinder was filled with water and weighed. Knowing the weight of the cylinder without water, the volume of water added, V_o, was calculated. Then the water was removed and the specimen placed into the cylinder which was filled with water to the same level as previously. The weight of the cylinder was measured and the volume of added water, V_I, determined. The average cross-sectional area, A, was then calculated as follows (Eq 3.1) (see Table 4.2):

$$A = 1000 \text{ x } (V_0\text{-}V_I)/L \qquad\qquad (4.1)$$

4.2.1.2 Fiber content

The glass fiber content was determined by pyrolysis according to (ASTM D 3171, 2011) – "Constituent Content of Composite, Method I: Procedure G". Three inch-long samples were accurately weighed (W_T) and heated at 600°C for 5 hr. Therafter, the sand (W_S) and glass fiber (W_F) weights were determined. The fiber content by weight was calculated as follows (Eq 3.1) (see Table 4.2):

$$F \text{ (Fiber Content by weight)} = 100 \cdot W_F/ (W_T - W_S) \qquad\qquad (4.2)$$

4.2.1.3 Transverse coefficient of thermal expansion

The transverse coefficient of thermal expansion, α, was determined according to (ASTM E 831, 2012) – "Linear Thermal Expansion of Solids Materials by Thermo-mechanical Analysis (TMA)". Three samples, 3 to 6 mm thick, were placed under the probe and the measurements conducted between -30° and 60°C with a heating rate of 3°C/min. The results of all the GFRP speicmens were reported in Table 4.2.

4.2.1.4 Water absorption

The Water/Moisture absorption was determined according to (ASTM D 570, 2010) - "Water Absorption of Plastics". Three inch- long specimens were cut, dried, and weighed. Then, the specimens were immersed in water at 50°C. After 24 hr, the samples were removed from water and the surface was dried and weighed. Thereafter, the specimens were immersed again and periodically weighed until fully saturated. The samples were considered as saturated when the weight became constant and then the samples were dried at 100°C and weighed. The water content in weight percent, W, was calculated as follows (Eq 3.3) (see Table 4.2):

$$W = 100 \cdot (P - P_d)/P_d \qquad\qquad (4.3)$$

where P and P_d were the weights of the bar after 24 h immersion (or full saturation) and in the dry state, respectively.

4.2.1.5   Cure ratio

The cure ratio was determinted according to (ASTM D 5028) – "Standard Test Method for Curing Properties of Pultrusion Resin by Thermal Analysis". The enthalpy of polymerization of the sample was measured by DSC and compared with the enthalpy of polymerization of the pure resin, taking into account the weight percentage of resin in the matrix. Thirty to fifty milligrams of samples were accurately weighed and placed in an aluminum crucible. Then, the samples were heated from room temperature to 200°C at 20°C/min and the area of the peak of polymerization was calculated. Table 4.2 shows a summary of the curing ratios results.

4.2.1.6   Glass transition temperature (Tg)

Glass transition temperature, Tg, was determined according to (ASTM D 3418) – "Transition Temperatures of Polymers by Thermal Analysis". The Tg was assigned by Differential Scanning Calorimetry (DSC) using ASTM E 1131 test method. Thirty to forty milligrams of composite samples were weighed and placed in an aluminum pan. Then, the samples were heated to 200°C under nitrogen at a heating rate of 20°C/min. The value of Tg was taken at the mid-height of the C_p jump.

4.2.1.7   Wicking

Three 2.54 mm (1-in.) length specimens were cut at random locations along the bars. To prevent the problem of wicking up the sides, a ring of clear nail polish was painted around the circumference of each specimen. A thin spongy material was placed on the bottom of glass pans to support the specimens and the pans were placed under a UV light source. A solution of 0.4% fuchsine aqueous solution was added to the pan such as the specimens will be immersed to a depth of 3.2 mm while resting on the sponge. The specimens were placed in the solution, such that their lower face was inserted into the dye (3 specimens of same size in each pan) and the time recorded. After 15 minutes, the number of upper face wicking dots was counted using a magnifier 5X and recorded. The test results are reported in Table 4.2.

4.2.2   Tensile properties

This section presents the tensile properties of two types of GFRP bars (Pultrall and Aslan GFRP bars), as part of the specification of the product to be used as internal reinforcement for concrete structures. The tensile properties were determined according to the (ACI-440.6M) and (CSA-S807).

4.2.2.1 Test specimens

A total of 88 specimens for each type [Pultrall GFRP bars (15.9 mm, No. 5) and Asaln GFRP bars (20 mm, (No. 6)] were tested in tension till failure and the tensile properties were determined. The GFRP bars were divided into two series: (1) the unconditioned control samples; and (2) the conditioned samples immersed in alkaline solution without load; (3) the conditioned samples immersed in alkaline solution under sustained load. The GFRP specimens were completely immersed in alkaline solution inside different stainless-steel containers. The alkaline solution was prepared using calcium hydroxide, potassium hydroxide, and sodium hydroxide (118.5 g of $Ca(OH)_2$ + 0.9 g of NaOH + 4.2 g of KOH in 1 L of deionized water) according to CSA S806 and ACI 440.3R. The pH of the alkali solution was 12.8. It is worth noting that the alkaline environment in concrete has a pH above 12 (ACI 440.4R-04). The GFRP specimens were kept at two different exposure temperatures (30°C and 60°C). The aging at ambient temperature (30°C) was performed by immersing the GFRP bars in a stainless-steel container filled with alkaline solution at room temperature. The stainless-steel containers were covered with polyethylene sheeting to prevent water evaporation during conditioning. Furthermore, the water level was kept constant throughout the study to avoid a pH increase resulting from a decreased water level and significant increase of alkaline ions in the solution. Two environmental chambers were used to accelerate the degradation of the GFRP specimens at 30°C, and 60°C, as shown in Figure 4.3. The immersion temperatures were chosen to accelerate the degradation effect of aging, but they were not high enough to produce any thermal-degradation mechanisms.

The GFRP specimen anchors were cast in a vertical position. The steel tubes and the GFRP specimens were axially aligned before the grout was poured according to ASTM D7205-A1.5 (Anchor Casting Procedure). CRAS expansive cement (Kayati 2014) was used in this study. The inside diameter and wall thickness of the steel tube were dependent on the bar diameter. The tensile tests were carried out using Baldwin testing machine in the structures laboratory in the Department of Civil Engineering at the University of Sherbrooke. The test specimens were instrumented with an extensometer of 200 mm (7.87 inch) length to capture elongation during testing. For each tensile test, the specimen was mounted in the tensile machine with the steel-pipe anchors gripped by the wedges of the machine's upper and lower jaws. The applied load and bar elongation were recorded with a computer data-acquisition system. Figure 4.4 shows the preparation of the test GFRP bar specimens.

(a) GFRP specimens (without load) in environmental chamber at 22ºC [72ºF]

(b) GFRP specimens (with load=30%) in environmental chamber at 60ºC [140ºF]

Figure 4.3: GFRP specimens (with load=30%) in environmental chamber at 60ºC [140ºF]

1- Fabricating the plastic rings

2- Installing the plastic rings with

2- Stell tubes preparation

4- Fill the grout

Figure 4.4: Preparation of the test GFRP bar specimens

4.2.2.2 Test method

The GFRP bars were tested in accordance with the (CSA-S806,-12), Annex C – "Test Method for Tensile Properties of FRP Reinforcement.", and (ACI-440.3R-04), Test Method B2 – "Test Method for Longitudinal Tensile Properties of FRP Bars". The test specimens were instrumented with two-linear -variable-displacement transducers (LVDTs) to capture the specimen elongation during testing. The tests were carried out using the Baldwin testing machine. The load was increased until the rupture failure occurred. The applied load and bar elongation were electronicaly recorded during the test using a computerized data acquisition system. Figure 4.5 shows the test setup and specimen during testing.

Figure 4.5: Test setup

4.2.2.3   GFRP specimens without load

This section presents the Pultrall GFRP bars (15.9 mm, No. 5) and Asaln GFRP bars (20 mm, No. 6) set in high pH solution (without load) under elevated temperature. A total of 40 specimens for each GFRP type were placed in alkali solution at 30 and 60°C environmental chamber for exposure time of 3,000; 5,000; and 7,000 hr. Thereafter, the test specimens were removed from the alkali solution and dried then test under tensile test.

4.2.2.3.1   Test specimens

For specimens without load, all GFRP bars were cut into lengths of 2,150 mm (84.6 inch) and 2,300 mm (90.5 inch), as specified in ASTM D7205, for Pultrall GFRP bars (No. 5) and Aslan GFRP bars (No. 6), respectively, as shown in Figure 4.6 and 4.7. The GFRP bars were divided into three series: (1) the unconditioned control samples, (2) the conditioned samples immersed in alkaline solution, and (3) the unconditioned samples under elevated temperature 60°C [140°F]. The GFRP specimens were completely immersed in alkaline solution inside different stainless-steel containers. The conditionings were conducted according to the (ACI-440.3R-04), Test method B.6, "Accelerated test method for alkali resistance of FRP bars" and (CSA-S806-12), Annex O, "Test method of alkali resistance of FRP rods". The GFRP samples were inserted in a conditioning container filled with an alkaline solution according to (CSA-S807-10) while the specimens were placed at 30 and 60°C environmental chamber for 3,000; 5,000; 7,000 hr. The level of alkaline solution and pH level were checked periodically and a new solution was added, when necessary. After each preiod of conditioning, the test specimens were dried and prepared with the steel anchorage tubes for the tensile test.

4.2.2.3.2 Test method

After three months of conditioning, the GFRP specimens were tested to deteremine the tensile properties according to (CSA-S806-12), Annex C – "Test Method for Tensile Properties of FRP Reinforcement", and ACI 440.3R-04, Test Method B2 - "Test Method for Longitudinal Tensile Properties of FRP Bars" same proceeding as mention previously in section 3.2.2. Figure 4.5shows the typical test specimen after drying and through the test. The ultimate tensile strength (f_u) and modulus of elasticity (E_L) of GFRP bars were reported in Table 4.3.
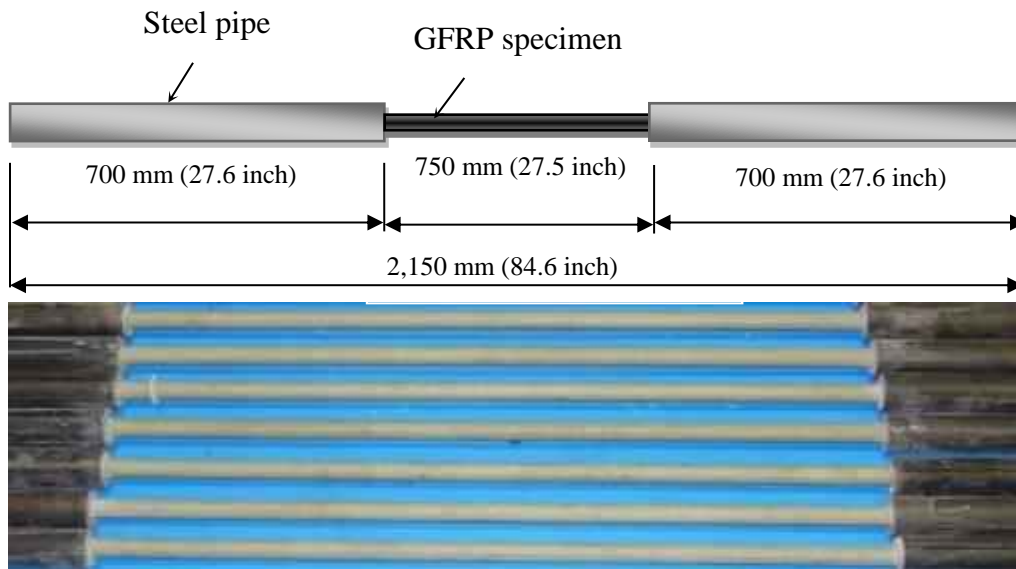
Figure 4.6: Dimensions of Pultrall GFRP specimens (without load)
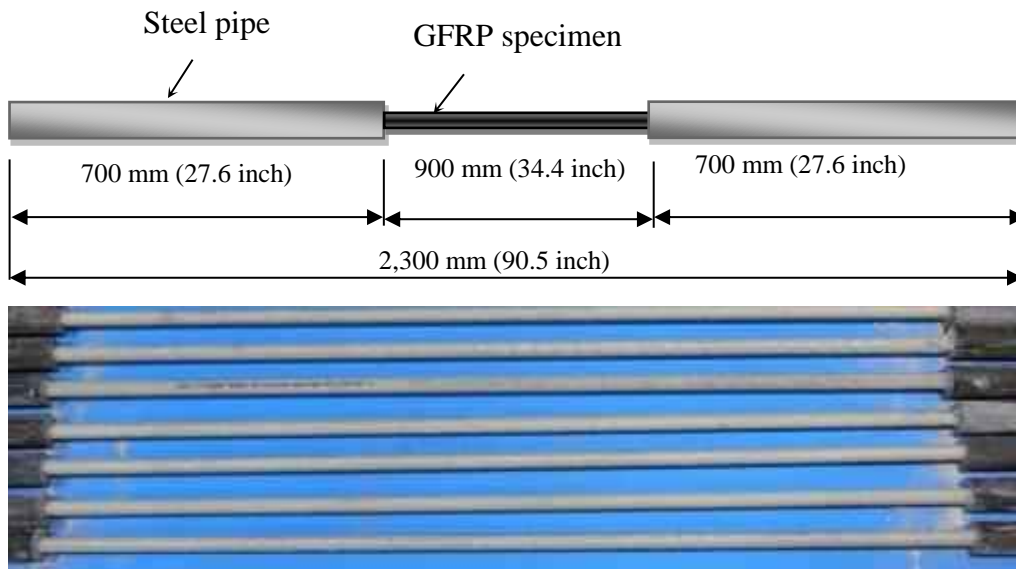
Figure 4.7: Dimensions of Aslan GFRP specimens (without load)

4.2.2.4   GFRP specimens with sustained load (30% of loading)

This section presents residual tensile properties of stressed GFRP bars [Pultrall GFRP bars (15.9 mm, No. 5) and Asaln GFRP bars (20 mm, No. 6)] exposed to harsh environments (alkaline soltion) at 30 and 60°C. A total of 48 speicmens for were placed under load in alkali solution at 30 and 60°C environmental chamber for exposure time of 3,000; 5,000; and 7,000 hr. The residual longitudinal tensile properties (f_u) and (E_L) of the GFRP conditioned specimens in high pH solution with load at elevated temperature, as required by (CSA-S807-10), were determined. The residual properties were compared to those of reference GFRP specimens (without conditioning).

4.2.2.4.1   Test specimens

For the specimens with sustained load (30% of loading), all GFRP bars were cut into lengths 2,400 mm (94.5 inch) as shown in Figure 4.8. The GFRP bars were divided into four series: (1) the unconditioned stress specimens at 22°C [72°F], (2) the unconditioned stress specimens at 60°C [140°F] and (3) the conditioned stress specimens immersed in alkaline solution at 22°C [72°F], and (4) the conditioned stress specimens immersed in alkaline solution at 60°C [140°F]. The GFRP specimens were completely immersed in alkaline solution inside different stainless-steel contain-ers. The specimens were prepared for conditioning on creep frame. Anchorage tubes and PVC cylinders for the alkaline solution were installed. Figure 4.8 presents the imensions of GFRP test specimens under sustained load, and the PVC cylinder installed directly on the bar and used for the conditioning in solution. The stressed specimens were tested under tensile test until failure, and the tensile properties [(modulus of elasticity (E_L), ultimate tensile strength (f_u), and ultimate strain (ε_u)] were determined.
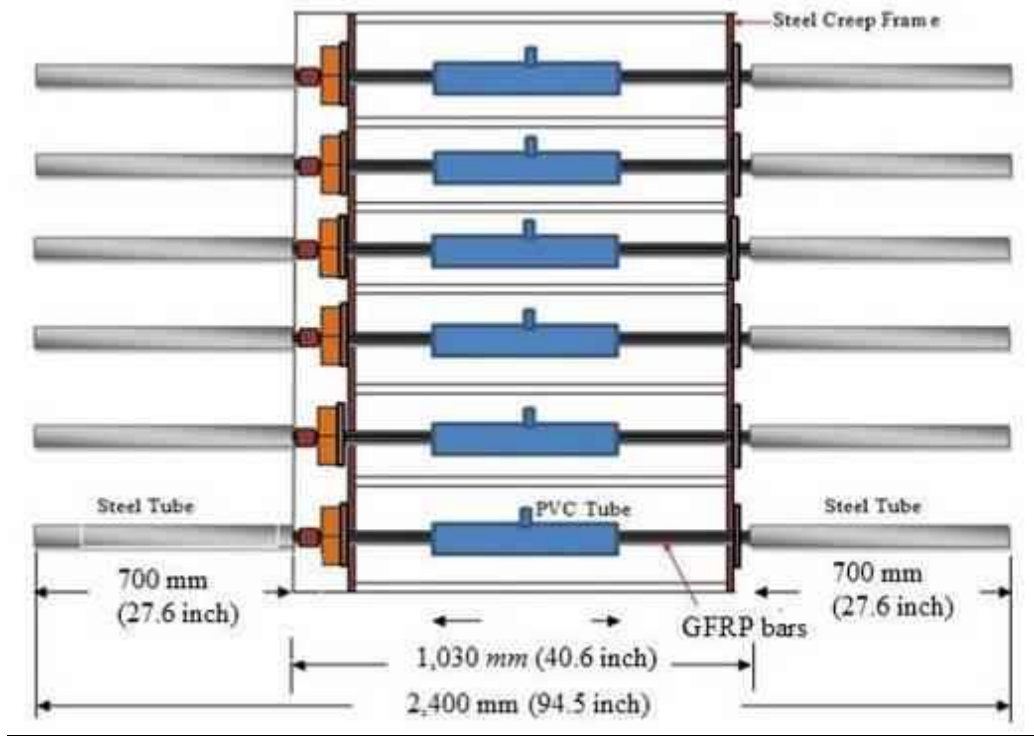
Figure 4.8: Dimensions of GFRP test specimens (under sustained load = 30%)

4.2.2.4.2 Test setup and procedure of specimens under sustained load

A specific sustained creep load frames were developed by the research group, at Sherbrooke University, to apply the sustained load on the GFRP bars, as shown in Figure 4.9. First, the axial load was applied using a hydraulic jack with the aid of a reaction frame and connector, and the applied load was monitored simultaneously using a load sensor. Second, the nut was tightened with a wrench and the hydraulic jack was unloaded after the load level was reached. According to preliminary research on the developed streel frame, a sustained load could be effectively maintained by the nut during the experiment. The middle test section of the bar was inserted into a PVC tube measuring 50 mm in diameter and 500 mm in length, which served as a reservoir, as shown in Figure 4.10. After the sustained load was applied, the two ends of the PVC tube were sealed with PVC capes. The prepared stressed specimen is shown in Figure 4.10. The preparation of the unconditioned stress specimens was the same as that of the conditioned stressed specimens except for the applied the alkaline solution. During the test, the pH value of the solutions was held constant according to regular inspection and solution supplement. Specimens were placed in a temperature (30 and 60°C) through the aging duration. A summary of the test program is presented in Table 4.7.

Figure 4.9: Test setup of stressed GFRP bars during the installation

Figure 4.10: GFRP stressed specimens (with 30% of loading) with sustained creep load frame

4.2.2.4.3 Test method

At the end of the conditioning, the 48 GFRP bars were tested in accordance with the (CSA-S806, 2012), Annex C – "Test Method for Tensile Properties of FRP Reinforcement", and ACI 440.3R (2004), Test Method B2 - "Test Method for Longitudinal Tensile Properties of FRP Bars" as perviuosly mentioned in section 3.2.2. The PVC cylinders were removed from the bars before the tests

to prevent any damage to the bar. The test specimens were then instrumented with an extensometer to capture the specimen elongation during testing (Figure 4.5). The tests were carried out using the Baldwin testing machine (Figure 4.5). The load was increased until tensile failure occurred. The applied load and bar elongation were electronically recorded during the test using a computerized data acquisition system. Through this test, the (f_u) and (E_L) were determined.

4.3 Results

4.3.1 Physical properties

Physical properties results of GFRP specimens on the Pultrall and Aslan bars showed that the tested GFRP bars satisfied the ACI and CSA requirements. The test results indicated that the fiber contents in weight of GFRP bars was 83.1% and 75.2%, respectively, for Pultrall and Asaln GFRP bars. The mass percentages of water uptake, for Pultrall and Asaln GFRP bars, after 24 hr were found to be 0.21% and 0.30% on average for the three grades, respectively. These values within the limits specified in CSA S807 (0.35%). Also, the mass percentages of water uptake at saturation for Pultrall and Asaln GFRP bars were found to be 0.24% and 0.9%, respectively. The water-absorption values obtained are within the limits specified in CSA S807 (0.75%). The material's cure ratio for all the tested Pultrall GFRP bars is high (close to 100%); while, the material's cure ratio for all the tested Aslan GFRP bars is less than 100 (close to 90%). The glass transition temperature for Pultrall and Asaln GFRP bars was visible from the thermograms obtained by Differential Scanning Calorimetry (DSC). Table 4.2 reported the physical properties for two types of GFRP bars.

Table 4.1**:** Properties, test method, number of specimens and specified limits

Property	Method	Number of specimens	Specified limit
Fiber content	ASTM D 3171 – "Constituent content of composite", Method I; Procedure G.	3	70% (by weight)
Transverse coefficient of thermal expansion	ASTM E 831 – "Linear Thermal Expansion of Solids Materials by Thermo-mechanical Analysis (TMA)".	3	$40 \cdot 10^{-6}\,^{\circ}C^{-1}$
Void Content	ASTM D 2734 – "Void Content of Reinforced Plastics"	3	1%
Water absorption	ASTM D 570 – "Water Absorption of Plastics"	5	1.00 % (D2) 0.75 % (D1)
Cure ratio	ASTM D 5028 – "Curing Properties of Pultrusion Resin by Thermal Analysis"	5	93 % (D2) 95 % (D1)
Glass transition temperature	ASTM D 3418 – "Transition Temperatures of Polymers by Thermal Analysis"	5	80°C (D2) 100°C (D1)

Table 4.2**:** Physical properties for GFRP bars

Bar type & Property	**Pultrall GFRP bars** No. 5 (15.9 mm)	Aslan **GFRP bars** No. 6 (20 mm)
Cross sectional area (mm^2)	181± 1.51	339± 0.91
Fiber content (%)	83.1 ± 0.0	75.2 ± 0.05
Transverse CET ($10^{-6}\,^{\circ}C^{-1}$)	22.1 ± 0.1	36.3 ± 1.03
T_g (ºC)	121 ± 2.1	87.0 ± 2.30
Water absorption @ 24 h (%)	0.20 ± 0.03	0.30 ± 0.03
Water absorption at saturation (%)	0.24 ± 0.03	0.90 ± 0.02
Cure ratio (%)	100 ± 0.0	90.6 ± 1.1
Wicking	0	0

4.3.2 SEM analysis

Cross sections of bar samples, one inch long, have been cut and placed in cylindrical molds, where epoxy resin was cast. After 24 hr of curing at room temperature, the samples were removed and cut using a low speed saw equipped with a diamond blade. Then, the specimens were polished using a polishing machine with three diamond pastes (15, 3, and 1 micron) before sputtering them with platinum. The specimens were then ready for analysis. Figures 4.11 and 4.12 show the typical views of the cross section of the Pultrall and Aslan GFRP Bars at low and high magnification, respectively. The degree of porosity of the material is high, in spite of a very low water absorption rate. However, no microcracks or poor fiber distribution were observed. Higher magnifications show that the fiber bonding is good since no free gaps are visible.
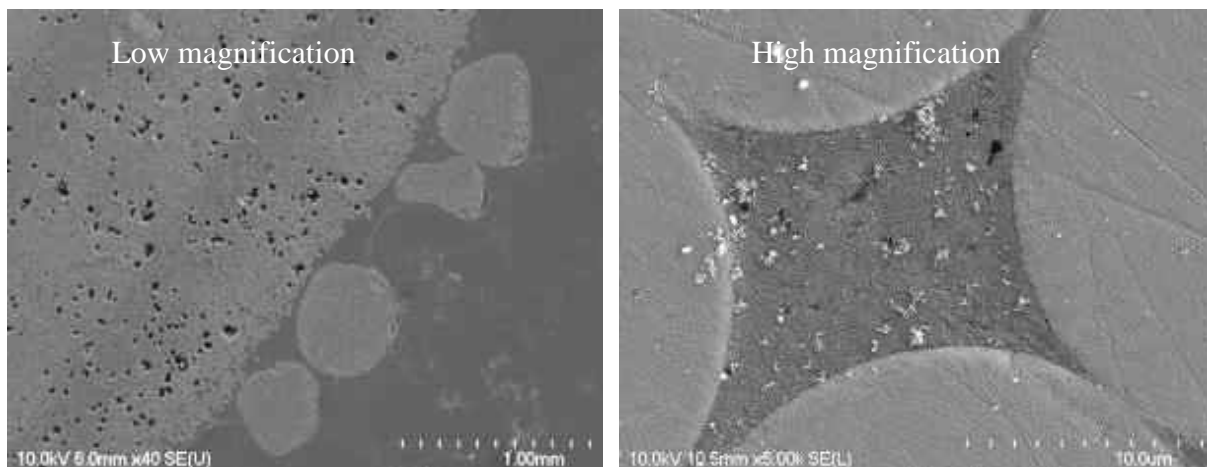
Figure 4.11: SEM picture of V-ROD Pultrall GFRP Bar No. 5
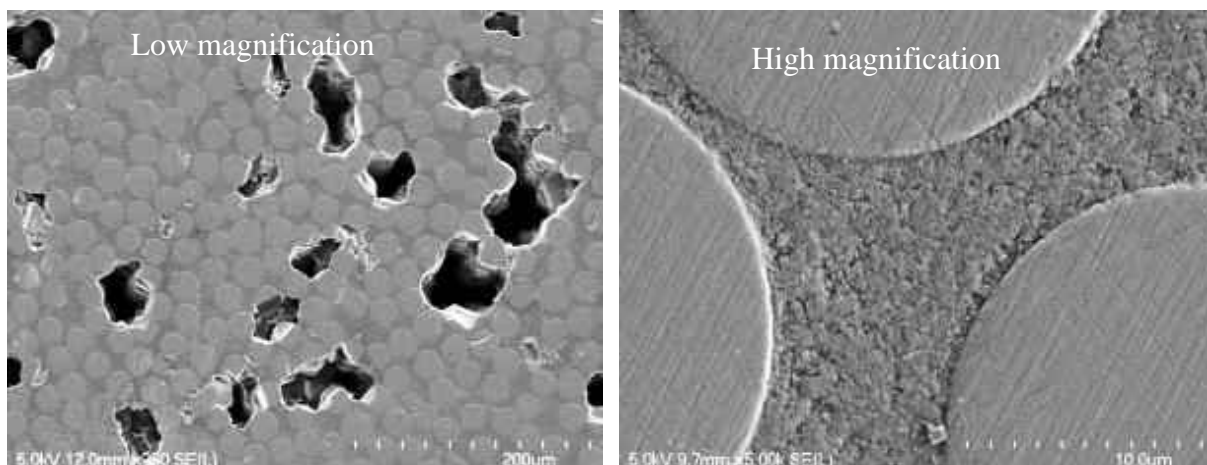
Figure 4.12: SEM picture of Aslan GFRP Bar No. 5

4.3.3 Tensile properties

Calculations

The tensile strength, f_{fu}, of GFRP bars was calculated according to the following equation:

$$f_u = \frac{F_u}{A}$$
(4.4)

where:

f_u = Tensile strength (MPa);
F_u = Tensile capacity (N); and
A = Cross-sectional area of the test bar (mm^2).

The tensile modulus of elasticity, E_L, was calculated from the difference between the load (stress)-strain curve values at 25 and 50% of the tensile capacity according to the following equation:

$$E_L = \frac{F_1 - F_2}{(\varepsilon_1 - \varepsilon_2)A}$$
(4.5)

where:

E_L = Longitudinal modulus of elasticity (MPa);
A = Cross-sectional area of the test bar (mm^2);
F_1 and ε_1 = Load and corresponding strain, respectively, at approximately 50% of the ultimate tensile capacity; and
F_2 and ε_2 = Load and corresponding strain, respectively, at approximately 25% of the ultimate tensile capacity, (N and dimensionless, respectively).

4.3.4 Test results and discussion

The test results of the tensile properties of the Pultrall and Aslan GFRP Bars GFRP were reported in Tables 4.3 to 4.9. The nominal cross-sectional areas provided by the (CSA-S807, 2010) were considered in the calculation of the tensile strength and the elastic modules for all the tested bars. The mode of failure is shown in Figure 4.13 and it can be noted that the tested bars failed in the middle of the bar (gauge length). It should be mentioned that the LVDTs were removed at about 80% of the ultimate capacity of the specimens not to break the LVDTs.

The test results indicated that the average reference tensile modulus of elasticity values for Putrall GFRP bars and Asaln GFRP bars were 51.5±0.8 and 54.8±1.1, respectively. The corresponding

ultimate tensile strengths were 1083±48.0 and 870 ±29.9MPa, respectively. Also, the corresponding ultimate strain values were 2.10±.07 and 1.6±0.1%. The tensile modulus of elasticity values were over the minimum limit of the ACI 440.6M and CSA-S807-10, 39.3 and 50 GPa, respectively. On the other hand, the ultimate tensile strengths and strains meet the requirements of the ACI 440.6M and CSA-S807-10. Table 4.3 shows the test results of the tensile modulus of elasticity, ultimate tensile strengths and strains of reference Putrall GFRP bars and Asaln GFRP bars. The results indicated that the tensile modulus for the bars of Putrall GFRP bars and Asaln GFRP bars ranged from 51 to 54 GPa, which it is over the ACI 440.6M and CSA-S807-10 limit (39.3 and 50 GPa, respectively). Also, the ultimate tensile meets the requirements of the ACI 440.6M and CSA-S807-10.
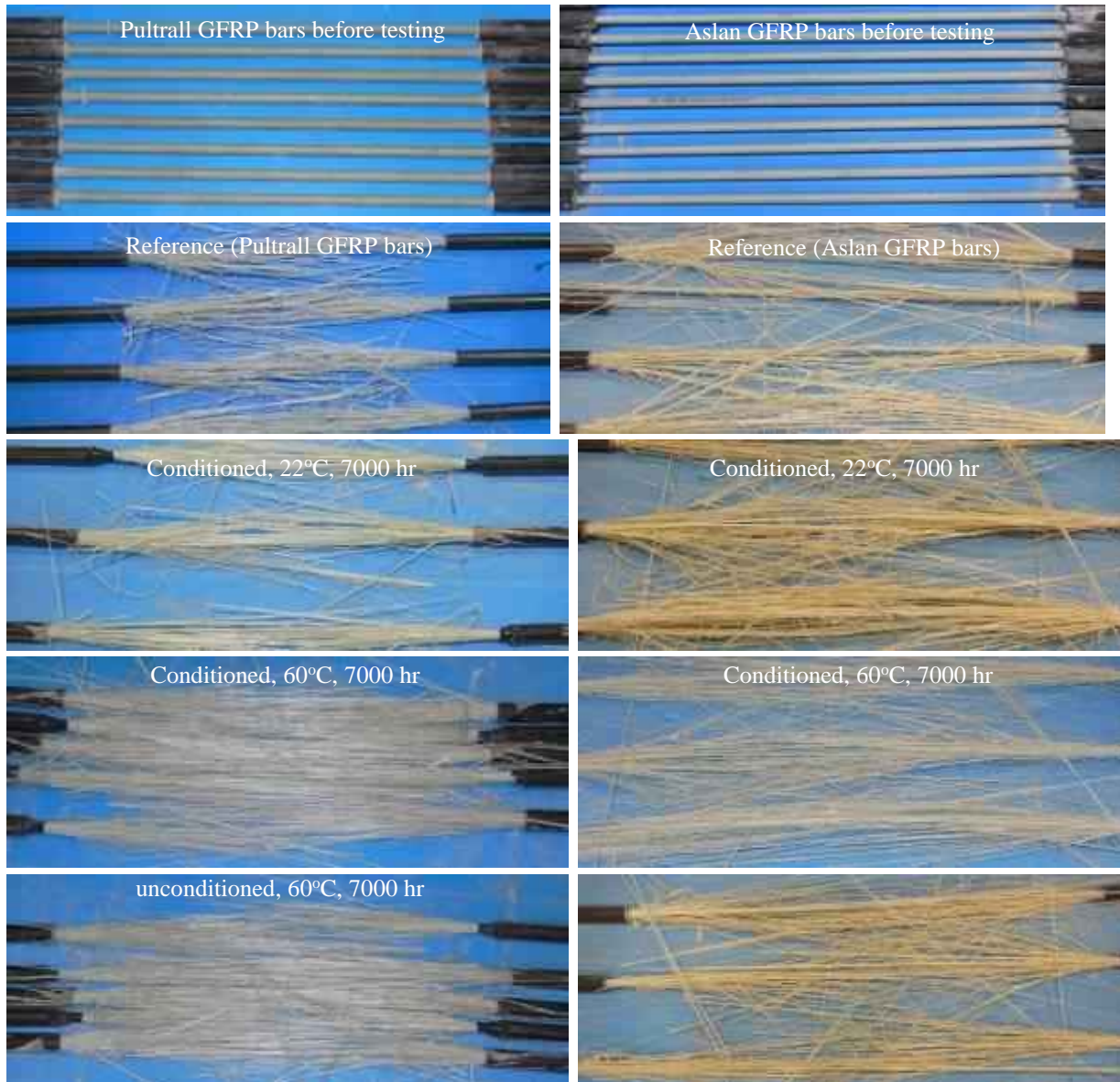
(a) Pultrall GFRP bars   **(b)** Aslan GFRP bars

Figure 4.13: Typical mode of failure for Pultrall and Aslan GFRP bars

4.3.4.1 GFRP specimens without load

4.3.4.1.1 Calculations

The f_u and E_L of GFRP bars were calculated by Eqns 4.4 and 4.5. The tensile property retention (strength and elastic modulus) was calculated according to the following equations:

$$R_{et} = (f_{u2}/f_{u1}) \times 100\% \tag{4.6}$$

$$E_{et} = (E_2/E_1) \times 100\% \tag{4.7}$$

Where,

R_{et} = Tensile capacity retention, %;

f_{u1} = Average tensile capacity of non-conditioned specimens (reference specimens), kN;

f_{u2} = Average tensile capacity of conditioned specimens, kN;

E_{et} = Elastic modulus retention, %;

E_1 = Average elastic modulus of non-conditioned specimens, GPa, and

E_2 = Average elastic modulus of conditioned specimens, GPa.

4.3.4.1.2 Test results and discussion

The test results of the tensile properties of the Pultrall and Aslan GFRP bars after 3,000; 5,000; and 7,000 hr conditioning and the retention of the tensile properties were reported in Tables 4.4 to 4.6. The nominal cross-sectional areas provided by the (CSA-S807, 2010) were considered in the calculation of the tensile strength and the elastic modules for all the tested bars. The typical mode of failure is shown in Figure 4.12 and it can be noted that the tested bars failed in the middle of the bar (gauge length). The failure was accompanied by the delamination of fibers and resin. The results for reference samples and conditioned specimens were compared in order to measure the effect of potentially high aging on short-term mechanical properties of Pultrall and Aslan GFRP bars. It can be noticed that the GFRP bars tested in this study show higher residual strengths compared to required limits of the Canadian codes (S807-10 and S806-12) and ACI 440. Tables 4.4 to 4.6 show the ultimate tensile properties of aged Pultrall and Aslan GFRP bars according to the duration of immersion at various temperatures. The tables show a decrease in the ultimate tensile strength of GFRP bars as the length of immersion increased. Furthermore immersion temperature clearly affected loss of strength. For Pultral GFRP bars without sustained load, the tables show that the loss of strength was 11% and 14.6% at 22ºC [72ºF] and 60ºC [140ºF], respectively, for 7,000 hr of immersion. While, the results of Asaln GFRP bars without sustained load showed that the loss of strength was 7% and 11% at 22ºC [72ºF] and 60ºC [140ºF], respectively, for 7,000 hr of immersion. All the tested GFRP bar presented a value greater than the specified limit for high durability (D_1) in (the CSA-S807, 2010) Standard (80%). Tables 4.4 to 4.6 present the change in the elastic modulus of aged bars with time of immersion at at 60°C. Indeed, it can be seen from the measured results that after 7,000 hr, the loss of elastic modulus is negligible and all aged bars are not affected by the higher temperature or alkaline solution.

This result shows that elastic modulus of bars is not significantly affected by aging in an alkali environment. The value of the modulus of elasticity retention for Pultral GFRP bars varied between 96 to 102% of the reference elastic modulus value.

Table 4.3: Tensile properties of GFRP reinforcing bars (refrence bars)

Bar Type	Bar Size	d_b (mm)	Area (mm²)	Modulus of elastic, E_L (GPa)			Ultimate tensile strength, f_u (MPa)	Ultimate tensile elongation, ε_u (%)
				Average value			Average value	Average value
Pultrall GFRP bars								
	No. 5	15.9	198	51.5±0.8 (7.4 x 10³ ksi)			1083±48.0 (157.1 ksi)	2.10±0.07
Aslan GFRP bars								
	No. 6	20.0	285	54.8±1.1 (8.0 x 10³ ksi)			870.1±29.9 (126.2 ksi)	1.6±0.1
ACI 440.6M limit				≥ 39.3 GPa			≥ 655 MPa	≥ 1.20 %
CSA-S807-10 limit				≥ 40 GPa (I)	≥ 50 GPa (II)	≥ 60 GPa (III)	(No.4, 5) ≥ 650 MPa; (No.6) ≥ 600 MPa;	≥ 1.20 %

Table 4.4: Tensile properties of conditioned GFRP reinforceing bars (after 3,000 hr of immersion), without load

Temp. (°C)	Bar Size	d_b (mm)	Area (mm²)	Modulus of elastic, E_L (GPa)	Ultimate tensile strength, f_u (MPa)	Ultimate tensile elongation, ε_u (%)
				Average value	Average value	Average value
Pultrall GFRP bars						
22°C, solution	No. 5	15.9	198	50.4±1.4 (7.3 x 10³ ksi)	1058±76 (153.0 ksi)	2.10±0.1
60°C, solution	No. 5	15.9	198	50.9±1.7 (7.4 x 10³ ksi)	985±62 (140.7 ksi)	1.95±0.1
60°C, no solution	No. 5	15.9	198	51.0±1.5 (7.4 x 10³ ksi)	1074±67 (155.8 ksi)	2.12±0.1
Aslan GFRP bars						
22°C, solution	No. 6	20.0	285	52.8±0.90 (7.7 x 10³ ksi)	836±6.0 (121.2 ksi)	1.58±0.02
60°C, solution	No. 6	20.0	285	50.9±2.1 (7.4 x 10³ ksi)	818±30.7 (118.6 ksi)	1.55±0.08
60°C, no solution	No. 6	20.0	285	50.8±1.7 (7.4 x 10³ ksi)	851±18.2 (123.4 ksi)	1.60±0.04

Table 4.5: Tensile properties of conditioned GFRP reinforceing bars (after 5,000 hr of immersion), without load

Temp. (°C)	Bar Size	d_b (mm)	Area (mm²)	Modulus of elastic, E_L (GPa)	Ultimate tensile strength, f_u (MPa)	Ultimate tensile elongation, ε_u (%)
				Average value	Average value	Average value
Pultrall GFRP bars						
22°C, solution	No. 5	15.9	198	50.1±1.1 (7.2 x 10³ ksi)	980±32 (142.1 ksi)	1.96±0.1
60°C, solution	No. 5	15.9	198	50.0±1.3 (7.2 x 10³ ksi)	964±42 (139.8 ksi)	1.93±0.1
60°C, no solution	No. 5	15.9	198	49.3±1.5 (7.1 x 10³ ksi)	1060±22 (153.7 ksi)	2.15±0.2
Aslan GFRP bars						
22°C, solution	No. 6	20.0	285	52.3±0.8 (7.7 x 10³ ksi)	821±3.5 (119.1 ksi)	1.57±0.05
60°C, solution	No. 6	20.0	285	51.2±2.1 (7.4 x 10³ ksi)	795±41.0 (115.3 ksi)	1.55±0.08
60°C, no solution	No. 6	20.0	285	50.0±1.9 (7.4 x 10³ ksi)	829±16.3 (120.2 ksi)	1.65±0.06

Table 4.6: Tensile properties of conditioned GFRP reinforceing bars (after 7,000 hr of immersion), without load

Temp. (°C)	Bar Size	d_b (mm)	Area (mm^2)	Modulus of elastic, E_L (GPa)	Ultimate tensile strength, f_u (MPa)	Ultimate tensile elongation, ε_u (%)
				Average value	Average value	Average value
Pultrall GFRP bars						
22°C, solution	No. 5	15.9	198	50.0±1.5 (7.3 x 10^3 ksi)	963±11 (139 ksi)	1.90±0.1
60°C, solution	No. 5	15.9	198	49.8 ±1.9 (7.2 x 10^3 ksi)	924±23 (134 ksi)	1.89±0.1
60°C, no solution	No. 5	15.9	198	51.6±2.1 (7.4 x 10^3 ksi)	1051±18 (152 ksi)	2.03±0.1
Aslan GFRP bars						
22°C, solution	No. 6	20.0	285	52.1±0.60 (7.6 x 10^3 ksi)	814±6.2 (117.6 ksi)	1.56±0.05
60°C, solution	No. 6	20.0	285	51.0±1.1 (7.4 x 10^3 ksi)	780±33.6 (110.9 ksi)	1.53±0.04
60°C, no solution	No. 6	20.0	285	50.8±1.4 (7.4 x 10^3 ksi)	816±15.2 (118.3 ksi)	1.61±0.05

4.3.4.2   GFRP specimens with sustained load (30% of loading)

The tensile strengths, f_u, of stressed Pultrall (No. 5) and Aslan (No. 6) GFRP bars after 3,000; 5,000; and 7,000 hr conditioning were calculated in accordance with Eqs 4.6 and 4.7. The nominal cross-sectional area as indicated in (CSA-S807, 2010) (198 and 285 mm^2 for No. 5 and No. 6, respectively) was considered in the calculation of the tensile strength and the elastic modulus of the bars. Tables 4.7 to 4.9 present the tensile properties of the Pultrall and Aslan GFRP bars after 3,000; 5,000; and 7,000 hr conditioning, under sustained load (30% of loading). There was no significant change noticed at the surface of GFRP bars due to aging high pH (pH = 13) solution under sustained load. Figure 4.12 shows that all the bars failed in the middle of the bars, as expected. The failure was accompanied by the delamination of fibers and resin. The tensile test of preloaded specimens showed almost a linear behavior up to failure.

As shown in Tables 4.7 to 4.9, the average residual tensile strengths for stressed Pultrall GFRP bars with sustained laod were equal to 957 and 906 MPa, at 22ºC [72ºF] and 60ºC [140ºF] for 7,000 hr of immersion respectively. The corresponding average residual tensile modulus of elasticity was 50.6 and 51.8 GPa, respectively. For the Asaln GFRP bars with sustained load, the residual tensile strengths for were equal to 802 and 716 MPa, at 22ºC and 60ºC [140ºF] for 7,000 hr of immersion, respectively. The corresponding average residual tensile modulus of elasticity was 50.8 and 49.5 GPa, respectively.The tested GFRP bars showed a value of tensile capacity retention over 85%. The tested GFRP bars meet the D1 requirement of (CSA-S807, 2010) for the alkali resistance in high pH solution with load (required limit is 70%).

Table 4.7: Tensile properties of conditioned GFRP reinforceing bars (after 3,000 hr of immersion), with sustained load (30%)

Temp. (ºC)	Bar Size	d_b (mm)	Area (mm²)	Modulus of elastic, E_L (GPa)	Ultimate tensile strength, f_u (MPa)	Ultimate tensile elongation, ε_u (%)
				Average value	Average value	Average value
Pultrall GFRP bars						
22ºC, no solution	No. 5	15.9	198	50.3±1.9 (7.3 x 10³ ksi)	1075±46 (155.9 ksi)	2.13±0.1
60ºC, no solution	No. 5	15.9	198	50.7±1.3 (7.4 x 10³ ksi)	1066±32 (155.4 ksi)	2.10±0.1
22ºC, solution	No. 5	15.9	198	51.3±1.6 (7.4 x 10³ ksi)	1039±38 (155.3 ksi)	2.03±0.1
60ºC, solution	No. 5	15.9	198	49.9±1.9 (7.3 x 10³ ksi)	975±22 (141.9 ksi)	1.95±0.0
Aslan GFRP bars						
22ºC, no solution	No. 6	20.0	285	52.1±1.90 (7.5 x 10³ ksi)	866±3.0 (125.6 ksi)	1.66±0.05
60ºC, no solution	No. 6	20.0	285	50.8±2.0 (7.4 x 10³ ksi)	847±13.2 (122.8 ksi)	1.67±0.10
22ºC, solution	No. 6	20.0	285	50.9±1.4 (7.4 x 10³ ksi)	831±1.9 (120.5 ksi)	1.63±0.08
60ºC, solution	No. 6	20.0	285	50.3±1.3 (7.3 x 10³ ksi)	813±11.2 (117.9 ksi)	1.61±0.03

Table 4.8: Tensile properties of conditioned GFRP reinforceing bars (after 5,000 hr of immersion), with sustained load (30%)

Temp. (ºC)	Bar Size	d_b (mm)	Area (mm²)	Modulus of elastic, E_L (GPa)	Ultimate tensile strength, f_u (MPa)	Ultimate tensile elongation, ε_u (%)
				Average value	Average value	Average value
Pultrall GFRP bars						
22ºC, no solution	No. 5	15.9	198	50.3±1.1 (7.3 x 10³ ksi)	1067±23 (154.8 ksi)	2.12±0.1
60ºC, no solution	No. 5	15.9	198	51.8±1.3 (7.5 x 10³ ksi)	1053±22 (152.7 ksi)	2.03±0.1
22ºC, solution	No. 5	15.9	198	52.1±1.5 (7.6 x 10³ ksi)	970±20 (141.3 ksi)	1.86±0.2
60ºC, solution	No. 5	15.9	198	50.8±1.5 (7.3 x 10³ ksi)	950±12 (137.9 ksi)	1.87±0.2
Aslan GFRP bars						
22ºC, no solution	No. 6	20.0	285	51.3±0.8 (7.4 x 10³ ksi)	857±7.5 (124.1 ksi)	1.67±0.06
60ºC, no solution	No. 6	20.0	285	51.3±2.1 (7.4 x 10³ ksi)	822±11.0 (119.3 ksi)	1.60±0.08
22ºC, solution	No. 6	20.0	285	51.0±1.9 (7.4 x 10³ ksi)	815±11.3 (118.2 ksi)	1.59±0.03
60ºC, solution	No. 6	20.0	285	50.0±1.9 (7.3 x 10³ ksi)	787±11.4 (113.6ksi)	1.57±0.04

Table 4.9: Tensile properties of conditioned GFRP reinforceing bars (after 7,000 hr of immersion), with sustained load (30%)

Temp. (ºC)	Bar Size	d_b (mm)	Area (mm^2)	Modulus of elastic, E_L (GPa)	Ultimate tensile strength, f_u (MPa)	Ultimate tensile elongation, ε_u (%)
				Average value	Average value	Average value
Pultrall GFRP bars						
22ºC, no solution	No. 5	15.9	198	50.1±1.7 (7.3 x 10^3 ksi)	1063±16 (154.1 ksi)	2.12±0.11
60ºC, no solution	No. 5	15.9	198	49.9 ±1.1 (7.2 x 10^3 ksi)	1048±21 (151.9 ksi)	2.10±0.12
22ºC, solution	No. 5	15.9	198	50.6±2.0 (7.3 x 10^3 ksi)	957±10 (138.8 ksi)	1.89±0.10
60ºC, solution	No. 5	15.9	198	51.8±2.0 (7.5 x 10^3 ksi)	906±13 (130.0 ksi)	1.75 ±0.10
Aslan GFRP bars						
22ºC, no solution	No. 6	20.0	285	52.6±0.1 (7.6 x 10^3 ksi)	848±3.4 (122.9 ksi)	1.61±0.02
60ºC, no solution	No. 6	20.0	285	51.9±1.1 (7.5 x 10^3 ksi)	805±13.8 (116.8 ksi)	1.55±0.03
22ºC, solution	No. 6	20.0	285	50.8±1.4 (7.4 x 10^3 ksi)	802±19.3 (116.3 ksi)	1.58±0.06
60ºC, solution	No. 6	20.0	285	49.5±1.4 (7.2 x 10^3 ksi)	716±16.3 (105.3 ksi)	1.46±0.10

4.4 Conclusions

4.4.1 Physical properties

Physical properties test results of Pultrall and Aslan bars showed that the test bars satisfied the ACI and CSA requirements (when applicable) for: 1) Glass fiber content, 2) Transverse coefficient of thermal expansion, 3) Moisture absorption, 4) Cure ratio, and 5) Glass transition temperature.

4.4.2 Tensile properties

Mechanical properties were given in this report as part of the certification of Pultrall and Aslan bars.

4.4.3 GFRP specimens without load

The average tensile strength retention of the tested Pultrall and Aslan GFRP bars conditioned during 3,000; 5,000; and 7,000 hr in high pH solution without load at 30°C and 60°C is over 85% for all the tested GFRP bars . All the tested Pultrall and Aslan GFRP bars presented a value greater than the specified limit for high durability (D1) in (the CSA-S807, 2010) Standard (80%). The modului of elasticity of the Pultrall and Aslan GFRP bars were not significantly affected by the immersion in high pH. The value of the modulus of elasticity retention for Pultral GFRP bars varied between 96 to 102 of the reference elastic modulus value.

4.4.4 GFRP specimens with sustained load (30% of loading)

The tested GFRP bars showed a value of tensile capacity retention over 83%. The tested GFRP bars meet the D1 requirement of (CSA-S807, 2010) for the alkali resistance in high pH solution with load (required limit is 70%).

The average residual tensile strengths for stressed Pultrall GFRP bars with sustained laod were equal to 957 and 906 MPa [138.8 and 131.4 ksi], at 22ºC [72ºF] and 60ºC [140ºF] for 7,000 hr of immersion respectively. The corresponding average residual tensile modulus of elasticity was 50.6 and 51.8 GPa, respectively. For the Asaln GFRP bars with sustained load, the residual tensile strengths for were equal to 802 and 716 MPa [116 and 103.8 ksi], at 22ºC [72ºF] and 60ºC [140ºF] for 7,000 hr of immersion, respectively. The corresponding average residual tensile modulus of elasticity was 50.8 and 49.5 GPa, respectively.

4.5 Degradation of GFRP Bars in High Alkali Environment and Elevated Temperature

4.5.1 Investigating the GFRP with different types of thermoset resins

In the last decade, noncorrosive glass fiber-reinforced-polymer (GFRP) bars have become more widely accepted as cost-effective alternatives to steel bars in many applications for concrete structures (bridges, parking garages, and water tanks). Also, these reinforcing bars are valuable for temporary concrete structures such as soft-eyes in tunneling works. The cost of the GFRP bars can be optimized considering the type of resin according the application. Yet limited research seems to have investigated the durability of GFRP bars manufactured with different types of resin matrix. In this study, the physical and mechanical properties of GFRP bars made with vinyl-ester, isophthalic polyester, or epoxy resins were evaluated first. The long-term performance of these bars under alkaline exposure simulating a concrete environment was then assessed in accordance with ASTM D7705. The alkaline exposure consisted in immersing the bars in an alkaline solution for 1000, 3000 and 5000 hr at different temperature (22, 40, and 60°C [140°F]) to accelerate the effects. Subsequently, the bar properties were assessed and compared with the values obtained on unconditioned reference specimens.

4.5.2 Test specimens

Three types of GFRP bars (isopolyester, vinyl ester, and epoxy GFRP Bars) manufactured by a German company (FIReP inc., 2013). The GFRP bars had a nominal diameter of 12 mm (0.472 inch) and were deformed with helical wrapping (Figure 4.14). The nominal cross-sectional area of three GFRP bars is 113 mm^2 (0.175 in^2.), as reported by the manufacture (FIReP inc., 2013). The GFRP specimen length and the length and diameter of the anchor to be used for the tensile test were calculated according to ASTM D7205 (ASTM 2011). Before the test was conducted, steel tubes were attached to the GFRP test specimens according to ASTM D7205 (ASTM 2011). Figure 4.15 shows the typical test of GFRP specimens.
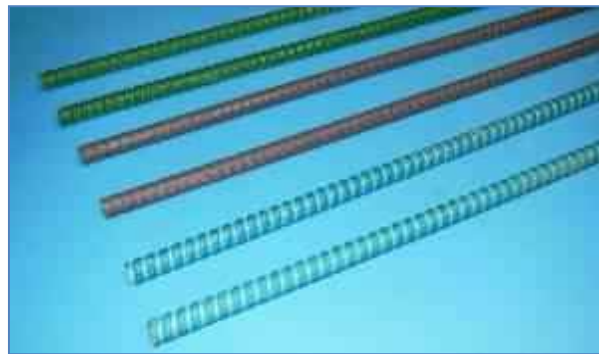
Figure 4.14: Overview of the GFRP specimens (12 mm, 0.472 inch)

Figure 4.15: Typical test GFRP specimens

4.5.3   Testing method

The GFRP bars were tested under tension according to the CSA-S806-12 (2012), Annex C–"Test Method for Tensile Properties of FRP Reinforcement", and ACI 440.3R-04 (2004), Test Method B2–"Test Method for Longitudinal Tensile Properties of FRP Bars". Each specimen was instrumented with a linear variable differential transformer (LVDT) to capture the elongation during testing. The test was carried out using a Baldwin testing machine in the structures laboratory of the Civil Engineering Department at the University of Sherbrooke. The load was increased until tensile failure occurred. For each tensile test, the specimen was mounted on the press with the steel pipe anchors gripped by the wedges of the upper and the lower jaw of the machine. The rate of loading ranged between 250 and 500 MPa/min (36.2 and 72.5 ksi/min). The applied load and bar elongation were recorded during the test using a data acquisition system monitored by a computer. Due to the brittle nature of GFRP, no yielding occurs and the stress-strain behavior was linear. Figure 4.16 shows typical test setup during testing. Through this test the ultimate tensile strength (f_u) and tensile modulus (E_L) of GFRP straight portions are determined.

Figure 4.16: Typical test setup

4.5.4 Environmental conditioning

The GFRP specimens were completely immersed in alkaline solution inside different metal containers. The alkaline solution was prepared using calcium hydroxide, potassium hydroxide, and sodium hydroxide (118.5 g of $Ca(OH)_2$ + 0.9 g of NaOH + 4.2 g of KOH in 1 L of deionized water) according to CSA S806 and ACI 440.3R. The pH of the alkali solution was 12.8. The GFRP specimens were kept at three different exposure temperatures (22°C, 40°C, and 60°C). The aging at ambient temperature (22°C) was performed by immersing the GFRP specimens in a metal container filled with alkaline solution at room temperature. The metal containers were covered with polyethylene sheeting to prevent water evaporation during conditioning. Furthermore, the water level was kept constant throughout the study to avoid a pH increase.

4.5.5 Physical properties results

Physical properties for the reference (unconditioned) and conditioned GFRP bars were determined according to ACI (2008) and CSA (2010) requirements, including: (1) fiber content, (2) moisture absorption, (3) cure ratio, and (4) glass transition temperature. The result showed that the glass/polyester and glass/epoxy FRP bars had approximately the same fiber content (78.8% and 79.4% by weight, respectively), while the glass/vinyl-ester FRP had the highest fiber–content ratio (83.9% by weight). The average cure ratios and transverse coefficients of thermal expansion of the tested bars were around 99.0±1.0 and 19.25±1.55×10−6°C−1, respectively, without significant differences between the three types of bars tested. On the other hand, significant differences were observed for Tg and moisture uptake. The vinyl-ester and polyester GFRP bars returned Tg values of 113°C and 93.0°C, respectively, while the epoxy GFRP bars had a Tg value of 126°C. Similarly, the vinyl-ester and polyester GFRP bars had water uptake ratios of 0.63% and 1.15%, respectively, while the epoxy GFRP bars had a moisture–uptake ratio of 0.23%. The limits of water absorption of the bars at saturation were <1% and <0.75% for high and medium durability, respectively, as recommended in CSA S807 (2010). The measured water absorption of the polyester GFRP bars was slightly higher than these limits, probably due to the resin-rich deformation pattern on the bar surface, which absorbed most of the moisture.

After 5,000 hr of conditioning, The Tg of the conditioned polyester GFRP bars were slightly higher than that of the reference specimens, as a result of post-curing at high temperature. The vinyl-ester and epoxy GFRP bars were almost fully cured (99.1% and 100%, respectively); their Tg values were lower than that of the reference specimens by 11.5% and 10.3%, respectively. Epoxy resin is known to lower Tg when water is absorbed (plasticizing effect). The water absorption of the epoxy GFRP bars was 0.2%. Table 4.10 presents the physical properties of the glass/polyester and glass/epoxy FRP bars.

Table 4.10: Cure ratio, *Tg*, and moisture uptake of the reference and conditioned GFRP bars

Property	GFRP bar type					
	Polyester		Vinyl-ester		Epoxy	
	Reference	5,000 hr	Reference	5,000 hr	Reference	5,000 hr
Cure ratio (%)	98	100	99	99	100	100
Tg (ºC)	93	98	113	100	126	112
Moisture uptake (%)	1.15	1.36	0.63	0.38	0.23	0.20

4.5.6   Microstructural analysis of the reference and conditioned GFRP bars

SEM observations were performed to investigate microstructural changes in the glass/polyester and glass/epoxy FRP bars before and after conditioning. The specimens were cut, polished, and coated with a thin layer of gold/palladium in a vapor-deposit process. The analysis was carried out on a JEOL JSM-840 A microscope (JEOL, Akishima, Tokyo, Japan). Figure 4.17 shows the SEM micrographs of the cross section of the reference glass/polyester and glass/epoxy FRP bars, while Figures 4.18 to 4.20 provide the SEM micrographs of the 5,000 hr conditioned specimens.

SEM analysis of the reference and conditioned specimens (Figures 4.17 to 4.22) indicates that the GFRP bars made with vinyl-ester and epoxy evidenced no significant changes, but presented a slight debonding at the interface between the fibers and vinyl-ester resin. Consequently, the vinyl-ester GFRP bars evidenced higher moisture uptake measured at saturation compared to the epoxy GFRP bars. On the other hand, the GFRP bars containing the polyester resin evidenced significant impact on the coating with the 5000 hr conditioning. Moreover, these bars experienced greater debonding at the fiber–resin interface than did the vinyl-ester and epoxy GFRP bars. Accordingly, the polyester GFRP bars had higher moisture uptake measured at saturation and higher degradation rate of mechanical properties after conditioning.

SEM was also performed on the fracture zones of the 1,000 hr specimens after short-beam testing (Figure 4.21) to investigate the mechanisms of failure at the interface fiber–matrix. The fiber surface of the vinyl-ester and epoxy GFRP bars had more resin coverage (Figure 4.21 [b and c]) than the polyester GFRP bars (Figure 4.21[a]). This observation corroborates the reduction ratio of the inter-laminar-shear strength and flexural strength after conditioning in the alkaline solution and characterizes the higher bonding of the glass fiber to the vinyl-ester and epoxy resins than the polyester resin.

4.5.7   Chemical changes in the conditioned GFRP bars

Fourier transform infrared spectroscopy (FTIR) was used to identify any chemical change/degradation after 5,000 hr of conditioning at 60ºC [140ºF]. FTIR spectra of the surface and core of the material

specimens were recorded using a Jasco 4600 spectrometer equipped with an attenuated total-reflectance device. Five hundred and twelve scans were routinely acquired at a resolution of 4 cm−1. Chemical degradation in the alkaline solution is mainly due to a hydrolysis reaction, which forms new hydroxyl (-OH) groups from sensitive units, such as ester groups. Hydroxyl groups appeared as a broad peak between 3200 and 3650 cm−1, which corresponds to the stretching mode of the hydroxyl groups in the polyester, vinyl-ester, and epoxy resins.

Figure 4.22 shows the FTIR spectra of the unconditioned and conditioned polyester, vinyl-ester, and epoxy GFRP specimens conditioned in the alkaline solution for 5,000 hr at 60°C. For each specimen—reference and conditioned—spectra of the surface and core of the specimen were recorded and the areas of the O–H and C–H peaks calculated as presented in Figure 4.23 presents the ratio of the (OH–) peak to the resin's carbon–hydrogen (C–H) stretching peak. The table indicates that none of the hydroxyl peaks for any of the tested vinyl-ester and epoxy GFRP specimens evidenced any significant changes, which equates to no increase in the amount of hydroxyl groups in the resins. This observation shows that the vinyl-ester and epoxy resins used did not degrade chemically while the specimens were immersed at 60ºC [140ºF] for 5,000 hr. On the other hand, the polyester resin showed significant differences on the surface and in the core of the tested specimens . The experimental O–H/C–H for the core and surface of the vinyl-ester and epoxy GFRP bars immersed for 5,000 hr were 1.5, 1.8, 1.2, and 1.5, respectively, compared to 1.80, 2.40, 1.25, and 1.6 for the unconditioned specimens, while the experimental ratios for the core and surface of the polyester GFRP bars immersed for 5,000 hr at 60ºC [140ºF] were 3.5 and 14.30, respectively. These results led to the conclusion that chemical degradation of the polymer occurred on the surface of the polyester bars, which was in direct contact with the solution during immersion. This observation explains the losses in mechanical properties of the polyester GFRP bars.
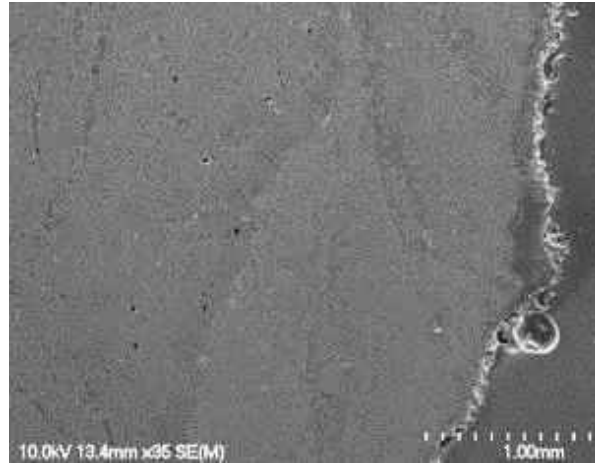
(a) Polyester GFRP bar
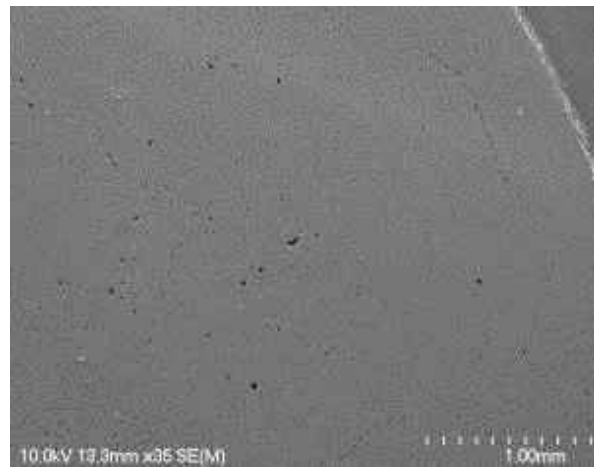
(b) Vinyl-ester GFRP bar
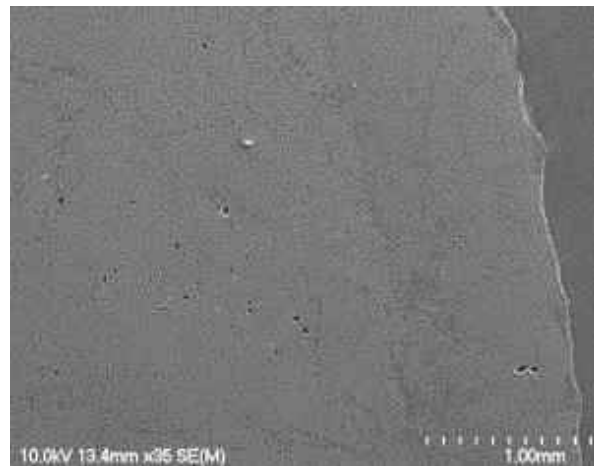
(c) Epoxy GFRP bar

Figure 4.17: Micrographs of the cross section of the reference GFRP bars
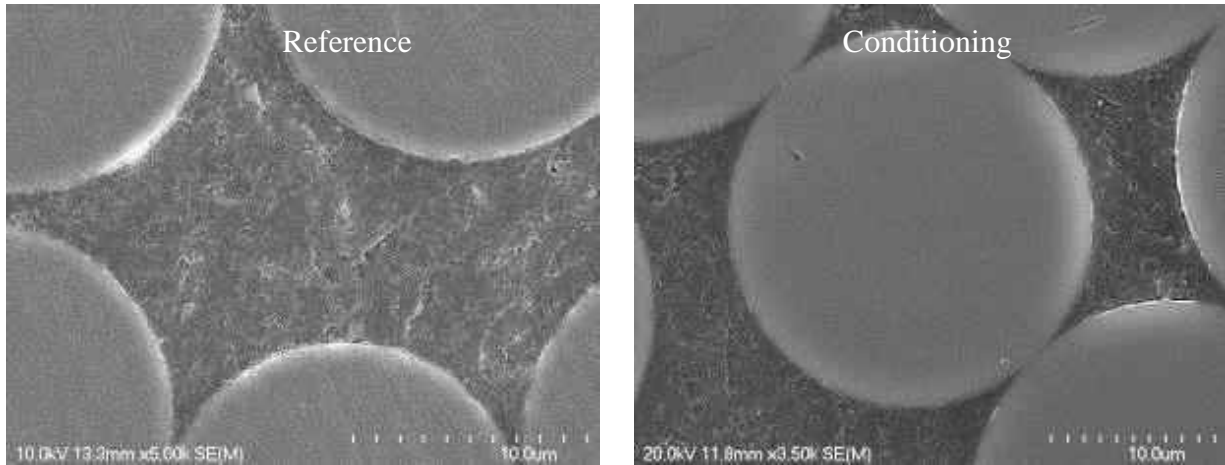
Figure 4.18: Micrographs of the fiber–matrix interface of an epoxy GFRP bars
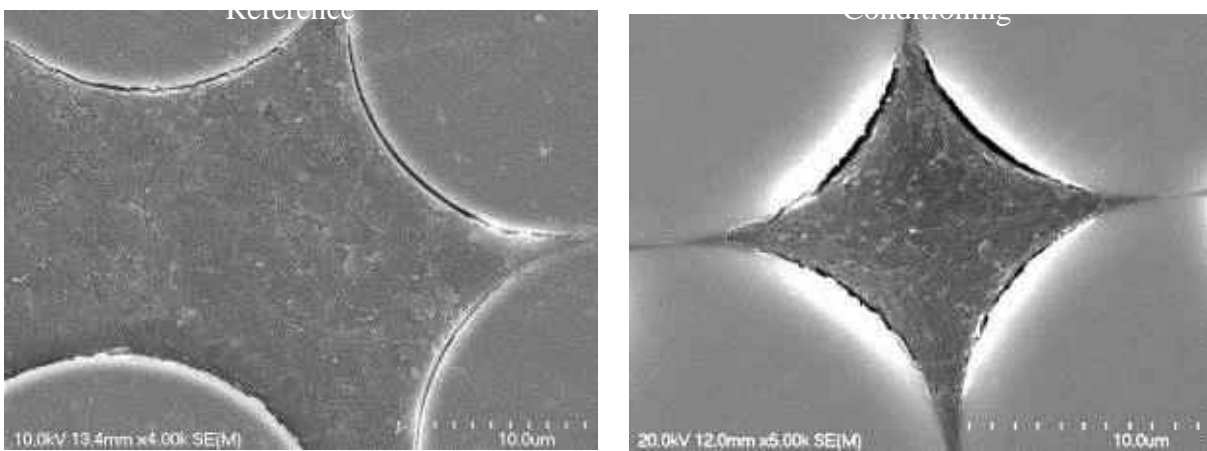
Figure 4.19: Micrographs of the fiber–matrix interface of a polyester GFRP bars
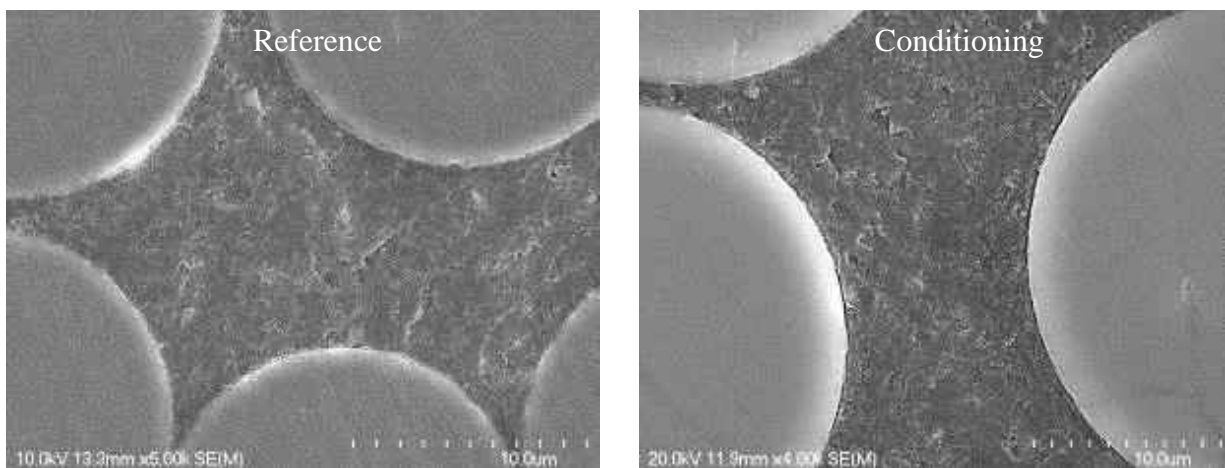
Figure 4.20: Micrographs of the fiber/matrix interface of a vinyl-ester GFRP bars before and after conditioning

4.5.8   Tensile properties results

4.5.8.1   Calculations

The f_u and E_L of GFRP bars were calculated by Eqns 4.4 and 4.5. The tensile property retention (strength and elastic modulus) was calculated according to the equations 4.6 and 4.7. The nominal cross-sectional areas provided by the (CSA-S807, 2010) were considered in the calculation of the tensile strength and the elastic modules for all the tested bars.

4.5.8.2   Test results and discussion

Table 4.11 reported the test results obtained during the tensile tests concerning the longitudinal tensile properties of the polyester, vinyl-ester, and epoxy GFRP aged bars tested after immersion at 22°C, 40°C, and 60°C for 1,000 hr, 3,000 hr, and 5,000 hr. The results indicate that the tensile strength was equal to 1015±21.7 Mpa [147.2±21.7 ksi], 1220±35.4 Mpa [176.9±35.4 ksi], and 1090±30.0 Mpa [158±30.0 ksi] for the unconditioned polyester, vinyl-ester, and epoxy GFRP bars, respectively. The tensile-strength reductions after 1,000, 3,000, and 5,000 hr of immersion at 60°C were about 14%, 16%, and 25.2% (for polyester GFRP bars), 2%, 5%, and 13.6% (for vinyl-ester GFRP bars), and 6%, 9%, and 14.5% (for epoxy GFRP bars), respectively. These results indicate that longer immersions at higher temperatures affected bar tensile strength. This phenomenon could be due to a higher solution diffusion rate within the sample and to the immersion temperature accelerating the chemical reaction of degradation, leading to a higher absorption rate for the same immersion time and accelerated degradation reaction. The typical mode of failure of epoxy, isoployester, and vinyl ester GFRP bars is shown in Figure 4.44 to Figure 4.26 and it can be noted that the tested bars failed in the middle of the bar (gauge length). The failure was accompanied by the delamination of fibers and resin.

Table 4.11: Tensile properties of reference and conditioned polyester, vinyl-ester, and epoxy specimens

Time of Immersion (h)	Temp. (°C)	Number of sample	Tensile Strength (MPa)					
			Polyester Bars		Vinyl-ester Bars		Epoxy Bars	
			Average	COV (%)	Average	COV (%)	Average	COV (%)
0	22	5	1015	2.1	1220	2.90	1090	2.80
1,000	22	3	963	1.0	1216	5.5	1070	1.9
	40	3	890	3.8	1211	2.6	1060	3.0
	60	3	870	4.7	1197	4.3	1024	1.2
3,000	22	3	960	1.2	1186	1.6	1069	3.1
	40	3	875	3.6	1178	1.4	1005	4.7
	60	3	860	4.4	1167	2.2	995	1.5
5,000	22	3	909	4.1	1139	4.2	1004	0.5
	40	3	835	5.3	1063	3.6	951	0.8
	60	3	760	5.0	1055	0.4	932	2.5
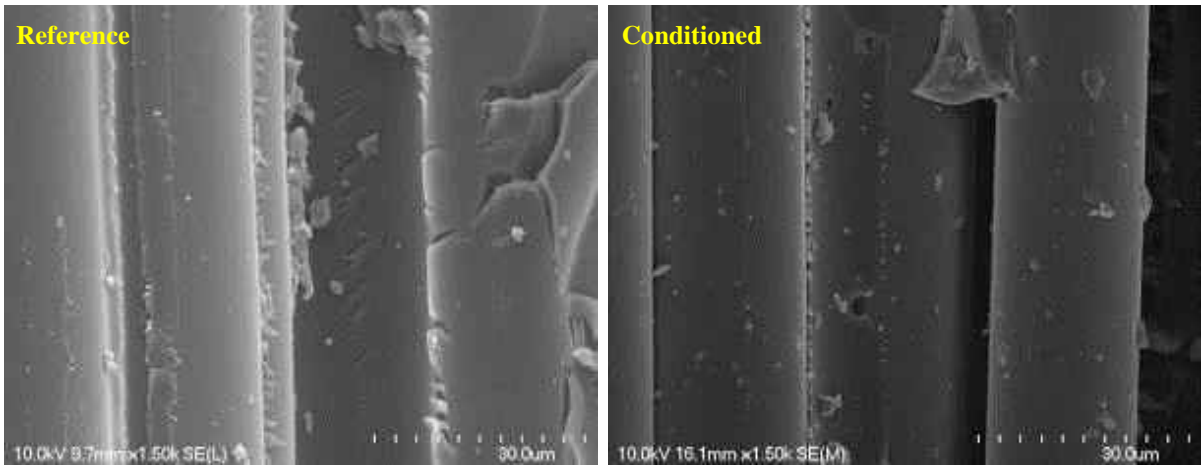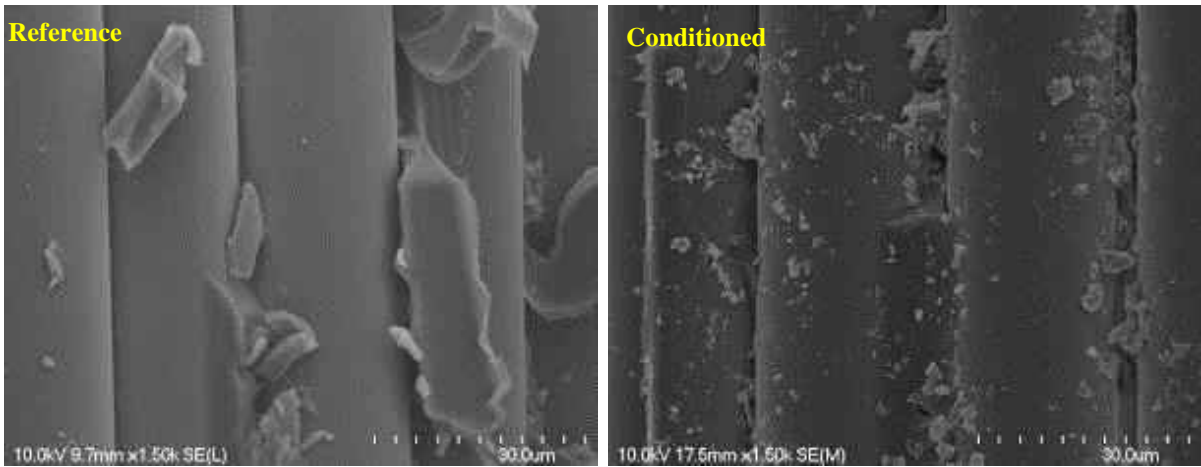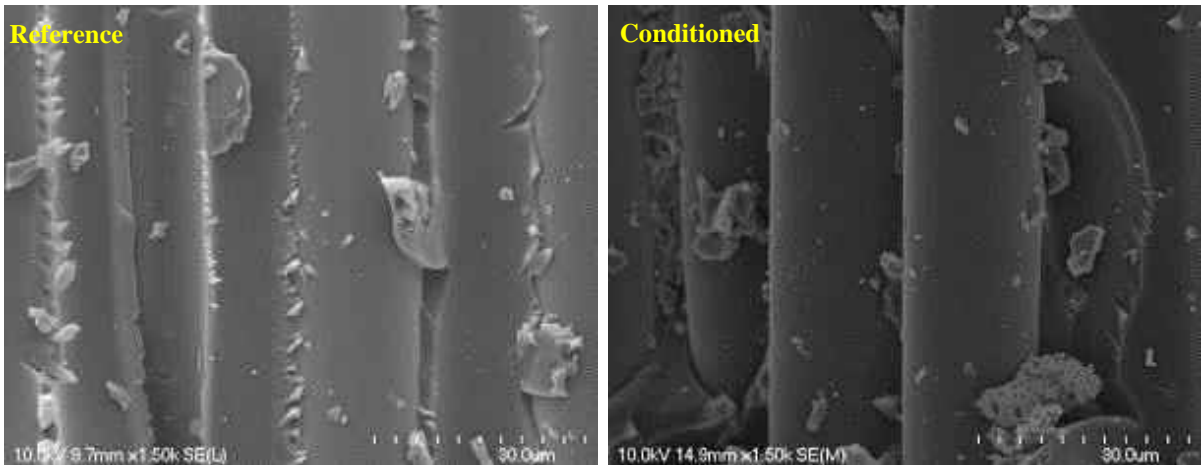
Figure 4.21: Micrographs of bars conditioned in the alkaline solution for 1,000 hr at 60°C (after interlaminar shear failure): (a) polyester GFRP; (b) vinyl-ester GFRP; (c) epoxy GFRP

(a) Polyester GFRP bars

(b) Vinyl-ester GFRP bars
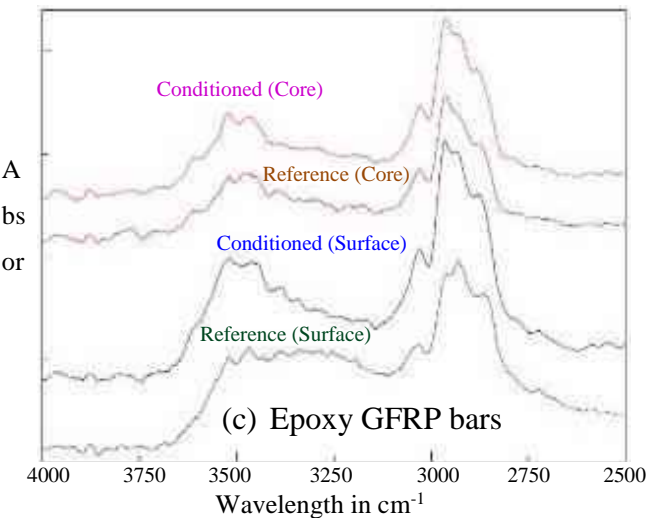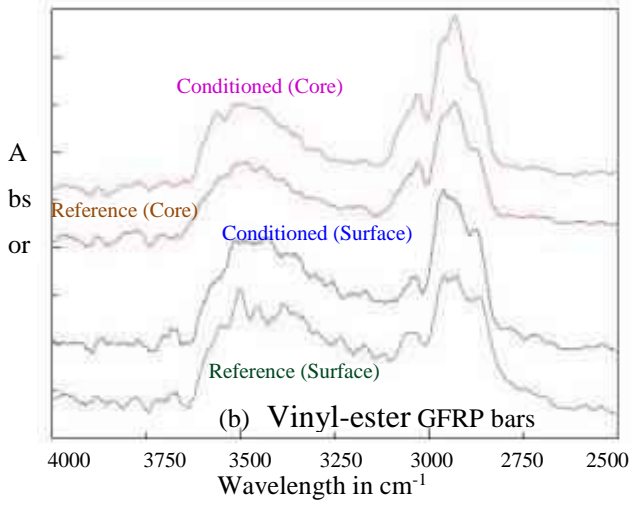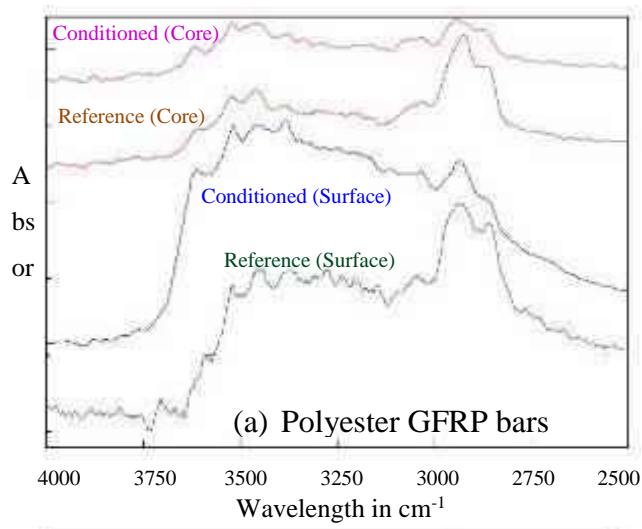
(c) Epoxy GFRP bars

Figure 4.22: FTIR spectra of reference and specimens conditioned for 5,000 hr
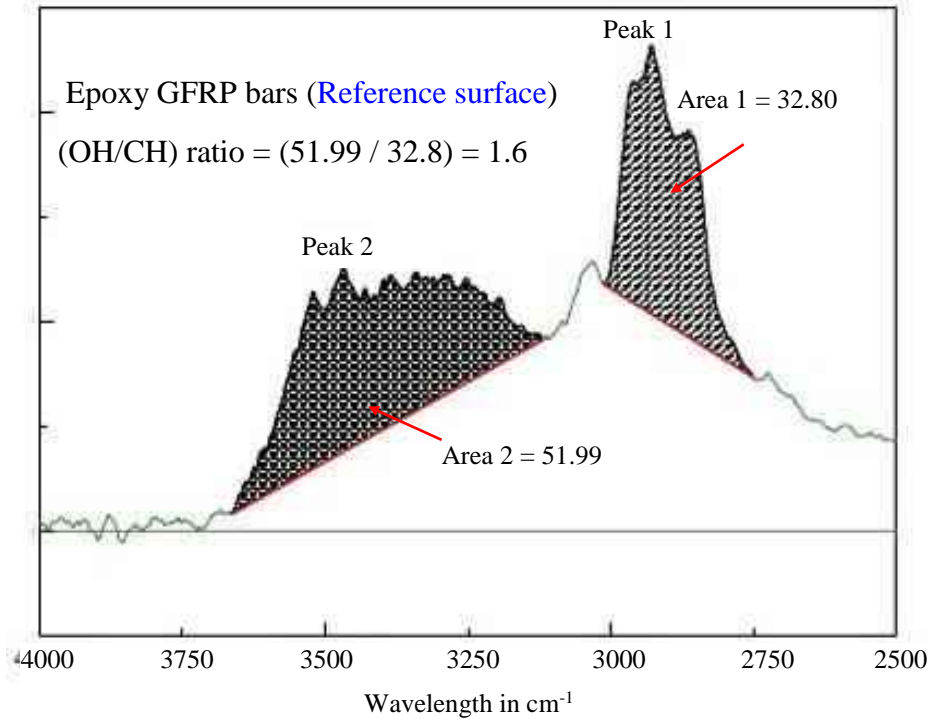
Figure 4.23: Peak areas used to calculate a O–H/C–H (Benmokrane et al. 2017)
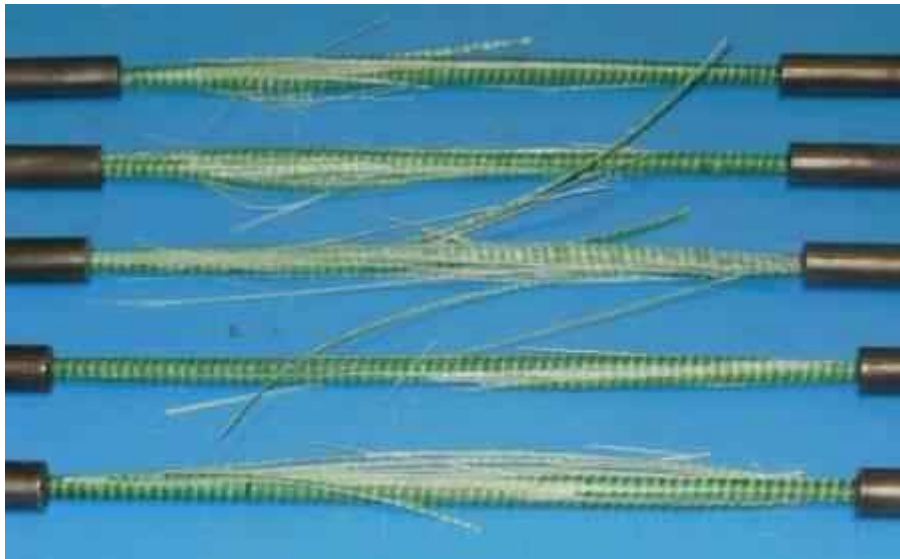
Figure 4.24: Typical mode of failure of epoxy GFRP bars

Figure 4.25: Typical mode of failure of isopolyester GFRP bars

Figure 4.26: Typical mode of failure of vinyl ester GFRP bars

4.5.9 Transverseeshear strength test

Transverse shear is the major structural force on dowels in jointed pavements or on stirrups in concrete beams. Transverse-shear tests were conducted according to ASTM D7617 (ASTM 2011) to characterize the tested bars. The setup consisted of a $230 \times 100 \times 110$ mm steel base equipped with lower blades spaced at 50 mm face to face, allowing for the double transverse-shear failure of the specimen caused by an upper blade, as shown in Figure 4.27. For each type of bar tested, six unconditioned specimens measuring 170 mm in length were tested under laboratory conditions on an MTS 810 (MTS Systems Corporation, Eden Prairie, Minneapolis) testing machine equipped with a 500 kN load cell. A displacement-controlled rate of 1.3 mm/min was used during the test, which yielded between

30 and 60 MPa/min until specimen failure. The loading was done without subjecting the test specimens to any shock.

4.5.9.1 Calculations

The transverse-shear strength was calculated with Eq. (4.8)

$$\tau_u = \frac{P_s}{2A} \tag{4.8}$$

where τ_u = transverse-shear strength (Mpa); P_s = failure load (N); and A = bar cross-sectional area (mm^2).

4.5.9.2 Test results and discussion

Table 4.12 shows that the transverse-shear strengths of the polyester and vinyl-ester GFRP bars were 250 ± 33 and 258 ± 32 MPa, respectively. The epoxy GFRP bars had the highest value of transverse-shear strength (270 ± 45 MPa). It is worth mentioning, however, that, although the resin delivers most of the transverse-shear strength, the fiber and the fiber/resin interface also play a role (Montaigu et al. 2013). The ratios between the shear strengths of the polyester and vinyl-ester GFRP bars and that of epoxy bars were 93% and 96%, respectively. The results indicate that the epoxy resin yielded higher transverse-shear strength than the polyester and vinyl-ester resin, although the standard deviation was high. Moreover, these values meet CSA requirements (2010), which specify a minimum transverse-shear strength of 160 Mpa [23.2 ksi] for GFRP bars.
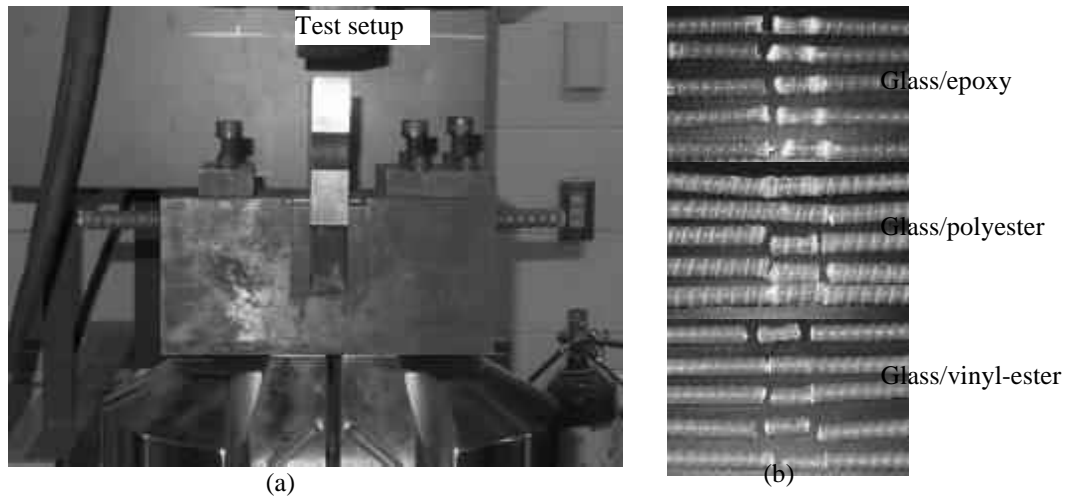
Figure 4.27: Setup for transverse-shear test and typical shear failure mode: (a) test setup; (b) failure mode

Table 4.13 shows the transverse-shear strength and strength-retention ratios of the tested bars after 1,000, 3,000, and 5,000 hr of immersion in the alkaline solution at 60°C. Table 4.13 indicates that the polyester GFRP bars were highly affected by accelerated aging with a transverse-shear strength reduction of 22.5% after 5,000 hr of immersion, while the vinyl-ester and epoxy bars had transverse-shear strength reductions of 15.9% and 11%, respectively.

Table 4.12: Mechanical properties of the reference GFRP bars

Bar type	τ_u (MPa)	f_u (MPa)	E (GPa)	ε_u (%)	S_u (MPa)
Glass/polyester	250±33	1150±59	56.9±2.4	2.02±0.16	47.2±0.4
Glass/vinyl-ester	258±32	1432±75	66.3±2.2	2.16±0.089	64.8±4.5
Glass/epoxy	270±45	1573±135	61.8±1.5	2.54±0.015	77.4±2.7

Figure 4.27 shows the effect of the alkaline solution on the transverse shear strength after different exposure times. Contrary to the polyester bars, the vinyl-ester and epoxy GFRP bars exhibited no significant reductions in the early stages (less than 3,000 hr).

Table 4.13: Retention of mechanical properties of the conditioned polyester bars, the vinyl-ester and epoxy GFRP bars

Fiber/resin	Conditioned period	τ_u (MPa)	Retention (%)	f_u (MPa)	Retention (%)	E (GPa)	Retention (%)	S_u (MPa)	Retention (%)
Glass/polyester	1,000	236	94.4	1133	99	55.0	96.6	43.8	93
	3,000	222	88.8	939	81	54.0	94.9	40.8	87
	5,000	194	77.5	863	75	50.8	89.3	37.4	79
Glass/vinyl-ester	1,000	248	96.1	1409	98	64.0	96.5	62.5	97
	3,000	234	90.7	1273	89	61.1	92.2	58.0	90
	5,000	217	84.1	1186	83	58.5	88.2	56.0	87
Glass/epoxy	1,000	267	98.9	1446	92	59.0	95.5	73.7	96
	3,000	248	92.0	1301	83	57.5	93.0	69.6	90
	5,000	239	89.0	1211	77	54.0	87.4	67.0	87
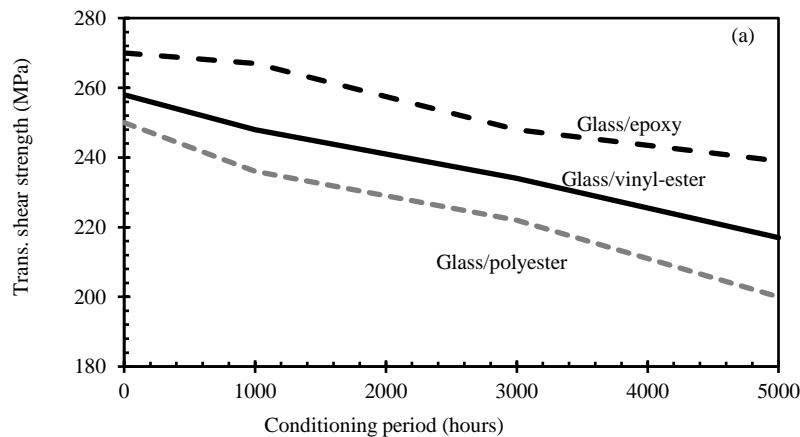
Figure 4.28: Effect of conditioning in the alkaline solution at 60°C on transverse-shear strength of three types of resins

4.5.10 Three-point flexural test

Flexural testing is especially useful for quality control and specification purposes. Flexural properties may vary with specimen diameter, temperature, weather conditions, and differences in rates of straining. The flexural properties obtained with this test method—ASTM D4476 (ASTM 2009)—cannot be used for design purposes but are appropriate for the comparative testing of composite materials. The test was conducted on specimens 240 mm long over a simply supported span equal to 20 times the bar diameter, as shown in Figure 4.29. Six unconditioned specimens were tested under laboratory conditions as references for each type on an MTS 810 testing machine equipped with a 500 kN load cell. The specimens were loaded at mid-span with a circular nose; the specimen ends rested on two circular supports that allowed the specimens to bend. A displacement-controlled rate of 3.0 mm/min was used during the test. The rate of loading was done without subjecting the test specimen to any shock. The applied load and deflection were recorded during the test on a data-acquisition system monitored by a computer.

4.5.10.1 Calculations

The flexural strength of tested FRP specimens was calculated with Eq. (4.9). The flexural modulus of elasticity (stiffness) is the ratio, within the elastic limit, of stress to corresponding strain. It was calculated with Eq. (4.10)

$$f_u = PLC / (4I) \tag{4.9}$$

$$E = PL^3 / (48IY) \tag{4.10}$$

where f_u = flexural strength in the outer fibers at mid-span (N/mm2); P = failure load (N); L = clear span (mm); I = moment of inertia (mm4); C= distance from the centroid to the extremities (mm); E = flexural modulus of elasticity in bending (N/mm2); and Y = mid-span deflection at load P (mm). The maximum outer fiber strain (ε_u) was calculated from Eq. (4.11)

$$\varepsilon_u = f_u / E \tag{4.11}$$

4.5.10.2 Test results and discussion

Table 4.12 provides the three-point flexural strength, flexural modulus of elasticity, and ultimate outer-fiber strain of the tested GFRP bars. The elastic behavior of all the specimens was maintained until flexural failure, at which point the specimens failed due to compression in the top fibers, as shown in Figure 4.29. The polyester GFRP bars showed the lowest flexural strength (1150±59 MPa), while the epoxy GFRP bars recorded the highest (1573±135 MPa). The vinyl-ester GFRP bars recorded a flexural strength of 1432±75 MPa. The vinyl-ester and epoxy GFRP bars, however, evidenced no significant differences in flexural modulus of elasticity (66.3 and 61.8 GPa, respectively). Lastly, the flexural modulus of elasticity of the polyester resin was lower than that of the vinyl-ester and epoxy resin (86% and 92% of the vinyl-ester and epoxy GFRP bars, respectively). The lower flexural

strength and modulus of the polyester GFRP bars is expected since the polyester had the lowest mechanical properties of the thermosetting resins considered. Castro and Carino (1998) pointed out that the resin system significantly affected the mechanical properties of FRP bars due to the efficiency of the stress transfer among the fibers.
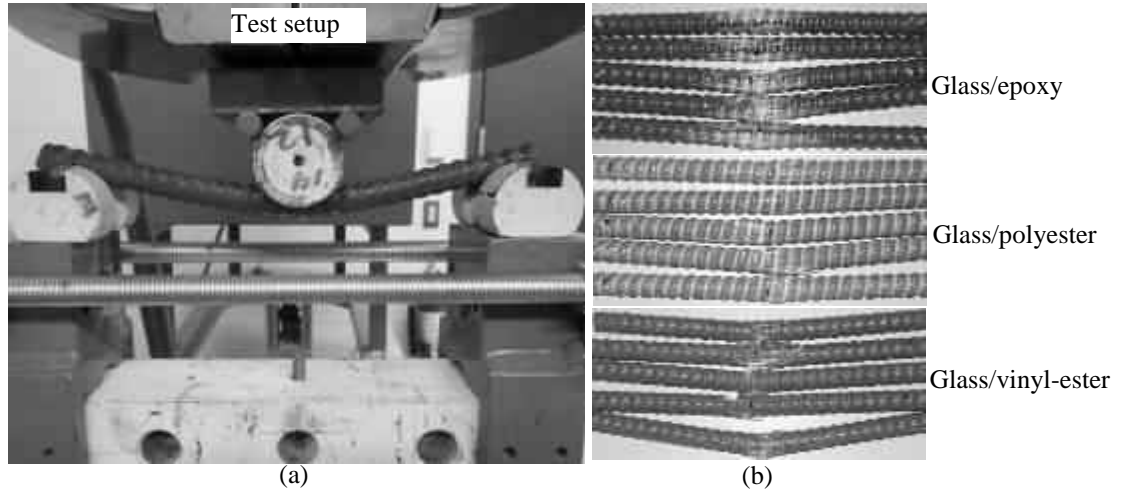
Figure 4.29: Setup for flexural testing and typical failure mode: (a) test setup; (b) failure mode

Table 4.13 provides the flexural strength and strength-retention ratios of the tested FRP bars after 1,000, 3,000, and 5,000 hr of immersion. Both the polyester and epoxy GFRP bars had similar flexural-strength reductions after 5,000 hr (25 and 23%, respectively), while the vinyl-ester GFRP bars showed a lower reduction of 17%. These observations confirm that the bond between the GFRP fibers and polyester resin—before and after conditioning—was lower than that between the glass fibers in the vinyl-ester or epoxy resin. Consequently, debonding occurring at the fiber–matrix interface caused the fibers to separate from the resin. Figure 4.30 shows the effect of the alkaline solution on flexural strength. The lowest reduction rate was observed with the vinyl-ester GFRP bars, which yielded the lowest degradation at the interface. The high degradation of the epoxy GFRP bars after 1,000 hr of conditioning resulted from the ingress of the alkaline solution through the initial voids. The polyester GFRP bars, however, returned an almost steady degradation rate between 1,000 and 5,000 hr.

4.5.11 Short-beam shear test

In FRP bars manufactured with a pultrusion process in which the fibers are arranged unidirectionally and bonded with the polymer matrix, the horizontal stresses would be more conducive to inducing interface degradation than transverse-shear stresses (Park et al. 2008). The short-beam shear test was conducted according to ASTM D4475 (ASTM 2008) on six specimens of each type of GFRP bar in order to calculate the interlaminar-shear strength, which is governed by the fiber–matrix interface. The tests were carried out with a 500 kN MTS 810 testing machine. The distance between the shear planes was set to 7 times the nominal diameter of the FRP bars. Figure 4.31 shows the test setup and typical modes of failure of the tested specimens. A displacement-controlled rate of 1.3 mm/min was

employed during the test. The applied load was recorded with a computer-monitored data-acquisition system.
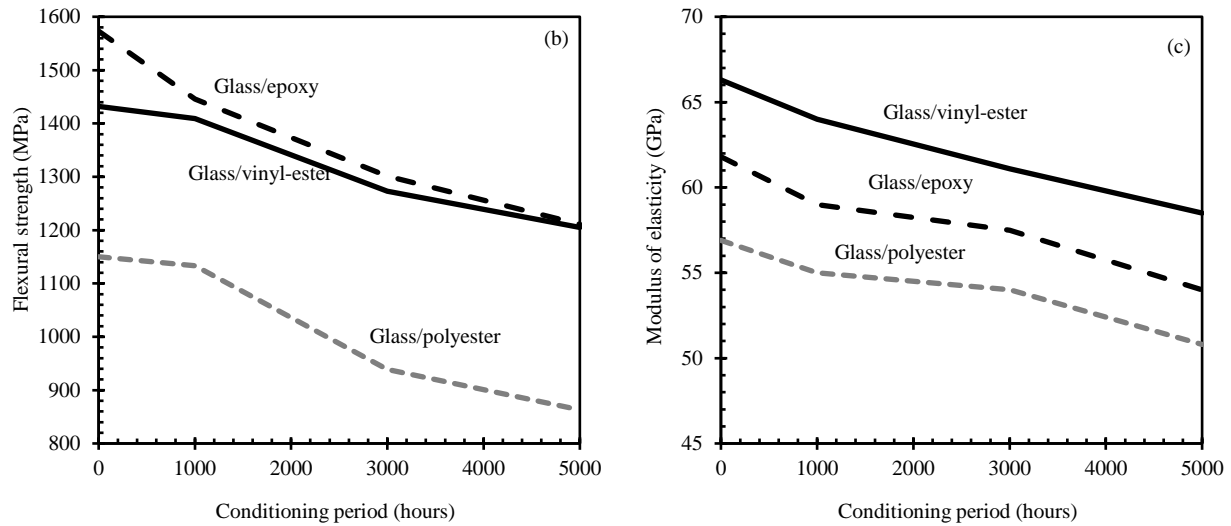
Figure 4.30: Effect of conditioning in the alkaline solution at 60°C on flexural properties

Figure 4.31: Setup for short-beam testing and typical failure mode

4.5.11.1 Calculations

The interlaminar-shear strength, S_u, of the GFRP bars was calculated from Eq. (4.12)

$$S_u = 0.849 P / d^2 \qquad (4.12)$$

where S_u = interlaminar-shear strength (MPa); P = shear failure load (N); and d = bar diameter (mm).

4.5.11.2 Test results and discussion

The short-beam shear test revealed that the epoxy GFRP bars had the highest interlaminar-shear strength (77.4±2.7 MPa), followed by the vinyl-ester GFRP bars (64.8±4.5 MPa) and the polyester GFRP bars (47.2±0.4 MPa). The results confirm that the interface between the glass fibers and polyester resin was not as strong as that within the vinyl-ester and epoxy GFRP bars. Table 4.12 shows the apparent horizontal shear strength of the tested GFRP bars. It is worth mentioning that the high values of the interlaminar-shear strength reveal a strong interface between the resins and reinforcing fibers, which will be clarified in the SEM analysis to follow.

Table 4.13 also shows the apparent horizontal shear (interlaminar shear) strength and strength-retention ratios of the tested FRP bars after 1,000, 3,000, and 5,000 hr of immersion. As for flexural testing, the vinyl-ester and epoxy GFRP bars offered excellent stability and durability after immersion in the alkaline solution, followed by the polyester GFRP bars. The reduction ratios for the vinyl-ester, epoxy, and polyester GFRP bars after 5,000 hr were 13%, 13%, and 21%, respectively. Again, this observation confirms the strong fiber–resin interface in the vinyl-ester GFRP bars, followed by the epoxy and polyester GFRP bars. As evidenced from these results, the fiber–resin interface stands out as one of the most important issues in manufacturing glass FRP. Figure 4.32 shows the effect of the alkaline solution on the interlaminar-shear strength, with the vinyl-ester GFRP bars exhibiting the lowest rate of degradation. Interestingly, the 21% reduction in the interlaminar-shear strength of the polyester GFRP bars in this study is significantly lower than with the polyester E-glass composite rods tested by Micelli and Nanni (2004), who observed a more than 90% reduction in interlaminar-shear strength. This indicates that the development of new material systems and advanced manufacturing methods now yield high-quality FRP bar products.
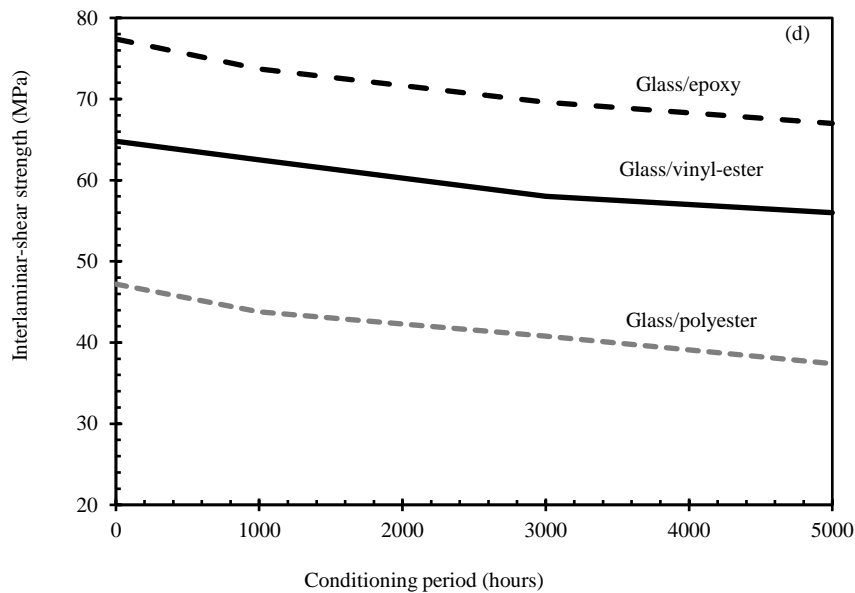
Figure 4.32: Effect of conditioning in the alkaline solution at 60°C on interlaminar shear properties

4.5.12 Conclusions

4.5.12.1 Mechanical properties observations

1. The epoxy and vinyl-ester GFRP bars exhibited higher fiber–resin bond, flexural strength, flexural modulus of elasticity, and interlaminar-shear strength, which is governed by the fiber–matrix interface. In addition, they showed lower moisture uptake.

2. Both the polyester and epoxy GFRP bars had similar flexural-strength reductions after 5,000 hr of immersion (25% and 23%, respectively), while the vinyl-ester GFRP bars returned a lower reduction of 17%. These observations confirm that the bond between the GFRP fibers and polyester resin—before and after conditioning—was lower than that between the glass fibers and the vinyl-ester or epoxy resin.

3. The unconditioned polyester GFRP bars exhibited lower transverse-shear strength, flexural strength, interlaminar-shear strength, and the weakest fiber–resin interface. The transverse-shear strength of the polyester GFRP bars was significantly affected by accelerated aging (22.5% reduction after 5,000 hr), while the epoxy and vinyl-ester GFRP bars were slightly affected by accelerated aging (11% and 15.9 % reductions, respectively, after 5,000 hr).

4. The flexural strength of the polyester GFRP bars was significantly affected by accelerated aging (25% reduction after 5,000 hr), while the vinyl-ester and epoxy GFRP bars were affected by accelerated aging (17% and 23% reductions, respectively, after 5,000 hr).

5. The interlaminar-shear strength of the polyester GFRP bars was highly affected by accelerated aging (21% reduction after 5,000 hr), while the vinyl-ester and epoxy GFRP bars were slightly affected by accelerated aging (13% reduction each after 5,000 hr). The fiber–resin interface plays a significant role in controlling the degradation due to conditioning.

4.5.12.2 Physical and microstructural observations

1. The microstructural observations revealed that GFRP bars made with vinyl-ester or epoxy resin were not significantly changed, but presented a slight debonding at the interface between the fibers and vinyl-ester resin. Consequently, the vinyl-ester GFRP bars evidenced higher moisture uptake measured at saturation compared to the epoxy GFRP bars.

2. The debonding at the interface between the fibers and polyester resin was higher than in the vinyl-ester and epoxy GFRP bars. Accordingly, the polyester GFRP bars evidenced higher moisture uptake measured at saturation and a higher degradation rate of mechanical properties after conditioning.

3. The polyester GFRP bars showed an increase in Tg of about 5°C after conditioning due to post-curing (cure ratio of the reference specimens was 98.1%). The vinyl-ester and epoxy GFRP bars, however, experienced a decrease in Tg after conditioning.

4. The polyester GFRP bars absorbed 18% more water than the vinyl-ester and epoxy GFRP bars after conditioning compared to the reference specimen.

4.6 Effects of Bars Size on the Durability of GFRP Bars Conditioned in alkaline solution

The sand-coated GFRP bars used in this study were made of continuous boron-free glass fibers (EC-R) impregnated in a vinylester-based resin matrix and were manufactured according to the pultrusion process by a Canadian company (Pultrall Inc., Thetford Mines, Quebec). Five diameters of GFRP bars were investigated (#3, #4, #5, #6, and # 8), which correspond to nominal diameters of 9.5 mm, 12.7 mm, 15.9 mm, 19.1 mm, and 25.4 mm, respectively.

4.6.1 Effect of bar diameter on physical properties

The bar diameter had no significant effect on most of the physical properties of the GFRP bars, including the transverse coefficient of thermal expansion, porosity, and *Tg*. Similarly, all of the bars tested evidenced an entirely cured resin, indicating that bar diameter did not affect the degree of cure. The development of an efficient production method makes this consistency possible. This is in contrast with the observations made by Yi and Hilton (1988), who indicated that laminate thickness might affect the degree of cure due to the higher thermal conductivity of thicker composite laminates. On the other, the fiber content and water absorption were found to increase and decrease, respectively, with increasing bar diameter. Since none of the FRP bars contained voids, the lower water absorption for the larger diameter bars can be correlated to increasing fiber content (by weight). Glass fibers absorb scarcely any water, therefore the bars with higher matrix contents evidenced higher absorption rates. In order to further correlate bar diameter to the percentage water absorption, the shape ratio of the GFRP bars were calculated and plotted (see Figure 4.33). Cinquin and Medda (2009) defined the shape ratio as the ratio between the sample's surface and volume. As can be seen in Figure 4.33a, the shape ratio was significant in the water absorption of the GFRP bars at 24 hr and at saturation (Saturation), i.e., the water absorption increased as did the shape ratio. It can also be observed that the relationship between the water absorption at 24 hr (%) and at saturation to that of the shape ratio is the same, as demonstrated by the almost equal slopes of the water absorption and shape-ratio relationship curves. On the another hand, there is a linear but negative correlation between the shape ratio and bar diameter. The shape ratio decreases as the bar diameter increases. This accounts for the smaller diameter bars having higher absorption rates than the larger diameter ones with the same length, since the exposed surface is greater with respect to volume. It is also worth noting that the decrease in the shape ratio is very similar to the decrease in the percentage of water absorption at saturation (%) for the various bar diameters.
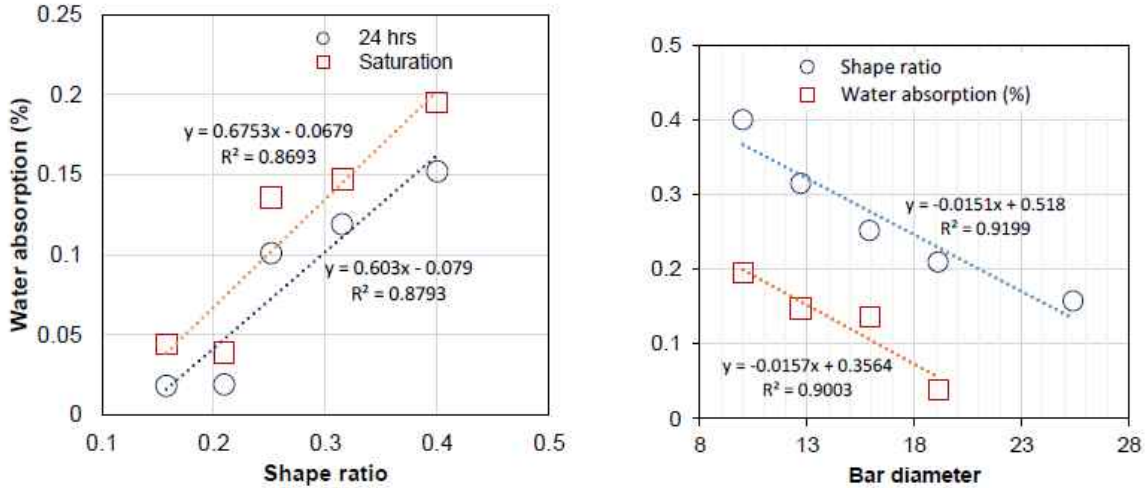
Figure 4.33: Relationship of water absorption to the shape ratio and bar diameter

4.6.2   Effect of bar diameter on mechanical properties

Many studies have revealed that the short-term mechanical properties of FRP bars decrease with increased bar diameter (Bank 2006; Hollaway 2008). This conclusion, however, was not clearly observed in our study. Figure 4.34 shows the normalized mechanical properties for the different sizes of GFRP bars. This graph provides the percentage of the interlaminar shear strength (ILSS), flexural strength (Flexure), tensile strength (Tensile), and tensile modulus (Modulus) for all of the bar diameters with respect to the mechanical properties of the #3 bars. The figure show no significant difference in the tensile properties of the GFRP bars regardless of bar diameter. While the highest tensile strength and modulus were observed for the #3 bars, the lowest tensile properties were exhibited by the #5 bars (94% compared to the #3 bars), with the #8 bars exhibiting more than 96% of strength and stiffness of the #3 bars. Kocaoz et al. (2005) suggested that modulus, which is an intrinsic property of the material, is not significantly affected by bar cross-sectional size but rather by the level of fibers contained in the bar. Since the percentage fiber content by weight (%) (Table 4.14) for different bar diameters was almost the same, then the bars should record the same elastic modulus. Moreover, the consistency in the measured tensile properties of the GFRP bars with different diameters can be due to an adequate anchor length, which resulted in a more efficient transfer of stresses from the bar surface to the center. Portnov and Bakis (2008) suggested that introducing a more uniform distribution of the applied shear stress near the grips could minimize the shear lag effect and increase the tensile-load carrying capacity of round pultruded rods. In contrast to the tensile properties, there was a size effect observed for ILSS and flexural strength. The #8 bars recorded ILSS and flexural strength almost 14% lower than the #3 bars. Significant size effects were also observed by Wisnom and Jones (1996) on the average ILSS for unidirectional glass-fiber/epoxy composites. They indicated that the lower ILSS with bigger specimens could be due to the larger defects inherent defects. Koller et al. (2007) also suggested that the probability of having large defects in composite materials increases with increased specimen volume. Moreover, it should be noted that ILSS is a matrix-dominated property. Wisnom and Jones (1996) suggested that matrix dominated failures show the largest size effects in

composite materials. Defects near the edge of the GFRP bars were very critical for the specimens subjected to the short-beam test as this location is subjected to higher levels of shear stress. Similarly, the lower flexural properties of the larger diameter bars can be explained by the high probability of defects. Carvelli et al. (2009) suggested that it is more difficult to keep the filaments parallel to one another in larger diameter FRP bars during the pultrusion process, increasing their tendency to buckle under compression. This is, in fact, the failure mechanism observed in the GFRP bars during the flexural test, in which the failure was initiated by the compression buckling of the top fibers.
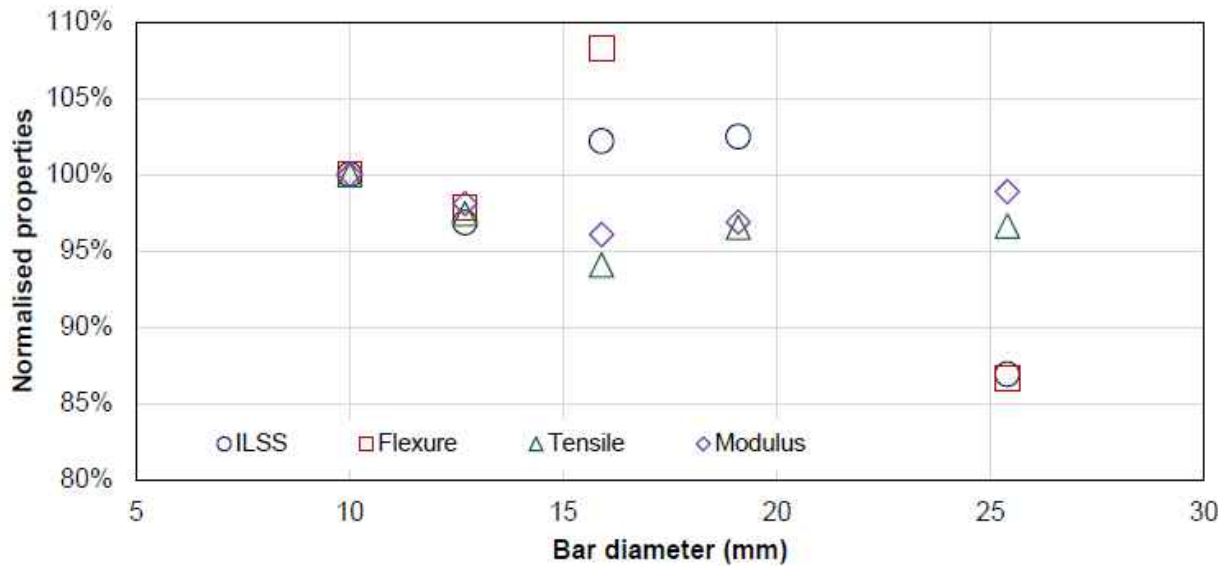
Figure 4.34: Normalized mechanical properties of the GFRP bars

4.6.3   Property retention of GFRP bars with different diameters

Tannous and Saadatmanesh (1999) indicated that the effect of an alkaline solution on FRP bars only involved a very thin layer on the exposed surface. Thus, the approximate layer thickness and area of the GFRP bars affected by the alkaline solution were calculated and reported in Table 4.15 to correlate with the property retention for different bar diameters. These values were determined by assuming that the affected portions of the GFRP bar were the same as the percentage of water absorption at saturation (%) (Table 4.14). It can be clearly seen that the affected thickness is only in the order of 0.0019 to 0.0054 mm. Moreover, the percentage of affected thickness with respect to the nominal diameter decreased as did bar diameter. Figure 4.35 provides the strength and stiffness retention properties of the GFRP bars with different diameters. Figures 4.35a to 4.35c clearly indicate that the strength properties were affected by conditioning in the alkaline solution, while Figure 4.35d shows that the modulus of elasticity was not affected. The almost 100% retention of the modulus of elasticity, which is a fiber-dominated property, for all bar diameters indicates that the damage caused by the moisture diffusion was confined to the very thin layer of the exposed surface and that the reinforcing fibers were not affected by the conditioning. As the modulus of elasticity was determined from the linear-elastic portion of the stress and strain curve, the matrix was still effectively transferring stresses

172

to the fibers. Nkurunziza et al. (2005) indicated that the diffusion of moisture and alkalis in composites can destroy the bond between the fiber and matrix, damaging the interface. This is difficult to see at lower loads, but higher mechanical loads increase the degradation of the fiber–matrix interface. This accounts for the noticeable decrease in strength properties, as these values were calculated at the point of failure of the GFRP bars at which the stress distribution along the fibers is less uniform. Figures 4.35a shows that the effect of conditioning on the ILSS of the GFRP bars was significant with the smaller diameter bars, but decreased as the diameter increased. In fact, the residual horizontal shear strength for the #8 bars was the same as that measured on the reference bars, while the #3 bars retained only 88% of their ILSS. This can be explained by the thinner layer affected by the alkaline solution in the case of the larger diameter bars, as reported in Table 4.15. As indicated in the previous section, ILSS is governed by the fiber–matrix interface. Thus, the decrease in ILSS can be correlated to interface degradation. Similarly, due to the very thin layer affected by conditioning in the alkaline solution in the larger diameter GFRP bars, its affected area was also significantly smaller with respect to the total area, compared to the smaller diameter bars. Figure 4.80b shows that the flexural-strength retention increased with bar diameter. The retention ranged from 88% retention for the #3 bars to more than 97% for the #8 bars. This behavior was also observed by Maranan et al. (2014), who found that larger diameter bars exhibited a slower rate of strength degradation at high temperature than small diameter bars. Cinquin and Medda (2009) also concluded that the residual mechanical properties were more affected in thin composites than thick composites. The higher flexural strength retention for the larger diameter bars could be due to the strength gradient through bar diameter during bending. During flexural tests, the outermost fibers are subject to the maximum stress. Thus, a smaller amount of fibers with respect to the total volume was under the maximum stress in the larger diameter bars. Moreover, the higher flexural-strength retention in the larger diameter bars can be correlated to the smaller reduction in the second moment of area of the conditioned specimens. Since only the bar surface was damaged, the fibers and matrix in the intact zone were undamaged and had the same initial mechanical properties, resulting in a better redistribution of load when the outer fibers progressively failed. Figure 4.35c shows a opposite trend than do Figures 4.35a and 4.35b, in which the smaller diameter bars exhibited higher tensile-strength retention. This figure shows that the #3 bars retained more than 95% of their tensile strength, while the #8 bars retained only 88%. This trend can be due to the shear lag effect. Achillides and Pilakoutas (2004) indicated that larger diameter FRP bars had more significant shear lag-effect than smaller diameter bars and had a noticeable effect on tensile strength. Castro and Carino (1998) further mentioned that the efficiency of the stress transfer from the bar surface to the interior fibers influences the mechanical properties of the FRP bars. Due to the shear lag effect, the outer fibers experience higher stresses than the inner fibers, even though all fibers resist the tensile load at the same time. Due to conditioning in alkaline solution, the outer surface of the bars was affected and might have decreased mechanical properties. As the specimens were loaded, the outer fibers— which were subjected to higher stress—initiated failure and the breakage moved instantly to the inner fibers, leading to the sudden and catastrophic failure of the GFRP bars. From the above results, it can be concluded that the conditioning in alkaline solution affected the strength properties of the GFRP bars, but not their moduli of elasticity. Moreover, the strength-

retention limit was affected by bar size. The ILSS and flexural strength of the smaller diameter bars was affected more than the larger diameter ones. This is in contrast to tensile strength: the larger diameter bars had lower strength retention. These results suggest that the conclusions drawn by most studies based on smaller diameter FRP bars do not apply to larger diameters. Based on the results in this study, it is more reasonable to use larger diameter bars in assessing the tensile-strength retention of FRP bars exposed to severe environmental conditions. Nevertheless, note should be taken of the very high load required cause failure of larger bars. That notwithstanding, the strength retention in all the bar diameters considered in this study is significantly higher than the 0.70 environmental reduction coefficient required by several codes.

Table 4.14: Physical properties of the GFRP bars

Property	Bar designation				
	#3	#4	#5	#6	#8
Nominal diameter (mm)	9.5	12.7	15.9	19.1	25.4
Nominal cross-sectional area (mm^2)	70.8	126.6	198.5	286.5	506.7
Actual cross-sectional area by immersion test (mm^2)	83.8 (1.9)	145.0 (1.7)	224.4 (1.2)	317.3 (1.9)	555.7 (5.2)
Fiber content by weight (%)	80.9 (1.0)	81.8 (0.1)	82.6 (0.1)	82.7 (0.2)	83.0 (0.2)
Transverse CTE, (x10^{-6}/°C)	20.7 (2.3)	20.5 (1.6)	21.5 (1.4)	22.0 (1.8)	21.3 (2.5)
Void content (%)	0 (0)	0 (0)	0 (0)	0 (0)	0 (0)
Water absorption at 24 hours (%)	0.152 (0.005)	0.119 (0.024)	0.101 (0.011)	0.019 (0.004)	0.018 (0.002)
Water absorption at saturation (%)	0.195 (0.012)	0.147 (0.048)	0.136 (0.012)	0.039 (0.010)	0.044 (0.003)
Cure ratio (%)	100 (0)	100 (0)	100 (0)	100 (0)	100 (0)
T_g (°C)	125.8 (1.3)	112.8 (2.5)	109.6 (1.5)	105.2 (1.3)	124.8 (4.9)

Table 4.15: Estimated affected portion of the GFRP bars

Affected Portion	#3	#4	#5	#6	#8
Area (mm^2)	0.1382	0.1862	0.2700	0.1117	0.2230
Thickness (mm)	0.0044	0.0047	0.0054	0.0019	0.0028
% of the nominal diameter	0.0463	0.0368	0.0340	0.0098	0.0110

(a) Interlaminar shear strength

(b) Flexural strength

(c) Tensile strength

(d) Modulus of elasticity
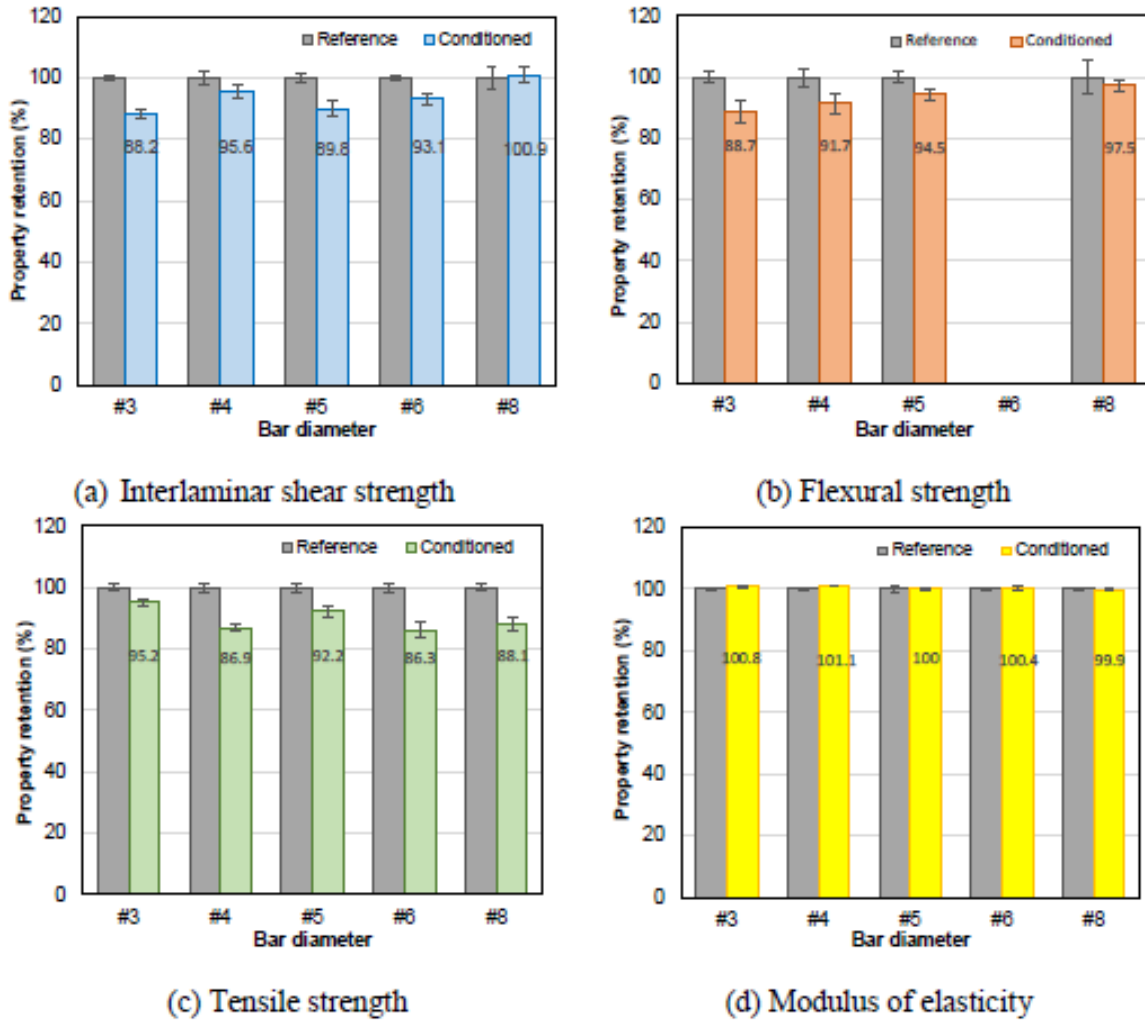
Figure 4.35**:** Property retention of GFRP bars with different diameters

4.6.4 SEM and FTIR observations

Scanning-electron-microscopy (SEM) observations were performed to assess the microstructure of the GFRP bars before and after conditioning. All of the specimens observed under SEM were cut, polished, and coated with a thin layer of gold–palladium using a vapor-deposit process. Microstructural observations were performed on a JEOL JSM-840A SEM. Similarly, Fourier Transformed Infrared Spectroscopy (FTIR) was conducted for each bar diameter to study the changes in the chemical composition of the matrix at the bar surface. These observations were conducted to determine the potential degradation of the polymer matrix, glass fibers, or interface, as applicable, due to the penetration of the alkaline solution. The aim was to link these observations to the possible evolution of mechanical properties and chemical composition of the bars after conditioning.

4.6.5   SEM

Figures 4.36 and 4.37 show the SEM micrographs of the cross section of the reference and conditioned GFRP bars, respectively. As shown in Figures 4.36a and 4.36b, there were no pores observed in the center or near the surface of the reference bars. There was also no noticeable gap at the fiber–matrix interface, indicating excellent adhesion between the fibers and matrix. This is also true in the center of the conditioned GFRP bars (Figure 4.37a). Small gaps between the fibers and matrix were observed near the exposed surface in some conditioned specimens (Figure 4.37b), suggesting that the bars were affected after exposure to the alkaline solution. This damage to the fiber–matrix interface reduces the transfer of loads between fibers and results in the reduction in strength properties. Benmokrane et al. (2002), however, indicated that the mechanical properties of GFRP bars are controlled by the fiber component. If the fibers have not deteriorated, FRP bars will preserve most of their mechanical strength and will be able to support loads. If the protective resin degrades, the bonding between the matrix and fibers located on the outer part of the bar will gradually reduce and bar resistance will start to decrease. This is the most probable reason why the strength properties of GFRP bars decreased after alkaline conditioning for 3 months. Nevertheless, the strength reduction is small as the SEM observation confirmed that only the exposed surface of the GFRP bars was affected, not the core section. This exposed surface can be considered as being an "all-resin" surface, which does not contribute much in resisting the applied load.
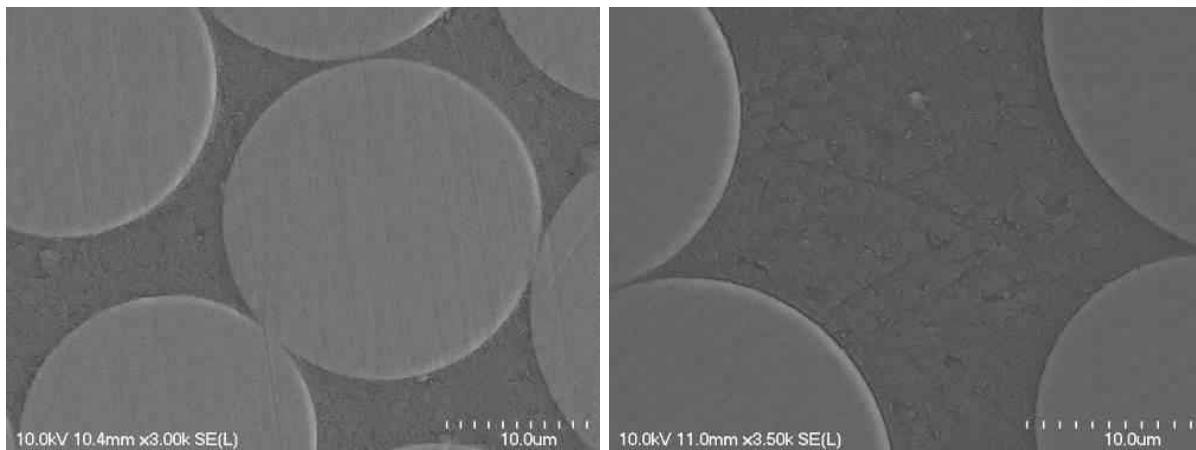
Figure 4.36: SEM micrographs of the reference GFRP bars
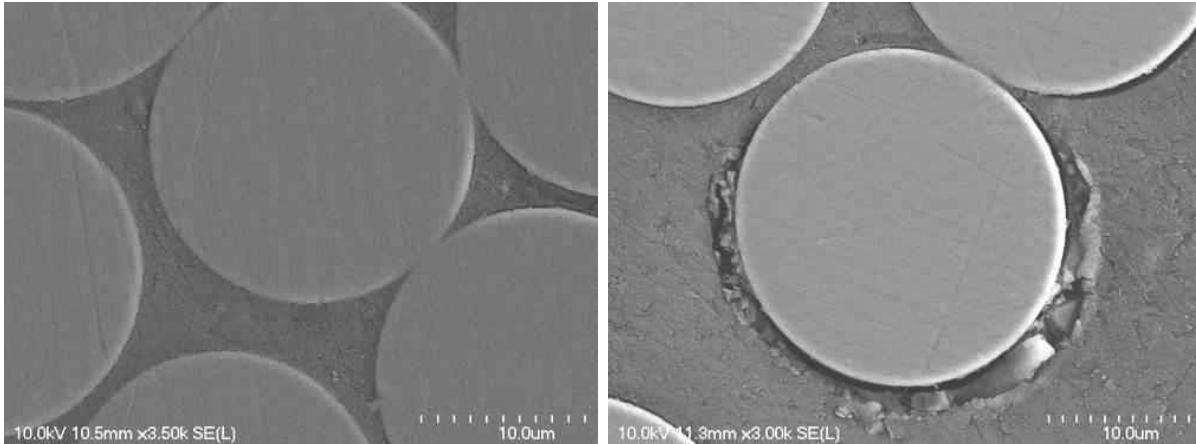
Figure 4.37: SEM micrographs of the conditioned GFRP bars

4.6.6 FTIR

Figure 4.38 shows the infrared spectroscopy (FTIR) spectra of the surface of the reference and conditioned GFRP bars. Only the FTIR for the #3 and #8 bars are provided for comparison. The FTIR for both bar diameters shows no clear differences between the infrared spectra of the reference and conditioned GFRP bars. Moreover, the FTIR did not show any significant changes in the chemical structure after exposure to the alkaline solution. These observations indicate that the surface of the bars exposed to the alkaline solution for 3 months at 60°C [140°F] had not been chemically modified and might possess the same initial mechanical properties. These results further confirm that the degradation of the matrix remains only at the exposed surface of the GFRP bars. This supports the findings by Nkurunziza et al. (2005) that vinylester epoxies are very resistant to chemical attack, which improves the environmental resistance of FRP bars made with these resins.

(a) #3 GFRP bars   (b) #8 GFRP bars
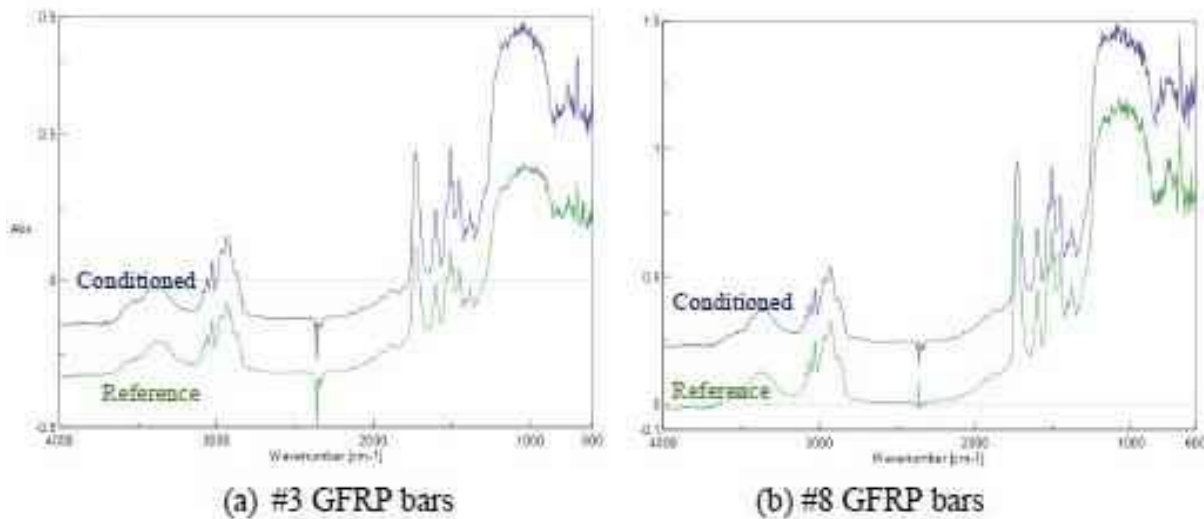
Figure 4.38: FTIR spectrum of the GFRP bars before and after conditioning.

4.7 Effects of solution type on GFRP

The experimental tests were conducted to determine the durability performance of glass fibers under different corrosive environment and observe how they reacted in specific chemical solutions at a fixed temperature for a different amount of time. Their test consisted of a weight loss analysis, tensile stress testing and scanning electron microscopy analysis (SEM) on different bare glass, all exposed in specific chemical solutions, at multiple temperature for different durations. The glass fibers were submerged in 4 chemical solutions, acidic, alkaline, saline and deionized water, for 24 h and 168 h and submitted to a weight loss analysis and SEM.

4.7.1 Glass fiber

Ten types of glass fibers were used in this study: V1, V2, V3, V4, V5, V6, V7, V8, V9, and V10. Glass fiber is commonly used as a reinforcing agent for polymers to create fiberglass, or glass-reinforced plastic (GRP). Glass fiber is known to be very strong in tension but weak in compression. When combined with plastic resins, which are strong in compressive loading but weak in tension, it forms a strong material in both compressive and tension loading. Its application usually include thermal electrical and sound insulation. It is very light and cheaper than carbon and basalt fiber.

4.7.2 Chemical solutions

They are four chemical solutions used in this experiment, each very different from one another; acidic, alkaline, saline and deionized or distilled water. Three were mixed using a specific chemical compound with ionized water while the last was just pure ionized water.

4.7.3 Deionized water

Deionized or distilled water, is water in its purest form. Deionization is a chemical process that removes mineral ions, cations and anions, such as sodium, calcium, iron and sulfate. The water was provided within the lab and it was used to create the other 3 solutions.

4.7.4 Acidic

The Owens Corning guide showed that the solution with the highest percentage of weight loss was hydrochloric (HCl) acid. To obtain an acidic environment of 10%, 200mL of pure HCl was mixed with deionized water in a 2L Florence flask.

4.7.5 Alkaline

Sodium hydroxide (NaOH) was used to create the alkaline solution. The pH level needed was 12.89, thus to reach that value, 3.2g/L of NaOH was mixed with deionized water. Again, the solution was mixed in a 2L Florence flask, hence, an average value of 6.4g of NaOH was used per flask.

4.7.6 Saline

In order to have maintain the same chemical level in each solution, approximately 200g of sodium chloride (NaCl) was combined with ionized water in a 2L Florence flask. The result was a saline solution of 10%.

4.7.7 Results

Table 4.16 presents all the percentage of weight loss for each specimen and charts to compare weight loss of the glass fibers with different conditioning time and specific chemical solutions. Also, Figure 4.39 shows the weight loss of glass fiber after 24hrs in every chemical solution.
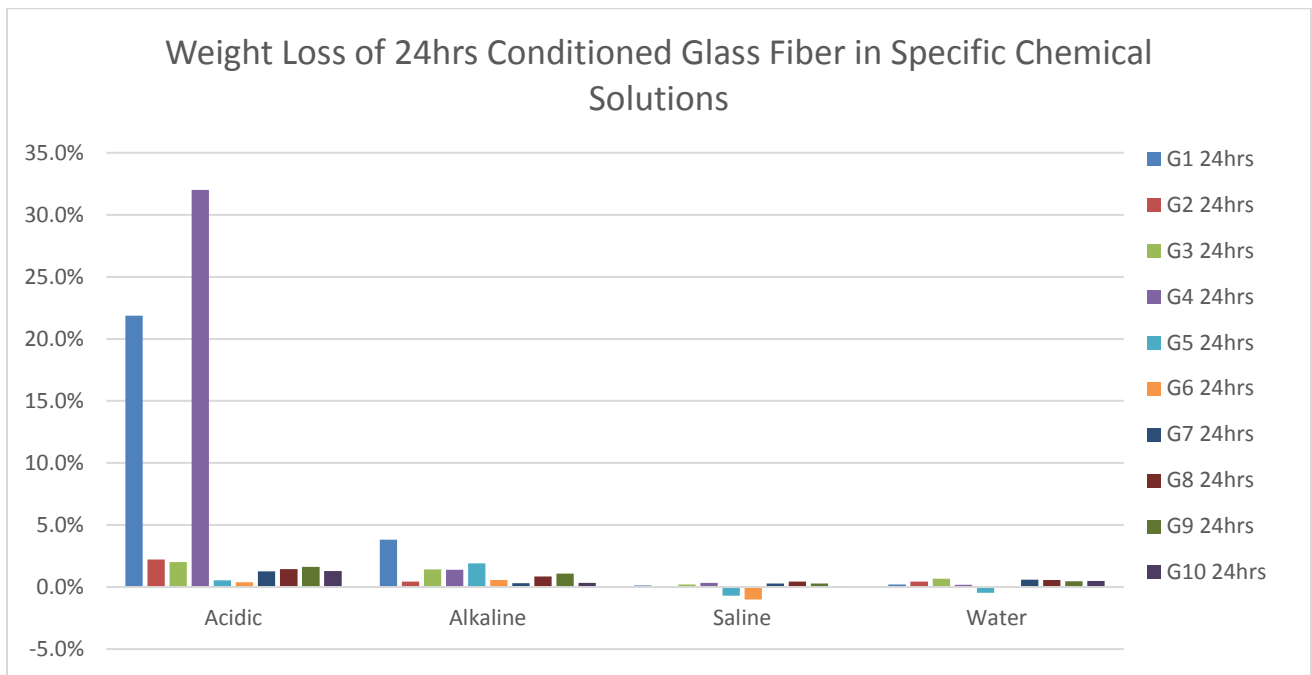
Figure 4.39**:** Weight loss of glass fiber after 24hrs in every chemical solution

4.7.8 Analysis

To simplify the analysis, all 10 types of glass fiber where divide into 2 groups. VI and V4, due to their low resistance in the acidic solution and the rest (V2,V3,V5,V6,V7,V8,V9 and V10) due to their very similar results in the weight lost analysis.

V1 and V4

V1 and V4 were the two fibers with the highest weight loss with approxmitely 22% and 33% respectively. The SEM and weight analysis showed that they were the weakest and least corrosion resistant fiber. In the figures below, the fibers from the acidic environment show signs of rupture and corrosion. Eventhought there was no sign of loss of mass in the alkaline solution, the SEM illustrated that the

fiber reacted witht the chemicals and created a lot of residue on the surface. Fiber mass lost may have been converted into the large amount of chemical deposit. The fibers from the saline solution didn't lose much weight and didn't show much sign of chemical reaction.

Table 4.16: Weight loss percentage for all 128 different specimens

Weight Loss of FRP			Acidic	Alkaline	Saline	Water
Glass Fiber	G1	24Hr	21.9%	3.8%	0.1%	0.2%
		168Hr	21.9%	2.9%	-0.1%	0.3%
	G2	24Hr	2.2%	0.4%	0.0%	0.4%
		168Hr	1.5%	1.9%	-0.1%	0.2%
	G3	24Hr	2.0%	1.4%	0.2%	0.7%
		168Hr	2.4%	2.2%	0.0%	1.1%
	G4	24Hr	32.0%	1.4%	0.3%	0.2%
		168Hr	35.1%	3.1%	0.0%	1.3%
	G5	24Hr	0.6%	1.9%	-0.7%	-0.5%
		168Hr	1.7%	-1.0%	-0.1%	0.4%
	G6	24Hr	0.4%	0.6%	-1.0%	0.0%
		168Hr	1.8%	-0.2%	0.2%	0.4%
	G7	24Hr	1.3%	0.3%	0.3%	0.6%
		168Hr	2.1%	-0.3%	-0.4%	0.4%
	G8	24Hr	1.4%	0.8%	0.4%	0.6%
		168Hr	2.0%	0.3%	-0.3%	0.4%
	G9	24Hr	1.6%	1.1%	0.3%	0.5%
		168Hr	2.5%	1.0%	-0.3%	0.5%
	G10	24Hr	1.3%	0.3%	0.1%	0.5%
		168Hr	2.7%	-1.1%	-0.1%	0.3%

(a)   (b)
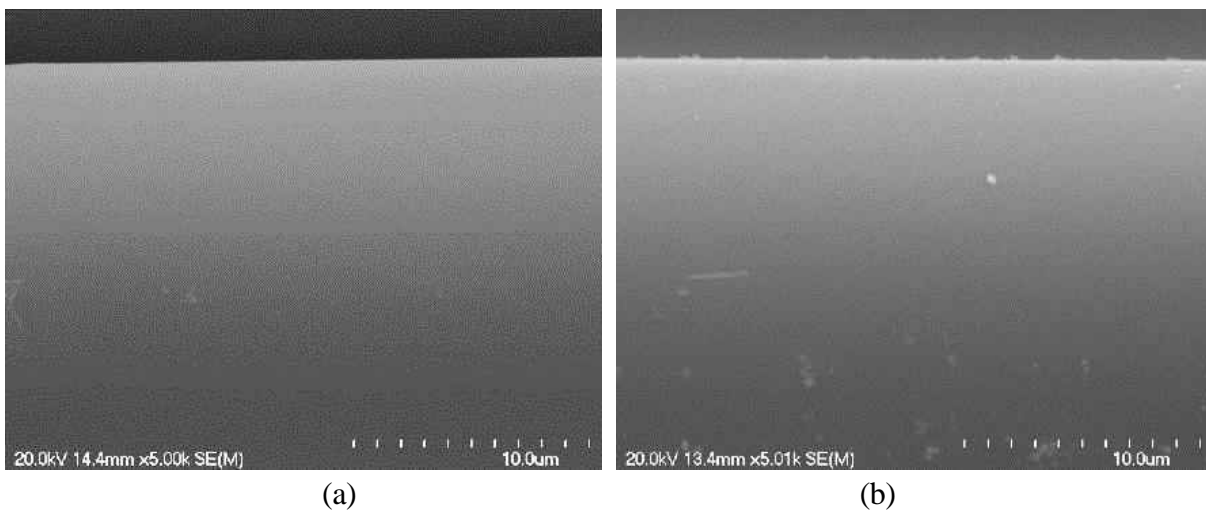
Figure 4.40**:** SEM analysis at 5000X of the reference glass fiber a)V1 and b)V4

180
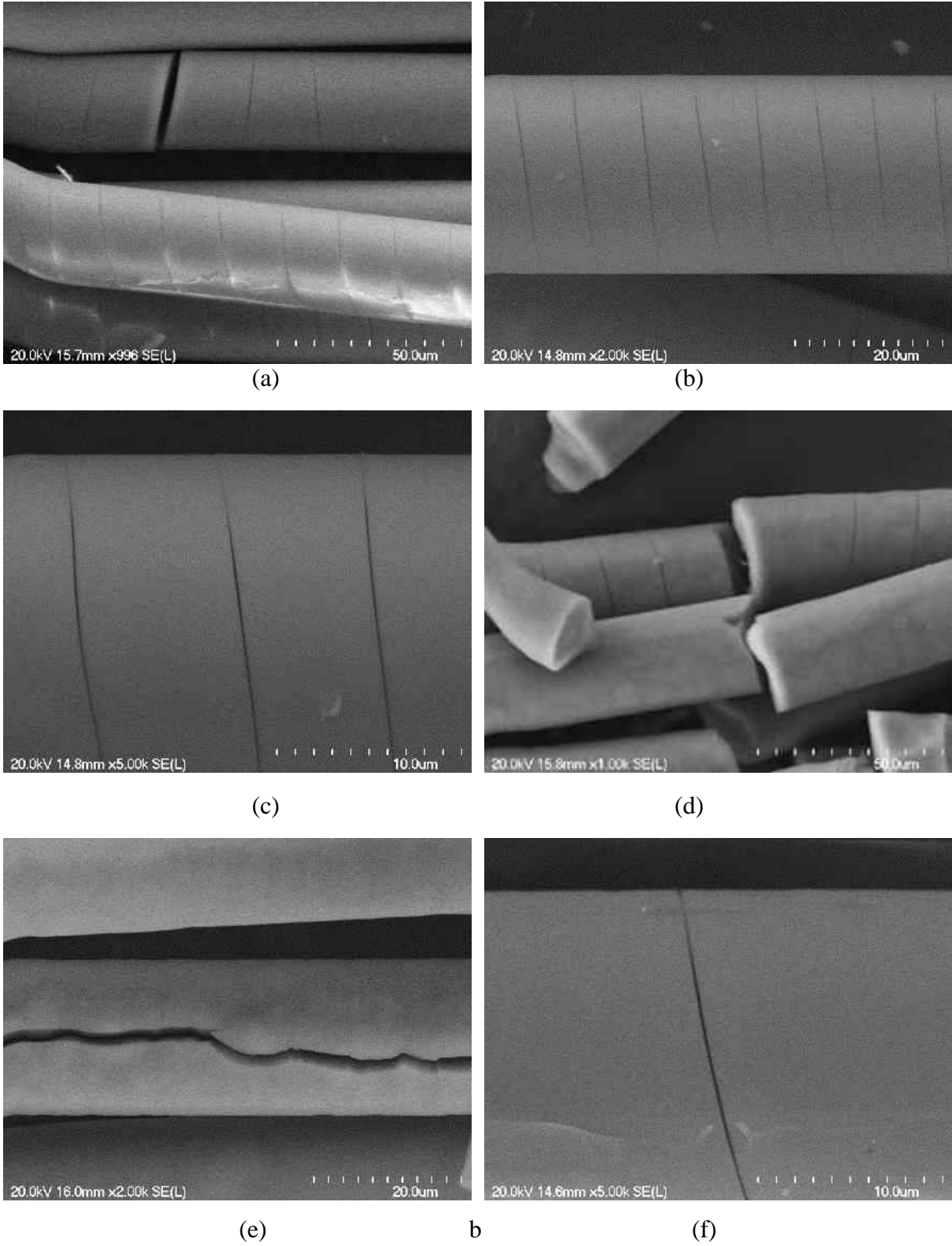
Figure 4.41: SEM analysis at of glass fiber submerged in HCl for 168 hr, a)V1 at 1000X, b)V1 at 2000X, c)V1 at 5000 d)V4 at 1000X, e)V4 at 2000X and f)V4 at 5000X

<center>(a)   (b)</center>
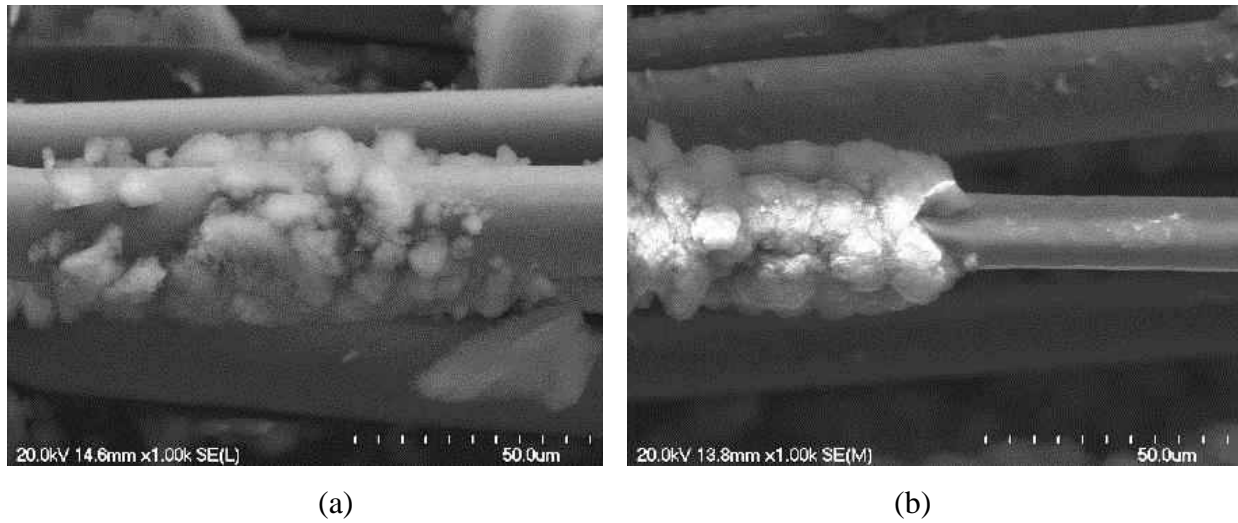
Figure 4.42: SEM analysis at 1000X of the glass fiber submerged in NaOH solution a)V1 and b)V4

<center>(a)   (b)</center>
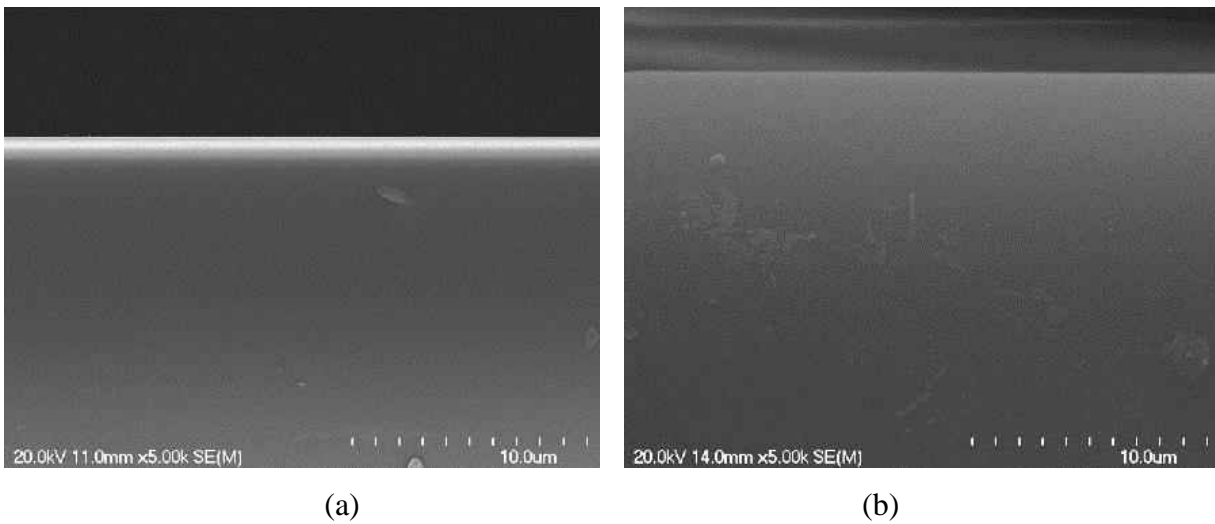
Figure 4.43: SEM analysis at 5000X of the glass fiber submerged in NaCl solution a)V1 and b)V4

<u>The rest (V2, V3, V5, V6, V7, V8, V9 AND V10)</u>

The first set of figures shows all the reference glass fibers from the second group.

<center>182</center>

(a)

(b)

(c)

(d)

(e)

(f)

183

(g)   (h)
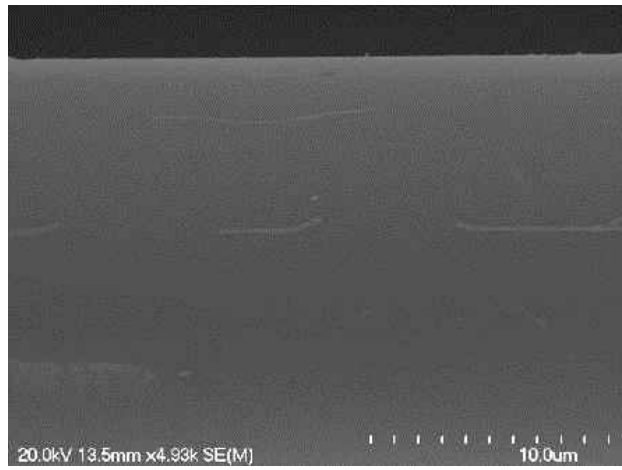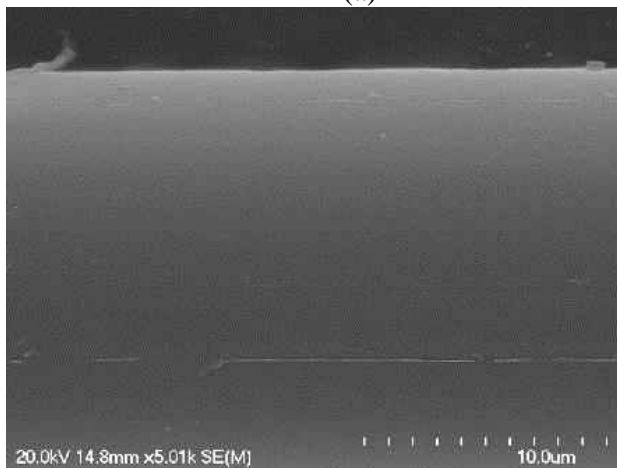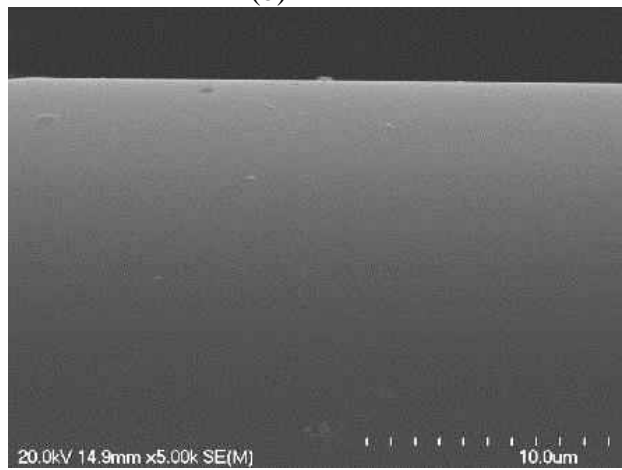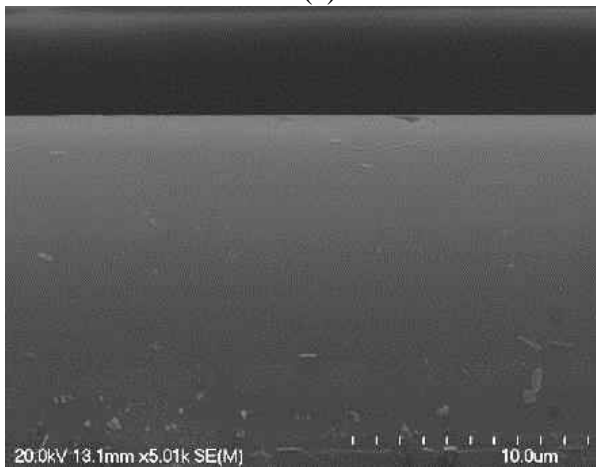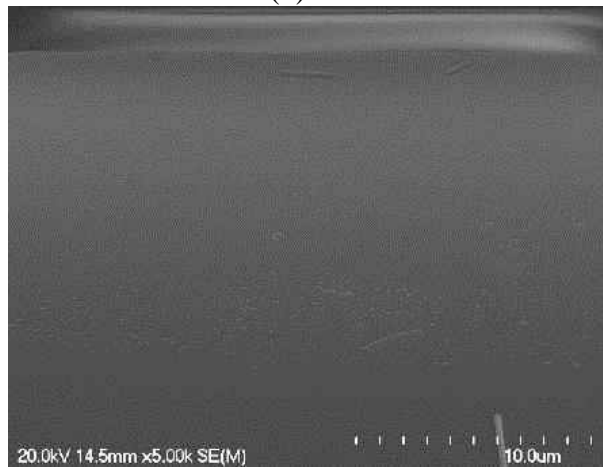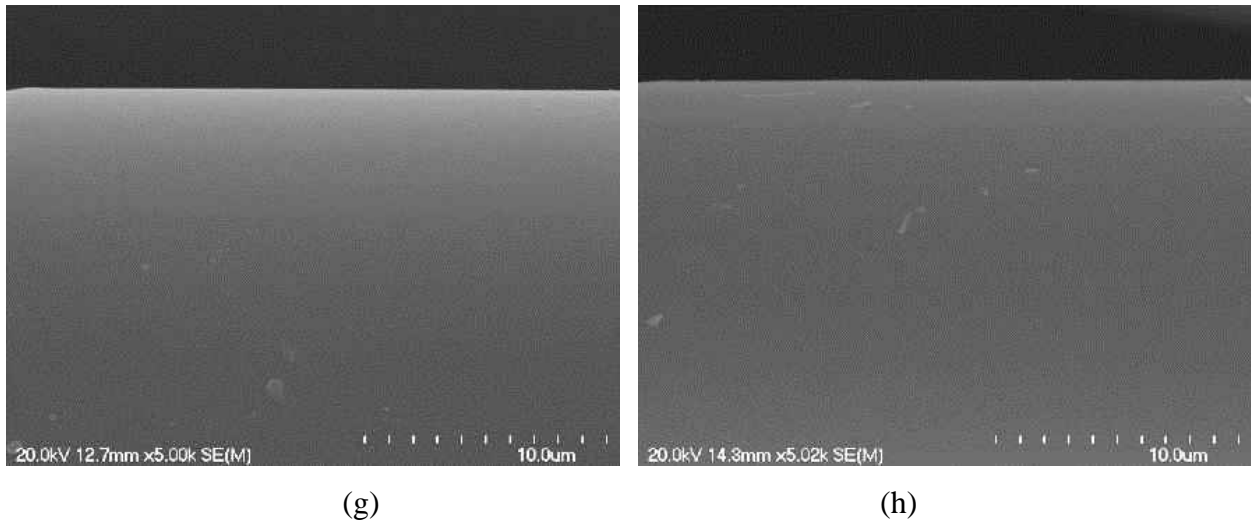
Figure 4.44**:** SEM analysis at 5000X of the reference glass fiber a)V2, b)V3, c)V5, d)V6, e)V7, f)V8 g)V9 and h)V10

All of these glass fibers were very resistant to the acidic solution. Barely any weight was loss and the SEM showed no change and no chemical reaction. These glass fibers resist even better than the basalt ones, losing only 1-2% of their mass.

(a)   (b)

(c)

(d)

(e)

(f)

(g)

(h)
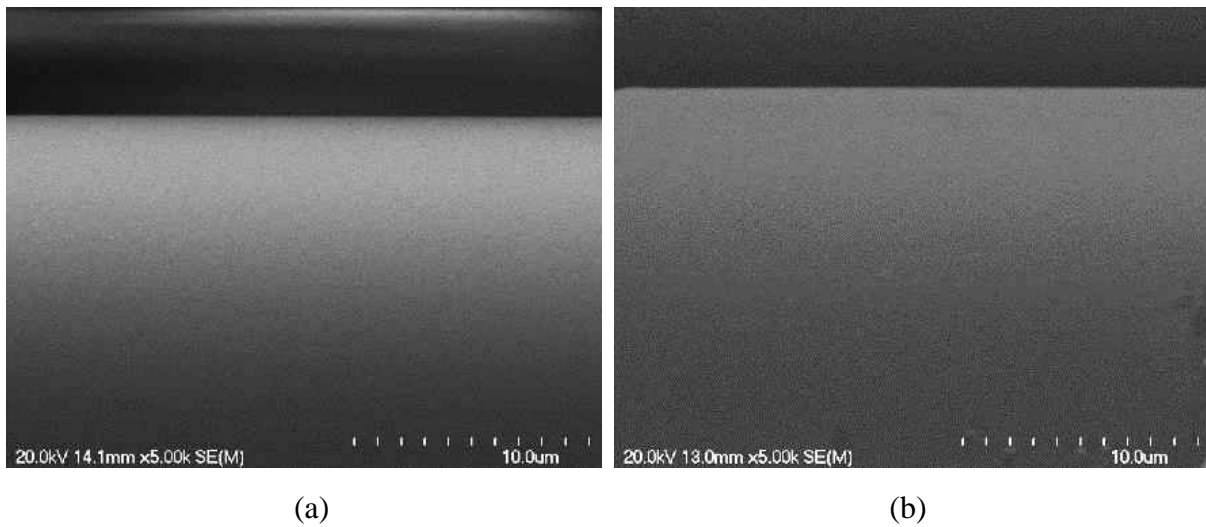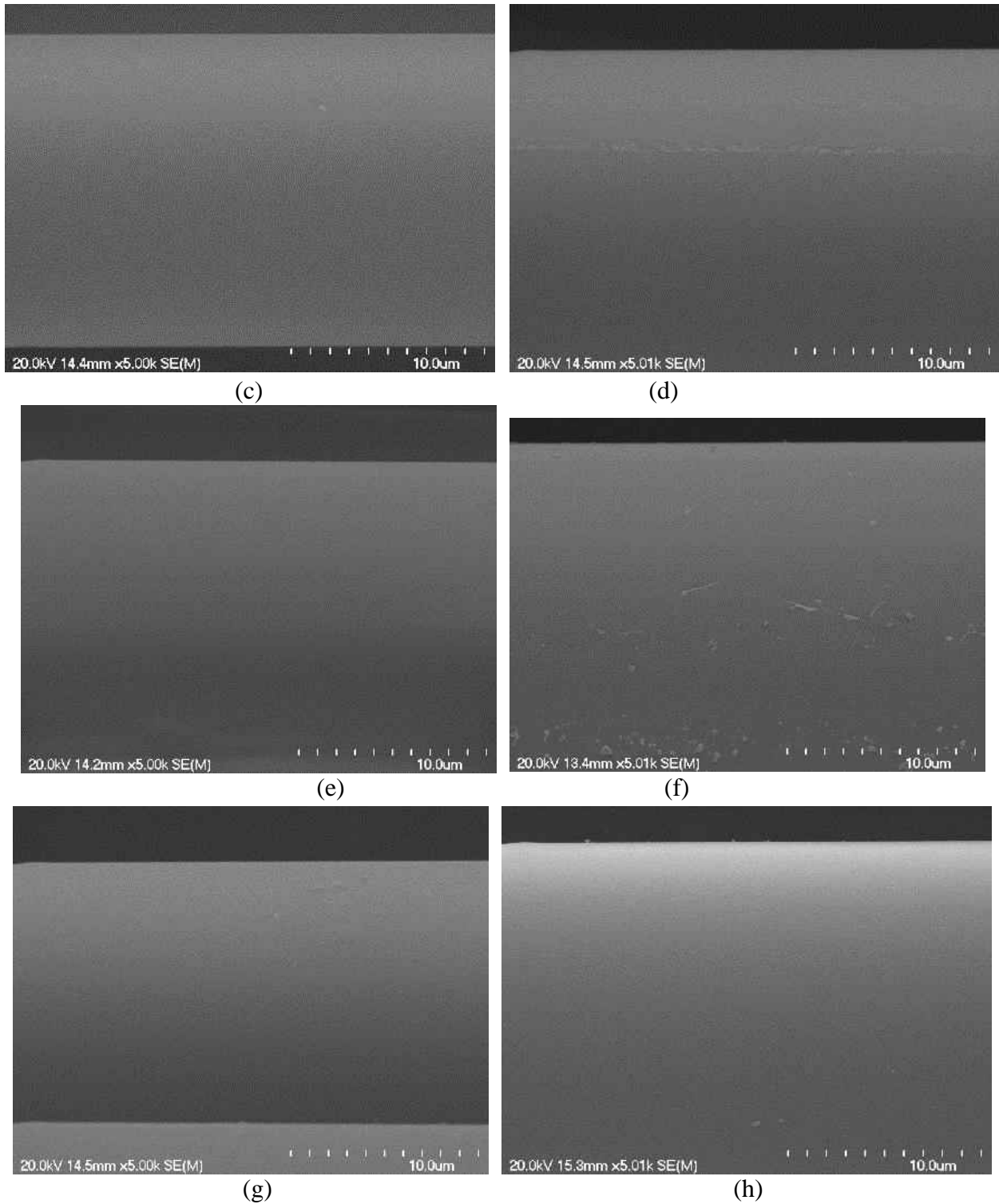
Figure 4.45**:** SEM analysis at 5000X of the glass fiber submerged in HCl for 168 hr, a)V2, b)V3, c)V5, d)V6, e)V7, f)V8 g)V9 and h)V10

Eventhought these glass fibers were highly resistant to hydrochloric acid, they produced a lot of chemical reaction and residue with the alkaline solution. The weight analysis showed very little weight loss for some, while V5, V6, V7 and V10 gained mass. To make sure there were no mistake, the test was done twice and both times, all four fiber showed to have gained mass instead of losing some. SEM analysis showed that the fiber was indeed corrode by the solution, however the chemical deposit formed would compensate for the loss fiber mass. For exemple, V5 showed weight loss after 24 hr but gained around 1% after 168 hr. This can be explained due to the fact that after 24 hr, the chemical would eat away the fiber but not have enough time to react and form alkaline residue, but after 168 hr, the chemicals had enough time to complete their reaction and deposit the extra mass onto the fiber.

The fibers showed almost no weight loss, around 0-1%, in a saline solution and the SEM analysis illustrate almost no corrosive activity but there was small chemical remains on the fibers. This explains the few mass gain from the weight loss analysis.
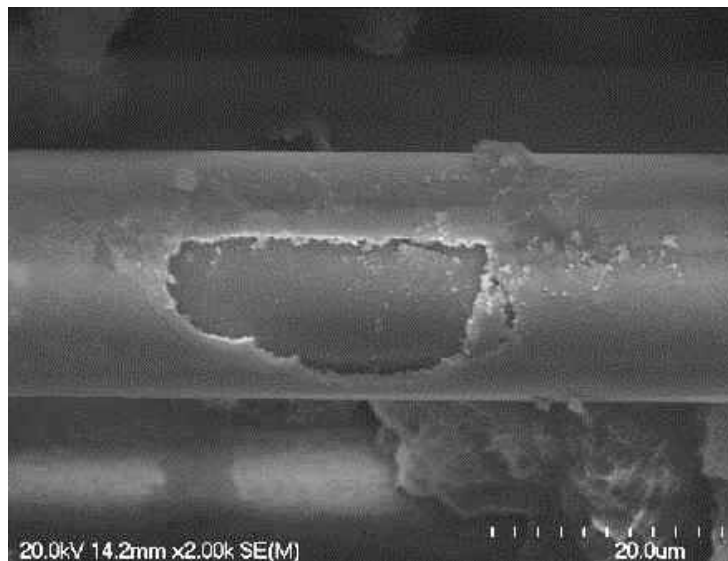
Figure 4.46: SEM analysis of V3 in alkaline solution for 168 hr with proof of corrosion and fiber loss

(a)
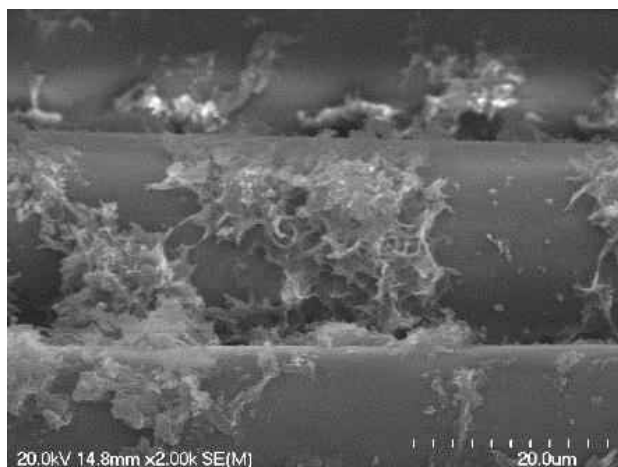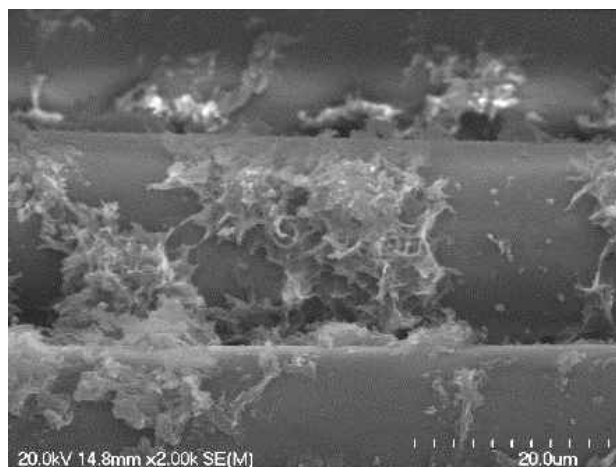
(b)
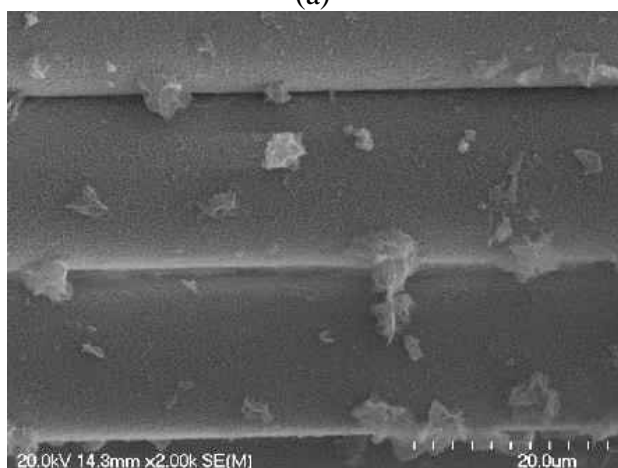
(c)
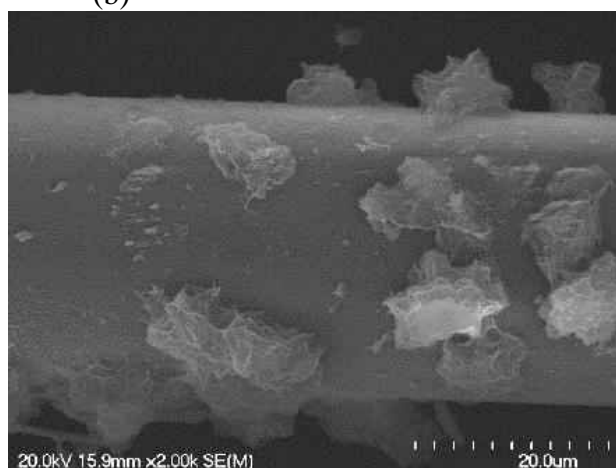
(d)
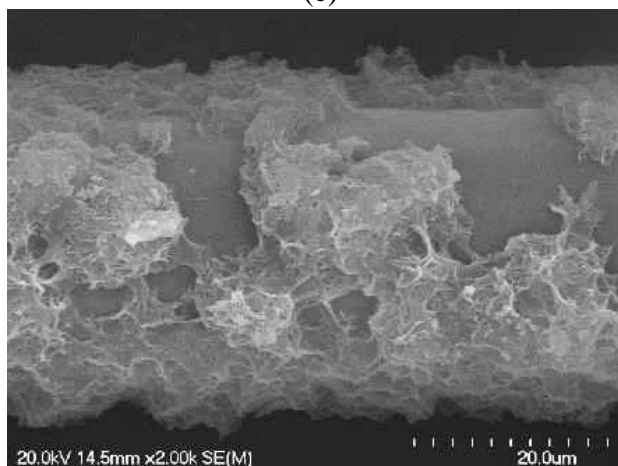
(e)
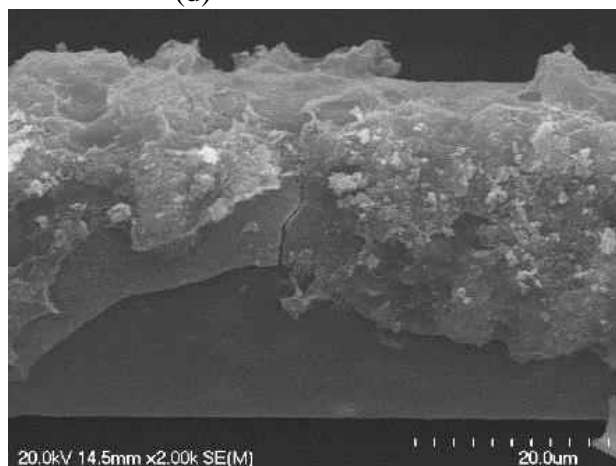
(f)
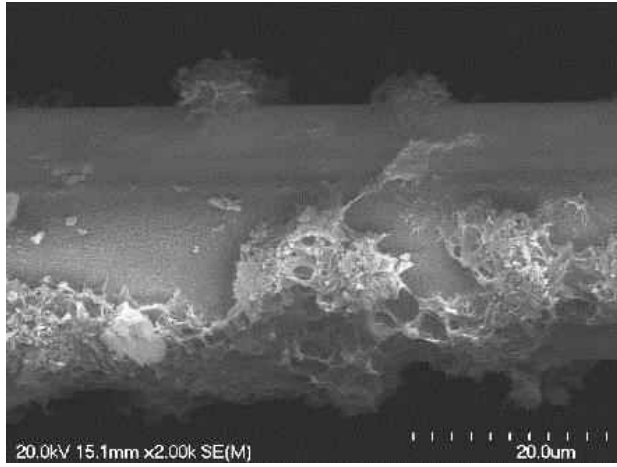
(g)
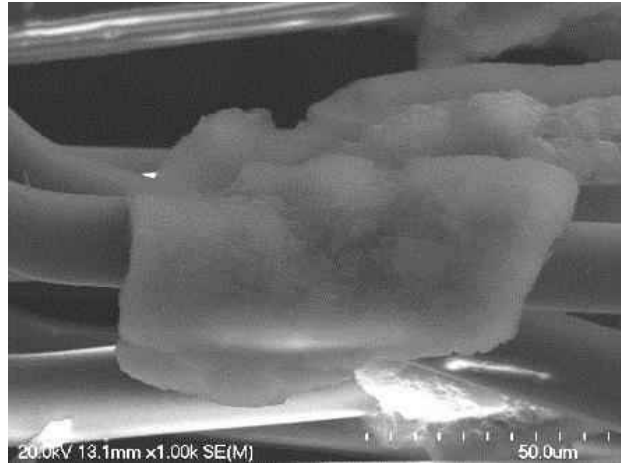
(h)

Figure 4.47**:** SEM analysis at 5000X (except for V10 at 1000X) of the glass fiber submerged in NaOH solution for 168 hr, a)V2, b)V3, c)V5, d)V6, e)V7, f)V8 g)V9 and h)V10
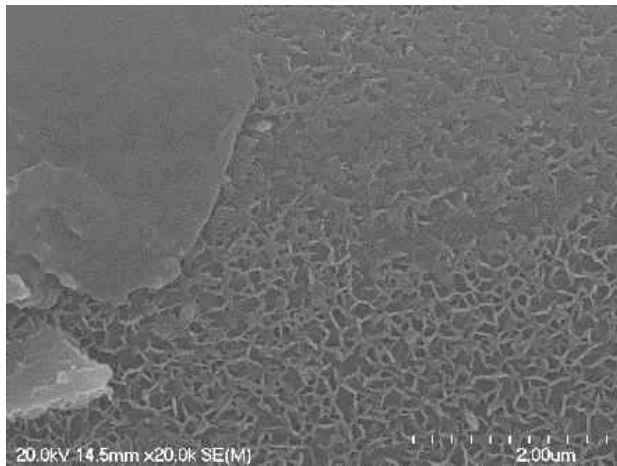
(a)
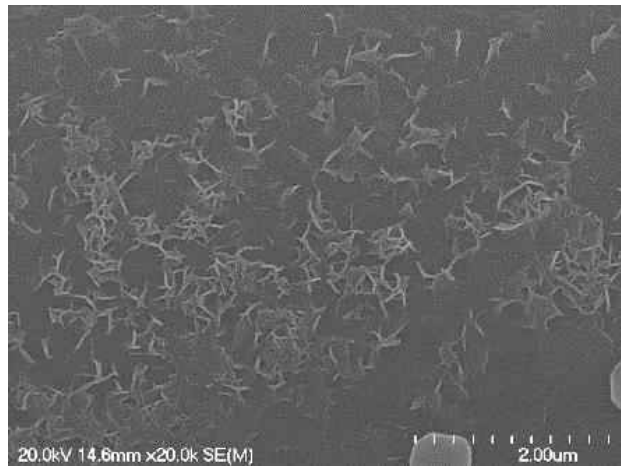
(b)
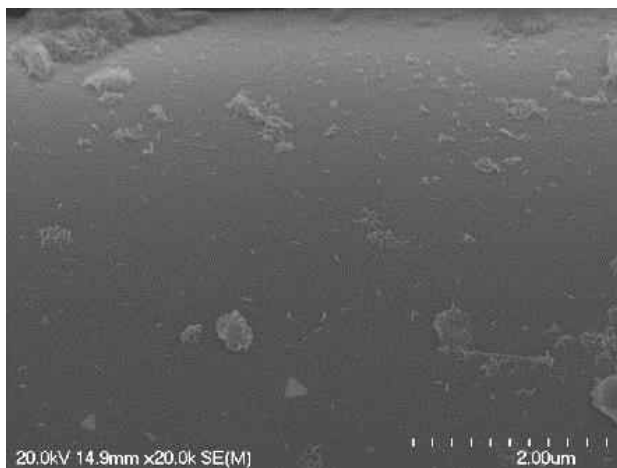
(c)
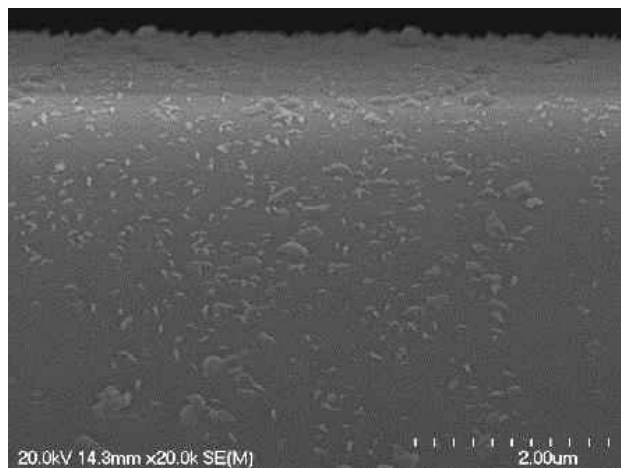
(d)
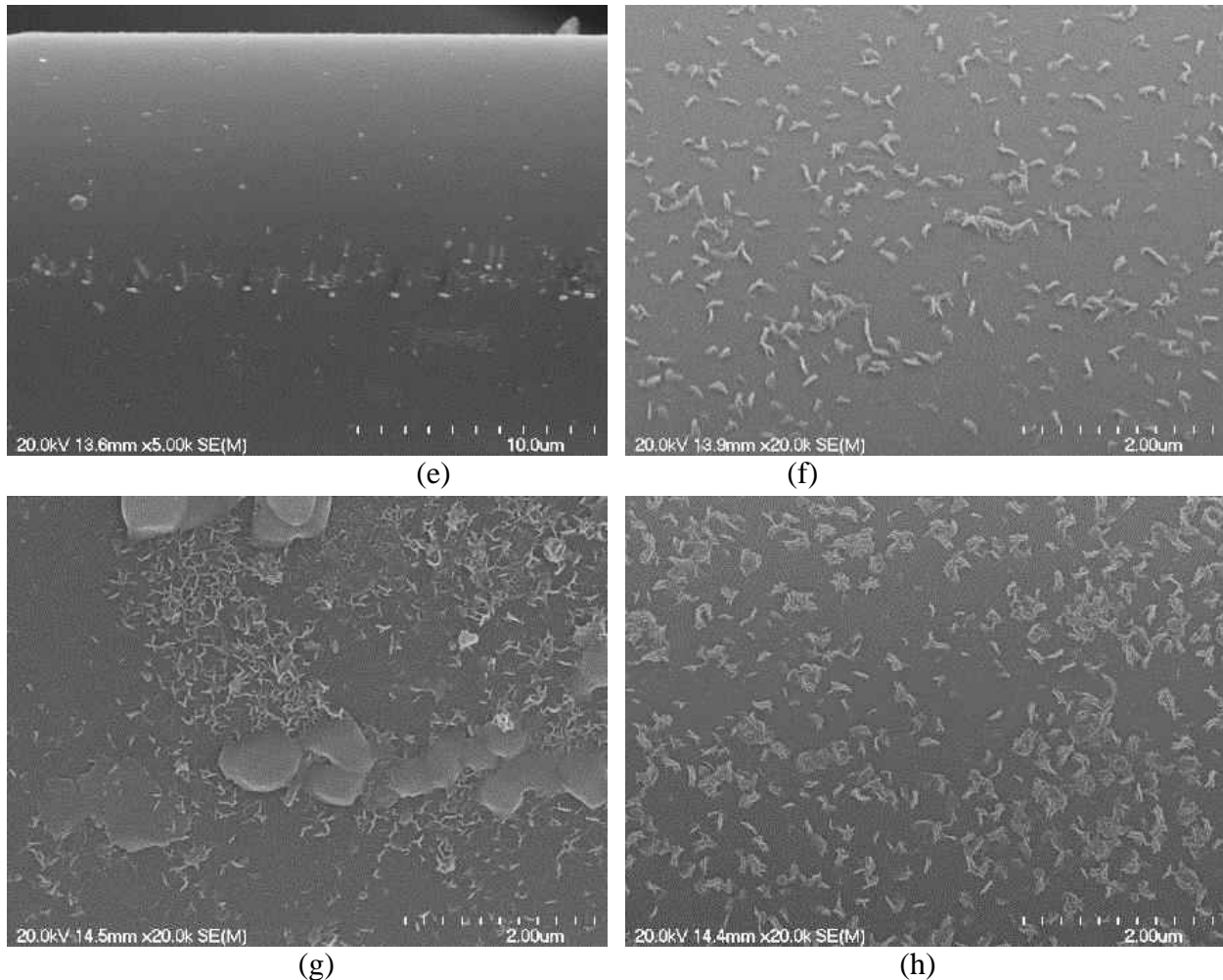
Figure 4.48: SEM analysis at 20 000X (except for V7 at 5000X) of the glass fiber submerged in NaCl solution for 168 hr, a)V2, b)V3, c)V5, d)V6, e)V7, f)V8 g)V9 and h)V10

4.8 Concrete beams testing with GFRP reinforcement

4.8.1 Introduction

This study investigates the combined effect of natural weathering conditioning and sustained tensile loads on the long-term flexural behavior of reinforced concrete (RC) members with glass fiber-reinforced polymer (GFRP) bars. The beams were previously manufactured. They were donated and made available for the project. A total of six beams with dimensions 9.8 x 9.8 x 78.7 inch (250 x 250 x 2000 mm) were designed with sand coated GFRP reinforcement (V-ROD, Pultrall Inc.) and tested. Three beams were subjected to sustained loads (40% of guaranteed tensile strength in tensile reinforcement) and natural Canadian weathering conditions (Brookside, Nova Scotia) for 10 years. The beams were subjected to harsh environmental conditions, including freeze–thaw cycles and moisture. This natural conditioning area is periodically subjected to

189

freeze–thaw cycles in which temperatures usually drop below -30ºC [-86ºF] during winter and exceed +30ºC [+86ºF] during summer. It also receives significant amount of snowfall and rainfall with an annual average of 47.2 inch (1200 mm).

The flexural behavior of the three GFRP-RC beams subjected to sustained high load equivalent to 40% of the ultimate tensile strength of the GFRP reinforcement and placed outdoor for 10 years under harsh natural environmental conditions, including freeze–thaw cycles and moisture was compared to that of the companion specimens without experiencing conditioning and sustained tensile load.

4.8.2   Dimensions of the beams and description of the materials

GFRP-RC beams

A total of six GFRP-RC beams, with dimension 9.8 x 9.8 x 78.7 inch (250 x 250 x 2000 mm), can be classified into two categories:
 1- Three specimens, real-time naturally conditioned and under sustained load for ten years;
2- Three control specimens kept with in the laboratory environment and no weather conditioning, no sustained load. Figure 1 illustrates the dimensions of the beams.

GFRP Reinforcement

GFRP bar size, tensile and compression GFRP longitudinal bars, and GFRP stirrups are shown in Figure 4.49. The properties of the GFRP reinforcement (V-ROD, Pultrall Inc.) are presented in the Table 4.17.

Concrete

A ready mix normal concrete with a target compressive strength of 5.0 ksi (35 MPa) was used. The average compressive strength of cylinder cores with dimensions of 4 inch (101.6 mm). Diameter and 9.84 inch (250 mm) height, extracted from the beams, was found to be 5.3 ksi (36.7 MPa), one year after casting of the beams.

Table 4.17: Tensile Properties of V-ROD GFRP #4 (2008)

Material properties	Value
Ultimate Tensile Strength (MPa)	757
Nominal Tensile Modulus of Elasticity (GPa)	40.8
Ultimate Tensile Strain	1.9%
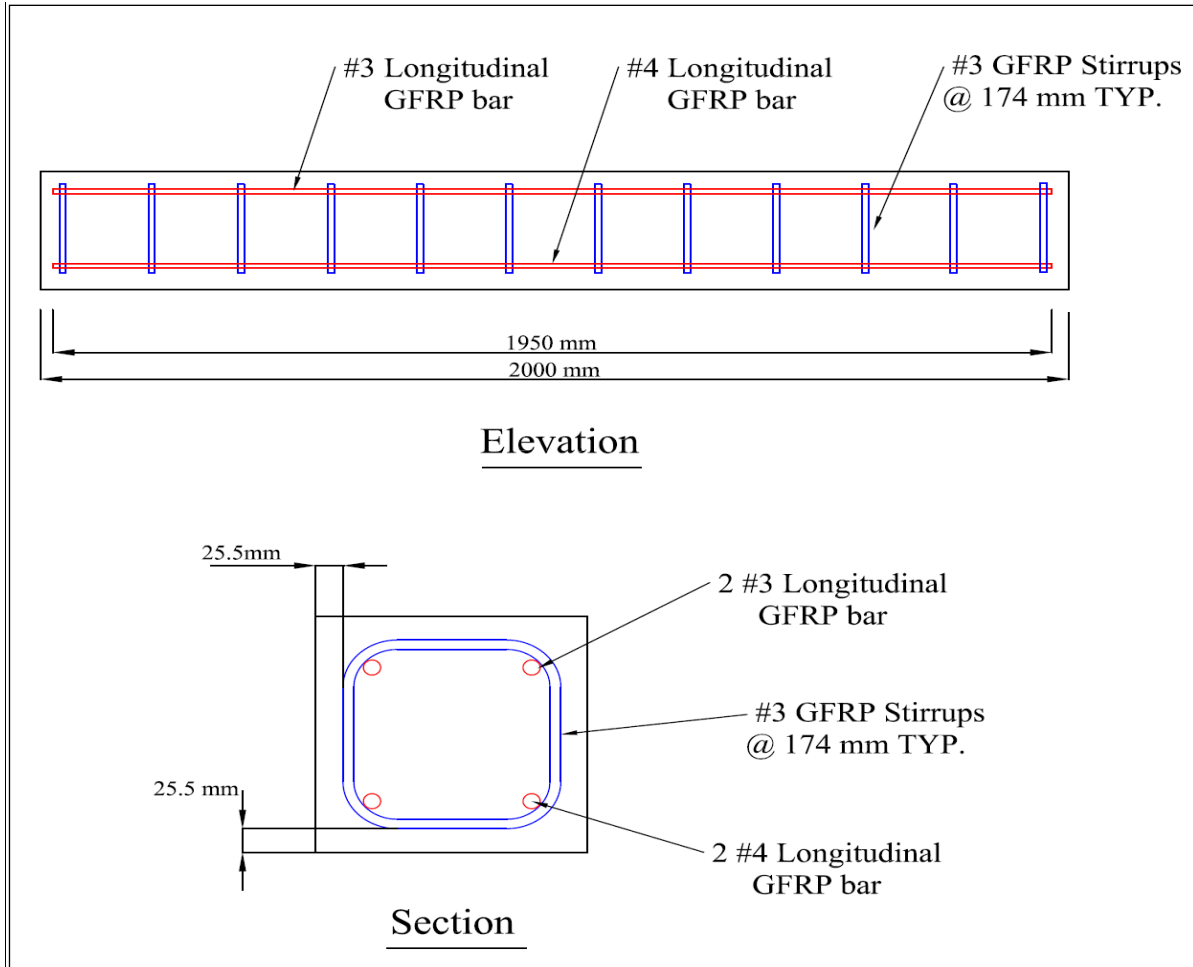
Figure 4.49: Beam geometry and cross section

4.8.3 Conditioning of the GFRP-RC beams and application of the sustained tensile load

The fabrication of the beams dates back to March 21, 2008, and was carried out at University of Dalhousie in Nova Scotia, Canada, through a collaborative research project between Prof. Brahim Benmokrane (University of Sherbrooke) and Prof. John Newhook (Dalhousie University). The beams had been left at a natural conditioning coupled with 40% sustained stress loading, until they were released from stress and delivered to University of Sherbrooke in March 2018 for testing. Figure 4.50 shows a view of the beams under sustained tensile load and natural weathering. All beams were clamped in pairs using externally transverse steel rods at the beam end to simulate crack damage under service conditions, as shown in Figure 4.50. Two roller supports were placed on the top surface of each beam at the one-third location of the beam length measured from each end. The region between two roller supports is considered as a pure bending zone (zero shear zone). The sustained load level in the tensile GFRP reinforcement was selected as 40% of the ultimate tensile strength, which is higher than two times of the allowed value by the FRP CSA

codes, AASHTO LFRD Code, and ACI 440.1R. A constant deformation was maintained during the test through clamping. The torque that was applied to the nuts at the end of each frame was determined through testing performed using a load cell. The torques and associated forces that were applied to the beams can be seen in Table 4.18. Three control beams were tested in flexure nearly one year after the fabrication at Dalhousie University University, and three beams of conditioned group were tested at University of Sherbrooke after ten years (19th of March 2018) under the supervision of Prof. Benmokrane. The aim was to assess whether there is any change in actual beam capacity over time or no.
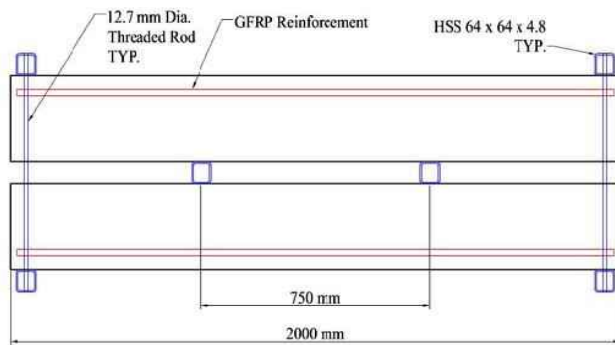
Figure 4.50: placed into long-term stressing frames and natural harsh weathering

Table 4.18: Forces applied to the beams in the long term stressing frames

Beam Reinforcement	Applied Moment	Applied Load	Reinforcement Stress	Applied Torque	
	kN.m	kN	%Ultimate	N-m	ft-lb
V-ROD bar	15.7	13.6	40	16.8	12.4

4.8.4 Four-point bending tests

The GFRP-RC beams were designed to fail through flexural tension using 4-point bending test; in that, the influence of the environmental conditioning and sustained load on the GFRP reinforcement can be assessed by the changes in the ultimate flexural strength of specimens. In other words, if the GFRP bars suffer from any degradation over time a decrease in the strength would be obtained as a result. However, this was not the only factor that was monitored during the tests. In fact four items were observed as the outcomes of the study: 1- Ultimate flexural strength, 2- Mid-span load-deflection curve, 3- Failure mode of the beams, and 4- Crack pattern.

4.8.5 Test sep-up

All beams were subjected to four-point bending after the natural weathering Conditioning. All tests were displacement-controlled at a rate of 0.15 mm/min. Figure 4.51 shows the test set-up and geometry of the beam specimens. The ultimate loads are defined as the maximum loads measured

by the load cell used with the data acquisition (DAQ) system. A hydraulic jack applied the load to the GFRP-reinforced concrete beams with GFRP through a spreader beam. In order to measure the deflection of the tested beam, two transducers (linear variable differential transducers and strain gauge-based transducers) were used in the mid-span section (pure bending region). Two LVDTs with an accuracy of 0.05 mm were used to measure crack widths at the location of the bottom reinforcement.
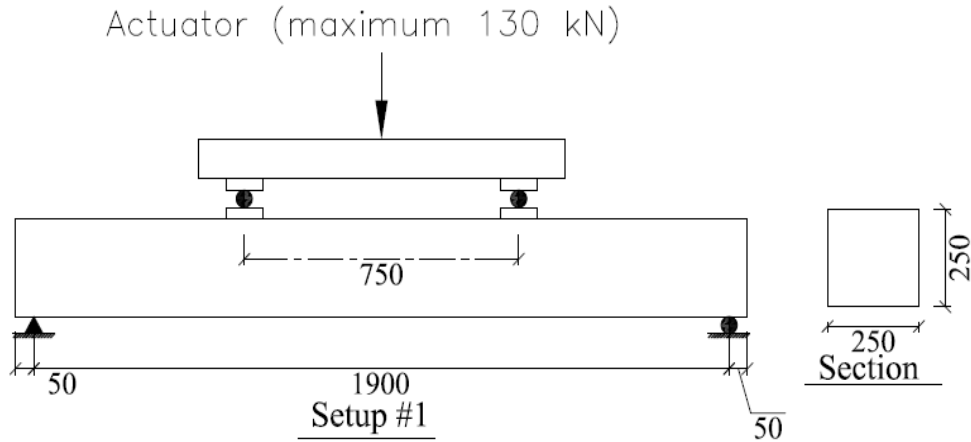
Figure 4.51: Test setup for the beam specimens

4.8.6 Test results

4.8.6.1 Mode of failure

The results obtained from the testing of the specimens were very consistent for all three specimens within each group. The observed failure mode of these beams was flexural-tension failure of the beam in the constant moment zone for all specimens (see Figure 4.52), which is the same mode of failure observed for the reference beams.

4.8.6.2 Moment-deflection response

The moment-deflection curve of the tested specimens is shown in Figure 4.53. It is observed that the average ultimate flexural strength of the conditioned beams was only decreased to 82% of average initial strength over 10 years of conditioning and undergoing a high sustained load equal to 40% of ultimate ensile strength of GFRP bars.

4.8.6.3 Crack pattern and crack-width

 Figures 4.54 and 4.55 depict crack pattern for the reference and conditioned specimens. The same crack pattern was observed. Additionally, crack width was also measured for the conditioned specimens for two major cracks by using two LVDT instruments, as shown in Figure 4.56. The

193

crack-width shown by the reference beams was equivalent to the crack-width shown by the con-ditioned beams.

Figure 4.52: Flexural tension failure mode observed in all of the control and conditioned specimens
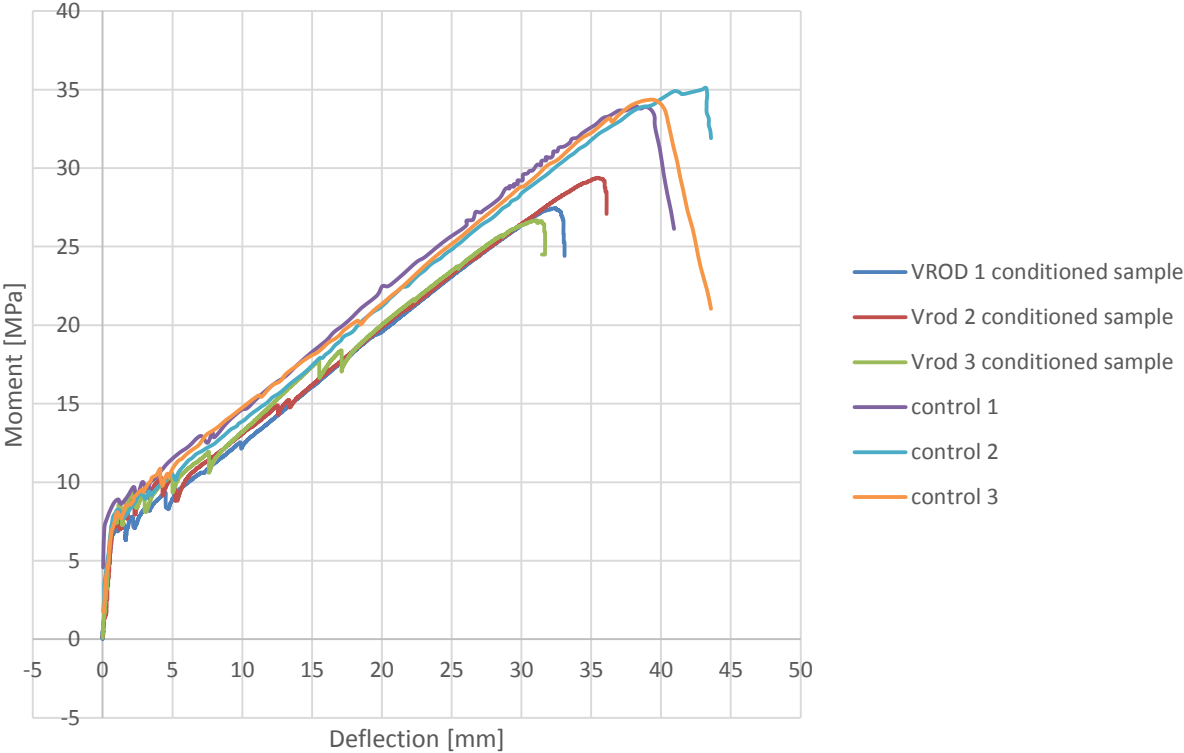
Figure 4.53: Moment-deflection curves of the beam specimens

Figure 4.54: Crack pattern of the conditioned beam specimens

Figure 4.55: Crack pattern of the control beam specimens
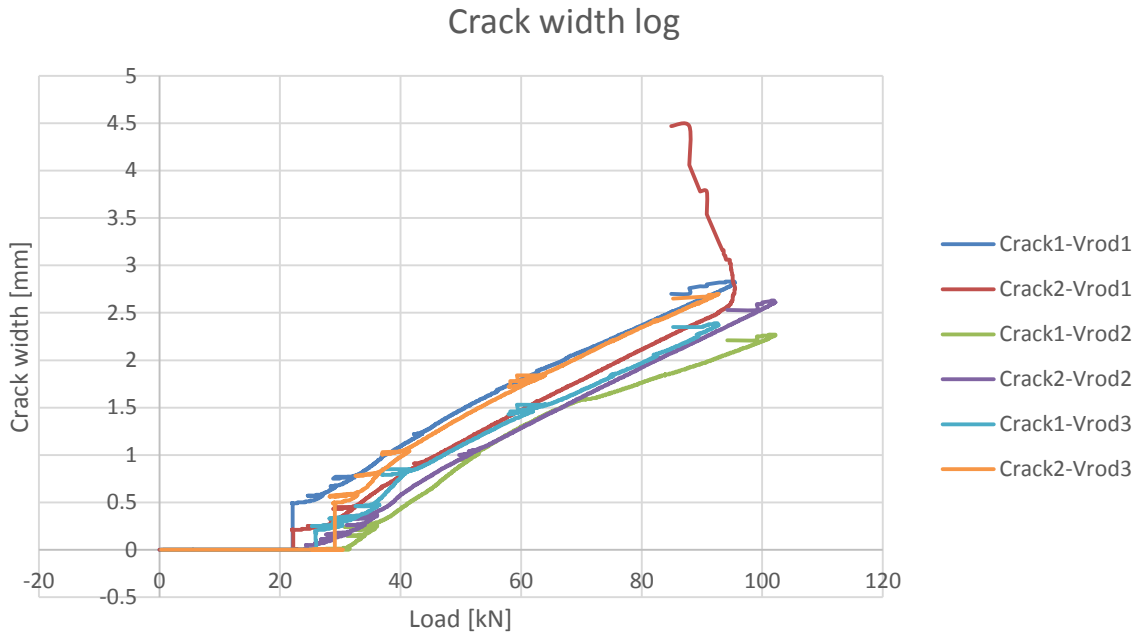
Crack width log

Figure 4.56: Measured crack-width for the conditioned beam specimens

4.8.7 Conclusions on Beams

This study presented the flexural behavior of concrete beams reinforced with GFRP bars that were subjected to sustained high load of 40% of the ultimate tensile strength of the GFRP reinforcement and placed outdoor for 10 years under harsh natural environmental conditions, including freeze–thaw cycles and moisture. The following conclusions have been developed:

1. The investigation of the GFRP beams after 10 years of aggressive environmental conditions and high sustained load of 40% guaranteed tensile strength was a very valuable asset that provided great information ensuring degradation of GFRP bars. The tensile strength retention was 82% after 10 years of service life.

2. There is a correlation between the degradation and performance of GFRP in beams and conditioned GFRP bars. Using the analytical model that incorporates the test results for conditioned GFRP bars, a 90% reduction is predicted in the ultimate strength after 10 years under sustained loading of 30% guaranteed tensile strength, temperature ranging from 10°c to 35°c, and alkaline exposure.

3. It is evident that the trend of degradation and strength reduction of GFRP bar reinforcement in concrete beams is similar to that for the conditioned GFRP bars. The discrepancy of the tensile strength retentions for the GFRP bars in beams (82%) and conditioned GFRP bars (90%) could be attributed to the higher sustained loading of 40% guaranteed tensile strength for the beams compared to only 30% guaranteed tensile strength for the conditioned GFRP bars, among other factors. These factors could include the freeze-thaw effect

196

due to the exposure to snow and freezing effects that could affect the concrete beam, in addition to any degradation at the interface between the FRP bars and the concrete that could occur due to long duration of exposure to outside harsh environment.

4. The mode of failure of the reference and conditioned beams was the same by tensile rupture of the GFRP reinforcement

5. The Crack pattern observed for the conditioned beams was equivalent to crack pattern recorded for the reference beams which is an indication no change in the bond of the GFRP reinforcement.

Recommendations:

Based on the tests results and the service-life prediction models that were developed, the tensile-strength retention can be predicted for GFRP bars and strength retention for GFRP beams, after 100 years of service life in moist alkaline environment with elevated temperatures and under sustained load.

4.9   Life prediction approaches for long-term performance of GFRP bars

4.9.1   Introduction

Significant work has assessed the performance and deterioration of FRP reinforcement for concrete. A wide range of results reports that clearly bar constituent materials and exposure conditions play a significant role in the performance of these systems. Researchers have used these results to generate deterioration models. These models can be used to predict the residual strengths at different times, thereby providing the designer with possible estimates of bar capacity at later ages. These residual strengths, or factored residual strengths, could then be used in the design of FRP reinforced concrete elements. In this study, the residual tensile strength of stressed GFRP bars (under sustained load) exposed to alkaline solution was used for long-term performance prediction based on the Arrhenius model and new model that incorporates the effects of temperature, design life, and relative humidity (RH) of exposure into the environmental reduction factor (RF) for the FRP bars used as concrete reinforcement.

4.9.2   Arrhenius relation

In endeavoring to assess the long-term durability performance of FRP in harsh environments, extensive studies have been conducted to develop accelerated aging procedures and predictive models for long-term strength estimates, especially for FRP bars (Davalos et al. 2012; Chen et al. 2006; Bank et al. 2003; Dejke 2001; Porter et al. 1997, Ali et al. 2015; Benmokrane et al. 2014, 2016, 2017). These models are based on the Arrhenius model. Research on the effects of temperature on the durability of FRP bars in concrete alkaline environments indicates that an accelerated factor for each temperature difference can be defined using Arrhenius laws. These factors differ for each product, depending on fiber and resin types and bar size. In addition, these factors are affected by environmental conditions,

such as surrounding solution media, temperature, pH, moisture, and freeze–thaw conditions. Predictive models based on Arrhenius laws make the implicit assumption that the elevated temperature will only increase the rate of degradation without affecting the degradation mechanism or introducing other mechanisms. Gerritse 1998 indicated that at least three elevated temperatures were necessary to perform an accurate predication based on Arrhenius laws. Moreover, the measured data should be in continuous time intervals. These recommendations were considered in this study.

Based on the short-term data from accelerated aging tests, the Arrhenius model was adopted to predict the long-term behavior of the GFRP bars. In the Arrhenius relation, the degradation rate is expressed as Eq. (4.13) (Nelson 1990).

$$k = A \exp\left(\frac{-E_a}{RT}\right) \tag{4.13}$$

where k = degradation rate (1/time); A = constant relative to the material and degradation process; E_a = activation energy of the reaction; R = universal gas constant; and T = temperature in Kelvin. The primary assumption of this model is that only one dominant degradation mechanism of the material operates during the reaction and that this mechanism will not change with time and temperature during the exposure (Chen et al. 2006). But the degradation rate is accelerated with the increase in temperature. Eq. (4.13) can be transformed into Eqs. (4.14) and (4.15):

$$\frac{1}{k} = \frac{1}{A} \exp\left(\frac{E_a}{RT}\right) \tag{4.14}$$

$$\ln\left(\frac{1}{k}\right) = \frac{E_a}{R}\frac{1}{T} - \ln(A) \tag{4.15}$$

Eq. (4.14) shows that the degradation rate k can be expressed as the inverse of the time required for a material property to reach a given value. Eq. (4.15), shows that the logarithm of the time required for a material property to reach a given value is a linear function of 1=T with a slope of $Ea=R$ (Chen et al. 2006). Ea and A can be easily calculated with the slope of the regression and the point of intersection between the regression and the y-axis, respectively. More details on using the Arrhenius model and long-term-durability prediction models of FRP reinforcement can be found in Davalos et al. (2012).

Dejke and Tepfers (2001) proposed another service life prediction approach for GFRP bar involving time shift factor (*TSF*) to estimate the service life of GFRP bars by describing the relationship between accelerated and nonaccelerated exposures. The *TSF* value between the reference temperature and selected temperature can be written as in Eq. (4.16).

$$TSF = e^{[B/(T1+273.15)] - [B/(T2+273.15)]} \tag{4.16}$$

where *TSF*=time shift factor; *B*=constant determined using the time shift of two known curves; and T_1, T_2 = temperatures between which the *TSF* is calculated (T_1: smaller temperature). As can be seen from expression (4.16), the TSF approach requires only two aging data sets at different temperatures. TSFT$_1$−T$_2$ can be obtained by simply taking the ratio of the time values required for the specified

strength loss from data at two different temperatures, then B value can be obtained by TSFT$_1$−T$_2$. Thereafter, any *TSF* for temperature T other than T_1 and T_2 can be obtained by substituting the temperature T value into Eq. (4.16). This approach can be used to determine the relative *TSF* between two exposure temperatures under the assumption that the Arrhenius timetemperature relationship is valid for the whole temperature range considered (Dejke and Tepfers 2001).

To date, in order to insure safe design of FRP bar for reinfoeced concrete members, environmental reduction factors (C_E) of FRP bar are adopted in the design codes/guidelines (Eq. 4.17) to account for the long-term durability of FRP bars, detailed as follows in American Concrete Institute (ACI 2015; FIB 2007); Norway Standard 1998; Japan Society of Civil Engineers (JSCE 1997); Canadian Standards Association International 2006; Canadian Standards Association (CSA S8-12).

$$f_{fu} = C_E \cdot f^*_{fu} \tag{4.17}$$

where f_{fu}=design tensile strength of GFRP bar; f^*_{fu} =guaranteed tensile strength of the GFRP bar defined as the average tensile strength of less than three times its standard deviation; and C_E =environmental RFs with 0.8 and 0.7 for concrete element nonexposed and exposed to the ground or moisture, respectively. The temperature effects are included in the value of C_E. In addition, the effects of applied stress during exposure are kept separate in ACI 440 due to insufficient data on combined weathering and applied stress. No more than 20% of the design rupture stress is recommended for safe design [American Concrete Institute (ACI 440.1R-2015)].

4.9.3 Degradation laws

Different mathematical equations describing the relationship between the strength retention and aging time have been proposed by researchers and are based on different theoretical foundations. Davalos et al. 2012 stated that there are generally four types of strength-degradation models for FRP bars and the prediction procedures for those models are all based on the Arrhenius equations shown in Eqns. (1) and (2). Serbescu et al. 2014 claimed that there are mainly two approaches for the performance prediction of FRP bars: measuring either "strength retention" or "moisture absorption." The following is a brief description of the four widely used mathematical models present in the literature. Tannous 1998 proposed the "moisture absorption" model:

$$Y = 100 \left(1- ((2.D.C.t)^2/r_o) \right)^2 \tag{4.18}$$

where Y is the strength retention (%) in this and all other equations presented in this paper, t is the exposure time, D is the diffusion coefficient, C is the concentration of the solution, and ro is the radius of the FRP bar. This model assumes that the affected area is completely degraded and unable to carry any load, which may not be entirely true. Additionally, the determination of the coefficients D and C from moisture absorption tests makes its use rather complicated. In addition, this equation cannot be used when the solution is distilled water, as the value of C would be zero. The second model adopted an exponential relationship between strength retention and aging time. Debonding at the fiber–matrix interface is assumed to be the major degradation mechanism in this model as is described via the following equation:

$$Y = 100 \exp\left(\frac{-t}{\tau}\right) \tag{4.19}$$

where τ is a fitted coefficient using the least squares method. It is worth noting that the tensile strength retention (%) at an infinite exposure time is assumed to be zero in this model. This model was originally used to predict the flexural-strength retention of composite laminates and had been adopted by many scholars [Chen et al. 2007, ACI 440.1R-2015] to predict the long-term performance of FRP bars. The third model adopted a linear relationship between the strength retention and the logarithm of the aging time via:

$$Y = a. \, log(t) + b \tag{4.20}$$

where a and b are regression constants. Litherland et al. 1981 first developed this model and successfully predicted the residual strength of glass-fiber concrete (GRC) using this model. It is worth noting that Eq. (5) is a widely used degradation model, but does not hypothesize the degradation mechanism. Some researchers have found, however, that the degradation lines at different temperatures in a single logarithmic scale from Eq. (5) are not parallel. Serbescu et al. 2014 used a double logarithmic scale in his study to plot the experimentally obtained tensile strength percentages in the fourth model described here:

$$\log(Y) = a.\log(t) + b \tag{4.21}$$

Based on Eq. (4.21), an approach for the calculation of the environmental-strength reduction factor ($\eta env,t$, which corresponds to $1/C_E$ in the ACI 440.1R-15) was established in Fib bulletin 40. For the detailed steps, the reader is referred to Fib bulletin 40. The aforementioned second, third, and fourth models all belong to the "strength-retention" approach.

4.9.4   New life prediction model for GFRP bars

In order to achieve more refined design of CFRP tendons reinforced concrete under service, environmental RFs need to be developed by taking all the effects of service temperature, RH, and design life into account. Several publications revealed that the degradation behavior of FRP bar subjected to solutions or moisture saturated concrete would follow Arrhenius empirical model (Bank et al. 2003; Dejke and Tepfers 2001; FIB 2007). In this study, based on the new model first proposed by Huang and Aboutaha (2010), that incorporates the effects of temperature, design life, and relative humidity (RH) of exposure into the environmental reduction factor (RF) for the FRP bars will be presented. Eq. (6) expresses the strength retention of FRP bar for specific design service life and service temperature [Huang and Aboutaha (2010)].

$$f_d = f_u \, . \, [1- \Delta_1- (\Delta_2+ \Delta_3)] \tag{4.22}$$

where f_d = design value or predicted value for tensile strength and f_u = characteristic value for tensile strength. The Δ_1 strength reduction value can be obtained by the experimental result as shown in

Figure 4.60. Δ_2 can be obtained by the triangular relationship from Figure 4.60 as presented in Eq. 4.23:

$$\Delta_2 = (tg\alpha) \cdot [\log(t_D) - \log(292)] = (-\phi) \cdot \log(t_D/292) = (-\phi) \cdot \log(DL) \qquad (4.23)$$

where ϕ = slope of the regression line as can be obtained by linear regression also; t_D = design lifetime in days; and DL = design life in years. Similarly, Δ_3 value can be obtained from Eq. 4.24:

$$\Delta_3 = (tg\alpha) \cdot [\log(ts) - \log(t_D)] = (-\phi) \cdot \log(ts/t_D) = (-\phi) \cdot \log(TSF) \qquad (4.24)$$

where t_S = lifetime in days by time temperature shift from T to T_1; and TSF is the time shift factor for temperature T and temperature T_1, which can be calculate based on proposed approach by Dejke and Tepfers (2001) as follows in Eq. 4.16.

By substituting the values of $\Delta2$ and $\Delta3$ into Eq. (1), fd can be rewritten as Eq. (4.25)

$$f_d = f_u \cdot [1 - \Delta_1 + \phi \cdot \log(DL \cdot TSF)] \qquad (4.25)$$

It is known that the contained water in concrete can be classified as capillary water, adsorbed water, interlayer water and chemically combined water. Huang and Aboutaha (2010) noted that the transportation of OH- can only occur in capillary water and some adsorbed water, which could be easily affected by the environmental relative humidity (RH). In moisture-saturated concrete, the degradation rate of FRP bars is the highest, and the degradation rate under less humidity can be adjusted using a correction factor (nH), which is closely related to the RH. The correction factor (nH) was assumed to be the same as the ratio of capillary and adsorbed water in the water content in concrete, as shown in Figure 4.61. The data presented in Fig. 4.61 are adapted from Huang and Aboutaha (2010). Thus the design tensile strength or predicted strength of GFRP bars in both saturated and unsaturated concretes can be written as Eq. (4.25)

$$f_d = f_u \cdot [1 - \Delta1 + \phi \cdot \log(DL \cdot TSF) \cdot n_H] = f_u \cdot RF \qquad (4.25)$$

where RF = reduction factor of tensile strength for the effects of service lifetime, temperature, and RH; nH would be equal to the ratio of mobile water in concrete under different RHs as shown in Figure 4.60. Δ_1, ϕ can be obtained by the accelerated aging data through linear regression. In this study, the residual tensile strength of stressed GFRP bars (under sustained load of 30%) exposed to alkaline solution was used for long-term performance prediction based on the Arrhenius model and new model that incorporates the effects of temperature, design life, and relative humidity (RH) of exposure into the environmental reduction factor (RF) for the FRP bars used as concrete reinforcement. The prediction results and discussion are presented in the following section.

4.9.5   Results and discussion for the prediction models of GFRP bars

4.9.5.1   Arrhenius model for GFRP bars under sustained load (30% of loading)

Predictions of the service life of the Pultrall and Aslan GFRP bars, at mean annual temperatures (MAT) of 10°C [50°F], 27°C [81°F] and 50°C [122°F] were performed according to the procedure based on previous work performed by Bank et al. (2003).The temperature of 10°C [50°F] is a close

approximation of the mean average temperature of northern regions, where deicing salts are often used. In addition, annual temperature (MAT) of 27°C [81°F] was performed according to weather condition of Florida State.The temperature of 50°C [122°F] exacerbates the combined effect of the mean annual temperature and the marine environment of the Middle East, and Caribbean (Robert and Benmokrane 2013). The Arrhenius plot can be used to extrapolate the service life necessary to reach the established tensile-strength retention levels (PR) for any temperature. Consequently, predictions were made for tensile-strength retention as a function of time for immersions at 10°C [50°F], 27°C [81°F] and 50°C [122°F]. Figure 4.57 and Figure 4.58 provide the general relationship between the PR and the predicted service life at the three MATs for Pultrall and Aslan GFRP bars, respectively. This figure shows that the predicted strength-property retention level (PR) for the Pultrall GFRP specimens immersed at an isotherm temperature of 10°C [50°F] would be slightly affected over 200 years. For the same specimen immersed at an isotherm temperature of 50°C [122°F], the service-life predictions are approximately 10 and 200 years for a PR of 88% and 84% (Pultrall GFRP bars) and 90% and 74% (Asaln GFRP bars), respectively. As expected, these results show that the long-term tensile strength of the GFRP was more affected by the alkaline environment in a warm climate. The predicted service life of GFRP embedded in an alkaline environment or aged in alkaline solution at an isotherm temperature of 10°C [50°F] to reach a PR of less than 80% can be estimated at more than 200 years. Figure 4.57 and 4.58 indicates that, even after a service life of 150 years—which corresponds to the longest design service life—the tensile-strength retention was still over 80% and 75% for MATs of 10°C [50°F] and 27°C [81°F], respectively. These predictions show that the GFRP bars are durable with respect to the concrete environment.
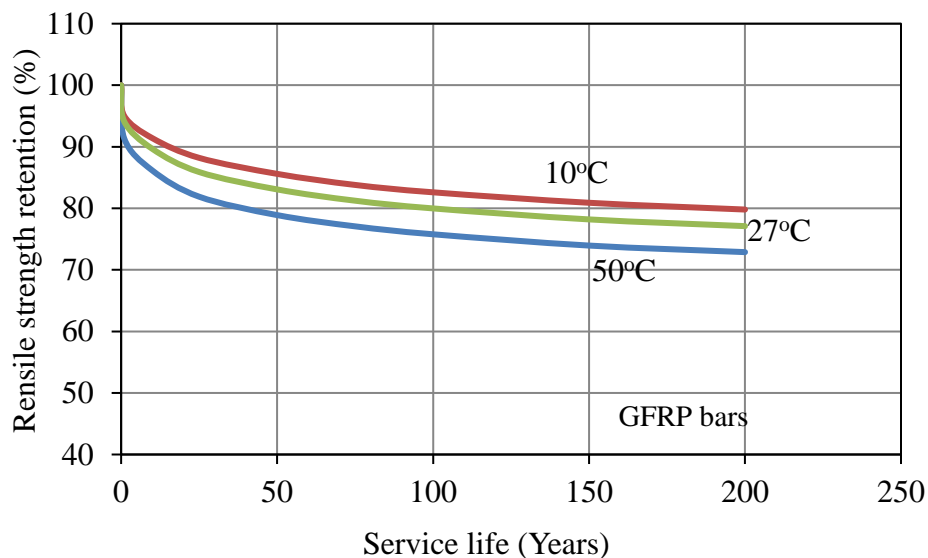
Figure 4.57: General relation between the PR and the predicted service life for Pultrall GFRP bars under sustained load, at mean annual temperatures of (10°C [50°F], 27°C [81°F], and 50°C [122°F])
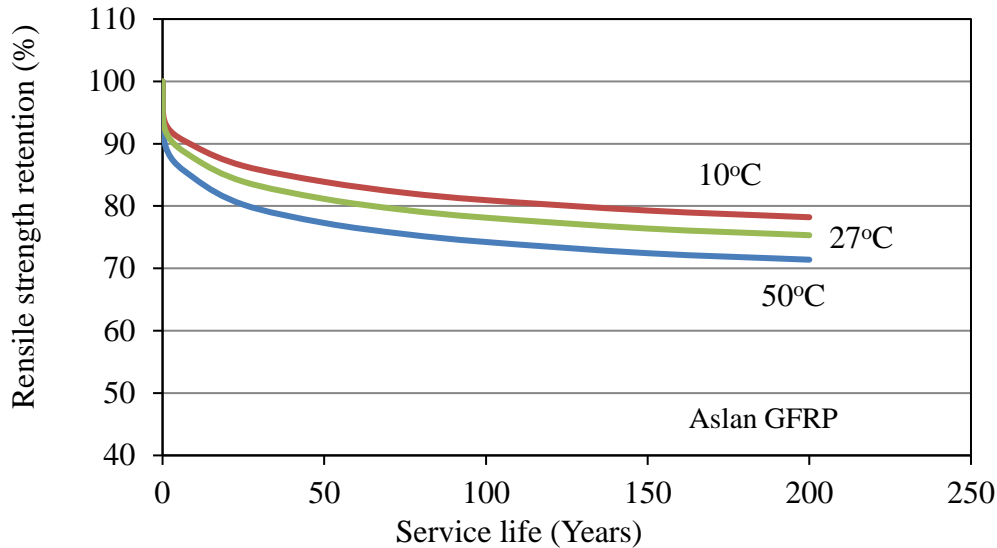
Figure 4.58: General relation between the PR and the predicted service life for Aslan GFRP bars under sustained load, at mean annual temperatures of (10°C [50°F], 27°C [81°F], and 50°C [122°F]).

4.9.5.2 Results and discussion for the new life prediction model of GFRP bars

Based on the reported data of the Pultrall and Aslan GFRP bars, the property tensile retention value for specimens tested at each temperature (30°C and 60°C [140°F]) and conditioning time (3,000, 5,000, and 7,000 hr) were calculated as the average property value at the time of testing (t) divided by the average property value for the reference specimen ($t=0$). These data were then plotted on a graph with time on the x-axis using a logarithmic scale (log-time), and the property retention value on the y-axis using a linear scale (Figure 4.59). Using linear regression, a line was fit through each data set (one for each conditioning temperature). The figure indicated that the slopes (ϕ) of the two regression lines are nearly the same, which is approximately equal to 0.079 and 0.1086 for Pultrall and Aslan GFRP bars, respectively. The regression line must have a minimum r^2 of 0.80.

In our case, the property tensile retention values used for the linear regression were chosen in the standard-deviation range to accommodate r^2 and all the r^2 values for regression lines at 22°C and 60°C [140°F] were greater than 0.80. Meanwhile, by substituting log[7000h (292 days)] as the value of x in the equation of y=−0.079x +1.3954 for Pultrall GFRP bars and y=−0.1086x +1.1879 for Aslan GFRP bars and, Δ_1 for T_1 (22°C) can be obtained as a value equal to 0.12297 and 0.081 for Pultrall and Aslan GFRP bars, respectively. The *TSF* value at each of the conditioning temperatures (60°C [140°F] and 22°C) was obtained as of approximately 5.10 and 8.25 for Pultrall and Aslan GFRP bars, respectively. Then by Then by substituting the value (5.10 and 8.25) into Eq. (4.26) as the TSF value, the constant B can be obtained as a value of 3,587.9 and 5,460.4 for Pultrall and Aslan GFRP bars, respectively. Thus, the TSF value between the reference temperature (22°C) and other selected temperature *T* can be obtained using Eq. (4.16). Figure 4.60 shows the *TSF* values versus temperatures.

$$TSF = e^{[B/(T1+273.15)] - [B/(T2+273.15)]}$$

(4.26)

By substituting *DL*=100 years, values of *TSF* from Figure 4.60 and values of n_H from Figure 4.61 into Eq. (4.25), the reduction factor (RF) can be obtained, as shown in Table 4.19 and Table 4.20, which present the retention factor for tensile strength of Pultrall and Aslan GFRP bars, respectively, for some typical application temperature and RH with 100-year design life. Tables 4.19 and 4.20 indicated that, for an environment with an RH of 100%, the values of the RFs of tensile strength are ranged between 0.74 and 0.76 (Pultrall GFRP bars) and 0.70 and 0.81 (Asaln GFRP bars), in which the lower temperature, the greater RF value. It can be also observed that GFRP bars have much better durability resistance in dry concrete than in moist concrete. For cases where RH<90% the values of the RFs, for the Pultrall GFRP bars, can retain over 87 % (for Pultrall) and (89 % for Asalan) of its original tensile strength after 100 years service in concrete environment. As long as RH is under 80%, the RFs are greater than 90% (ACI 440.1R-15), even with elevated temperatures (up to 60°C).
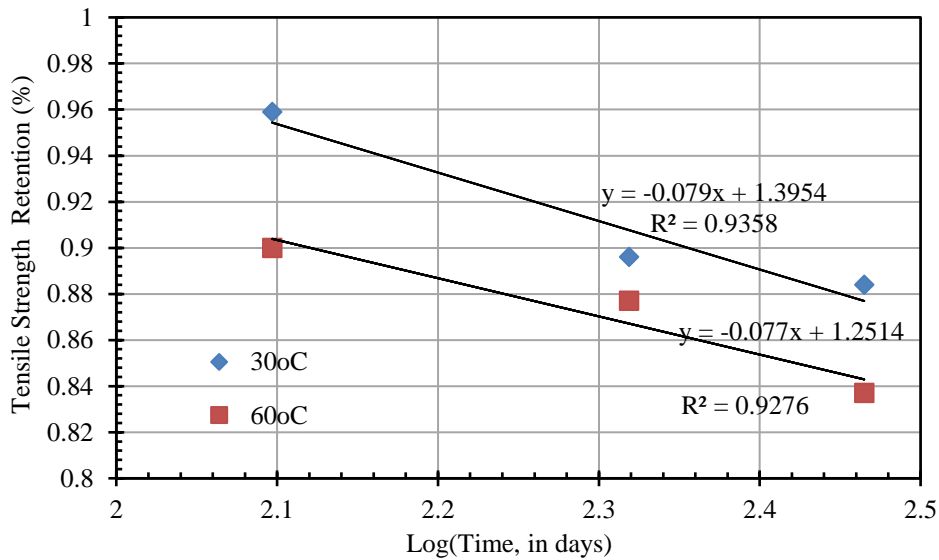
(a) Pultrall GFRP bars
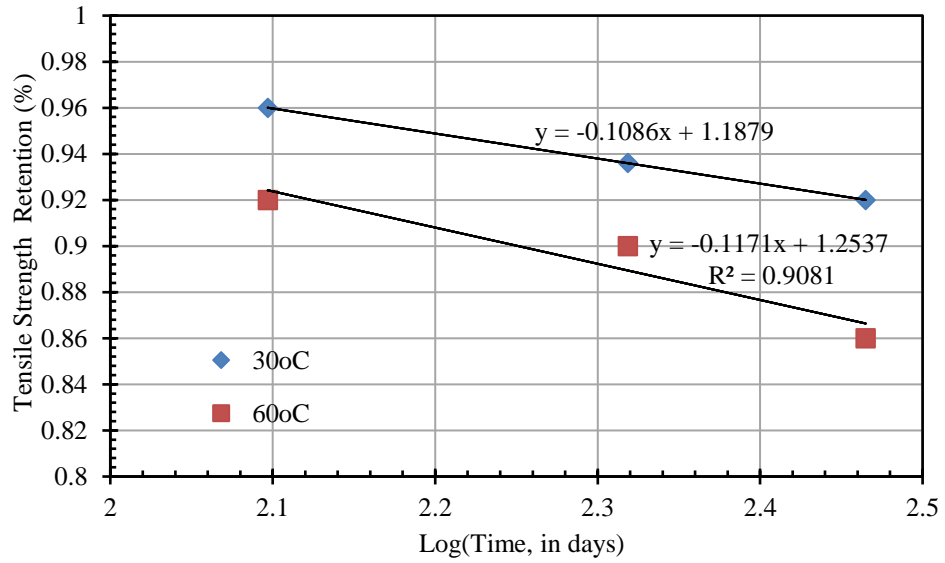
(b) Aslan GFRP bars

Figure 4.59: Strength retention versus log(time) for Pultrall and Aslan GFRP bars after being embedded in solution at 30 and 60°C
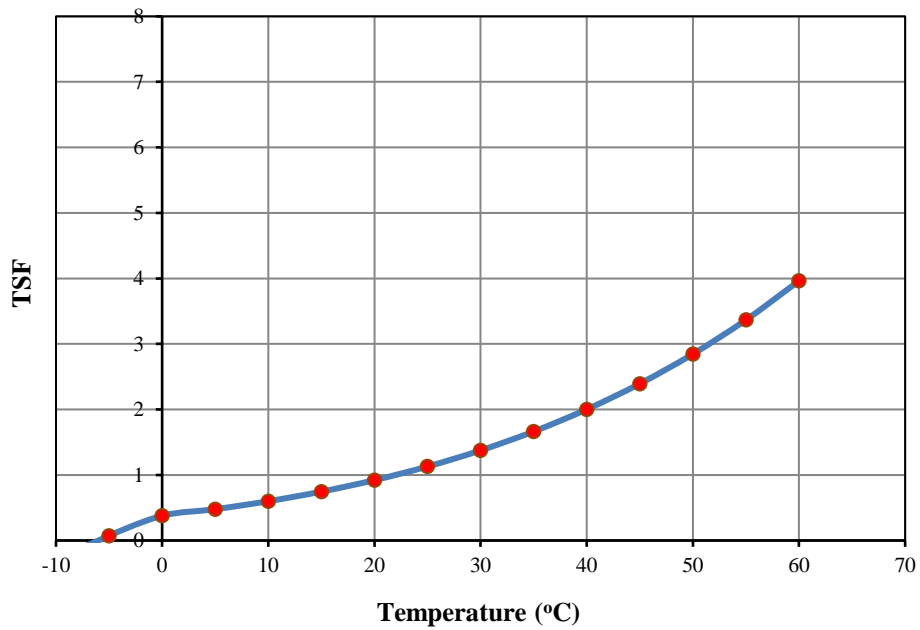
(a) Pultrall GFRP bars
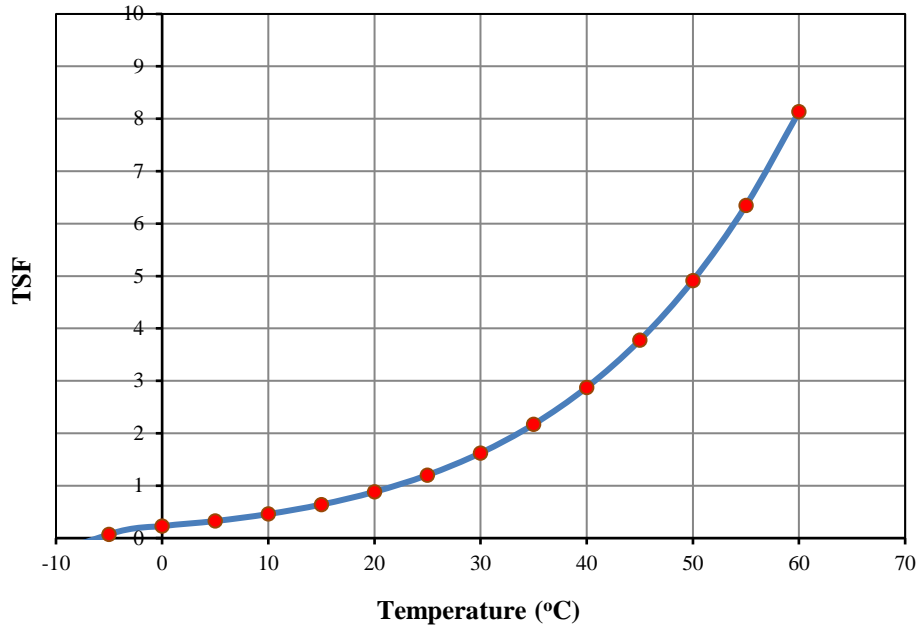
(b) Aslan GFRP bars

Figure 4.60: TSF versus temperature
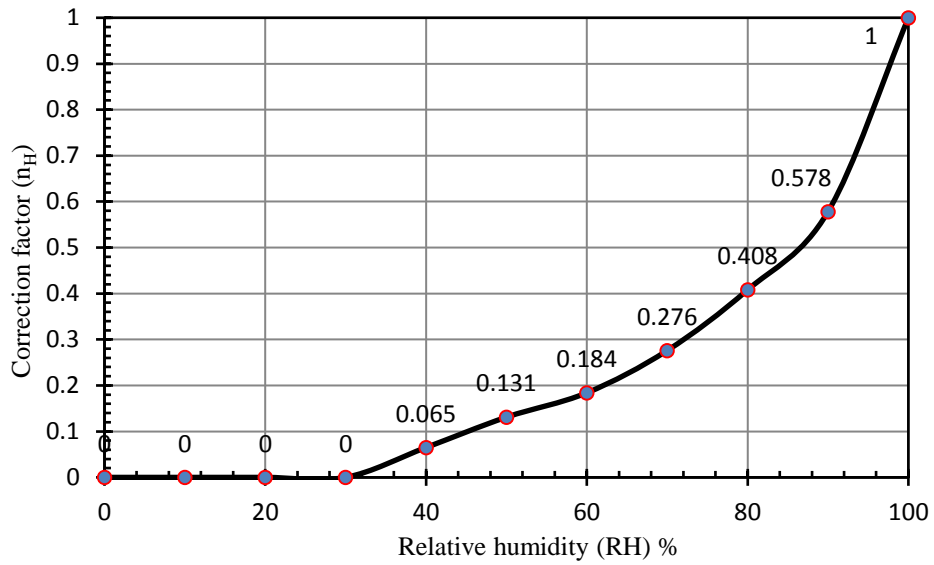
Figure 4.61: Relationship between the correction factor and the relative humidity

4.10 Test Protocol to Evaluate the Service Life and Degradation of GFRP Reinforcements

The research team conducted an extensive number of tests (mechanical, physical, durability characterization, and microstructure analysis) on FRP reinforcements. Based on the test results, the research team concluded that the most sensitive test method is the "Tensile Test under sustained load, elevated temperature of 140°F (60°C), alkaline solution of pH=12.8, and exposure duration of 3 months). The reason for choosing this tensile test and its associated factors as the most dominant effects (sustained load, elevated temperature, and alkaline exposure) is that the conditioned FRP reinforcements that performed properly in tensile test meeting the threshold (80% guaranteed tensile strength under un-sustained loading and 70% guaranteed tensile strength under sustained loading) also performed well under shear tests. In addition, the FRP reinforcement with acceptable tensile capacity retention did not reveal remarkable defects in the interface between the resin and fibers under microstructural analysis. In conclusion, the shear capacity retention and microstructure analysis were related to and consistent with the recommended tensile capacity retention. This recommended test was based on the reported results for GFRP on the tensile capacity, shear capacity, and microstructural analysis.

Therefore, based on the observed degradation mechanisms and test results, a test protocol is recommended for rapid assessment of the durability and service life performance of FRP materials; which is the "Tensile Test for conditioned GFRP bars". The recommended test protocol is detailed for GFRP and listed in the following section.

Recommended Test Protocol: Tensile Test for Conditioned GFRP Bars:

1. **Specimen preparation should be conducted according to ASTM D7205 as follows:**
   1.1 Specimens should be representative of the lot or batch being tested.
   1.2 During the sampling and preparation of test specimens, all deformation, heating, outdoor exposure to ultraviolet light, and other factors possibly causing changes to the material properties of the specimen should be avoided.
   1.3 The length of the specimen should be the sum of the length of the test section and the lengths of the anchoring sections. The length of the test section should not be less than 100 mm, nor should it be less than 40 times the diameter of the FRP bar.
   1.4 The number of test specimens should not be less than five. If the specimen fails at or slips out of an anchoring section, an additional test should be performed on a separate specimen taken from the same lot as the failed specimen.

2. **Conditioning**

    2.1 Standard conditioning procedure—Conditioning according to Procedure A of ASTM D 618 is recommended. Store and test specimens at the standard laboratory atmosphere (23 ± 3°C [73°F] and $60 \pm 10\%$ [140°F] relative humidity) and sustained load.

    2.2 As a minimum time, FRP samples should be immersed in the alkaline solution at 60 ± 3°C [140°F] for exposure times of 3 months.

    2.3 Sustained load should be 30% for GFRP bars.

3. **Test method:**

    3.1 When mounting the specimen on the testing machine, care should be taken to ensure that the longitudinal axis of the specimen coincides with the line joining the two anchorages fitted to the testing machine.

    3.2 The load should be increased until tensile failure occurs. Strain measurements should be recorded until the load reaches at least 50% of the tensile capacity or the guaranteed tensile capacity, whichever is higher.

4. **Specified limits:**

    4.1 Alkali resistance in high at least pH of 12.8 a solution (without load): Tensile capacity retention should be greater than 80% guaranteed tensile strength for FRP bars.

    4.2 Alkali resistance in high pH solution (with sustained load): Tensile capacity retention should be greater than 70% guartneed tensile strength for FRP bars.

In this testing protocol, the tensile test for conditioned GFRP (under 30% sustained load, elevated temperature of 140°F (60°C [140°F]), alkaline solution of pH=12.8, and exposure duration of 3 months) is the most sensitive test method that also includes the most dominating effects (elevated temperature and alkaline solution) to material degradation.

The minimum exposure duration is specified to be 3 months and that is consistent with the CAN/CSA 806-12 and ACI 440.3R-4. The research team took into consideration the test results reported for the 3-months exposure (for GFRP) and the available test results in the literature (Ali et al. 2018). The research team concluded that the minimum exposure duration of 3 months is representative of the degradation and can predict the long-term degradation of FRP reinforcements and the service life of FRP.

4.11 Conclusions on Models

Based on the results of this research, the following conclusions may be drawn:

1- Long-term-behavior predictions of the conditioned GFRP specimens were made with a method based on the Arrhenius theory. Accordingly, the GFRP specimen immersed at an isotherm temperature of 50°C [122°C], the service-life predictions are approximately 10 and 200 years for a PR of 92% and 79.8% (GFRP bars). As expected, these results show that the long-term tensile strength of the GFRP was more affected by the alkaline environment in a warm climate compared to the

cold climate. While, the predicted service life of GFRP embedded in an alkaline environment or aged in alkaline solution at an isotherm temperature of 10°C to reach a PR of less than 80% (GFRP) can be estimated at more than 200 years.

2- Based on the test results and proposed service life prediction model, the tensile strength retentions (RF) for CFRP strands under sustained load, were predicted to be 91% and 82% (for CFRP) at a relative humidity (RH <90%) and a moisture saturated environment (RH=100%), respectively.

2- Based on the test results and proposed service life prediction model, the tensile strength retentions (RF) for GFRP bars, under sustained load, were predicted to be 89% and 74% (for GFRP) at a relative humidity (RH <90%) and a moisture saturated environment (RH=100%), respectively.

4.12 Recommendation

1- Based on the test results, the research team concluded that the most sensitive test method is the "Tensile Test under sustained load, elevated temperature of 140°F (60°C), alkaline solution of pH=12.8, and exposure duration of 3 months.
2- The Recommended test protocol of tensile test for conditioned FRP bars should be conducted in according with ASTM specifications.
3- The sustained load should be applied as 30% for GFRP.
4- Based on results of different performed tests, the tensile test for conditioned GFRP (under 30% sustained load, elevated temperature of 140°F (60°C), alkaline solution of pH=12.8, and exposure duration of 3 months) is the most sensitive test method that also includes the most dominating effects (elevated temperature and alkaline solution) to material degradation.
5- Based on the test results conducted on FRP reinforcements in this study, considering the recommendation of the CAN/CSA 806-12 and ACI 440.3R-4, the minimum exposure duration is specified to be 3 months.
6- The new proposed service life prediction models (detailed in the previous section 4.9.4) incorporate the effects of temperature, design life, and RH of exposure into the environmental reduction factor for the FRP bars. Based on the service-life prediction models, the tensile-strength retention is predicted to retain over 74% of guaranteed tensile strength (CFRP), after 100 years of service life in moist alkaline environment with elevated temperatures and under sustained load.

Table 4.19: Strength retention factor (RF) under different temperatures and RH for 100-years design life for pultrall GFRP bars under sustained load (30% of loading)

T ºC	Tensile Retention Factor (RF)							
	100% RH	90% RH	80% RH	70% RH	60% RH	50% RH	40% RH	Less than 30 % RH
0	0.82	0.895	0.925	0.949	0.966	0.976	0.988	1
5	0.81	0.888	0.921	0.946	0.964	0.974	0.987	1
10	0.80	0.881	0.916	0.943	0.962	0.973	0.986	1
15	0.79	0.875	0.912	0.940	0.960	0.971	0.986	1
20	0.78	0.869	0.907	0.937	0.958	0.970	0.985	1
25	0.77	0.863	0.903	0.934	0.956	0.969	0.984	1
30	0.76	0.858	0.899	0.932	0.954	0.967	0.984	1
35	0.76	0.852	0.895	0.929	0.953	0.966	0.983	1
40	0.75	0.847	0.892	0.927	0.951	0.965	0.982	1
45	0.75	0.842	0.888	0.924	0.949	0.964	0.982	1
50	0.74	0.837	0.884	0.922	0.948	0.963	0.981	1
55	0.74	0.832	0.881	0.919	0.946	0.962	0.981	1
60	0.73	0.827	0.878	0.917	0.945	0.960	0.980	1

Table 4.20: Strength retention factor (RF) under different temperatures and RH for 100-years design life for Aslan GFRP bars under sustained load (30% of loading)

T ºC	Tensile Retention Factor (RF)							
	100% RH	90% RH	80% RH	70% RH	60% RH	50% RH	40% RH	Less than 30 % RH
0	0.818	0.895	0.925	0.949	0.966	0.976	0.988	1
5	0.806	0.888	0.921	0.946	0.964	0.974	0.987	1
10	0.795	0.881	0.916	0.943	0.962	0.973	0.986	1
15	0.784	0.875	0.912	0.940	0.960	0.971	0.986	1
20	0.774	0.869	0.907	0.937	0.958	0.970	0.985	1
25	0.764	0.863	0.903	0.934	0.956	0.969	0.984	1
30	0.754	0.858	0.899	0.932	0.954	0.967	0.984	1
35	0.744	0.852	0.895	0.929	0.953	0.966	0.983	1
40	0.735	0.847	0.892	0.927	0.951	0.965	0.982	1
45	0.730	0.842	0.888	0.924	0.949	0.964	0.982	1
50	0.730	0.837	0.884	0.922	0.948	0.963	0.981	1
55	0.720	0.832	0.881	0.919	0.946	0.962	0.981	1
60	0.720	0.827	0.878	0.917	0.945	0.960	0.980	1

CHAPTER 5
QUANTIFYING THE DEGRADATION OF RESIN MATRIX AND FIBERS IN HIGH ALKALI ENVIRONMENT

5.1 Constituent Materials of CFRP

The objective of this chapter is to evaluate the mechanical properties of the constituent materials of the CFRP tendons and examine the effect of environmental conditioning on their durability. CFRP tendons are comprised of carbon fibers and epoxy resin. The carbon fibers provide the tensile strength and stiffness while the epoxy resin provide the interlaminate shear mechanism to transfer the load among fibers. To examine the effect of environmental conditioning on the durability of CFPR constituent materials, the fibers and epoxy resin were exposed to an alkaline environment and water at room and elevated temperature. Upon completion of the exposure duration, the specimens were tested to determine their mechanical properties as compared to the original unexposed materials. The following sub-section presents a detailed description of the experimental program undertaken for each material.

5.2 Carbon Fibers

The carbon fibers used to fabricate CFRP tendons are shown in Figure 5.1. The environmental parameters considered in this study included subjecting the carbon fibers to water and alkaline solution at room temperature and high temperature of 130 ºF for an exposure duration of 3000, 5000 or 7000 hr. The testing matrix for conditioning the carbon fibers is given in Table 5.1. Upon completion of the exposure duration, the carbon fibers were tested to evaluate their residual tensile capacity compared to the fibers as received. The carbon fibers were cut from the spool into 12 inches (304.8 mm) long and placed in glass containers that were filled with water and others filled with alkaline solution. Three glass containers of each solution were kept at room temperature and additional three containers of each solution were kept at high temperature of 130 ºF as shown in Figure 5.2.

Figure 5.1: Carbon fibers as received from the manufacturer.

Table 5.1: Testing matrix of carbon fibers.

Solution	Duration of exposure (hr)	Temperature (^{o}F)
N/A	As received	N/A
Water	3000	73 & 130
Water	5000	73 & 130
Water	7000	73 & 130
Alkali	3000	73 & 130
Alkali	5000	73 & 130
Alkali	7000	73 & 130

Figure 5.2: Carbon fibers in glass containers undergoing conditioning in room temperature.

5.2.1 Testing of fibers

The carbon fibers were removed from the glass jars upon completion of the specified durations and cut in smaller specimens with total length of 3 inches. Three specimens were tested for each type of exposure. The specimens were anchored at the ends using metal tabs as shown in Figure 5.3 and tested to determine the tensile strength before and after exposure as shown in Figure 5.4. A typical failure of the tested carbon fiber specimens is shown in Figure 5.5.
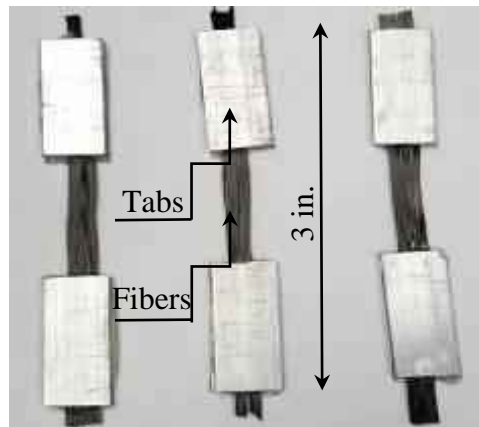
Figure 5.3: Typical carbon fiber specimen after tabbing.

Figure 5.4: Tensile testing of carbon fibers specimen.

Figure 5.5: Typical carbon fiber specimens after testing.

5.2.2 Test results

Table 5.2 presents the tensile test results of carbon fiber specimens. The table provides the average failure load for each type of exposure, the standard deviation and coefficient of variation for each category.

Table 5.2: Tensile test results of carbon fibers.

Exposure Type	Temp. (°F)	Exposure Duration	Number of Specimens	Average Failure load (lbs)	Standard Deviation	Coefficient of variation
As Received			6	215	31	14.5%
Water	73	3000	3	222	25	11.5%
		5000	3	218	31	14.2%
		7000	3	225	22	9.7%
Water	130	3000	3	244	4	1.6%
		5000	3	221	31	14.2%
		7000	3	212	6	2.8%
Alkaline Solution	73	3000	3	139	6	4.2%
		5000	3	82	15	18%
		7000	3	126	16	12%
Alkaline Solution	130	3000	3	75	15	20%
		5000	3	75	17	23%
		7000	3	133	14	10%

5.2.3 Analysis of test results

Carbon fibers were exposed to water and alkaline solution at room and elevated temperature for 3000, 5000 and 7000 hr. Figure 5.6 presents a comparison of average failure load between the unconditioned specimens and the specimens exposed to water at room and elevated temperature

for the three specified durations 3000, 5000, 7000 hr. The comparison is given as a percentage of the average failure load. Also, given in the figure are the maximum and minimum failure loads as a percentage of the average failure load for each exposure type.
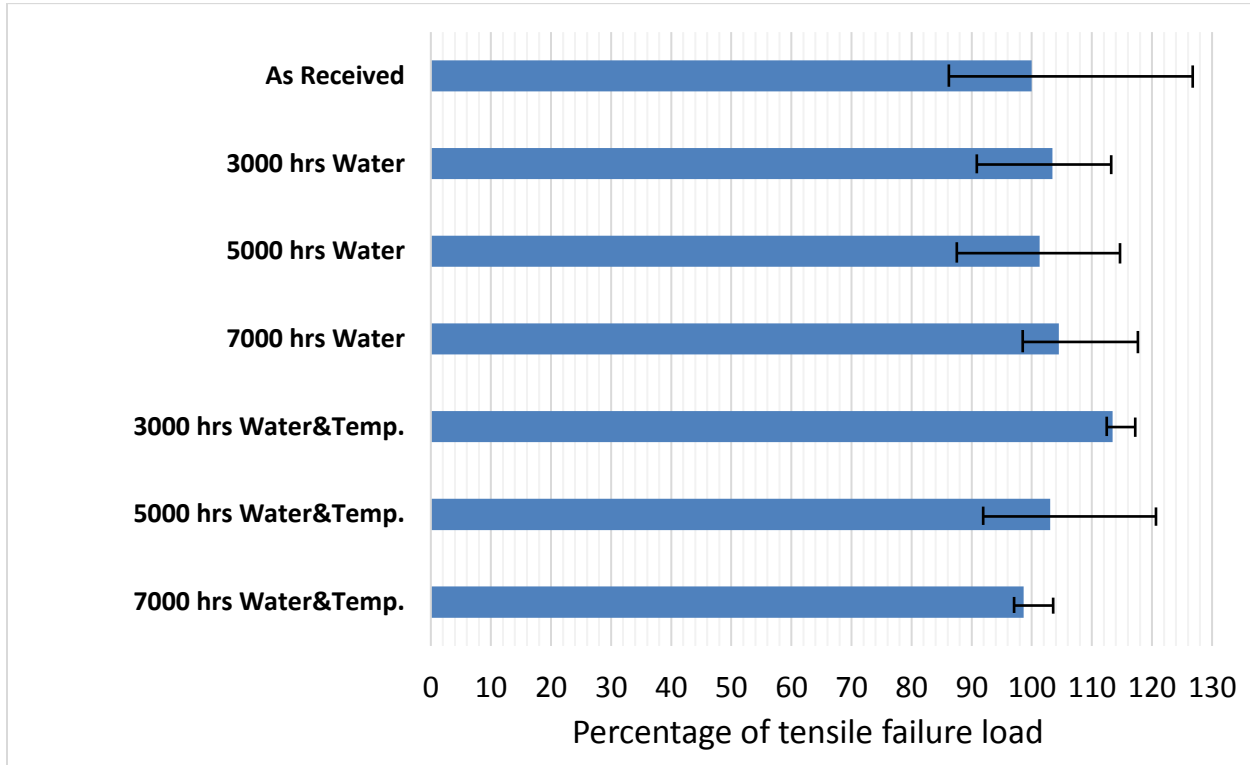
Figure 5.6: Effect of water at room and elevated temperature on the tensile strength of carbon fibers.

Test results clearly indicate that the average failure load of the as received specimens was similar to the conditioned ones. In most cases, the standard deviations of the test results were within the same range. Based on the test results presented in the above figure it can be concluded that exposing the carbon fibers to water at room and elevated temperature did not have an effect on the tensile capacity of the fibers.

The effect of exposing carbon fibers to alkaline solution at room and elevated temperatures was also studied. Figure 5.7 presents a comparison of average failure load between the unconditioned specimens and the conditioned ones for the three specified durations of 3000, 5000 and 7000 hr. Also given in the figure are the maximum and minimum failure loads for each type of conditioning presented as a percentage of average failure load.
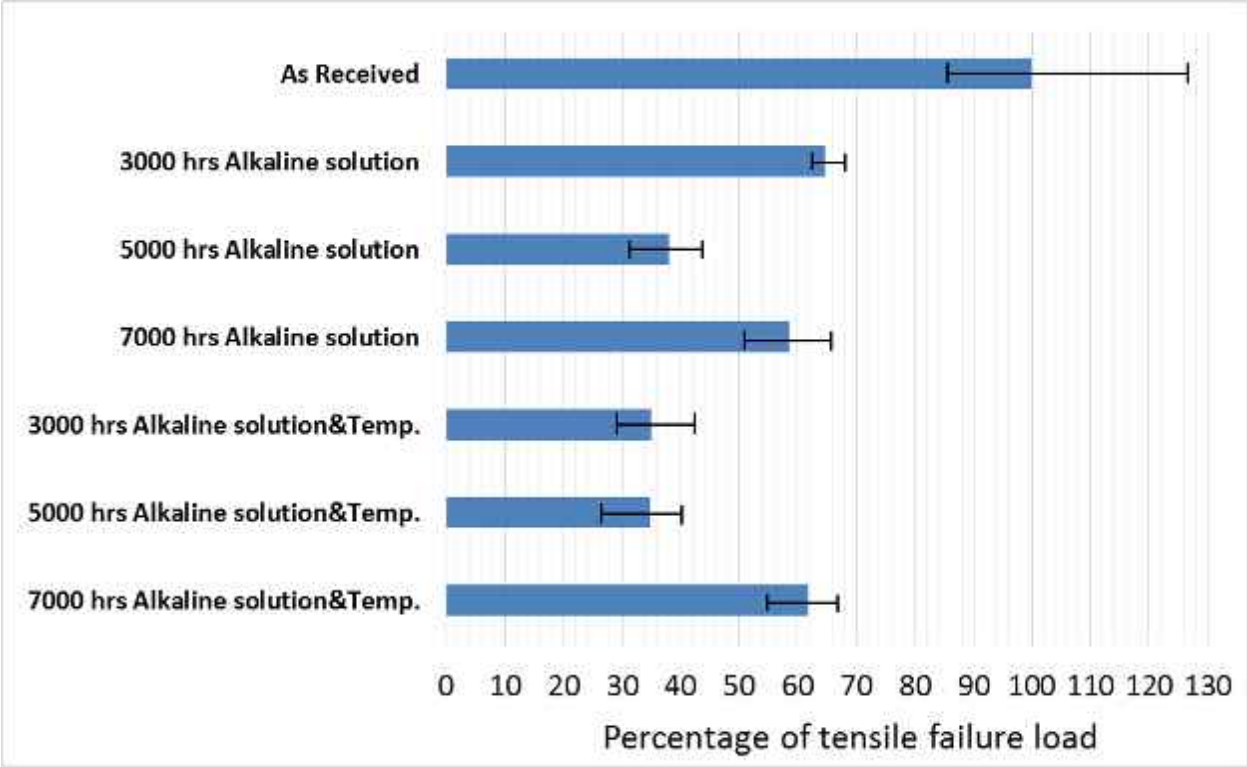
Figure 5.7: Effect of alkaline solution on tensile strength of carbon fibers.

Test results reflect significant reduction of the average tensile strength of the carbon fibers when exposed to alkaline solution. The reduction in some cases exceeds 50%. The geometry and the physical condition of the tests specimens exposed to alkaline solution were also severely affected. As a result, the size, number of fibers, and their alignment within the tabs were not uniform and similar to those of unconditioned samples.

Figure 5.8 presents a comparison between the specimens conditioned in alkaline solution and specimens conditioned in water before testing. This figure provides a clear evidence that the specimens exposed to alkaline solution were "tangled" and "matted." It is very likely that the alkaline solution had an effect on the material used for sizing the fibers. It should be noted that this was not observed for the CFRP tendons exposed to alkaline solution since fibers are protected by the epoxy used to fabricate the strands and not directly exposed to the alkali solution.

Figure 5.8: Comparison between specimens exposed to alkaline solution (left) and water (right).

Based on the test results and the observed shape of the carbon fibers, it can be concluded that exposing carbon fibers to alkaline solution at room and elevated temperature led to significant misalignment problems, which translated into a significant reduction of the tensile strength. The results indicated clearly that the degradation is mainly of the sizing, which consequently caused misalignment of the fibers and caused significant reduction of the tensile strength. However, this behavior does not confirm that the fibers are affected by the alkaline solution and it cannot be determined by the undertaken tests. Exposure of CFRP tendons to alkaline solution, presented in chapter 3 clearly indicate that exposure of CFRP tendons to alkaline solution had an insignificant effect on the overall tensile strength.

5.3 Epoxy Resin

The resin matrix used to manufacture the CFRP was also tested after being exposed to water and alkaline solution at room and elevated temperature for 3000 and 7000 hr. The typical epoxy plate used in this study and provided by the manufacturer is shown in Figure 5.9. A total of six epoxy resin plates were received. The plates were 7-7/8 inches (200 mm) long, 5-1/8 inches (130 mm) wide and 0.12 inches (3 mm) thick. A total of 27 specimens were produced from the 6 plates. The specimens were cut from the plates into a dog-bone shaped configuration. The total length of each specimen was 7 inches (177.8 mm) and a width of 1 inch (25.4 mm). Each specimen had a gage length of 3 inches (76.2 mm) and gage width of 0.5 inch (12.7 mm). Figures 5.10a and 5.10b show a sketch for the geometrical configuration of the specimens and an actual specimen respectively. It should be noted tat the color of the plates were not uniform which may significantly affect the strength of the test specimens.

Figure 5.9: Epoxy resin plate as received from the manufacturer.
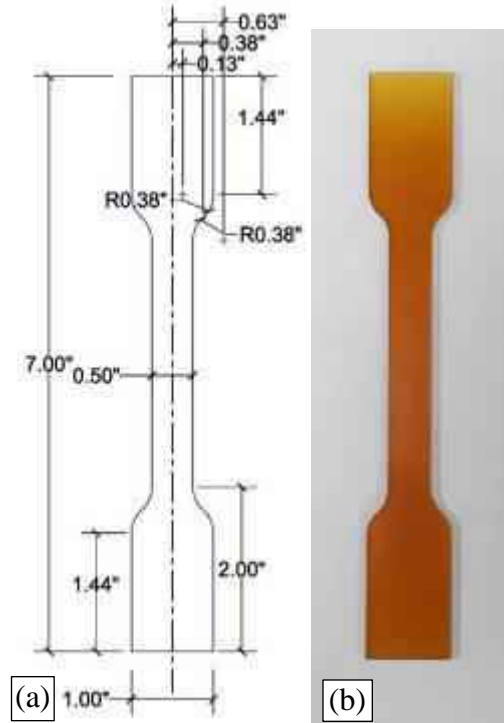
Figure 5.10: a) Sketch for the geometrical configuration of epoxy coupons. b) Actual epoxy specimen.

The test matrix for the testing program, given in Table 5.3, included a total of 27 specimens. The parameters considered in the experimental program included exposing the epoxy coupons to water or alkaline solution at room or high temperature of 130 ºF for an exposure duration of 3000 or 7000 hr.

Table 5.3: Testing matrix of epoxy resin.

Solution	Duration of exposure (hr)	Temperature (ºF)	No. of specimens
N/A	As received	N/A	3
Water	3000	73 & 130	6
Water	7000	73 & 130	6
Alkali	3000	73 & 130	6
Alkali	7000	73 & 130	6
Total			27

The epoxy coupons were placed in plastic containers and submerged in water or alkaline solution as shown in Figure 5.11. The plastic containers were kept with glass containers containing the carbon fibers at the same temperatures.

Figure 5.11: Epoxy resin specimens undergoing conditioning at room temperature.

5.3.1 Testing of epoxy resin coupons

Upon completion of the exposure duration, the epoxy coupons were tested to determine their tensile capacity. All the specimens were tested using MTS machine to apply the load and an extensometer was used to measure the strain during the test. Figure 5.12 shows one specimen during testing and Figure 5.13 shows the typical failure mode of specimens after testing.

Figure 5.12: Epoxy coupon during testing.
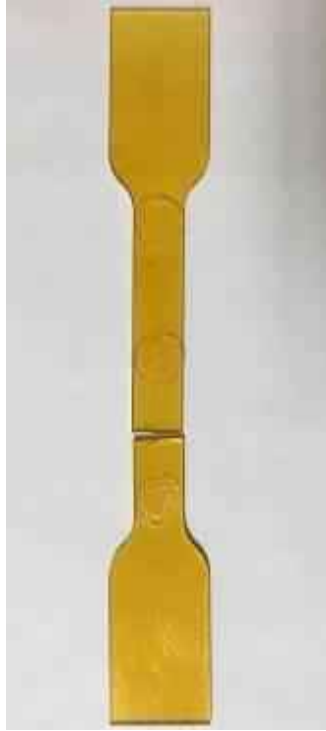
Figure 5.13: Typical failure mode of epoxy resin coupons.

5.3.2 Test results of epoxy resin coupons

Tensile test results of the epoxy specimens are given in Table 5.4. Test results include the average tensile strength, the ultimate strain and the modulus of elasticity.

Table 5.4: Tensile test results of epoxy resin coupons

Exposure Time	Temp. (ºF)	Type of Solution	Tensile Strength ksi (Mpa)		Ultimate Strain (%)		Modulus of Elasticity ksi (Gpa)	
			Average	COV (%)	Average	COV (%)	Average	COV (%)
0	72	-	5.8 ± 0.5 (40 ± 3.5)	7.5	1.3 ± 0.2	10.5	445 ± 13 (3.1 ± 0.1)	2.5
3000 hrs	72	Water	5.8 ± 0.4 (40 ± 2.8)	5.8	1.3 ± 0.1	6.7	428 ± 10 (3.0 ± 0.1)	2
	72	Alkaline	5.5 ± 0.6 (38 ± 4.1)	7.5	1.3 ± 0.15	8.1	423 ± 4 (2.9 ± 0.03)	0.7
	130	Water	5.0 ± 0.1 (35 ± 0.3)	0.9	1.1 ± 0.02	1.9	447 ± 6 (3.1 ± 0.04)	1.1
	130	Alkaline	5.0 ± 0.8 (35 ± 5.5)	14.1	1.1 ± 0.2	16.3	449 ± 11 (3.1 ± 0.1)	2.3
7000 hrs	72	Water	6.6 ± 0.1 (46 ± 0.7)	1.5	1.4 ± 0.02	1.3	473 ± 2 (3.3 ± 0.01)	0.5
	72	Alkaline	7.0 ± 0.2 (48 ± 1.4)	3.2	1.4 ± 0.02	1.4	483 ± 9 (3.33 ± 0.1)	2
	130	Water	6.5 ± 0.1 (45 ± 0.3)	0.3	1.3 ± 0.01	0.9	493 ± 2 (3.4 ± 0.01)	0.5
	130	Alkaline	5.5 ± 0.4 (38 ± 2.8)	6.5	1.2 ± 0.1	9.5	477 ± 14 (3.3 ± 0.1)	3

222

5.3.3 Analysis of epoxy resin test results

Epoxy resin coupons were exposed to water and alkaline solution at room and elevated temperature for 3000 and 7000 hr. Figure 5.14 presents a comparison of average tensile strength of the as received specimens and the specimens exposed to water or alkaline solution at room and elevated temperature for the specified durations of 3000, 7000 hr. The comparison is presented as a function of the average tensile strength of the as received specimens. Also, given in the figure are the maximum and minimum tensile strengths for each exposure type.
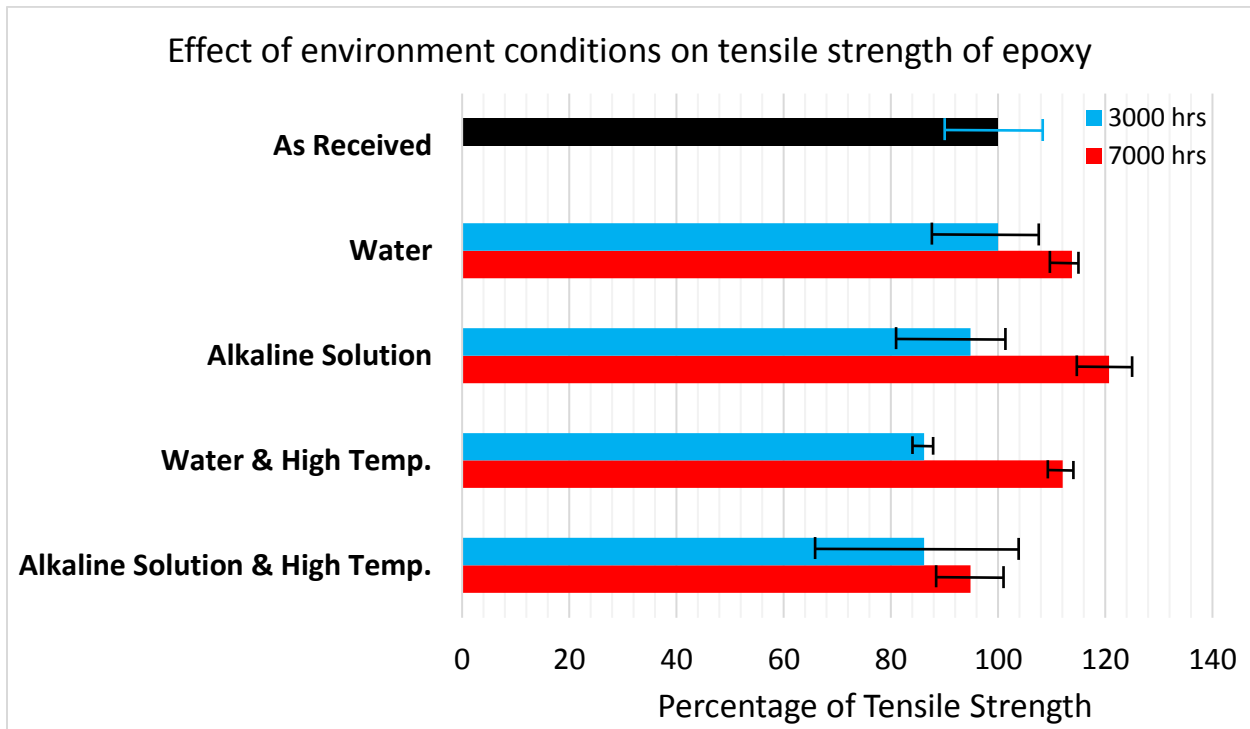
Figure 5.14: Effect of environmental conditions on tensile strength of epoxy specimens.

Test results indicated a reduction in the range of 10 percent in the average tensile strength of epoxy resin after 3000 hr of exposure to water or alkaline solution at elevated temperature. However, the results should be interpreted in the light of the observed scatter of the data, i.e., standard deviation and coefficient of variation. Scatter of the data is evident by the increase in the average tensile strength of the epoxy specimens exposed to environmental conditions for 7000 in comparison to the as received specimens. The following remarks should be considered in the analysis of these test results:

- The preparation process of epoxy used to produce the plates was different from the preparation process of epoxy used in CFRP tendons and the manufacturer performed several trials in order to produce these plates.

- Variation of the color of epoxy within the same plate can be observed as shown in Figure 5.15. This non-uniform color indicates the inconsistency of epoxy resin material within the same plate where several coupons were cut from which led to inconsistency of the test results.
- It is important to note that there are two opposing mechanisms occurring during conditioning of epoxy coupons, first is the possible degradation of epoxy due exposure to environmental conditions and second post-curing of the material which possibly increases the strength. Due to the initial variation of the materials, these two processes may affect different samples in different ways.

Figure 5.15: Inconsistency of epoxy resin within the same plate.

Based on the results we have obtained we believe that test results are inconclusive. However, we would like to point out that the tensile strength of CFRP is mainly a function of the tensile strength of the fibers and slight reduction in the tensile strength of matrix would not affect the tensile strength of CFRP significantly as presented in chapter 3.

5.4   Degradation of GFRP Constituent Materials

Durability of resins and fibers used in FRP manufacturing is a major key for determining the long-term performance of GFRP composites. This research item addressing the degradation of GFRP constituent materials includes two tasks. One task includes some tests to assess the durability/degradation of glass fibers and resins, while the other task investigates the durability of GFRP samples fabricated with the tested constituents.

5.4.1   Assessing the durability/degradation of glass fibers and resins

The aim of this task 1 is to: (a) study the chemical resistance in alkaline solution simulating concrete environment of current resins and glass fibers used for GFRP reinforcement, (b) investigate mechanisms of water absorption in pure resins and GFRP composites, and (c) assess the effect of water ingress on the long-term behavior of GFRP composites.

5.4.2   Materials under investigation

Three pultrusion-grade thermoset resins were tested in this study: 1) a vinylester resin –VE -, which is the main resin used in GPRF reinforcement, 2) a polyurethane –PU- (RIMLINE SK 97007 + SUPRASEC 9700 MDI) and 3) an epoxy –EP- (AMPREG 22) as alternative resins. The plates of resin were prepared according to the manufacturer recommendations as shown in Figure 5.16. DSC measurements were carried out to assess that the resin samples were fully cured before tests.

Figure 5.16: View of Samples of PU, EP et VE

Three glass fibers identified as ECR glass fiber (ECR-GF), boron free glass fiber for epoxy resin (EP-BF-GF) and multi-compatible boron free glass fiber (MC-EP-BF-GF) were investigated. The composition of these fibers were determined by X Ray Fluorescence, as shown in Table 5.5. We note that the chemical composition of EP-BF-GF and MC-EP-BF-GF fibers is the same, as reported in Table 5.5. However, these two glass fibers have different sizings. All these materials were provided by a Canadian GFRP bar manufacturer (Pultrall Inc).

Table 5.5: Composition of fibers by X Ray Fluorescence

Type of fiber	SiO$_2$	Al$_2$O$_3$	CaO	MgO	Na$_2$O	Fe$_2$O$_3$	K$_2$O
ECR-GF	58.3	10.5	21.7	3.1	0.5	0.8	0.3
BF-GF	59.8	16.0	12.1	8.6	0.6	1.1	0.3
MC-EP-BF-GF	59.8	16.0	12.1	8.6	0.6	1.1	0.3

GFRP composite samples made with these selected fibers and resins were fabricated in the laboratory at Sherbrook University following the manufacturer recommendations. Fiber rovings dipped in the liquid resin were introduced into 30 cm long glass tubes with a rectangular section. The bottom of the tubes were then immersed in the resin and a vacuum pump was plugged to the other edge to suck the resin along the tubes. After completion, the edges were sealed and the tubes placed in an oven for curing. After curing, the GFRP composite samples were removed from the tubes and cut. DSC measurements were carried out to assess that the samples are fully cured (cure ratio around 100%), Figure 5.17.
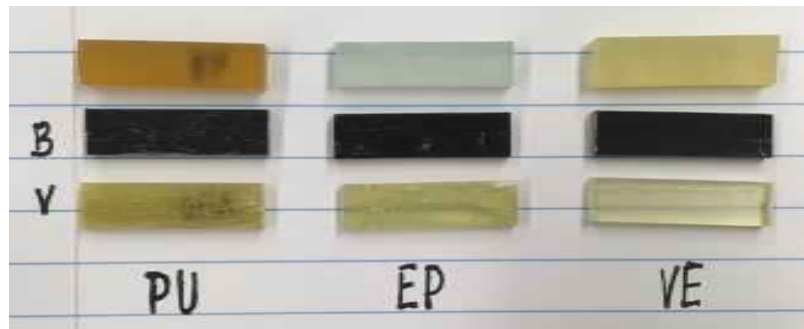
Figure 5.17: Resin samples

5.4.3 Test method

An alkaline solution of 1.0 g Ca(OH)$_2$ + 4.2 g KOH + 0.9 g NaOH per liter was prepared. The pure resin and GFRP samples were immersed in deionized water and alkaline solution up to 2 months at 24°, 40° and 65°C. The samples were periodically removed, surface dried, and weighed for water uptake. Then, they were analyzed using SEM and FTIR. DSC measurements were also conducted to assess the effect of water and alkaline solution on glass transition temperature, Tg. The dry glass fibers were immersed in alkaline solution for 7 days at 65°C. After flushing with water and drying, SEM/EDS and X-Ray Fluorescence were performed to assess any degradation of the glass fibers.

5.4.4 Results and discussion

Pure Resin Samples: Figures 5.18 to 5.20 present micrographs of the surface of resin samples before and after 1 month conditioning at 60°C in water and alkaline solution. It can be seen that

the surface of the EP samples is not affected by the exposure conditions (Figure 5.19), whereas the surface of VE samples is degraded in alkaline solution and slightly degraded in water (Figure 5.20). PU resin offers an intermediate chemical resistance between EP and VE samples. However, it has to be noted that only the surface of resin samples, which is in direct contact with the alkaline solution, was affected. The core of the resin samples can only be affected if enough water containing corrosive species diffuses/penetrates inside the material. The durability of resins and GFRP composites should therefore be assessed by investigating the mechanism of water absorption, as reported below.
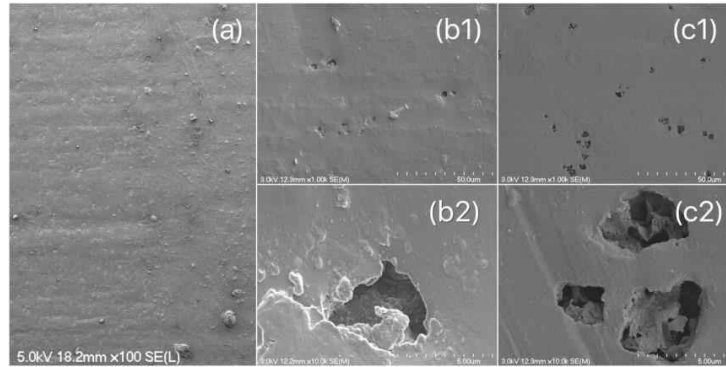
Figure 5.18: SEM micrographs of the surface of PU specimens: (a): Reference; (b): 1 month in water; (c): 1 month in alkaline solution.
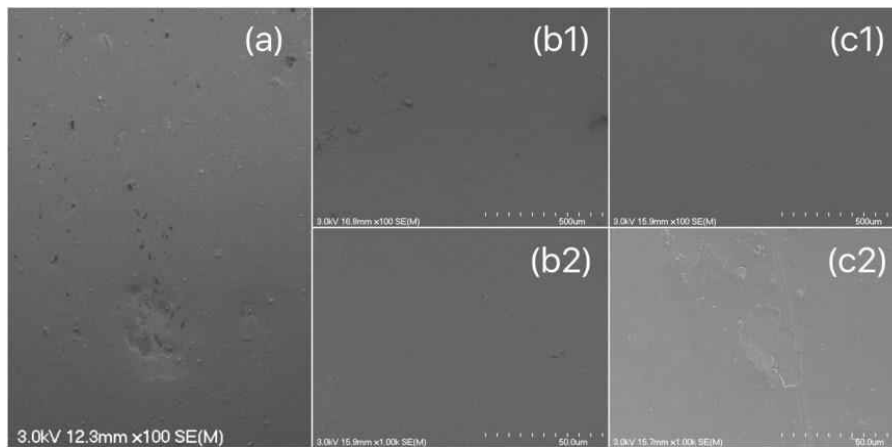
Figure 5.19: SEM micrographs of the surface of EP specimens: (a): Reference; (b): 1 month in water; (c): 1 month in alkaline solution.

227
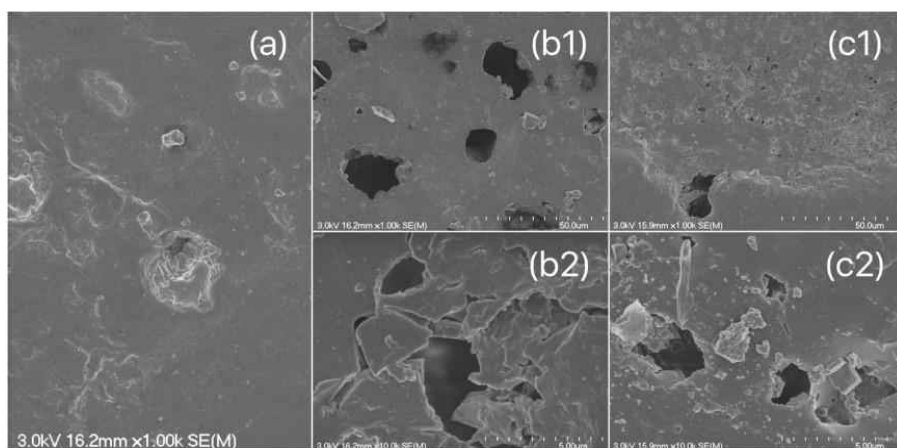
Figure 5.20: SEM micrographs of the surface of VE specimens: (a): Reference; (b): 1 month in water; (c): 1 month in alkaline solution.

Figures 5.21 to 5.23 exhibit FTIR spectra of the surface of resin samples before and after conditioning in alkaline solution during 1 and 2 months at 24°, 40° and 65°C. The broad band located above 3000 cm^{-1} corresponds to OH groups, whereas the sharp peaks below 3000 cm^{-1} are characteristic of C-H units. When degradation occurs, the amount of OH groups increases, which can be detected by an increase of the intensity of the OH peak with respect to the one of C-H groups. As for the SEM analysis, FTIR shows that the EP resin is not degraded (Figure 5.22), whereas a hydrolysis mechanism affect the VE resin after 2 month conditioning (Figure 5.23). PU resin is only slightly degraded after immersion in alkaline solution. Here also, it must be mentioned that this analysis has been conducted on the surface of the specimens. Below the surface, no degradation occurs.
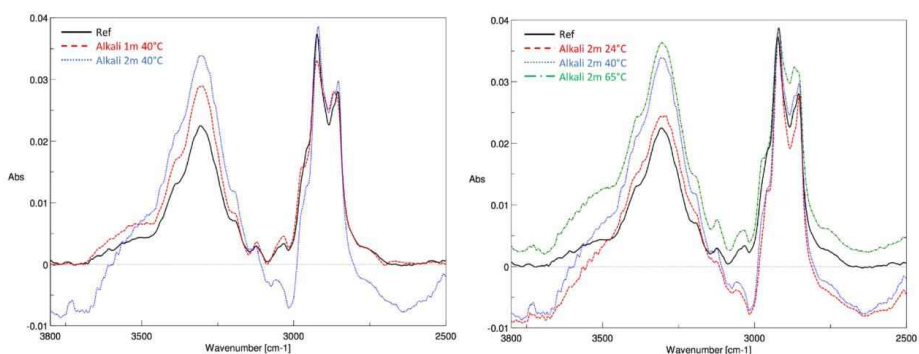
Figure 5.21: FTIR spectra of PU before (black) and after conditioning in alkaline solution. Left: After 1 (red) and 2 months (blue) at 40°C. Right: After 2 months at 24°C (red), 40°C (blue) and 65°C (green).
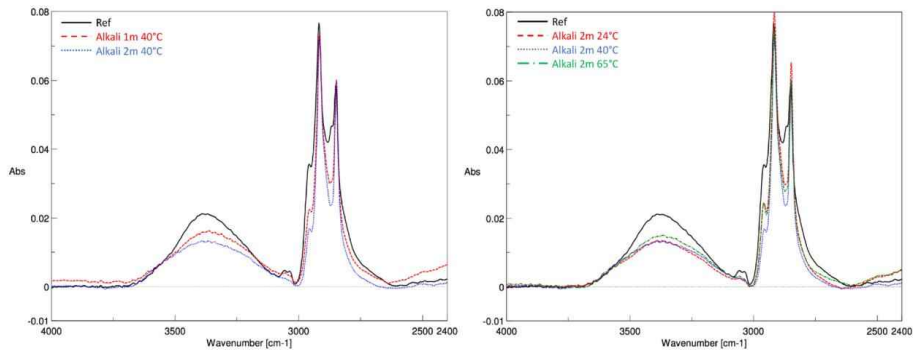
Figure 5.22: FTIR spectra of EP before (black) and after conditioning in alkaline solution. Left: After 1 (red) and 2 months (blue) at 40°C. Right: After 2 months at 24°C (red), 40°C (blue) and 65°C (green).
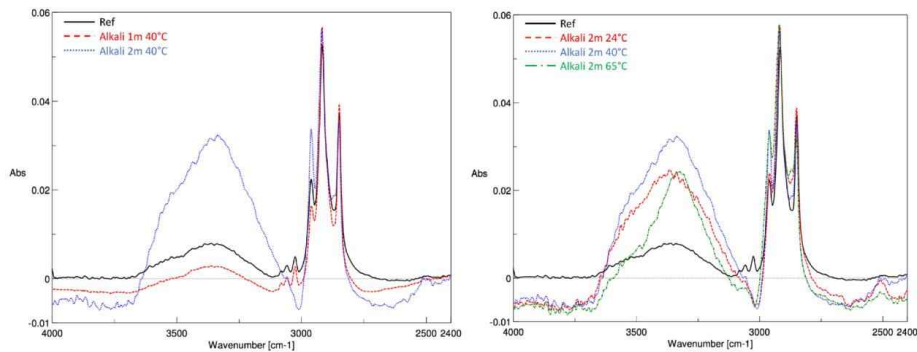
Figure 5.23: FTIR spectra of VE before (black) and after conditioning. Left: After 1 (red) and 2 months (blue) at 40°C. Right: After 2 months at 24°C (red), 40°C (blue) and 65°C (green).

Table 5.6 presents the values of Tg after immersion in water and alkaline solution for 2 months at 24°, 40° and 65°C. Runs 1 and 2 correspond to the measurement on the specimens before and after a first heating, i.e. to humid and dry specimens, respectively. It can be observed that the Tg measured in runs 1 decreases as a function of temperature: the higher the temperature, the lower the Tg. At 65°C, the Tg of PU and EP are reduced by 30°C, whereas the difference is only 10°C for VE. This effect is similar in alkaline solution and water, which shows that only water affect Tg. After the first heating, Tg returns to a value slightly lower than its original value (run 2).

Table 5.6: Glass transition temperature of specimens after 2 month immersion in water and alkaline solution at different temperatures (°C)

			Water			Alkaline solution		
		Ref	24°C	40°C	65°C	24°C	40°C	65°C
PU	*Run 1*	133	114	105	102	112	109	102
	Run 2	138	126	124	131	125	124	131
EP	*Run 1*	97	80	71	69	79	72	68
	Run 2	97	91	87	86	89	82	82
VE	*Run 1*	127	123	121	117	122	120	119
	Run 2	128	128	124	122	124	124	125

Water uptake has been determined at different temperatures. Figure 5.24 displays the curves obtained at 65°C for the three resins as a function of the square root of immersion times, whereas Table 5.7 reports the value of water absorption at saturation for the three temperatures of conditioning. The absorption rates obey to Fick law. Vinylester resin absorbs much less water (<1%) than polyurethane and epoxy resins (2.5-3.5%), which explains the lower decrease of *Tg* of VE specimens immersed in water, reported just above. These results confirm data obtained in a previous study on the behavior of several VE, PU and EP resins, which also showed that VE absorbs less water than EP and PU resins.
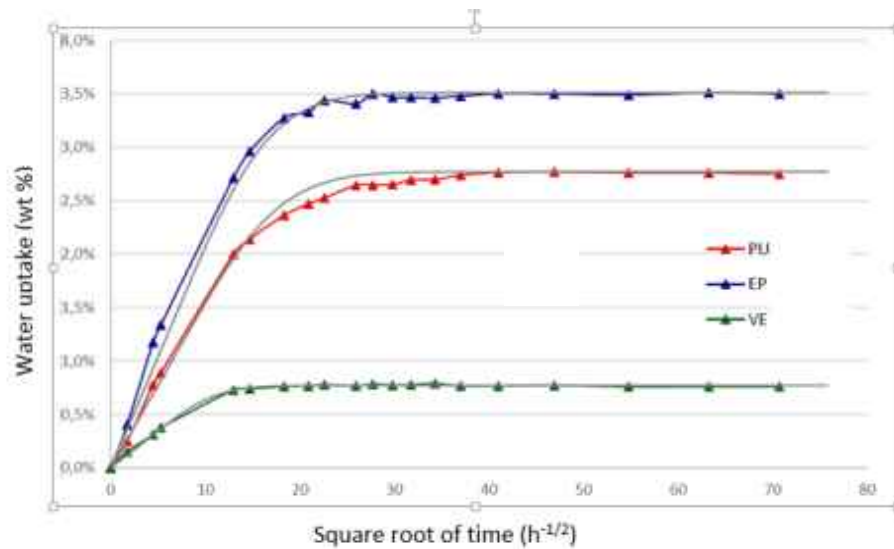
Figure 5.24: Water uptake of the three resins at 65°C as a function of time

Table 5.7: Water uptake at saturation (wt %)

	PU	EP	VE
@ 24°C	2.45	2.85	0.68
@ 40°C	2.64	3.30	0.77
@ 65°C	2.77	3.51	0.69

Figure 5.25 presents the effect of temperature on water uptake of PU resin. Two observations may be noted. Increasing the temperature accelerates water absorption and shortens the time to saturation (plateau). However, the water uptake at saturation is minimally affected. These phenomena may be explained by a higher mobility of polymeric chains, which facilitate water diffusion (rate increase) and a very small increase of the volume of the specimens (thermal expansion), which corresponds to an increase of free volume and therefore a slightly higher capacity of the resins to retain water. EP and VE resins behave in the same way.
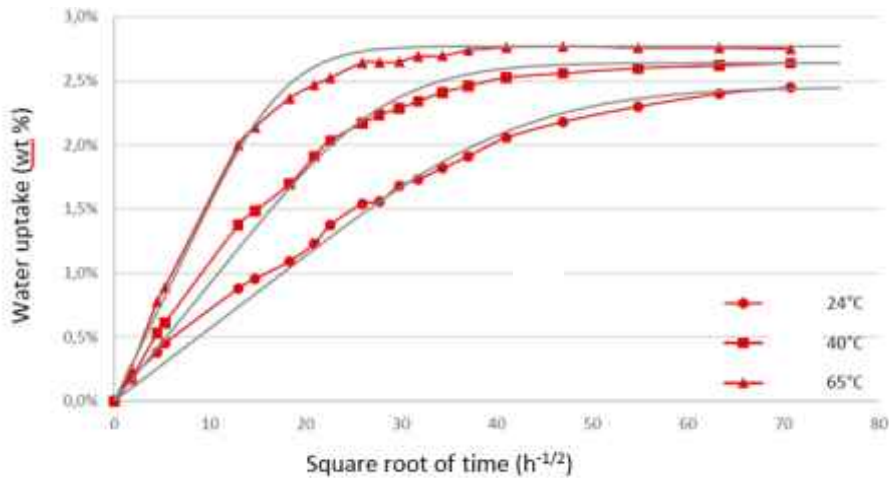
Figure 5.25: Water uptake of PU at 24°, 40° and 65°C as a function of time

5.4.5 Fibers

Figures 5.26 to 5.28 display SEM micrographs of the three fibers before and after 7 days conditioning. No degradation was observed on the surface of the three glass fibers.
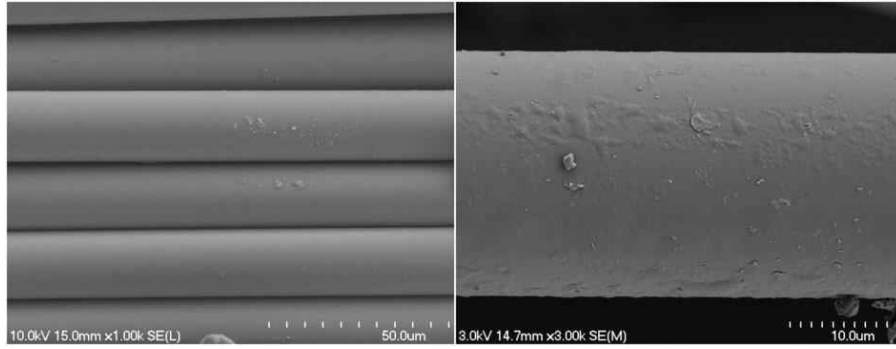
Figure 5.26: ECR-GF fibers before and after conditioning
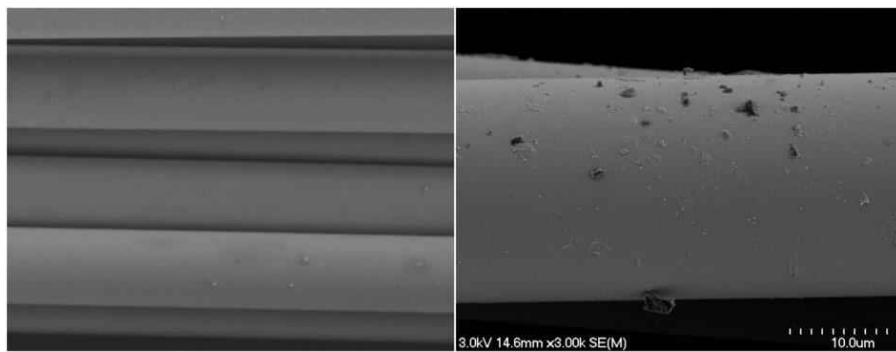
Figure 5.27: EP-BF-GF fibers before and after conditioning
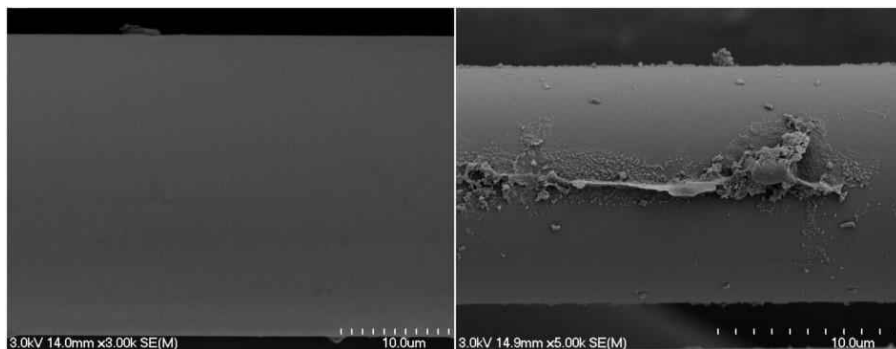
Figure 5.28: MC-EP-BF-GF fibers before and after conditioning

X-Ray Fluorescence has been carried out on ECR-GF and BF-GF fibers in order to verify if some metals have been leached during the conditioning in alkaline solution. This phenomenon is well documented for conditioning in acidic solutions. Table 5.8 reports the content of the main oxides present in the fibers. Only minimally decrease of silica content is detected. The concentration of the different metals can therefore be considered constant, which is confirmed by EDS analysis. EDS mapping shows an even distribution of Silicon, Calcium and Aluminum through the cross section of ECR-GF fiber before and after conditioning in alkaline solution (Figure 5.29). However,

as reported above, conditioning in acid causes the leaching of Calcium and Aluminum in the outer area of the fiber.

Table 5.8: Composition of fiber before and after conditioning

Type of fiber		SiO_2	Al_2O_3	CaO	MgO	Na_2O	Fe_2O_3	K_2O
ECR-GF	Ref.	58.3	10.5	21.7	3.1	0.5	0.8	0.3
	Cond.	57.3	10.5	21.5	3.0	0.7	0.9	0.3
BF-GF	Ref.	59.8	16.0	12.1	8.6	0.6	1.1	0.3
	Cond.	58.9	15.9	12.3	8.5	0.6	1.0	0.3

Note: Only fibers with different composition have been analyzed. It has been considered that the sizing does not modify the composition.
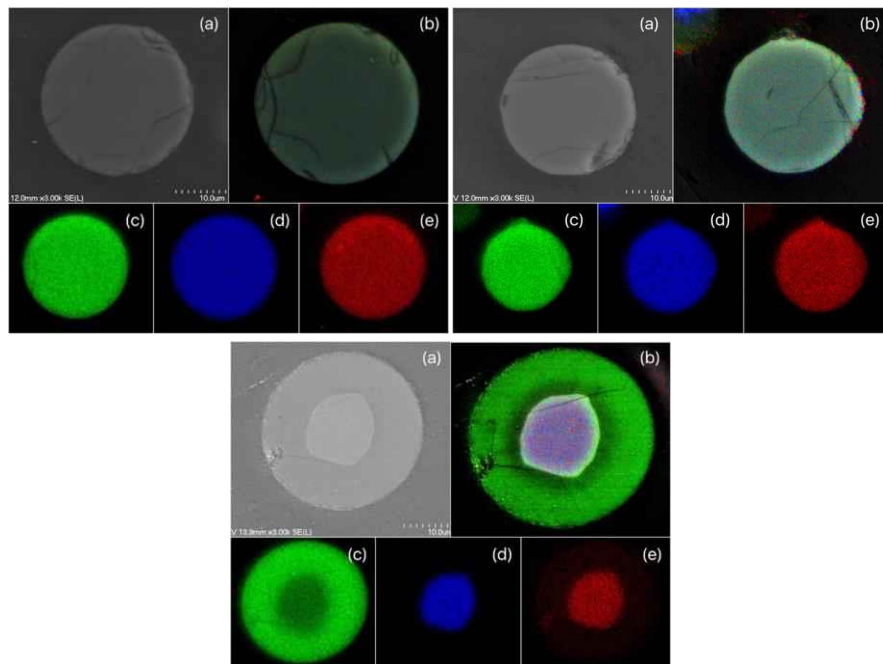
Figure 5.29: EDS analysis of ECR-GF fiber: Left: Before conditioning; Middle: Conditioned in alkaline solution; Right: Conditioned in acidic solution. (a) SEM micrograph; (b) Mapping of all species; (c) Mapping of silicon; (d): Mapping of calcium; (e) Mapping of aluminium.

5.4.6 GFRP composite samples

GFRP composite samples were immersed in water and alkaline solution at 24°, 40° and 65°C for 1 and 2 months. Water uptake was recorded periodically. Figure 5.30 displays water uptake as a function of the square root of the time. At equilibrium, the water content of VE composites is below 0.5 wt%, whereas EP composites absorb 1 to 1.5% water. However, PU composites do not follow a fickian type water diffusion model and absorbs a large amount of water. No equilibrium

is even reached after 2 months. Table 5.9 reports the average values of water uptake at equilibrium for the composites immersed during 2 months at 24°, 40° and 65°C. The VE composites absorb significantly less water than the PU and EP composites.
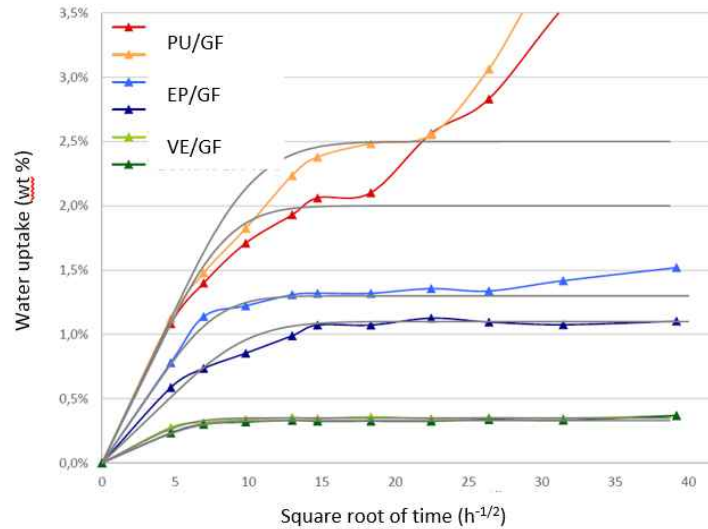
Figure 5.30: Water uptake of VE, EP and PU composites at 65°C (measurements have been duplicated)

Table 5.9: Water uptake at saturation of composites at 24°, 40° and 65°C.

	PU	EP	VE
$M_{\infty}24$	1.4	0.8	0.2
$M_{\infty}40$	1.9	0.9	0.3
$M_{\infty}65$	2.2	1.2	0.4

Figures 31 to 33 report the evolution of the water absorption rate at 65°C of pure PU, EP and VE resins and composites as a function of the square root of the time, respectively. The data have been smoothed according to the fickian model and normalized to the water absorption at equilibrium. M_t and M_s are the water at time t and saturation, respectively. The water absorption rate depends on the microstructure of the resin, pores generated during the manufacturing process, barrier effect created by inorganic particles or fibers, such as glass fibers, and voids located at the interface between the resin and the surface of fibers. The effect of these voids on the water diffusion will be all more important that the adhesion of the fibers will be poor. The three figures show the same behavior. Composites absorb water more rapidly than pure resins. Assuming that the microstructure of the resins in the bulk (far from the fiber surface) is the same in the composite and the pore content negligible, it may be concluded that barrier effect created by the impervious fiber, also known as tortuous path, does not compensate the diffusion of water along the fibers, through the interface. The interface may contain free gaps but is also constituted of an entanglement of surrounded resin molecules and fiber sizing, which apparent produces a lower density with mobile molecules and a higher free volume, which facilitate water diffusion.
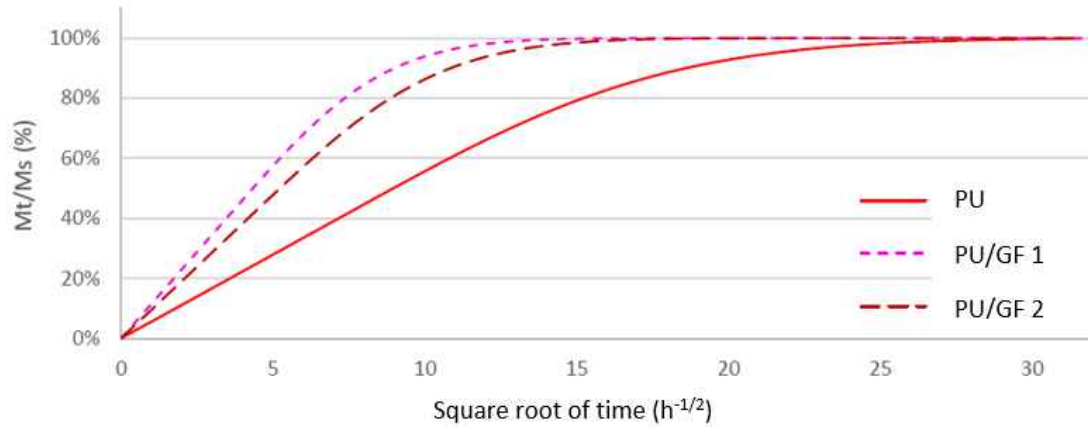
Figure 5.31: Normalized water absorption rate of PU composite vs square toot of time at 65°C

Figure 5.32: Normalized water absorption rate of EP composite vs square root of time at 65°C
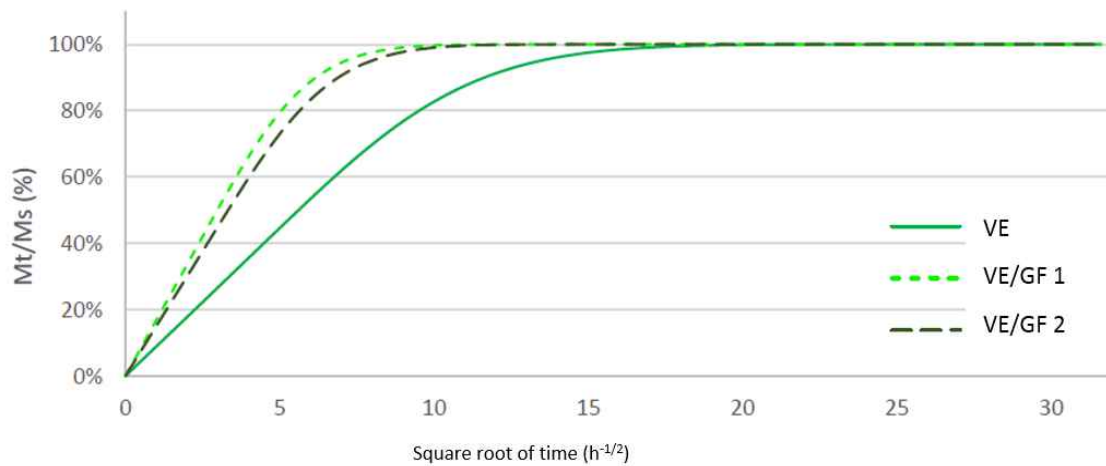
Figure 5.33: Normalized water absorption rate of VE composite vs square toot of time at 65°C.

The coefficient of diffusion can be calculated for the pure resins and their composites according to Fick's law:

$$\frac{M_t}{M_S} = \frac{4}{h}\sqrt{\frac{D \cdot t}{\pi}}$$

Where h, D and t are the half thickness of the same, the coefficient of diffusion and the time.

Table 5.10 reports the ratio of the coefficient of diffusion of composites with respect to pure resins. The coefficient of diffusion of PU and EP composites is twice larger than for the pure resins. However, it is only 60% higher for VE composites. This indicates that the quality of the interface of glass fiber with VE resin is better than with PU and EP resins, which are approximately equivalent.

Table 5.10: Ratio of coefficients of diffusion at 65°C

	PU	EP	VE
$D_{composite}/D_{resin}$	1.96	2.03	1.61

The quality of the interface has been analyzed by Scanning Electronic Microscopy. Figure 5.34 exhibits three micrographs of the cross section of PU, EP and VE composites at high magnification. It may be observed that the three samples visually present a similar interface with no free gap or sign of debonding. Consequently, it may be assumed that the differences of water absorption rates and diffusion is not due to the diffusion of water through voids present between the fiber surface and the surrounding resin, but to the ingress through an interphase eventually constituted of sizing molecules and resin molecules surrounding the fibers. It has to be noted that the sizing coating the fiber surface is composed of several chemicals and not only of coupling agents, such as silanes. In fact, silanes are not the main constituent of sizing agents, which also contain lubricants, emulsifiers, etc. These chemicals may also interact with the resin and affect the properties of the interphase. The existence ot the interphase has been highlighted by Joliff *et al.* by Atomic Force Microscopy (AFM) and Micro-Thermal Analysis in epoxy/glass fiber composites. The AFM analysis showed that the modulus of the resin located at less than 1 micron of the surface of fibers is much lower than the one of the bulk resin (Figure 5.35), whereas micro-TA showed a significant decrease of the softening temperature of the resin surrounding the fibers (Figure 5.36). In this case, the thickness of the interphase would lay between 4 and 10 microns. Figure 5.37 shows the interphase determined by these two techniques. The mechanical strength of the resin is highly reduced in the first micron surrounding the fiber (left picture), whereas the resin is physically affected up to 10 microns (right picture).
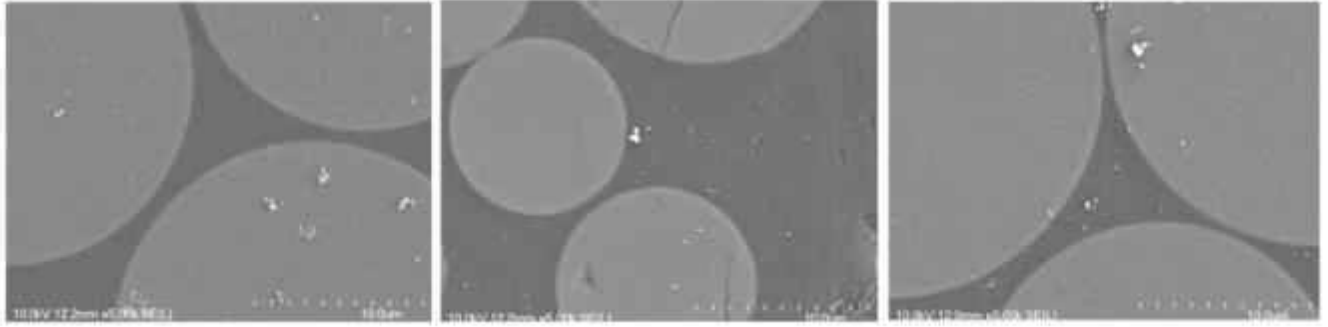
Figure 5.34: Interface in PU, EP and VE composites at same magnification
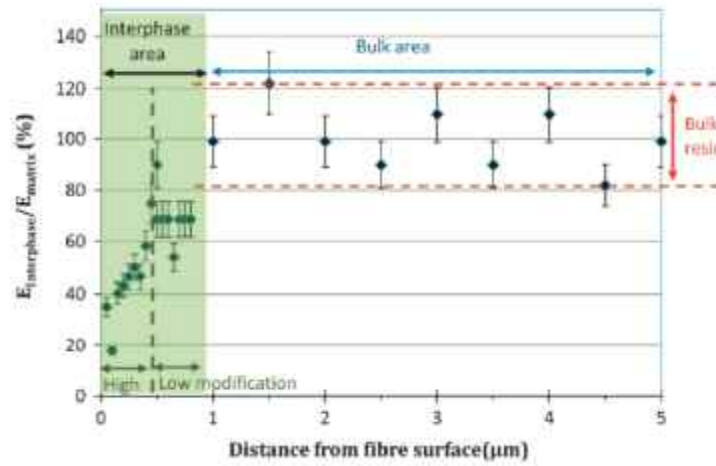
Figure 5.35: Elasticity modulus of resin matrix versus distance to fiber surface by AFM (Joliff *et al*., 2014).
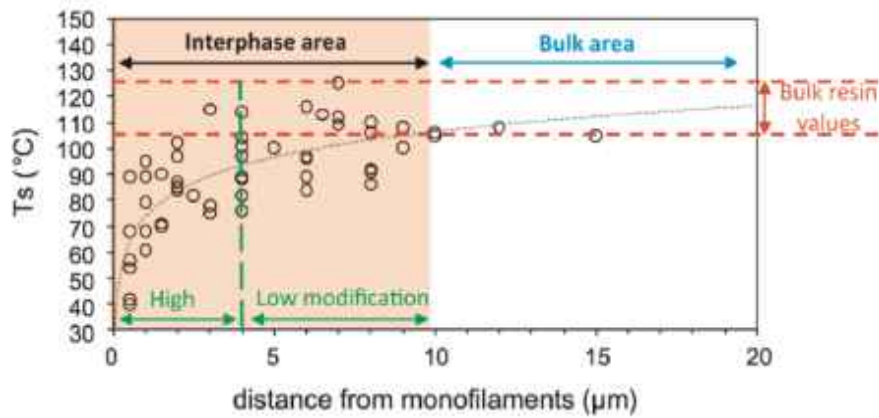
Figure 5.36: Softening temperature of resin matrix versus distance to fiber surface by μ-TA (Joliff *et al*., 2014).

237
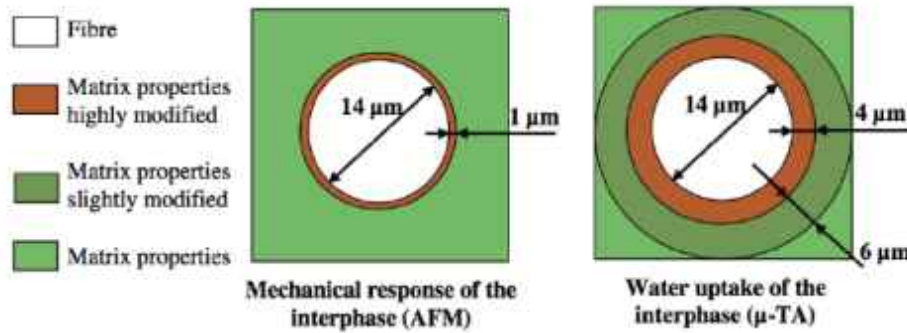
Figure 5.37: Interphase thickness estimated mechanically (left) and thermally (right) (Joliff *et al*., 2014).

The phenomena involved in the formation of this interphase may be explained in two ways. As seen above, the first one is the interaction of the sizing agent with the resin. Cross *et al.* have showed a decrease of the polymerization around fibers treated with a silane, whereas Mallarino *et al*. have showed a decrease of the density of reticulation and local plasticization at the interphase by DMA. Mallarino *et al*. have also showed by micro-TA that the temperature of relaxation of composites composed of fibers without sizing agent is the same as for pure resin. The other reason for the presence of an interphase is the effect of water. It is well known that water may act as a plasticizer, which increases the mobility of the molecular chains. Yu *et al.* have performed DMA analyses on a vinylester resin and composites immersed in water during several periods of time. Figure 38 presents the effect of water immersion on the glass transition temperature of VE resin. It appears that the *Tg* of the pure resin is equal to 135°C. After immersion, a second *Tg* appears at a lower temperature (115°C). It may therefore been assumed that a molecular rearrangement occurs, leading to the presence of two phases: a denser phase with less mobile polymeric chains presenting a higher *Tg* and a softer phase with more mobile chains presenting a lower *Tg*. Since it has been demonstrated that water diffuse faster in composites than in pure resins and that this extra-diffusion is located along the fiber, we may conclude that the resin surrounding the fibers is more affected by the plasticizing effect of water. Consequently, the effect of water ingress along the fibers increases the plasticizing effect of the sizing via a synergistic mechanism: The less dense resin phase diffuses more water and more water softens the resin.
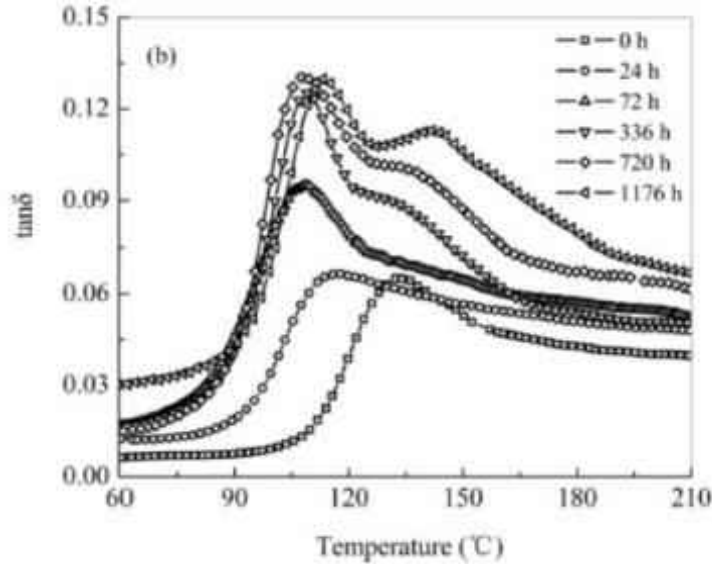
Figure 5.38: *Tg* (taken as maximum of the peak of tan delta) of VE resin immersed in water (Yu *et al.,* 2009.

5.4.7 Conclusions on GFRP constituent materials

From the analyses performed on three thermoset resins used in FRP bar manufacturing, it may be concluded that the chemical resistance of these materials in alkaline solution is as following:

EPOXY > POLYURETHANE > VINYL ESTER

However, it has to be noted that the conditionings used in this study are harsher than the environment surrounding composite material in concrete. Moreover, only a thin layer in direct contact with the solution is affected. Below the resin surface, the three resins are not degradated. Consequently, in spite of their lower chemical resistance VE resins are resistant to concrete environment, as observed in several studies on GFRP reinforcing bars.

As glass fibers are concerned, the main conclusions drawn from this study are:

(a) ECR-type and boron free glass fiber are resistant to alkalis.
(b) Sizing can act as a protector against alkali corrosion.
(c) Conditioning in alkaline solution does not modify the content of metals in the fiber. No metal leaching is observed.

Concerning the composites prepared at the laboratory with these fibers and resins, several conclusions may be drawn:

- Composites absorb water faster than pure resins.
- SEM analysis shows that the bonding at the fiber-matrix interface is excellent. No significant debonding was detected.

239

- The presence of fibers in a resin matrix creates an interphase, which is caused by the diffusion of sizing molecules through the surrounding resin molecules. The thickness of this interphase is between 1 and 10 microns depending on the technique used.
- This interphase is constituted of a less dense and more "porous" resin, which is responsible of the increase of water diffusion.
- VE composites absorb less water than PU and EP composites. VE resin and the interphase in VE composites are less permeable to water diffusion and should therefore offer an excellent durability for vinyl-ester GFRP bars in humid/moist environments like in Florida.

CHAPTER 6
STRUCTURAL PERFORMANCE OF CONCRETE BEAMS PRESTRESSED WITH CFRP TENDONS

6.1   Introduction

This chapter focuses on the structural behavior of concrete beams prestressed with CFRP tendons. A total of 12 prestressed concrete beams were tested during this research. Eight beams were placed in two tanks and subjected to wet and dry cycles of saltwater, which simulated the aggressive exposure to seawater and also mimicked the environmental condition of Florida State. The accelerated aging process was facilitated by applying a sustained load to induce cracks into the beams. The sustained load was equivalent to 50 percent of the flexural capacity of the beam. Two control beams were tested at the beginning of the experimental program to determine the flexural capacity of the beams. In addition, two beams were subjected to sustained load only and tested at the end of the exposure duration, in order to exclude the aging effect of concrete from the effect of exposure to saltwater cycles.

In order to evaluate any degradation in the CFRP tendons, the concrete beams were designed to fail by rupture of strands before crushing of concrete. The guaranteed mechanical properties of CFRP, provided by Tokyo Rope Company, were used in the design process. It should be noted that the ultimate strength is significantly higher than the guaranteed strength reported by the manufacturer. All twelve beams have the same geometrical configuration of 11 ft. (3.35 m) long, a total height of 12 inches (305 mm), a web width of 12 inches (305 mm), a flange width of 36 inches (914 mm) and a flange thickness of 3 inches (76 mm). Each concrete beam was prestressed with two 15.2 mm (0.6 inch) diameter CFRP strands to 65% of their guaranteed tensile strength. The cross-sectional dimensions and reinforcement details are shown in Figure 6.1.
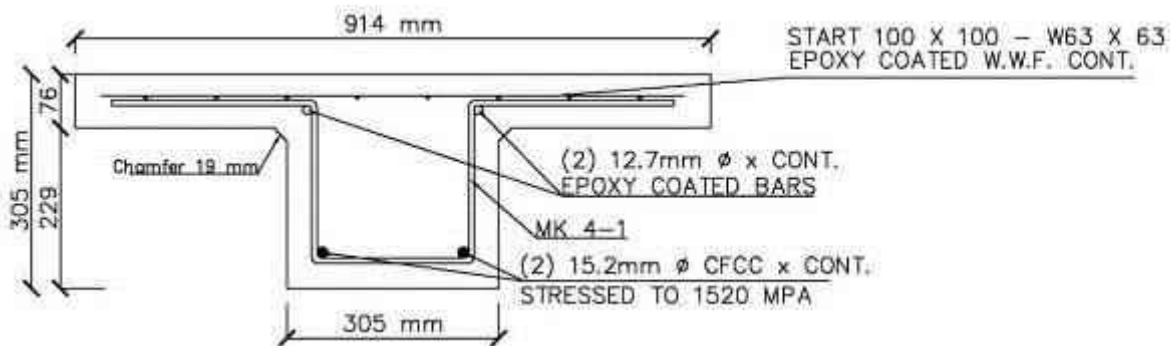
Figure 6.1: Beam cross-sectional dimensions and reinforcement details

6.2   Casting of Beams

Twelve prestressed beams were cast at Gate Precast Plant in Jacksonville, FL on November 4th, 2015. All beams were cast using one casting bed and one concrete batch was used to ensure consistency of concrete strength for all beams. Figure 6.2 through Figure 6.8 show the tensioning and the casting process.   Tensioning of CFRP tendons required special preparations. Both ends of strands were coupled to prestressing steel strands. Figure 6.2 shows the coupler used to join the CFRP to the steel strand. The interior of the CFRP coupler was sprayed with a lubricant spray and then was slid onto the strand as shown in Figure 6.2 (a) and (b) respectively. A helical buffer material was wrapped around the ends of strands as shown in Figure 6.2 (c). The buffer material was tightly twisted around the CFRP and taped to the strand with electrical tape. Figure 6.2 (d) shows the second layer of braid grip that was placed over the buffer mesh. The grip was tightly squeezed around the CFRP and taped to the strand. A wedge guide was placed onto the strand, the wedges were inserted into the guide and pushed by hand into the sleeve as shown in Figure 4.2 (e) and (f), respectively. Then the wedges and sleeve were placed into the seating ram assembly as shown in Figure 6.2 (g). The wedges were pushed into the sleeve using a hand pump connected to the seating ramp as shown in Figure 6.2 (h). Figure 6.2 (i) shows the CFRP sleeve with wedges pressed inside it. The other part of the coupler was slid into the standard chuck of the steel strand as shown in Figure 6.3. The coupler was pulled tightly and screwed to the sleeve, as shown in Figure 6.4. The final shape of the coupler is shown in Figure 6.5. Figure 6.6 shows the CFRP tendons before and after tensioning. The couplers were placed in a staggered configuration to avoid interference with each other. The strands were tensioned to the desired load in two steps to ensure that the CFRP tendons were straight. Figure 6.7 shows the casting process of the beams. Finally, the beams were shipped to NC State University and stored as shown in Figure 6.8.

| (a) Spraying of CFRP sleeve | (b) Sliding sleeve into CFRP |

(c) Wrapping CFRP with buffer material

(d) Placing braid grip over buffer material

(e) Placing wedges in wedge guide

(f) Placing wedge guide into the CFRP sleeve

(g) Wedges and sleeve are placed in seating ram

(h) A hand pump presses the wedges into the sleeve

(i) Sleeve with wedges pressed inside it

Figure 6.2: Preparation of CFRP part of the coupler

Figure 6.3: Preparation of steel strand part of the coupler

Figure 6.4: Screwing the two halves of the coupler

Figure 6.5: Final shape of coupler

Figure 6.6: CFRP strands before and after tensioning.

Figure 6.7: Casting of Concrete

Figure 6.8: Beams stored at NCSU lab

6.3 Conditioning of beams

Two beams were tested as control specimens upon arrival to NC State University. Eight beams were subjected to sustained load equivalent to 50 percent of their flexural capacity to induce cracks into the beams and facilitate the adding process. In addition to the sustained load, the eight beams were also exposed to wet and dry cycles of saltwater for 3, 6, 12 and 18 months. The last two beams were subjected to sustained load only and tested at the end of the exposure duration of 18 months, in order to exclude the aging effect of concrete from the effect of exposure to saltwater cycles. The testing matrix for accelerated aging of CFRP prestressed concrete beams is given in Table 6.1. The sustained load was applied by tying two beams together at the two ends using high strength stainless steel bars. A 4x4 inch stainless steel hollow structural solutions (HSS) was placed between the two beams at the mid span to induce a concentrated applied load on the two beams. Figure 6.9 shows a sketch of the beams under sustained loading and Figure 6.10 shows the actual beams subjected to sustained load only. The eight beams under sustained load were placed in tanks and subjected also to wet and dry cycles using 3.5 % saltwater. Figure 6.11 shows the loading process of the beams in tanks and Figure 6.12 shows the beams subjected to wet and dry cycles of salt water. At the end of each exposure period, the beams were tested monotonically using 3-point bending configuration up to failure to determine the residual strength of the beams prestressed with CFRP.

Table 6.1: Testing matrix for accelerated aging of CFRP prestressed concrete beams

Sustained Load	Wet and Dry Cycles of Salt Water	Duration of exposure (month)	Temperature (^oF)	No. of specimens
-	No	0 (control)	Outdoor	2
Cracking (50% of beam capacity)	Yes	3	Outdoor	2
	Yes	6	Outdoor	2
	Yes	12	Outdoor	2
	Yes	18	Outdoor	2
	No	18	Outdoor	2
Total				12
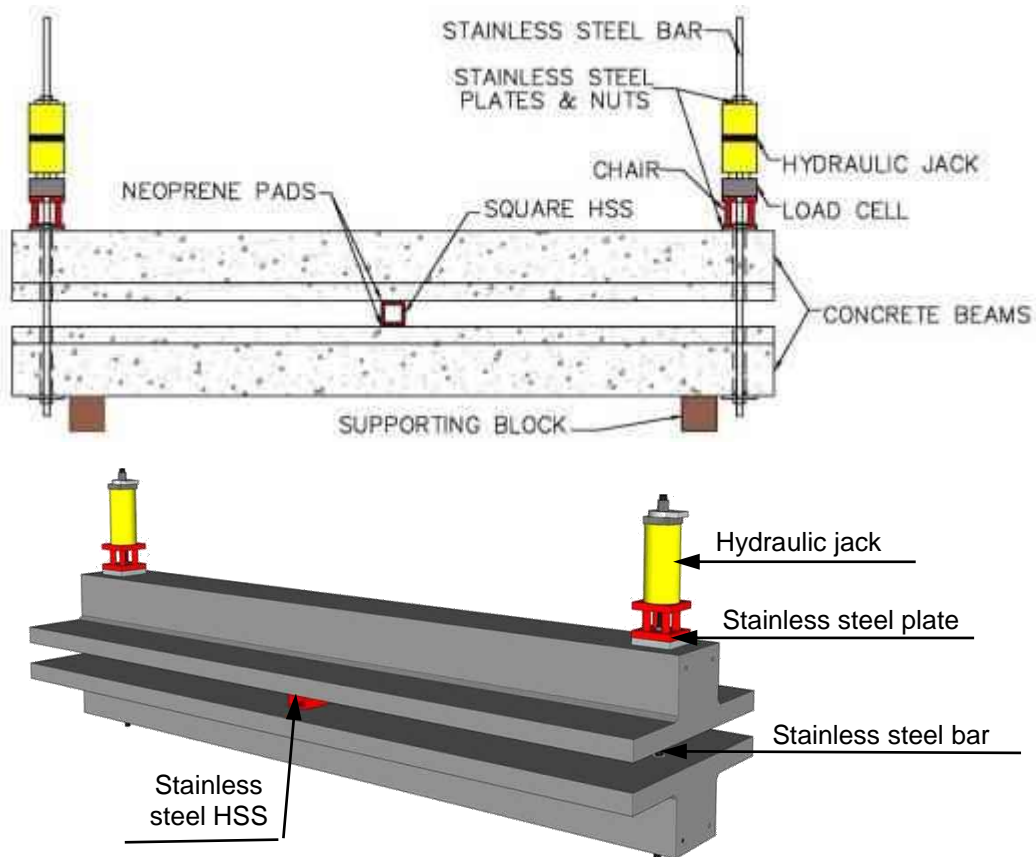
Figure 6.9: Sketch for beams under sustained loading.
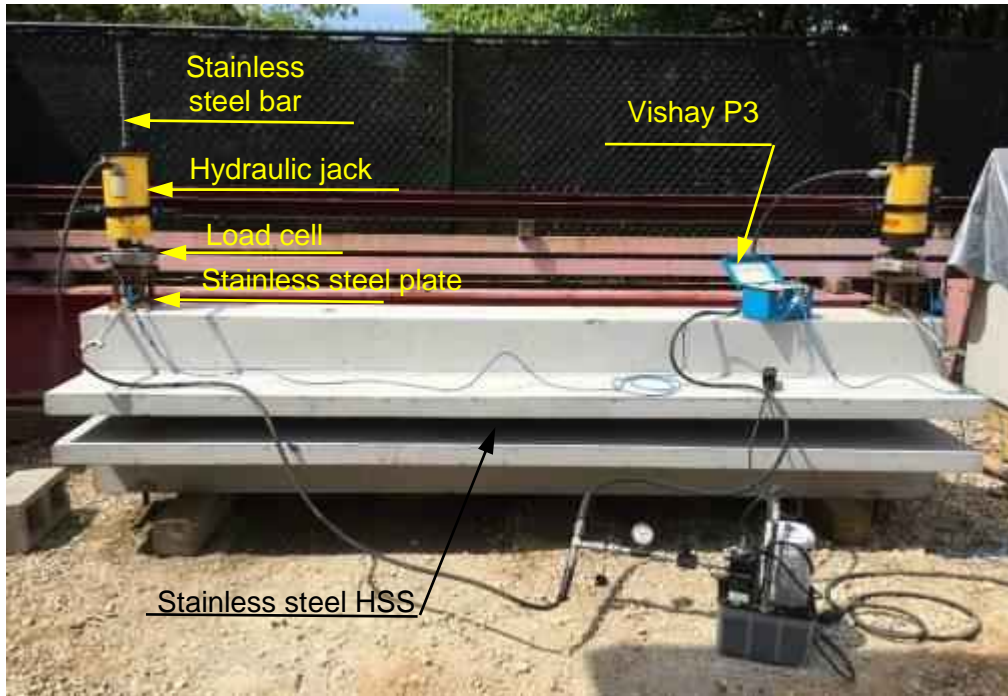
Figure 6.10: Actual beams under sustained loading.

Figure 6.11: Concrete beams in first tank subjected to sustained load.

Figure 6.12: Concrete beams in two tanks undergoing wet and dry cycles

6.4 Test Setup

The concrete beams prestressed with CFRP were tested using a simply supported configuration and loaded monotonically up to failure. The supports were located six inches away from the edge. The load was applied at the mid-span using two 120 kips hydraulic jacks and a 4 ft. long spreader beam. The load was transferred to the beam through a 4x4 inch stainless steel hollow structural solutions (HSS) placed under the spreader beam. The HSS had a length of 18 inches and rested on top of the beam specimen. Figure 6.13 and Figure 6.14 show the schematic view and the actual test setup respectively. Four types of instrumentations were used to monitor the response during testing. All instruments were connected to an electronic data acquisition system to monitor and record the data during testing. Load cells were used to measure the applied load from the hydraulic jack to the spreader beam. String potentiometer were used to measure the vertical deflection of beam specimen at the mid span. Four linear potentiometers were placed at the end of each strand to measure any possible movement of the strands during testing. A total of three PI gauges were used to measure the strain of concrete. One PI gauge was placed at the bottom of the web at mid span and two PI gauges were placed on the top flange of the beam on the left and right of the HSS to measure the concrete strain in tension and compression respectively.
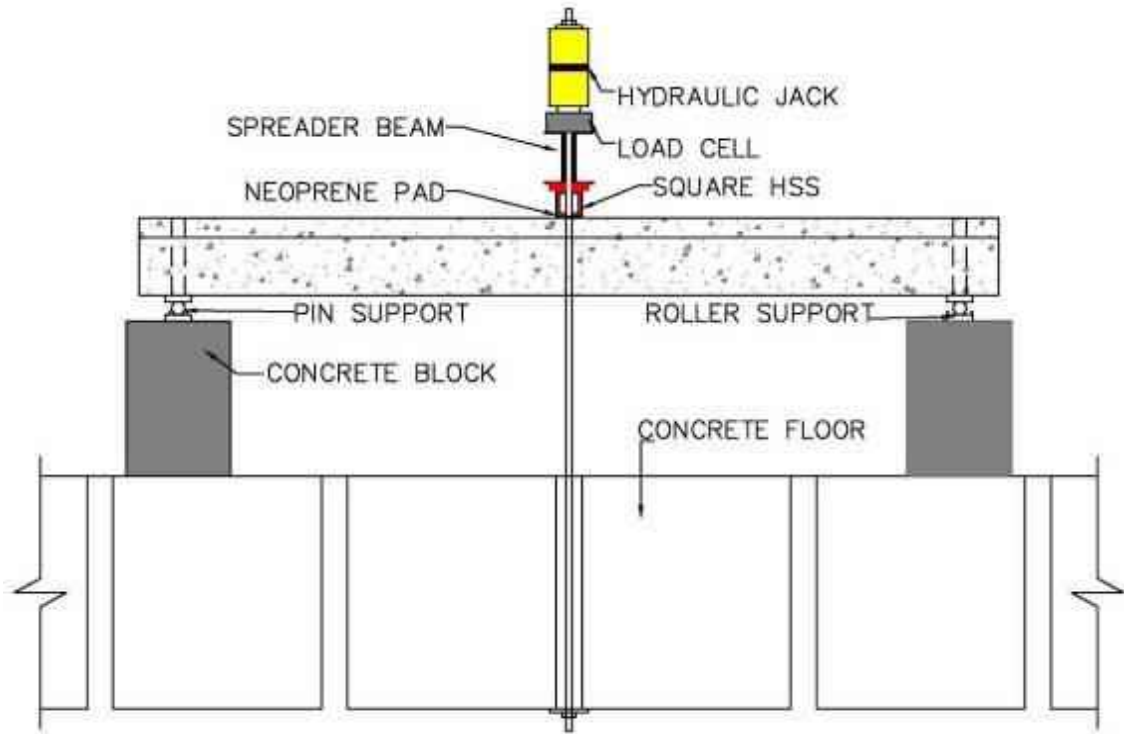
Figure 6.13: Schematic view of test setup
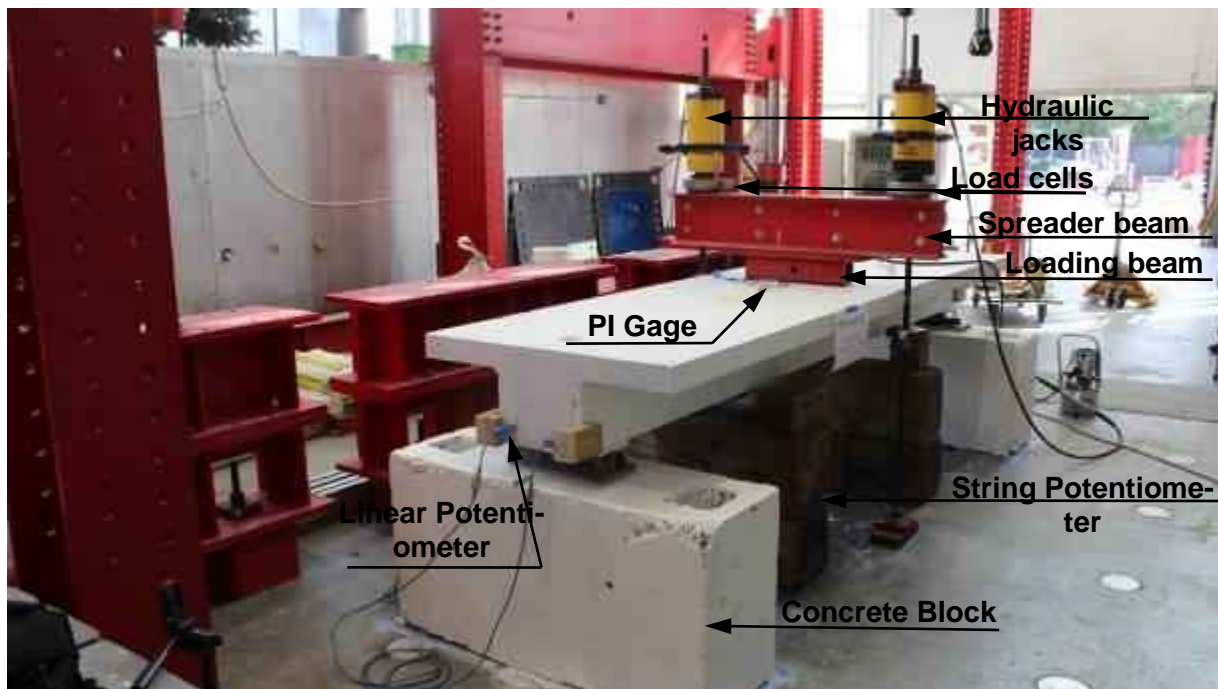
Figure 6.14: Actual test setup

6.5   Test Results

The beams were designed to fail by rupture of strands before crushing of concrete in order to evaluate any possible degradation of CFRP in concrete after exposure to salt water and sustained load for specified durations. The actual mechanical properties of CFRP, provided by the manufacturer are given in Table 6.2. It should be noted that the actual ultimate strength of the strands is higher than the guaranteed strength. The CFRP tendons were stressed to 65% of their guaranteed strength as recommended by ACI 440.4R-04 design guideline.

Table 6.2: Guaranteed and actual mechanical properties of Tokyo Rope CFRP tendons

	Breaking load Kips (KN)	Tensile Strength Ksi (Mpa)	Ultimate Strain (%)	Tensile Modulus Ksi (Gpa)
Guaranteed values	60.70 (270)	337.2 (2335.6)	1.51	22480.80 (155)
Actual values	82.93 (368.9)	463.3 (3191.2)	2.0	22915.96 (158)

The following sub-section discusses the test results of all tested beams.

6.5.1   Control Beams

The observed behavior under the applied load for the tested beams indicated that the first flexural crack was initiated at mid span of the beam at a load of about 22 kips (118 KN). As the load increased, the cracks extended in depth and width followed by initiation fo several other cracks along the span. Both beams failed by rupture of the strands at approximately the same load level. The first beam experienced slippage of one of the strands after the rupture of the strands. The second beam failed also by rupture of strand followed by crushing of concrete. Table 6.3 presents a summary of the test results in terms of cracking load, failure load and mid span deflection at failure. Figure 6.15 and Figure 6.16 show failure of beams #1 and #2 respectively. After the test was completed, the cracked concrete was chipped to verify the failure mode of beams. Figure 6.17 (a) and (b) show a close up of the ruptured strands for the control beam #1 and #2, respectively.

Table 6.3: Test results of control beams

Conditioning period		Cracking load kips (KN)	Failure load kips (KN)	Mid span deflection Inches (mm)
Control Beams	Beam #1	22.00 (98)	58.50 (260)	1.80 (45.7)
	Beam #2		59.00 (262)	2.10 (53.3)

Figure 6.15: Failure of control beam#1

Figure 6.16: Failure of control beam#2
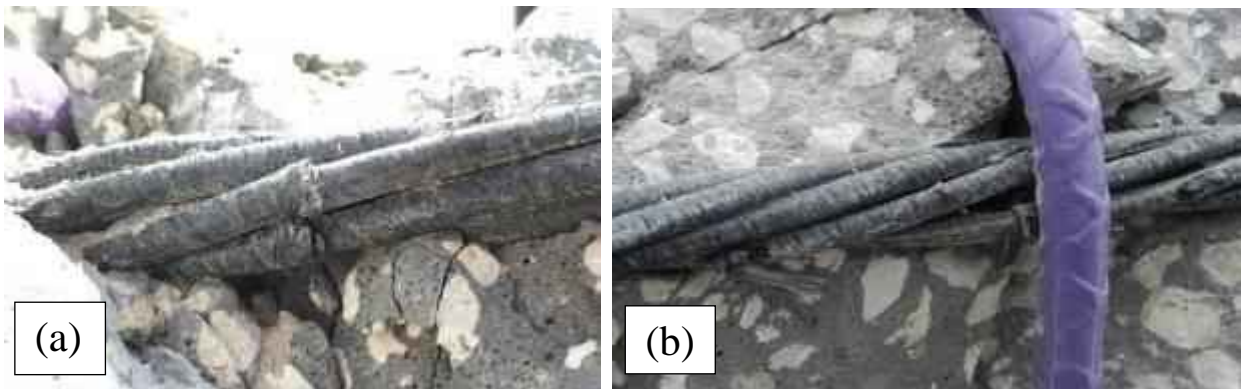
Figure 6.17: Rupture of strands (a) Control beam #1 (b) Control beam #2

6.5.2 Beams exposed to sustained load and environmental conditions for 3 months

Two duplicate beams were subjected to sustained load equivalent to 50 percent of their flexural capacity and exposed to wet and dry cycle of salt water every two weeks for 3 months. Upon completion of the exposed duration, the sustained load was removed at the end of a dry cycle. The pre-existing cracks were marked before the test. During testing the preexisting cracks increased in width as expected as typical behavior of prestressed beam. New cracks started to develop when the applied load reached 35 kips (156 KN). Figure 6.18 (a; b) show the crack pattern of the top and bottom concrete beams respectively, during the test at a load level of 40 kips (178 KN). Failure of the first exposed beam, placed on top during the exposed period, failed at a load of 59 kips (262 KN). The second exposed beam, placed at the bottom, failed at load of 56.50 kips (251 KN). The test results of control beams and beams conditioned for 3 months are given in Table 6.4. It should be noted that the measured mid span deflection for the top beam was slightly higher due to an instrumentation error in the string potentiometer discovered after the test. This was confirmed when testing the duplicate beam conditioned for 3 months and the mid span deflection was 1.8 inches similar to control beams Figure 6.19 and Figure 6.20 show failure of beams #3 and #4 respectively. The failure of both beams was due to rupturing of strands and in this case, no slippage or concrete crushing took place. The cracked concrete was chipped off to verify the rupture of strands. Figure 6.21 (a; b) show a close up view of the ruptured strands for beams exposed for 3 months #1 and #2 respectively. There was no change in the flexural carrying capacity of beams after exposed for 3 months relative to control beams.

Table 6.4: Summary of test results of beams up to 3 months of exposure

Exposed period		Cracking load kips (KN)	Failure load kips (KN)	Mid span deflection Inches (mm)
Control Beams	Beam #1	22.00 (98)	58.50 (260)	1.80 (45.7)
	Beam #2		59.00 (262)	2.10 (53.3)
3 months	Top Beam	Pre cracked	59.00 (262)	3.4 (86.4)*
	Bottom Beam		56.50 (251)	1.8 (45.7)

*Confirmed instrumentation error
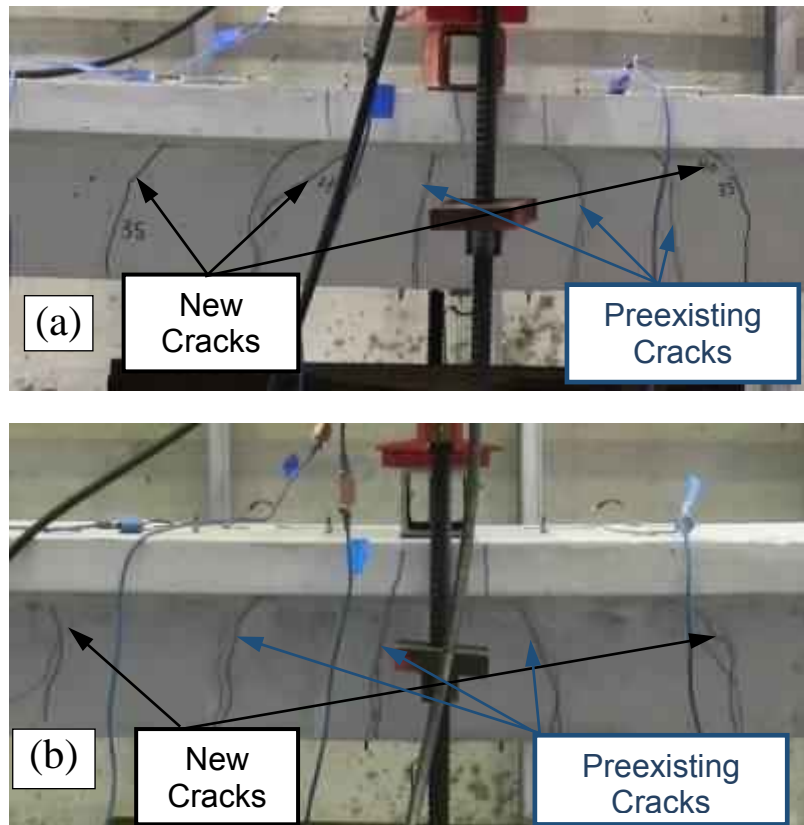
Figure 6.18: Crack pattern at load level of 40 kips after 3 months exposure (a) top beam (b) bottom beam.

Figure 6.19: Failure of beam#3 after 3 months of exposure (Top Beam).

Figure 6.20: Failure of beam#4 after 3 months of exposure (Bottom Beam).

Figure 6.21: A close up view of the strand rupture after 3 months exposure (a) top beam (b) bottom beam.

6.5.3 Beams exposed to sustained load and environmental conditions for 6 months

Similar to the beams conditioned for 3 months, two duplicate beams were tested to determine their residual flexural capacity after conditioning for 6 months. The observed behavior during the testing of the two beams was similar to the previous tested beams. The pre-existing cracks became wider as the load increased and new cracks were developed at a load level equals to 35 kips (156 KN). Figure 6.22 (a; b) show the crack pattern of the top and bottom concrete beams respectively, during the test at a load level of 40 kips (178 KN). The failure of the beam which was placed on top during the conditioning period, failed at a load equals to 60.50 kips (269 KN). The beam placed at the bottom failed at load equals to 57.50 kips (256 KN). The test results of all beams up to 6 months of exposure are given in Table 6.5. Figure 6.23 and Figure 6.24 show the failure of beams #5 and #6 respectively. Failure of both beams was due to rupturing of strands. The cracked concrete was chipped off to verify the rupture of strands. Figure 6.25 (a; b) show a close up view of the ruptured strands for beams conditioned for 6 months #5 and #6 respectively.

Table 6.5: Summary of test results of beams up to 6 months of exposure.

Conditioning period		Cracking load kips (KN)	Failure load kips (KN)	Mid span deflection Inches (mm)
Control Beams	Beam #1	22.00 (98)	58.50 (260)	1.80 (45.7)
	Beam #2		59.00 (262)	2.10 (53.3)
3 months	Top Beam	Pre cracked	59.00 (262)	3.4 (86.4)*
	Bottom Beam		56.50 (251)	1.8 (45.7)
6 months	Top Beam		60.50 (269)	2.0 (50.8)
	Bottom Beam		57.50 (256)	1.9 (48.3)

*Confirmed instrumentation error

Figure 6.22: Crack pattern at load level of 40 kips after 6 months exposure (a) top beam (b) bottom beam.
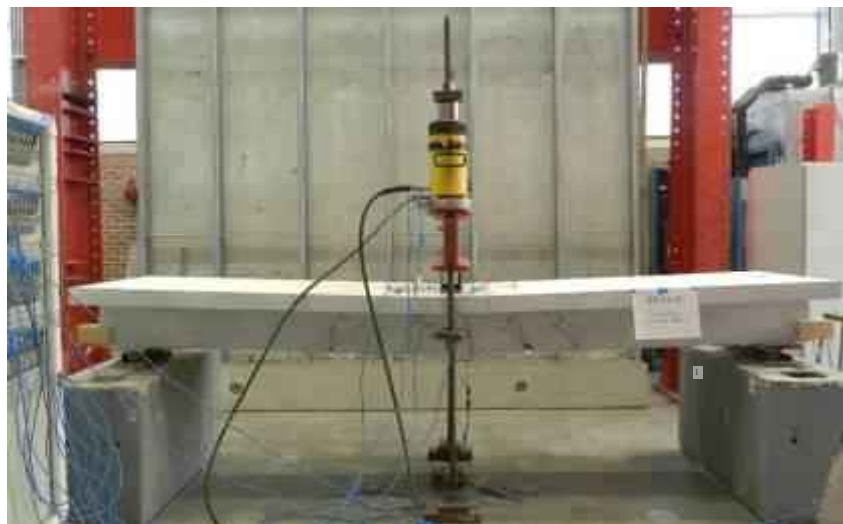
Figure 6.23: Failure of beam#5 after 6 months of exposure (Top Beam).

Figure 6.24: Failure of beam#6 after 6 months of exposure (Bottom Beam).
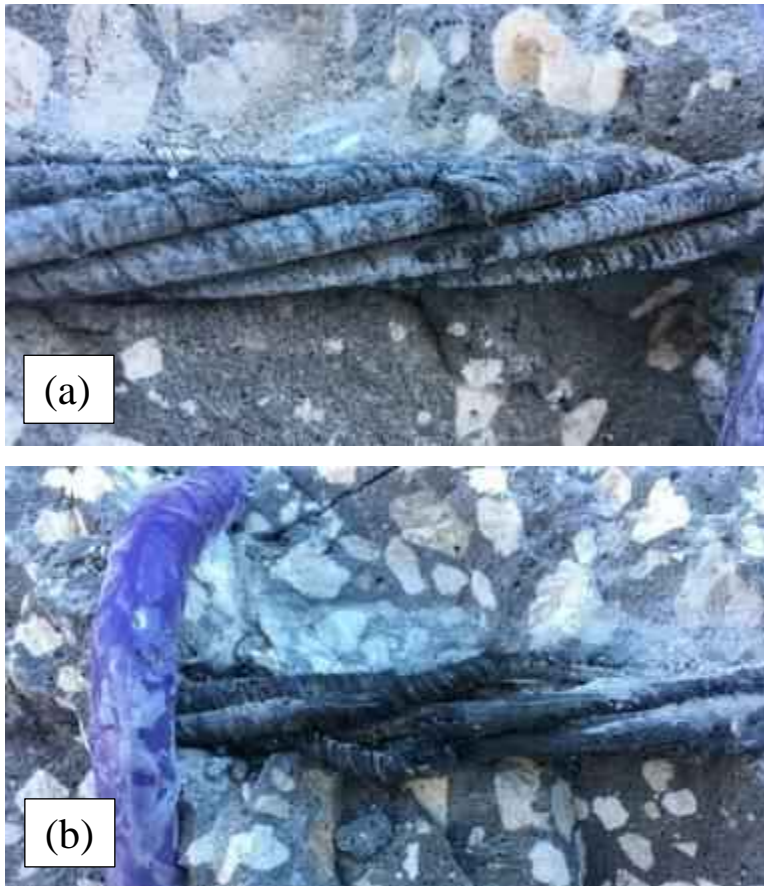
Figure 6.25: A close up view of the strand rupture after 6 months exposure (a) top beam (b) bottom beam.

6.5.4 Beams exposed to sustained load and environmental conditions for 12 months

Two duplicate beams were tested to determine their residual flexural capacity after aging for 12 months. The observed behavior during the testing of the two beams was similar to the previous tested beams. The pre-existing cracks became wider as the load increased and new cracks were developed at a load equals to 35 kips (156 KN). The beam, placed on top during the aging period, failed at a load equals to 59.00 kips (262 KN). The beam, placed at the bottom, failed at load equals to 57.50 kips (256 KN). Table 6.6 provides a summary of all the tested beams up to 12 months of conditioning. Figure 6.26 (a; b) show the crack pattern of the top and bottom concrete beams respectively, during the test at a load level of 40 kips (178 KN). Figure 6.27 and Figure 6.28 show the failure of beams #7 and #8 respectively. Failure of both beams was due to rupturing of strands. The cracked concrete was chipped off to verify the rupture of strands. Figure 6.29 (a; b) show a close up view of the ruptured strands for beams exposed for 12 months #7 and #8 respectively.

Table 6.6: Summary of test results of beams up to 12 months of exposure.

| Aging period		Cracking load kips (KN)	Failure load kips (KN)	Mid span deflection Inches (mm)
Control Beams	Beam #1	22.00 (98)	58.50 (260)	1.80 (45.7)
	Beam #2		59.00 (262)	2.10 (53.3)
3 months	Top Beam	Pre cracked	59.00 (262)	3.4 (86.4)*
	Bottom Beam		56.50 (251)	1.8 (45.7)
6 months	Top Beam		60.50 (269)	2.0 (50.8)
	Bottom Beam		57.50 (256)	1.9 (48.3)
12 months	Top Beam		59.00 (262)	1.9 (48.3)
	Bottom Beam		57.50 (256)	1.8 (45.7)

*Confirmed instrumentation error
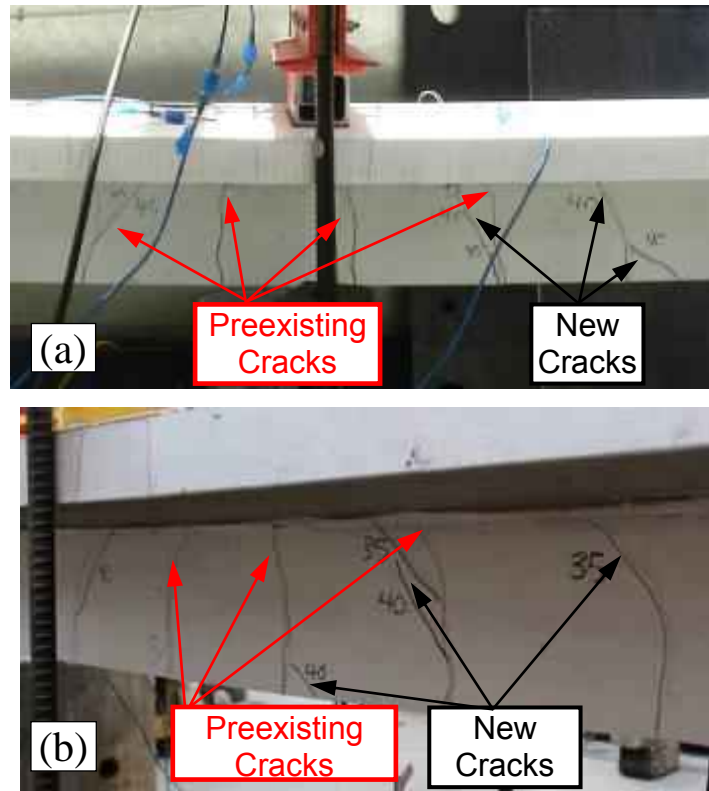
Figure 6.26: Crack pattern at load level of 40 kips after 12 months exposure (a) top beam (b) bottom beam.
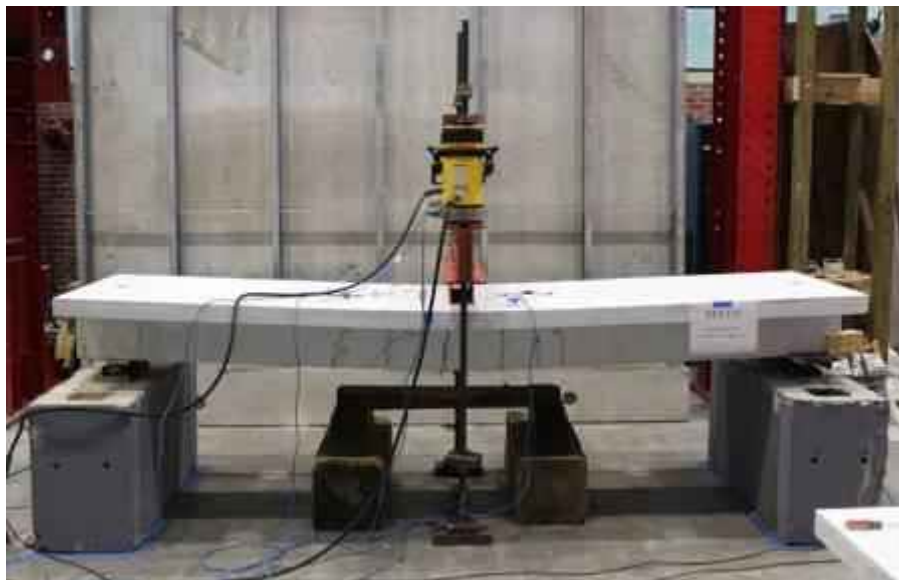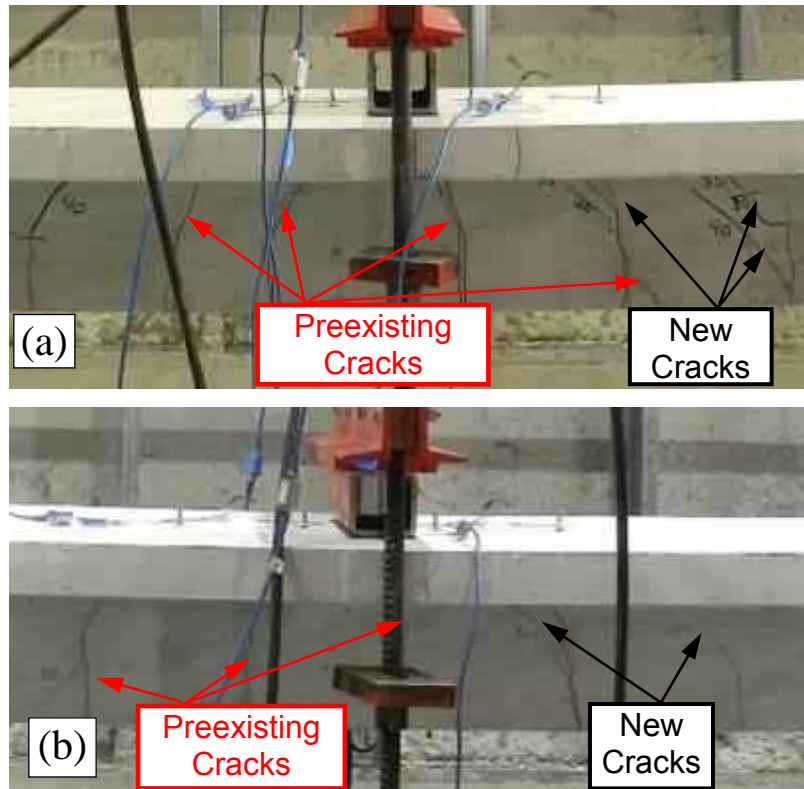

Figure 6.27: Failure of beam#7 after 12 months of exposure (Top Beam).

Figure 6.28: Failure of beam#8 after 12 months of exposure (Bottom Beam).

(a)

(b)

Figure 6.29: A close up view of the strand rupture after 12 months exposure (a) top beam (b) bottom beam

6.5.5 Beams exposed to sustained load and environmental conditions for 18 months

Similar to the previous beams, two duplicate beams were tested to determine their flexural capacity after exposure to sustained load and environmental conditioning for 18 months. The two duplicate beams had the same behavior during the test similar to all previous beams. The beam, placed on top during the aging period, failed at a load equals to 58.60 kips (261 KN). The beam placed at the bottom failed at load equals to 58.10 kips (258 KN). Table 6.7 provides a summary of all the tested beams up to 18 months of conditioning. Figure 6.30 and Figure 6.31 show the failure of beams #9 and #10 respectively. Failure of both beams was due to rupturing of strands. The cracked concrete was chipped to verify the rupture of strands. Figure 6.32 (a; b) show a close up view of the ruptured strands for beams exposed for 18 months #9 and #10 respectively.

Table 6.7: Summary of test results of beams up to 18 months of exposure.

| Aging period		Cracking load kips (KN)	Failure load kips (KN)	Mid span deflection Inches (mm)
Control Beams	Beam #1	22.00 (98)	58.50 (260)	1.80 (45.7)
	Beam #2		59.00 (262)	2.10 (53.3)
3 months	Top Beam	Pre cracked	59.00 (262)	3.4 (86.4)*
	Bottom Beam		56.50 (251)	1.8 (45.7)
6 months	Top Beam		60.50 (269)	2.0 (50.8)
	Bottom Beam		57.50 (256)	1.9 (48.3)
12 months	Top Beam		59.00 (262)	1.9 (48.3)
	Bottom Beam		57.50 (256)	1.8 (45.7)
18 months	Top Beam		58.60 (261)	1.8 (45.7)
	Bottom Beam		58.10 (258)	1.8 (45.7)

*Confirmed instrumentation error

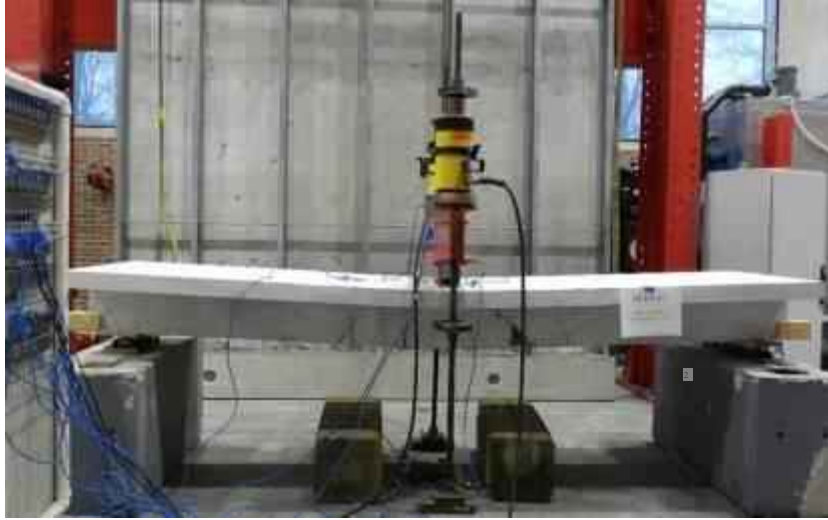Figure 6.30: Failure of beam#9 after 18 months of exposure (Top Beam).

Figure 6.31: Failure of beam#10 after 18 months of exposure (Bottom Beam).

Figure 6.32: A close up view of the strand rupture after 18 months exposure (a) top beam (b) bottom beam.

6.5.6 Beams exposed to sustained load only for 18 months

In order to exclude the aging effect of concrete from the effect of exposure to saltwater cycles, two duplicate beams, subjected to sustained load only, were tested at the end of the exposure duration of 18 month. Figure 6.33 shows the two beams during the exposure duration subjected to sustained load only. The beams had similar behavior during testing as all previous beams. The same failure load was achieved and the same mode of failure occurred. The beam, placed on top during the aging period, failed at a load equals to 59.80 kips (266 KN). The beam placed at the bottom failed at load equals to 56.80 kips (253 KN). Table 6.68 provides a summary of all the tested beams. Figure 6.34 and Figure 6.35 show the failure of beams #11 and #12 respectively. Failure of both beams was due to rupturing of strands. The cracked concrete was chipped to verify the rupture of strands. Figure 6.36 (a; b) show a close up view of the ruptured strands for beams subjected to sustained load only for 18 months #11 and #12 respectively.

Figure 6.33: Two beams subjected to sustained load only for 18 months.

Table 6.8: Summary of all tested beams.

Aging period		Cracking load kips (KN)	Failure load kips (KN)	Mid span deflection Inches (mm)
Control Beams	Beam #1	22.00 (98)	58.50 (260)	1.80 (45.7)
	Beam #2		59.00 (262)	2.10 (53.3)
3 months	Top Beam	Pre cracked	59.00 (262)	3.4 (86.4)*
	Bottom Beam		56.50 (251)	1.8 (45.7)
6 months	Top Beam		60.50 (269)	2.0 (50.8)
	Bottom Beam		57.50 (256)	1.9 (48.3)
12 months	Top Beam		59.00 (262)	1.9 (48.3)
	Bottom Beam		57.50 (256)	1.8 (45.7)
18 months	Top Beam		58.60 (261)	1.8 (45.7)
	Bottom Beam		58.10 (258)	1.8 (45.7)
18 months (No water cycles)	Top Beam		59.80 (266)	1.9 (48.3)
	Bottom Beam		56.80 (253)	1.8 (45.7)

*Confirmed instrumentation error

Figure 6.34: Failure of Beam#11 after exposure to sustained load for 18 months (Top Beam)

Figure 6.35: Failure of Beam#12 after exposure to sustained load for 18 months (Bottom Beam)
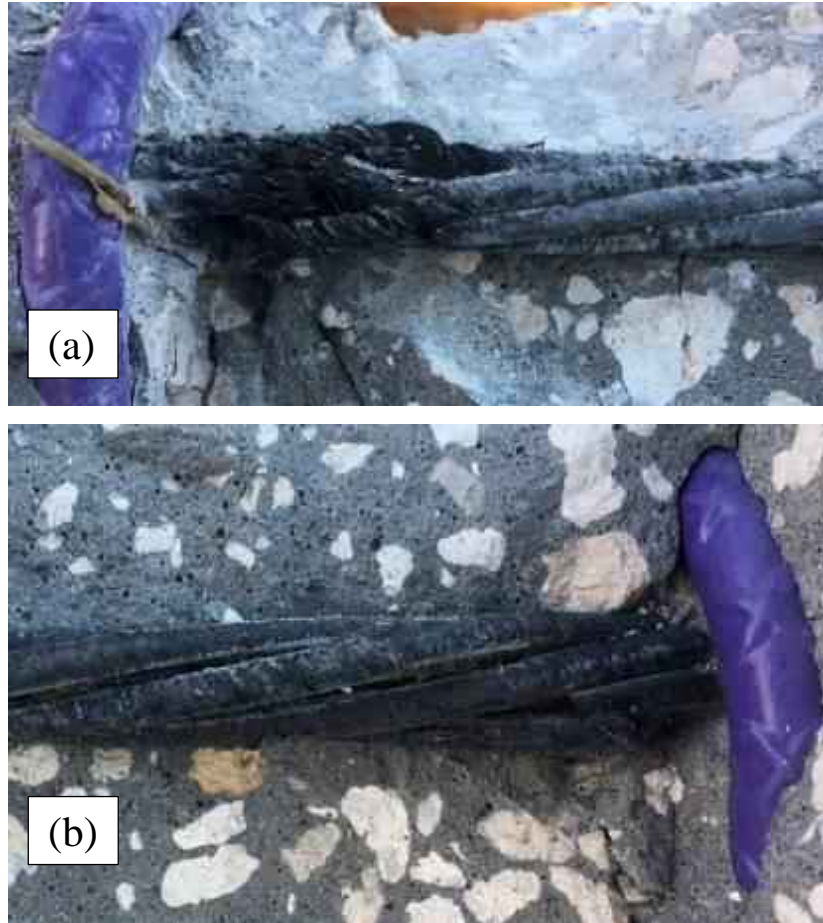
Figure 6.36: A close up view of the strand rupture after 18 months exposure to sustained load only (a) top beam (b) bottom beam.

6.6 Analysis of Test Results

All beams were loaded monotonically up to failure using load control system. The failure load of concrete beams ranged from 56.5 kips to 60.5 kips (251 KN to 269 KN). Figure 6.37 shows the load deflection curves of all the tested beams. The curves of load – concrete strain behavior at the top and bottom of the concrete beams are given in Figure 6.38.
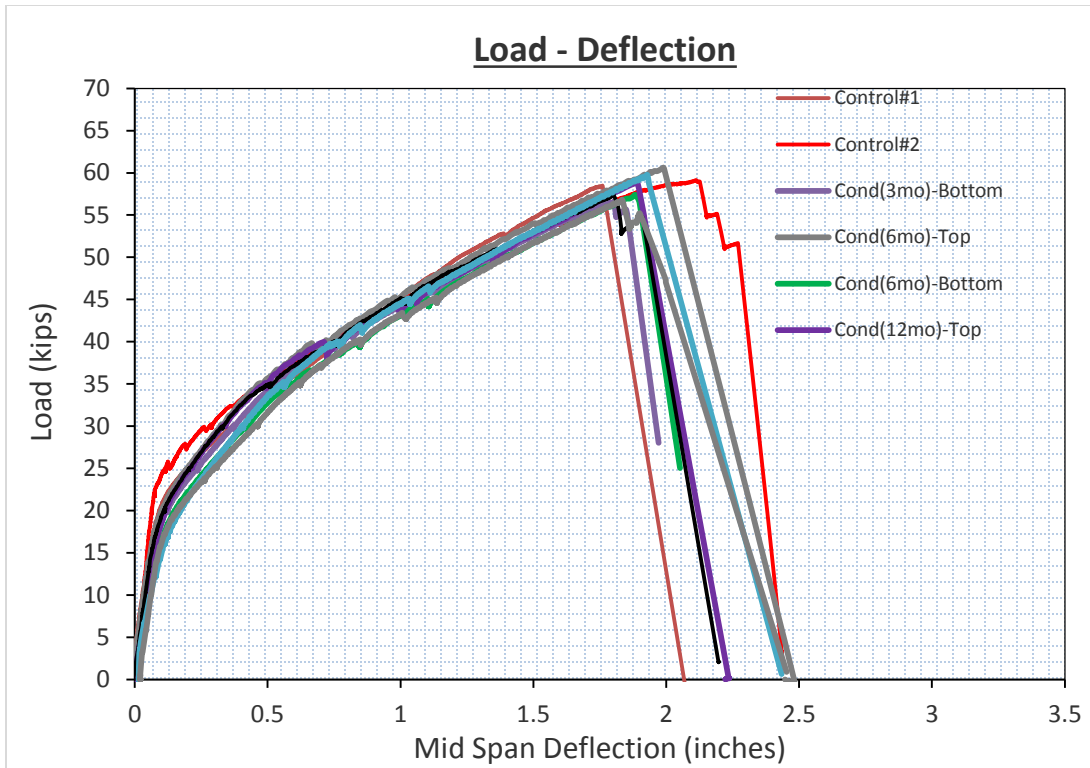
Figure 6.37: Load deflection curves of all concrete beams.
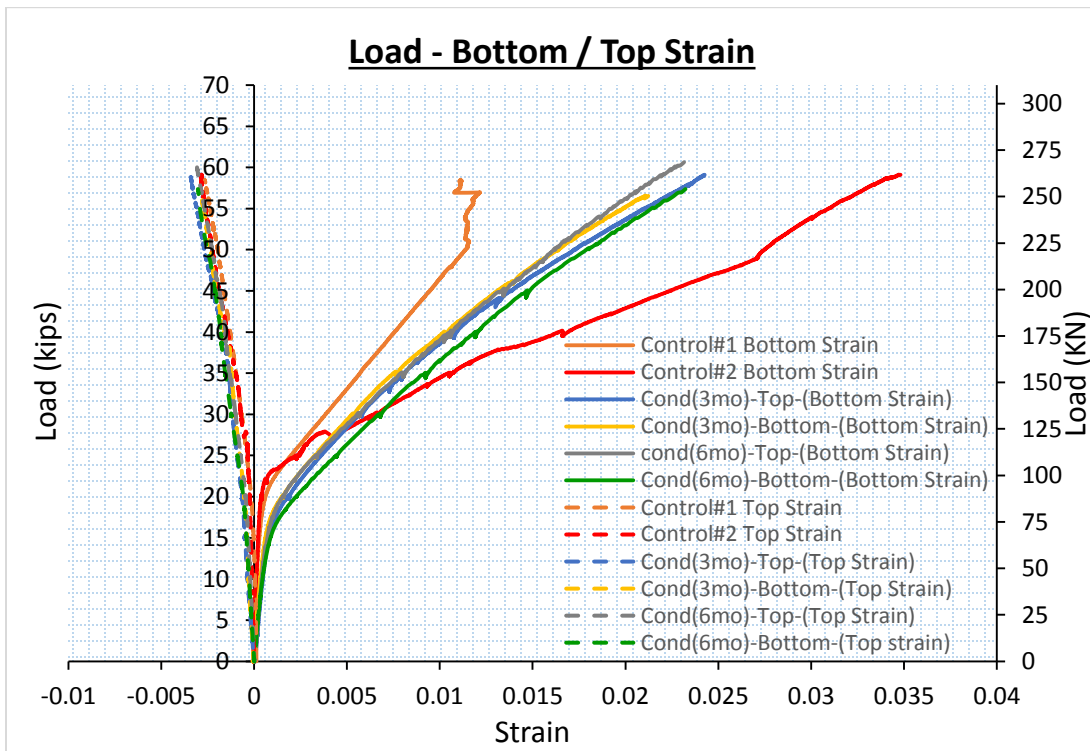
Figure 6.38: Load – bottom / top strain curves of all concrete beams.

Behavior of all tested beams was identical with similar load capacity and the failure was due to rupture of strands. Failure loads of the beams placed at the bottom during the exposure duration were slightly different than those placed in the top since the bottom beams were subjected to higher loads due to the self-weight of the top beam. The measured strain at the bottom of the beams indicated that at failure, the strands reach the ultimate rupture strain of the CFRP. The measured concrete strain at the top was also close to the crushing strain of concrete.

6.7   Conclusion

Test results indicated that all tested beams subjected to sustained load equivalent to 50 percent of their ultimate flexural capacity and exposed to environmental conditions for 18 months had an identical behavior during testing. Based on the observed behavior and measured failure load, it can be concluded that no degradation of the concrete beams presetressed with CFRP was observed up to 18 months of exposure.

CHAPTER 7
CONCLUSIONS AND RECOMMENDATIONS

Based on the experimental and analytical results obtained in this research considering the previous parameters associated with this research program, the following general conclusions are drawn:

7.1   CFRP Tendons under Sustained Load

7.1.1   Physical characteristics:

Physical and microstructural analyses were conducted on Tokyo Rope CFRP tendons (diameter: 7.5 mm). The carbon fiber content was 82.5% by weight, and the water uptake at saturation is equal to 11.6%. The cure ratio of the material was very high (close to 100%). The DMA measurements show a slight increase of Tg after conditioning at 60°C. At 22°C, the increase is insignificant since the temperature is too low to post-cured/consolidate the material. Optical and electronic scanning microscopy analysis showed that a few voids were visible in the coating.

7.1.2   Tensile and transverse shear strength:

This research focuses on studying the possible degradation of CFRP prestressing strands due to exposure to simultaneous high alkali environment and sustained loading at an elevated temperature of 140 ºF (60 ºC) for durations up to 7,000 hr. The high alkali environment simulated the concrete pore solution and the elevated temperature was used to accelerate the aging process. The applied sustained load on the CFRP tendons was equivalent to 40% and 65% of their guaranteed strength. Based on the results of this research, the following conclusions may be drawn:

a) For specimens without load:

1- The results indicate that specimen strength was affected by increased immersion time at higher temperatures. The test results after 7,000 hr of immersion in the alkaline solution at 60ºC [140ºF] reveal a 10.5 % reduction in tensile strength. The tensile-strength reduction was attributed to the development of microcracks in the epoxy resin, resulting essentially from the existing defects in the material. Diffusion of water along these microcracks and the fibers might also have weakened the interfacial adhesion between the carbon fibers and epoxy resin, which reduces the stress transfer between carbon fibers and, consequently, the composite's tensile strength.

2- The transverse-shear strength of the Tokyo Rope CFRP tendons was significantly affected by accelerated aging (16.5 % reduction after 7,000 hr).

b) For specimens with load = 65%:

3- The results indicate that specimen strength was affected by increased immersion time at higher temperatures. The test results after 7,000 hr of immersion in the alkaline solution at 60°C [140°F] reveal a 12.3 % reduction in tensile strength.

c) For specimens with load = 40%:

4- The test results after 7,000 hr of immersion in the alkaline solution at 60°C [140°F] reveal a 9.4 % reduction in tensile strength.

7.2 GFRP Bars under Sustained Load

7.2.1 Physical properties

Physical properties test results of Pultrall and Aslan bars showed that the test bars satisfied the ACI and CSA requirements (when applicable) for: 1) Glass fiber content, 2) Transverse coefficient of thermal expansion, 3) Moisture absorption, 4) Cure ratio, and 5) Glass transition temperature.

7.2.2 Tensile properties

Mechanical properties were given in this report as part of the certification of Pultrall and Aslan bars.

7.2.3 GFRP specimens without load

The average tensile strength retention of the tested Pultrall and Aslan GFRP bars conditioned during 3,000; 5,000; and 7,000 hr in high pH solution without load at 30°C and 60°C is over 85% for all the tested GFRP bars . All the tested Pultrall and Aslan GFRP bars presented a value greater than the specified limit for high durability (D1) in (the CSA-S807, 2010) Standard (80%). The modulus of elasticity of the Pultrall and Aslan GFRP bars is not significantly affected by the immersion in high pH. The value of the modulus of elasticity retention for Pultral GFRP bars varied between 96 to 102 of the reference elastic modulus value.

7.2.4 GFRP specimens with sustained load (30% of loading)

The tested GFRP bars showed a value of tensile capacity retention over 83%. The tested GFRP bars meet the D1 requirement of (CSA-S807, 2010) for the alkali resistance in high pH solution with load (required limit is 70%).

The average residual tensile strengths for stressed Pultrall GFRP bars with sustained laod were equal to 957 and 906 MPa, at 22°C [72°F] and 60°C [140°F] for 7,000 hr of immersion respectively. The corresponding average residual tensile modulus of elasticity was 50.6 and 51.8 GPa, respectively. For the Asaln GFRP bars with sustained load, the residual tensile strengths for were equal

to 802 and 716 MPa, at 22ºC [72ºF] and 60ºC [140ºF] for 7,000 hr of immersion, respectively. The corresponding average residual tensile modulus of elasticity was 50.8 and 49.5 GPa, respectively.

7.3   GFRP with Different Types of Thermoset Resins

7.3.1   Mechanical properties observations

1- The epoxy and vinyl-ester GFRP bars exhibited higher fiber–resin bond; flexural strength; flexural modulus of elasticity; and interlaminar-shear strength, which is governed by the fiber–matrix interface. In addition, they showed lower moisture uptake.

2- Both the polyester and epoxy GFRP bars had similar flexural-strength reductions after 5,000 hr of immersion (25% and 23%, respectively), while the vinyl-ester GFRP bars returned a lower reduction of 17%. These observations confirm that the bond between the GFRP fibers and polyester resin—before and after conditioning—was lower than that between the glass fibers and the vinyl-ester or epoxy resin.

3- The unconditioned polyester GFRP bars exhibited lower transverse-shear strength, flexural strength, interlaminar-shear strength, and the weakest fiber–resin interface. The transverse-shear strength of the polyester GFRP bars was significantly affected by accelerated aging (22.5% reduction after 5,000 hr), while the epoxy and vinyl-ester GFRP bars were slightly affected by accelerated aging (11% and 15.9 % reductions, respectively, after 5,000 hr).

4- The flexural strength of the polyester GFRP bars was significantly affected by accelerated aging (25% reduction after 5,000 hr), while the vinyl-ester and epoxy GFRP bars were affected by accelerated aging (17% and 23% reductions, respectively, after 5,000 hr).

5- The interlaminar-shear strength of the polyester GFRP bars was highly affected by accelerated aging (21% reduction after 5,000 hr), while the vinyl-ester and epoxy GFRP bars were slightly affected by accelerated aging (13% reduction each after 5,000 hr). The fiber–resin interface plays a significant role in controlling the degradation due to conditioning.

7.3.2   Physical and microstructural observations

1- The microstructural observations revealed that GFRP bars made with vinyl-ester or epoxy resin were not significantly changed, but presented a slight debonding at the interface between the fibers and vinyl-ester resin. Consequently, the vinyl-ester GFRP bars evidenced higher moisture uptake measured at saturation compared to the epoxy GFRP bars.

2- The debonding at the interface between the fibers and polyester resin was higher than in the vinyl-ester and epoxy GFRP bars. Accordingly, the polyester GFRP bars evidenced higher moisture uptake measured at saturation and a higher degradation rate of mechanical properties after conditioning.

3- The polyester GFRP bars showed an increase in *Tg* of about 5°C after conditioning due to post-curing (cure ratio of the reference specimens was 98.1%). The vinyl-ester and epoxy GFRP bars, however, experienced a decrease in *Tg* after conditioning.

4- The polyester GFRP bars absorbed 18% more water than the vinyl-ester and epoxy GFRP bars after conditioning compared to the reference specimen.

7.4 Effects of Bars Size on the Durability of GFRP Bars Conditioned in alkaline solution

The effects of diameter on the physical, mechanical, and durability properties of GFRP bars were investigated. Based on the results of this study, the following conclusions were drawn for the tested GFRP bars:

1- With the bar sizes considered, bar diameter did not affect fiber content, transverse coefficient of thermal expansion, porosity, or glass transition temperature. On the other hand, the water absorption was found to decrease as the diameter increased. This can be correlated to the ratio of the surface area to the volume (shape ratio) of the GFRP bars.

2- The tensile strength and modulus of the reference bars were not significantly affected by the cross-sectional size, but a size effect was observed for interlaminar shear strength and flexural strength. The consistency in the measured tensile properties for GFRP bars with different diameters is due to the efficient stress transfer from the bar surface to the center. On the other hand, the higher probability of defects contained in the larger diameter bars may have caused the lower interlaminar shear strength and flexural strength in comparison to the smaller diameter bars. The elastic moduli of the reference and conditioned bars were same for all bar diameters, which is due to nearly same fiber content of the GFRP bars.

3- The interlaminar shear strength and flexural strength of the larger diameter GFRP bars were less affected after exposure to the alkaline solution than the smaller bar diameter. The higher strength retention for the larger bar sizes was due to the lower affected thickness. As a result, the penetrated area was proportionally small relative to the total cross-sectional area of the bar.

4- The tensile-strength retention was highest for the smallest diameter bar. This suggests that the impact of conditioning on the tensile properties of GFRP bars is expected to be greater for larger than smaller diameters.

5- The scanning-electron-microscope and FTIR observations showed no changes in the material properties and chemical structure in the exposed surface of the bars after conditioning in the alkaline solution for 90 days at 60°C [140°F]. This shows that the degradation remained at the surface for all the bar diameters.

6- Nevertheless, the variations in the physical and mechanical properties of the GFRP bars investigated in this study, from one diameter to another, remained low. Thus, the suggestions of the current standards and specifications of not relating the strength-retention limit to the size of the FRP bars are

acceptable. Further research, however, is needed to investigate other bar types and diameters to clearly determine how the diameter might affect the design of GFRP-reinforced concrete structures.

7.5   Concrete Beams Testing with GFRP reinforcement

This study presented the flexural behavior of concrete beams reinforced with GFRP bars that were subjected to sustained high load of 40% of the guaranteed tensile strength of the GFRP reinforcement and placed outdoor for 10 years under harsh natural environmental conditions, including freeze–thaw cycles and moisture. The following conclusions have been developed:

1- The investigation of the GFRP beams after 10 years of aggressive environmental conditions and high-sustained load of 40% guaranteed tensile strength was a very valuable asset that provided great information ensuring degradation of GFRP bars. The tensile strength retention was 82% after 10 years of service life.

2- There is a correlation between the degradation and performance of GFRP in beams and conditioned GFRP bars. Using the analytical model that incorporates the test results for conditioned GFRP bars, a 90% reduction is predicted in the ultimate strength after 10 years under sustained loading of 30% guaranteed tensile strength, temperature ranging from $50\,^{\circ}$F to $86\,^{\circ}$F ($10\,^{\circ}$c to $35\,^{\circ}$c), and alkaline exposure.

3- It is evident that the trend of degradation and strength reduction of GFRP bar reinforcement in concrete beams is similar to that for the conditioned GFRP bars. The discrepancy of the tensile strength retentions for the GFRP bars in beams (82%) and conditioned GFRP bars (90%) could be attributed to the higher sustained loading of 40% guaranteed tensile strength for the beams compared to only 30% for the conditioned GFRP bars, among other factors. These factors could include the freeze-thaw effect due to the exposure to snow and freezing effects that could affect the concrete beam, in addition to any degradation at the interface between the FRP bar surface and the concrete that could occur due to long duration of exposure to outside harsh environment.

4- The mode of failure of the reference and conditioned beams was the same by tensile rupture of the GFRP reinforcement

5- The Crack pattern observed for the conditioned beams was equivalent to crack pattern recorded for the reference beams which is an indication of no change in the bond of the GFRP reinforcement.

7.6   Constituent Materials of GFRP

From the analyses performed on three thermoset resins used in FRP bar manufacturing, it may be concluded that the chemical resistance of these materials in alkaline solution is as following:

$$EPOXY > POLYURETHANE > VINYL ESTER$$

However, it has to be noted that the conditionings used in this study are harsher than the environment surrounding composite material in concrete. Moreover, only a thin layer in direct contact

with the solution is affected. Below the resin surface, the three resins are not degradated. Consequently, in spite of their lower chemical resistance VE resins are resistant to concrete environment, as observed in several studies on GFRP reinforcing bars.

As glass fibers are concerned, the main conclusions drawn from this study are:

  (d) ECR-type and boron free glass fiber are resistant to alkalis.
  (e) Sizing can act as a protector against alkali corrosion.
  (f) Conditioning in alkaline solution does not modify the content of metals in the fiber. No metal leaching is observed.

Concerning the composites prepared at the laboratory with these fibers and resins, several conclusions may be drawn:

  - Composites absorb water faster than pure resins.
  - SEM analysis shows that the bonding at the fiber-matrix interface is excellent. No significant debonding was detected.
  - The presence of fibers in a resin matrix creates an interphase, which is caused by the diffusion of sizing molecules through the surrounding resin molecules. The thickness of this interphase is between 1 and 10 microns depending on the technique used.
  - This interphase is constituted of a less dense and more "porous" resin, which is responsible of the increase of water diffusion.
  - VE composites absorb less water than PU and EP composites. VE resin and the interphase in VE composites are less permeable to water diffusion and should therefore offer an excellent durability for vinyl-ester GFRP bars in humid/moist environments like in Florida.

7.7 Structural Performance oF Concrete Beams Prestressed with CFRP Tendons

Test results indicated that all tested beams subjected to sustained load equivalent to 50 percent of their ultimate flexural capacity and exposed to environmental conditions for 18 months had an identical behavior during testing. Based on the observed behavior and measured failure load it can be concluded that no degradation of the concrete beams presetressed with CFRP was observed up to 18 months of exposure.

.

7.8 Recommendations

1- Based on the test results, the research team concluded that the most sensitive test method is the "Tensile Test under sustained load, elevated temperature of 140ºF (60ºC), alkaline solution of pH=12.8, and exposure duration of 3 months.

2- The Recommended test protocol of tensile test for conditioned FRP bars should be conducted in according with ASTM specifications.

3- The sustained load should be applied as 30% for GFRP and 65% for CFRP.

4- Based on results of different performed tests, the tensile test for conditioned GFRP and CFRP, under (30% for GFRP or 65% for CFRP) sustained load, elevated temperature of 140ºF (60ºC), alkaline solution of pH=12.8, and exposure duration of 3 months, is the most sensitive test method that also includes the most dominating effects (elevated temperature and alkaline solution) to material degradation.

5- Based on the test results conducted on FRP reinforcements, considering the recommendation of the CAN/CSA 806-12 and ACI 440.3R-4, the minimum exposure duration is specified to be 3 months.

6- The new proposed service life prediction models (detailed in the previous sections 3.5.4 and 4.9.7) incorporate the effects of temperature, design life, and RH of exposure into the environmental reduction factor for the FRP bars. Based on the service-life prediction models, the tensile-strength retention is predicted to retain over 82% of guaranteed tensile strength for CFRP and over 74 % of guaranteed tensile strength for GFRP, after 100 years of service life in moist alkaline environment with elevated temperatures and under sustained load.

REFERENCES

ACI (American Concrete Institute). (2008). "Specification for carbon and glass fiber-reinforced polymer bar materials for concrete reinforcement." ACI 440.6M-08, Farmington Hills, MI.

ACI 224R-01. 2001. Control of cracking in concrete structures, Farmington Hills (MI): American Concrete Institute.

ACI 440.1R-15, 2015, "Guide for the Design and Construction of Structural Concrete Reinforced with FRP Bars" American Concrete Institute, Farmington Hills, Michigan, USA, 44 p.

ACI 440.3R-04, 2004, "Guide Test Methods for Fiber-Reinforced Polymers (FRPs) for Reinforcing or Strengthening Concrete Structures," American Concrete Institute, Farmington Hills, Michigan, USA, 41 p.

Advanced Composites Materials, vol. 1, no.3, p. 55 – 67.

Ahmed H. Ali, Awad El hashimy, Hesham Haggag, and Tarek El-Sayed. (2015). "Physical, Mechanical, and Durability Performance of GFRP Square Reinforcing Bars Exposed to Alkaline Solution." International Journal of Engineering Sciences & Research Technology, Vol. 4, Issue 6, 548-553.

Ahmed H. Ali, Bahira Abdulsalam, Hamdy M. Mohamed, Mohammad Z. Afifi (2015). "Enhancing the behaviour of FRP RC Slabs using square FRP bars and Fiber Concrete." International Journal of Civil Structural Engineering, Vol. (6), Issue (1), 70-90.

Ahmed H. Ali, Bahira Abdulsalam, Hamdy M. Mohamed, Mohammad Z. Afifi (2015). "Enhancing the behaviour of FRP RC Slabs using square FRP bars and Fiber Concrete." International Journal of Civil Structural Engineering, Vol. (6), Issue (1), 70-90.

Ahmed H. Ali, Mohammad Z. Afifi, Bahira Abdulsalam, Hesham Haggag, Awad El Hashimy, Tarek El-Sayed, Hamdy M. Mohamed (2015). "Performance Evaluation of One-Way Concrete Slabs Reinforced with New Developed GFRP Bars" Materails Science and Application, Vol. (6), May (2014), 420-435.

Ali, A. H. (2016). "Shear strength and behavior of circular concrete members reinforced with FRP bars and spirals." Doctoral thesis in Civil Engineering, April 2016, Sherbrooke University, Canada.

Ali, A. H., Benmokrane, B., Mohamed, H., Manalo, A., and El-Safty, A. (2018). "Statistical Analysis and Theoretical Predictions of the Tensile Strength Retention of GFRP Bars based on Resin Degradation." Journal of Composite Materials, 1-20.

Ali, A. H., Mohamed, H. M., and Benmokrane, B., (2017) "Shear Strength of Circular Concrete Beams Reinforced with Glass-FRP Bars and Spirals". ACI Structural Journal, Vol. 114, Issue 1, 39-49.

Ali, A. H., Mohamed, H. M., Benmokrane, B., and ElSafty, A. (2017). "Influence of Resin Type on Physical, Mechanical and Durability Performance of Glass-FRP Bars in Concrete Environment at Elevated Temperature." Fifth International Conference on Durability of Fibre Reinforced Polymer (FRP) Composites for Construction and Rehabilitation of Structures (CDCC 2017), 19-21th July, 2017, Sherbrooke, Qc, Canada.

Ali, A. H., Mohamed, H.M., Benmokrane, B., and El-Safty, A. (2018). "Effect of Applied Sustained Load and Severe Environments on Durability Performance of Carbon-Fiber Composite Cables (CFCCs)." Journal of Composite Materials, Accepted on July 2018.

Ali, A. H., Mohamed, H. M., and Benmokrane, B. (2016). "Shear Behavior of Circular Concrete Members Reinforced with GFRP Bars and Spirals at Shear Span-to-Depth Ratios between 1.5 and 3.0." J. Compos. Constr., 10.1061/(ASCE)CC.1943-5614.0000707 , 04016055.

Ali, A. H., Mohamed, H. M., and Benmokrane, B. (2016). "Strength and Behavior of Circular FRP-Reinforced Concrete Sections without Web Reinforcement in Shear." J. Struct. Eng., 10.1061/(ASCE)ST.1943-541X.0001684 , 04016196.

Ali, A., Mohamed, H., ElSafty, A., and Benmokrane, B. (2015). "Long-term durability testing of tokyo rope carbon cables." 20th International Conference on Composite Materials Copenhagen, 19-24th, Denamark.

Allred, R. E. (1984). "The effects of temperature and moisture content on the flexural response of Kevlar/epoxy laminates: Part II [45/0/90] filament orientation." Environmental effects on Composites Materials, vol. 2, ed. Springer, G., Lancaster, PA: Technomic Publishing Company Inc.

Allred, R. E., 1984, The effects of temperature and moisture content on the flexural response of

Almusallam T.H., Al-Salloum Y.A, Alsayed S.H., Sherif El-Gamal, and Aqel, M. (2013). "Tensile properties degradation of glass fiber-reinforced polymer bars embedded in concrete under severe laboratory and field environmental conditions." Journal of Composite Materials, 47(4), 393-407.

Al-Zahrani, M. (2005) Effect of accelerated laboratory conditions on tensile strength and moisture absorption of two GRFP bars, Proceedings of Composites in Construction 2005-Third International Conference, Lyon, France, p. 775-782.

Ando, N., Matsukawa, H., Hatorri, A., Mashima, A. (1997) Experimental studies on the long-term tensile properties of FRP tendons, Proceeding of the 3rd International Symposium on Non-Metallic (FRP) Reinforcement for Concrete Structures, FRPRCS-3, Japan Concete Institute, Saporro, Japan, vol. 2, p. 203-210.

ASTM D3418, 2012, "Standard Test Method for Transition Temperatures and Enthalpies of Fusion and Crystallization of Polymers by Differential Scanning Calorimetry". American Society for Testing and Materials, Conshohocken, USA, 7 p.

ASTM. (2003). "Standard test method for compositional analysis by thermogravimetry." ASTM E1131, West Conshohocken, PA.

ASTM. (2003). "Standard test method for curing properties of pultrusion resins by thermal analysis." ASTM D5028, West Conshohocken, PA.

ASTM. (2010). "Water absorption of plastics." ASTM D570, West Conshohocken, PA.

ASTM. (2011). "Tensile properties of fiber reinforced polymer matrix composite bars." ASTM D7205, West Conshohocken, PA.

Bahira Abdulsalam, and Ahmed H. Ali (2014). "The Preservation of Historical Masonry Heritage Structures using Advanced Composite Materials." International Journal of Engineering Sciences and Research Technology, Vol. (4), Issue (8), August 2014, 14-24.

Bank, L. C., Gentry, T. R., Thompson, B. P., and Russell, J. S. (2003). "A model specification for composites for civil engineering structures." Constr. Build. Mater., 17(6-7), 405-437.

Banthia, N., Benmokrane, B., and Karbhari, V. (Editors) (2006). Durability of Fiber Reinforced Polymers in Civil Infrastructure. ISIS Canada Monograph, 243 p.

Ben Daly, H., Ben Brahim, H., Hfaied, N., Harchay, M., Boukhili, R., 2007, "Investigation of

Benmokrane B and Mohamed H.M (2013) "Durability Issues of FRP for Civil Infrastructures" 11th International Conference on Fibre Reinforced Polymer (FRP) Reinforcement for Concrete Structures (FRPRCS-11), Portugal, Porto, 15p.

Benmokrane, B. (2000) Improvement of the Durability Performance of Glass Fiber Reinforced Polymer (GFRP) Reinforcements for Concrete structures, Technical Report, Civil Engineering Department, University of Sherbrooke, 50 p.

Benmokrane, B., Ahmed, E., Dulude, C., and Boucher, E., 2012, "Design, Construction, and

Benmokrane, B., Ali, A. H., Mohamed, H. M., ElSafty, A., Manalo, A. (2017). "Laboratory Assessment and Durability Performance of Vinyl-Ester, Polyester, and Epoxy Glass-FRP Bars for Concrete Structures." Journal Composites: Part B, Vol. 114, 163-174.

Benmokrane, B., Ali, A. H., Mohamed, H. M., ElSafty, A., Manalo, A. (2017). "Laboratory Assessment and Durability Performance of Vinyl-Ester, Polyester, and Epoxy Glass-FRPBars for Concrete Structures." Journal Composites: Part B, Vol. 114, 163-174.

Benmokrane, B., Robert, M., Mohamed H., Ali, A. H., and Cousin, P. (2016). "Durability Assessment of Glass FRP Solid and Hollow Bars (Rock Bolts) for Application in Ground Control of Jurong Rock Caverns in Singapore." J. Compos. Const., 10.1061/(ASCE)CC.1943-5614.0000775.

Benmokrane, B., Wang, P., Pavate, T., Robert, M. (2006). "Durability of materials and structures in building and civil engineering. Chapter 12: durability of FRP composites for civil infrastructure applications." Yu, C. W. (Editors), Whittles Publishing, Dunbeath, Scotland, 44 p.

Benmokrane, B., Ali, A. H., Mohamed, H., Robert, M., and ElSafty, A. (2016). "Durability Performance and Service Life of CFCC Tendons Exposed to Elevated Temperature and Alkaline Environment." J. Compos. Constr., 10.1061/(ASCE)CC.1943-5614.0000606, 04015043.

Benmokrane, B., Ali, A. H., Mohamed, H., Robert, M., and ElSafty, A. (2016). "Durability Performance and Service Life of CFCC Tendons Exposed to Elevated Temperature and Alkaline Environment." J. Compos. Constr., 10.1061/(ASCE)CC.1943-5614.0000606, 04015043.

Benmokrane,B., Mohamed, H. M., and Ali, A. H. (2018). "Service-Life-Prediction and Field Application of GFRP Tubular and Solid Bolts based on Laboratory Physical and Mechanical Assessment." Journal of Composite Materials, 1-15, https://doi.org/10.1177/0021998318764806.

Benzarti, K., and Colin, X., (2013). Understanding the Durability of Advanced FRP Composites for Structural Applications." Chapter 12, 361-439, in book: Advanced FRP Composites for Structural Applications, Woodhead Publishing, Edited by Jiping Bai, 906p.

Benzarti, K., and Colin, X., (2013). Understanding the Durability of Advanced FRP Composites for Structural Applications." Chapter 12, 361-439, in book: Advanced FRP Composites for Structural Applications, Woodhead Publishing, Edited by Jiping Bai, 906p.

Browning, C.E., (1978) "The mechanism of elevated temperature property losses in high performance structural epoxy resin matrix materials after exposure to high humidity environments". Polymers Engineering and Science, 18 (1), p. 16-24.

Canadian Journal of Civil Engineering 27: 949–959.

Canadian Standards Association (CSA), 2010, "Specification for Fibre-Reinforced Polymers.", (CAN/CSA S807–10), Rexdale, Ontario, Canada, 27 p.

Canadian Standards Association (CSA), 2012, "Design and Construction of Building Components with Fibre Reinforced Polymers (CAN/CSA S806–12).", Rexdale, ON, Canada.

Canadian Standards Association (CSA), 2014, "Canadian highway bridge design code-Section 16, updated version for public review." CAN/CSA-S6-14, Rexdale, Ontario, Canada.

Chen, Y., Davalos, J. F., and Ray, I. (2006). "Durability prediction for GFRP bars using short-term data of accelerated aging tests." J. Compos. Constr., 10(4), 279-286.

Chen, Y., Davalos, J.F., Ray, I. and Kim, H.Y. (2007). "Accelerated aging tests for evaluation of durability performance of FRP reinforcing bars reinforcing bars for concrete structures." Composite Structures. 78(1), 101-111.

Chin, J., Aouadi, K., Haight, M. R., Hughes, W. L., Nguyen, T. (2001) Effects of Water, Salt Solution and Simulated Concrete Pore Solution on the Properties of Composite Matrix Resins Used in Civil Engineering Applications, Polymer Composites, vol. 22, no 2, p. 282-297.

Chu, W., and Karbhari, V. (2002). "Characterization and moisture and alkali effects on E-glass/vinylester composites." In: Proceedings of 2nd International Conference on Durability of Fibre Reinforced Polymer Composites for Construction, Montreal, Quebec, Canada, 359–369.

Chu, W., Wu, L. and Karbhari, V. (2004). "Durability evaluation of moderate temperature cured E-glass/vinylester systems." Compos. Struct. 66, 367–376.

Composites Materials, vol. 2, ed. Springer, G., Lancaster, PA: Technomic Publishing Company

Davalos, J .F., Chen, Y., and Ray, I. (2012) "Long-term durability prediction models for GFRP bars in concrete environment." J. Comp. Mater., 46: 1899-1914.

Dejke, V., and Tepfers, R. (2001). "Durability and service life time prediction of GFRP for concrete reinforcement." Proc., 5th Int. Symp. on Fiber Reinforced Polymers for Reinforced Concrete Structures (FRPRCS-5), Vol. 2 , Thomas Telford, Cambridge, U.K., 505–513.

Dejke, V., and Tepfers, R. (2001). "Durability and service life time prediction of GFRP for concrete reinforcement." Proc., 5th Int. Symp. on Fiber Reinforced Polymers for Reinforced Concrete Structures (FRPRCS-5), Vol. 2 , Thomas Telford, Cambridge, U.K., 505–513.

Dell'Anno, G., and Lees, R. (2011). "Effect of Water Immersion on the Interlaminar and Flexural Performance of Low Cost Liquid Resin Infused Carbon Fabric Composites." Composites Part B: Engineering, 43(3), 1368-1373.

Dénève, B., Shanahan, M. E. R. (1995) "Physical And Chemical Effects In An Epoxy-Resin Exposed To Water-Vapor." Journal of Adhesion, 49: 165-176

Elsafty, A., Benmokrane, B., Rizkalla, S., Mohamed, H.M., and Hassan, M. (2014) "Degradation Assessment of Internal Continuous Fiber Reinforcement in Concrete Environment" BDK82-977-05, College of Computing, Engineering, and Construction, University of North Florida.

El-Salakawy, E., Benmokrane, B., and Desgagné, G. (2003). "FRP composite bars for the concrete deck slab of Wotton Bridge." Can. J. Civ. Eng., 30(5), 861-870.

Gerritse A. (1998). "Assessment of long term performance of FRP bars in concrete structures." Proc., Durability of Fiber Reinforced Polymers (FRP) Composites for Construction, Sherbrooke, Québec, Canada; 285-297.

Gerritse, A. (1998) Assessment of long term performance of FRP bars in concrete structures, Proceedings of Durability of Fiber Reinforced Polymers (FRP) Composites for Construction, eds. B. Benmokrane and H. Rahman, p.285-297.

GFRP Bars." 6th International Conference on FRP Composites in Civil Engineering.CD proceeding, CICE 2012, Rome, Italy.

Grace, N., Enomoto, T., Baah, P., and Bebawy, M. (2012). "Flexural behavior of CFRP precast prestressed decked bulb T-beams." J. Compos. Constr., 16(3), 225-234.

Grace, N., Rout, S., Ushijima, K., and Bebawy, M. (2014). "Performance of carbon-fiber-reinforced polymer stirrups in prestressed-decked bulb T-beams." J. Compos. Constr., 10.1061/(ASCE)CC.1943-5614.0000524, 04014061.

Green, M. F., Bisby, L. A., Beaudoin, Y. and Labossière, P., 2000, "Effect of freeze–thaw cycles

Hancox, N. L., Mayer, R. M. (1994). "Design data for reinforced plastics." Chapman & Hall, New York, NY, 202-204.

Hancox, N. L., Mayer, R. M., 1994, "Design data for reinforced plastics", Chapman & Hall,

Hojo, H., Tsuda, K., Ogasawara, K., 1991, "Form and rate of corrosion – resistance FRP resins",

Huang, J. and Aboutaha, R. (2010). "Environmental Reduction Factors for GFRP Bars Used as Concrete Reinforcement: New Scientific Approach." J. Compos. Constr., 14(5), 479–486.

Inc.

ISIS Canada 2001; 2006; 2007, "Reinforcing concrete structures with fiber reinforced polymers." ISIS-M03-2001; 2006; 2007, The Canadian Network of Centers of Excellence on Intelligent Sensing for Innovative Structures, Univ. of Winnipeg, Manitoba, Canada.

Japanese Society of Civil Engineers JSCE, 1997, "Recommendations for Design and Construction of Concrete Structures using Continuous Fiber Reinforced Materials", 120 p.

Journal of Composites for Construction, vol. 6, no 4, p. 280-287.

Judd, N. C. W. (1971). "The chemical resistance of carbon fibers and a carbon fiber\polyester composites." The First International Conference of Carbon Fibers, Plastics Institute, 1 – 8.

Kang, H. M, Yoon, T. H., Bump, M., and Riffle, J. S. (2001). "Effect of Solubility and Miscibility on the Adhesion Behavior of Polymer-Coated Carbon Fibers with Vinyl Ester Resins." Journal of Applied Polymer Science, Vol. 79, 1042–1053.

Katsuki, F., and Uomoto, T. (1995). "Prediction of deterioration of FRP rods due to alkali attack." Proc., Non-Metallic (FRP) Reinforcement for Concrete Structures, L. Taerwe, ed., E & FN Spon, London, 108–115.

Katsuki, F., Uomoto, T. (1995) Prediction of deterioration of FRP rods due to alkali attack, Non-metallic (FRP) Reinforcement for Concrete Structures, FRPCS-2, Ghent, Belgium, p. 108 – 115.

Kevlar/epoxy laminates: Part II [45/0/90] filament orientation, Environmental effects on

Liao, K., Schultheisz, C. R., Hunston, D. L., Brinson, L. C. [1998] Long-term durability of fiber-reinforced polymer-matrix composite materials for infrastructures application: a review, Journal of Advanced Materials, vol. 30, no 4, p. 3-40.

Liao, K., Schultheisz, C. R., Hunston, D. L., Brinson, L. C. [1998] Long-term durability of fiber-reinforced polymer-matrix composite materials for infrastructures application: a review, Journal of Advanced Materials, vol. 30, no 4, p. 3-40.

Liao, T.-T. (1989). "A Study of Glass Fiber-Epoxy Composite Interfaces." Polymer Composites 10(6), 424-428.

Litherland, K. L., Okley, D. R., and Proctor, B. A. (1981). "The use of accelerated aging procedures to predict the long term strength of GRC composites." Cem. Concr. Res., 11, 455-466.

Mashima, M., Iwamoto, K. (1993) Bond Characteristics of FRP Rods and Concrete after Freezing and Thawing Deterioration, ACI SP 138, International Symposium on FRP Reinforcements for Concrete Structures, Vancouver, Canada, p. 51-69.

Mashima, M., Iwamoto, K. (1993) Bond Characteristics of FRP Rods and Concrete after Freezing and Thawing Deterioration, ACI SP 138, International Symposium on FRP Reinforcements for Concrete Structures, Vancouver, Canada, p. 51-69.

McKague, E.L., Reynolds, J.D., Halkias, J.E., (1978) "Swelling and glass transition relations for epoxy matrix in humid environments". J. Appl. Polymer Sci., 22, p. 1 643-54.

Micelli, F. and Nanni, A. (2004). "Durability of FRP rods for concrete structures." Construction and Building Materials, 18, 491-503.

Mohamed, H. M., and Benmokrane, B., 2012b, "Recent field applications of FRP composite

Mohamed, H., Ali, A. H., and Benmokrane, B. (2016). "Behavior of Circular Concrete Members Reinforced with Carbon-FRP Bars and Spirals under Shear." J. Compos. Constr., 10.1061/(ASCE)CC.1943-5614.0000746 , 04016090.

Mohamed, H.M., and Benmokrane, B. (2014). "Design and performance of reinforced concrete water chlorination tank totally reinforced with GFRP bars." J. Compos. Constr, 18(1), 05013001.

Mohamed, H.M., and Benmokrane, B. (2014). "Design and Performance of Reinforced Concrete Water Chlorination Tank Totally Reinforced with GFRP Bars: Case Study." J. Compos. Constr., Volume 18, Issue 1, 10.1061/(ASCE)CC.1943-5614.0000429, 05013001.

Monitoring OF the First Worldwide Two-Way Flat Slab Parking Garage Reinforced with

Mufti A, Onofrei M, Benmokrane B. (2005). "Durability of GFRP reinforced concrete in field structures. ACI Spec. Publ., 230: 1361–1378.

Nanocomposites in Civil, Offshore and Mining Infrastructure, 14 – 16 November 2012 Melbourne, Australia, 6p.

Nelson, W. (1990). "Accelerated testing-Statistical models, test plans, and data analyses." Wiley, New York.

New York, NY, p. 202-204.

Nkurunziza, G., Benmokane, B., Debaiky, A. S., Masmoudi, R. (2005) Effect of sustained load and environment on long-term tensile properties of glass FRP reinforcing bars, ACI Structural Journal, vol 102, no 4, p. 615-621.

on the bond durability between fibre-reinforced polymer plate reinforcement and concrete",

Perez-Pachero, E., Canich-Capul, I., Veladez-Gonzalez, A., and Herrera-Franco, P.J. (2013). "Effect of Moisture Absorption on the Mechanical Behavior of Carbon Fiber/Epoxy Matrix Composites." J . Mater. Scien., 48, 1873-1882.

piles", Research Report, Department of Civil Environmental Engineering, University of

Polymer Composites, 28(3), 355-364.

Porter, M. L., Mehus, J., Young, K. A., O'Neil, E. F., and Barnes, B. A. (1997). "Aging for fiber reinforcement in concrete." Proc., 3rd Int. Symp. on Non-Metallic (FRP) Reinforcement for Concrete Structures, Vol. 2, Japan Concrete Institute, Sapporo, Japan, 59-66.

reinforcing bars in civil engineering infrastructures", ACUN6 –Composites and

Robert M, Cousin P and Benmokrane B. (2009). "Durability of GFRP reinforcing bars embedded in moist concrete." J Compos Constr., 13,66–73.

Robert, M. and Benmokrane, B., (2013). "Combined effects of saline solution and moist concrete on long-term durability of GFRP reinforcing bars." Construction and Building Materials, 38: 274-284.

Robert, M., and Benmokrane, B. (2013). "Combined effects of saline solution and moist concrete on long-term durability of GFRP reinforcing bars." Construction and Building Materials, 38, 274–284.

Robert, M., Wang, P., Cousin, P., and Benmokrane, B. (2010). "Temperature as an accelerating factor for long term durability testing of FRPs should there be any limitations." J. Compos. Constr., 14(4), 361-367.

Saadatmanesh, H. Tannous, F. E. (1999) Long-Term Behavior of Aramid Fiber Reinforced Plastic Tendons, ACI Material Journal, pp. 297-305.

Saadatmanesh, H., Ehsani, M. R. (1998) International Conference on Composites for Infrastructure, Proceedings of ICCI'98, Tucson, Arizona, USA, vol. 1, 723 p., vol. 2, 783 p.

Santoh, N., (1993) "CFCC (Carbon Fiber Composite Cable)," Fiber-Reinforced-Plastic (FRP) Reinforcement for Concrete Structures: Properties and Applications, Developments in Civil Engineering, 42, A. Nanni editor, Elsevier Science Publishers, pp. 223-247.

Santoh, N., Kimura, H., Enomoto, T., Kiuchi, and T., Kuzuba, Y., (1993) "Report on the Use of CFCC in Prestressed Concrete Bridges in Japan," Fiber-Reinforced-Plastic Reinforcement for Concrete Structures (FRPRCS), Vancouver, Canada, March 1993, pp. 895 - 911.

Sen, R., Ross, J., Sukamar, S., Snyler, D., 1996, "Durability and bond of AFRP pretensioned

Shao, Y., Kouadio, S. ,2002, "Durability of Fiberglass Composite Sheet Piles in Water",

South Florida.

Suzuki, Y., Maekawa, Z., Hamada, H., Kibune, M., Hojo, M., and Ikuta, N. (1992). "Influence of Adsorption Behaviour of a Silane Coupling Agent on Interlaminar Fracture in Glass Fibre Fabric-Reinforced Unsaturated Polyester Laminates" Journal of Materials Science, 27 (24), 6782-6790.

Tokyo Rope. (2012). "Technical data on CFCC." Manufacturer Rep., Tokyo, Japan.

Water Absorption in Pultruded Composites Containing Fillers and Low Profile Additives",

Weitsman, Y., J., Elahi, M. [2000] Effects of fluids on deformation, strength and durability of polymeric composites-an overview, Mechanics of time-dependent materials 4, p. 107-126.

Xiao, G. Z., Shanahan, M. E. R. (1997) "Water Absorption and Desorption in an Epoxy Resin with Degradation." J Polym Sci B: Polym Phys, 35: 2659–2670.